METAL INERT GAS (MIG) WELDING OF ASTM A500 GRADE B STEEL PIPES: INFRARED THERMAL IMAGING AND ANALYSIS

By

CATHERINE ANTES HIGGINS

Bachelor of Science

Oklahoma State University

Stillwater, Oklahoma

2003

Submitted to the Faculty of the
Graduate College of the
Oklahoma State University
in partial fulfillment of
the requirements for
the Degree of
MASTER OF SCIENCE
December 2005

METAL INERT GAS (MIG) WELDING OF

ASTM A500 GRADE B STEEL PIPES:

INFRARED THERMAL IMAGING

AND ANALYSIS

Thesis Approved:

Dr. R. Komanduri
Thesis Adviser

Dr. C.E. Price

Dr. R.D. Delahoussaye

Dr. G. Emslie
Dean of the Graduate College

SUMMARY

Welding is a complex manufacturing process that generates extremely high temperatures and temperature gradients at and near the weld bead. Metallurgical damage and residual thermal stresses in pipe welds can restrict their widespread usage in industry especially for critical applications. A better understanding of the heat generated in welding and associated thermal gradients can shed light on the metallurgical quality of welded pipes and reliability of welds in practice. Most investigations on welding deal with joining flat pieces of material. In this investigation welding of circular pipes is undertaken. An experimental setup was designed and built to observe the welding process and gather thermal images under different welding conditions.

In the present experimental investigation thermal images of the welding of ASTM A500 Grade B steel pipes are collected using an infrared camera. An analytical solution is used to calculate the temperature isotherms for comparison with the experimental data. The conditions used for the analytical solutions were essentially the same as the experimental. A V-groove on the welded pipe simulates welding of two pipes using a metal inert gas (MIG) welding process as the workpiece rotates in a pipe welding machine.

An analytical approach, developed by Komanduri and Hou, uses Jaegers moving heat source method, is extended to calculate spot temperature data in pipe welding to determine the temperature profiles under various welding conditions. The analytical and experimental temperature isotherms were compared. Some differences in the

temperature distributions produced by the analytical and experimental results were observed. They include the geometry and magnitude of the temperature distributions. An attempt has been made to explain for these differences.

ACKNOWLEDGEMENTS

I would like to thank my family for their constant love, support, inspiration, and guidance; especially my father, Dr. Joseph Higgins, my mother, Mrs. Sunny Higgins, and brothers, Joseph, Brian, Daniel, and Jimmy.

I would like to thank my advisor, Dr. Ranga Komanduri, for his time, guidance, and valuable advice during my graduate career.

I would like to thank Dr. C.E. Price and Dr. R.D. Delahoussaye for serving on my committee and for their valuable guidance during my college career. I want to thank the professors who have instructed and advised me throughout my college career.

I would like to thank Dr. Z.B. Hou for his support and guidance. Special thanks are extended to Dr. Robert Ivester, Dr. Robert Polvani, Eric Whitenton, and the staff of NIST for their extended help and valuable guidance throughout this work.

I would like to thank the MAE and ATRC staff for their guidance especially Mr. Jerry Dale, Mrs. Sharon Green, and the office staff of Engineering North, Room 218.

I would like to thank my research partners Mr. Amol Bhome, Mr. Robert Gerlick, and Mr. Sean Ong, for their help in experimental work. I would like to thank the personal of office 142 throughout my graduate career for their valuable discussions. I would like to thank everyone else involved in my OSU career for their advice and support.

TABLE OF CONTENTS

LIST OF TABLES

LIST OF FIGURES

LIST OF SYMBOLS

ε	Emissivity Value
σ	Stefan-Boltzmann Constant (5.67051×10^{-8} $(W/(m^2K^4))$
ρ	Density (g/cm^2)
τ	Time (s)
a	Thermal Diffusivity (cm^2/s)
A	Area
AISI	American Institute Standard Insturments
ASCII	American Standard Code for Information Interchange
ASM	American Society of Materials
ASTM	American Society of Thermal Mechanics
C	Constant Value
CCD	Charge Coupled Device
DC	Digital Current
DSAW	Double Sided Arc Welding
E_b	Radiant Energy (W)
FCAW	Flash Core Arc Welding
FEA	Finite Element Analysis
FEM	Finite Element Method
FPA	Focal Plane Array
FOV	Field of View or Field of Vision

GMA	Gas Metal Arc
GMAW	Gas Metal Arc Welding
GTAW	Gas Tungsten Arc Welding
H_2S	Hydrogen Sulfide
HAZ	Heat Affected Zone
InSb	Indium Antimonide
INTG_TIME	Integration Time
IR	Infrared
LOF	Lack of Fusion
LOP	Lack of Penetration
MIG	Metal Inert Gas
MWIR	Mid-Wavelength Infrared
NDF	Neutral Density Filter
NDF2	Neutral Density Filter with OD of 2
NDT	Non-Destructive Testing
NIST	National Institute of Standards and Technology
NUC	Non-Uniformity Correction
OD	Optical Density
OSHA	Occupational Safety and Health Association
PC	Personal Computer
q_{pl}	Heat Liberation Rate for a Moving Circular Disc Heat Source (J/s)
Q_{pt}	Heat Liberated by an Instantaneous Point Heat Source (J)
Q_{Rg}	Heat Liberation by a Ring Heat Source (J)

r	X-Y Distance to the Temperature Point from the Instantaneous Heat Source (cm)
R'	Distance from the Edge of the Instantaneous Point Heat Source to the Location of the X-Y Coordinates of the Instantaneous Point Heat Source (cm)
R	Distance Between the Center of the Moving Disc Heat Source and the Point at which the Temperature Rise at a Specified Time is Concerned (cm)
ROIC	Readout Integrated Circuit
SMAW	Shielded Metal Arc Welding
T	Temperature (K)
$T_{background}$	Room Temperature (K)
T_{camera}	Real Temperatures (K)
T_{object}	Workpiece (Object) Temperature (K)
th	Pipe Thickness (mm)
TIG	Tungsten Inert Gas
UNS	Universal Numbering System
USA	United States of America
UV	Ultra-Violet
VBA	Visual BASIC for Application
WM	Weld-Metal

X_1	Distance in the X-Direction from the Center of the Heat Source to the Primary Heat Source (mm)
X_2	Distance in the X-Direction from the Center of the Heat Source to the Image of the Primary Heat Source (mm)
X_3	Distance in the X-Direction from the Center of the Heat Source to the Secondary Heat Source (mm)
X_4	Distance in the X-Direction from the Center of the Heat Source to the Image of the Secondary Heat Source (mm)
Z_1	Distance in the Z-Direction from the Center of the Heat Source to the Primary Heat Source (mm)
Z_2	Distance in the Z-Direction from the Center of the Heat Source to the Image of the Primary Heat Source (mm)
Z_3	Distance in the Z-Direction from the Center of the Heat Source to the Secondary Heat Source (mm)
Z_4	Distance in the Z-Direction from the Center of the Heat Source to the Image of the Primary Heat Source (mm)

CHAPTER 1

INTRODUCTION

1.1 Introduction to Welding

Welding of steels is a metal-joining process used in various manufacturing industries. The United States of America is currently the third largest producer of steel behind China and Japan. [1] Welding is a widely used manufacturing process in multiple production fields, namely, recreational equipment, defense technology, transportation, pipelines, and structural design. The widespread applications of steel piping in corrosive environments can be hindered by metallurgical damage caused by extremely high temperatures generated during welding. Welding is extensively used in industry though with a known failure rate as there are no good alternatives to replace it. Pipe industries utilize carbon steels in millions of miles of non-submerged and submerged pipelines for the transport of multiple media; water, natural gas, oil, sewage, drainage. Overall, welding is a necessary but an unfavorable manufacturing process.

Welding processes are classified into two main categories solid-phase welding and fusion-phase welding. The main difference is the lack of pressure in the solid-phase and dependence on pressure in the fusion-phase. The current investigation utilizes a fusion-state welding process, specifically, metal inert gas (MIG) welding. Effects observed in fusion welding of carbon steel include changes in the material strength, metallurgical phase transformations, transient thermal stresses, and metal splashing. Welding of two pipes requires melting and solidification of a filler wire and two base

metals over a span of time. The filler wire must be of a similar material to prevent corrosion and non-uniformity in the weld. Steel microstructure and material property changes are directly affected by sudden extreme temperature increases, especially in the heat affected zone (HAZ) of the welding process. It is important to consider non-uniformity of the weld in primary and post weld analysis. High carbon steels are used for economical reasons in pipe industries although carbon content increases the chance of corrosion and inclusions when welded. Welding parameters determine the success or premature failure of a weld; specific welding process, material composition, maximum and minimum temperatures, preheating processes, connection method, voltage, current, wire feed speed, standoff distance, weld geometry, weld velocity, thermal conductivity, specific heat, microstructure, cooling rates. Parameters are chosen and monitored in the experimental welds to study specific effects before, during, and after completion of the welding process. Transient thermal conditions can cause defective metallurgical changes in the HAZ region and cracking in the weld-metal (WM) region. The main welding parameters and their effects on weld production include [3]:

- Weld current effects on the temperature penetration in the base metal and the weld bead size
- Voltage effects on the weld bead shape and the temperature of penetration in the base metal
- Travel speed effects on the weld bead size and the temperature penetration in the base metal
- Gas flow rate of the shield gas which controls the porosity
- Wire diameter which controls the size of the weld and the porosity

MIG welding generates the following discontinuities, as described in the 1st volume of the ASM Handbook Online:

- Porosity formed by gas entrapment during solidification
- Inclusions, such as slag, tungsten metal, oxides
- Lack of fusion (LOF) and lack of penetration (LOP)
- Geometric discontinuities, such as poor weld contours, undercut, underfill, overlap, excessive reinforcement, fillet shape, melt-through, misalignment, and distortion
- Shrinkage voids formed during solidification
- Carters or depressions that form at the termination of a weld bead or in the molten weld pool
- Spatter that occurs when metal particles are expelled during welding
- Arc strikes that form from any localized remelted metal, heat affected metal, or change in the surface profile or any part of a weld or base metal resulting from the arc

Porosity, the main discontinuity found in welds, consists of cavities or pores that form in the weld metal. To prevent and control porosity in a weld the following factors are suggested, as given in the 11th and 15th volumes of the ASM Handbook Online:

- Remove scale, rust, paint, grease, oil, and moisture from the pipe surface
- Eliminate moisture from the flux or the shield gas
- Use a short arc length
- Keep the weld molten long enough (use preheating) to allow the gas to escape
- Provide sufficient shield gas

- Improve fit-up
- In steel, remove slag residue, particularly in butt welds
- Use low-hydrogen electrodes when welding steels that are low in carbon and manganese and high in sulfur and phosphorus
- Minimizing formation of hydrogen sulfide (H_2S)
- Decrease surface tension and viscosity of both the liquid weld metal and the molten flux
- Prevent contamination of GMAW filler-metal wire

Teardrop and circular shaped porosity is uniformly distributed throughout a weld, usually concentrated at the root of the weld. Larger forms of porosity increase the probability of weld failure.

Techniques have been developed to prevent weld failure; preheating, post heating, parameter comprehension. Preheating and post heating are suggested to reduce thermal shock in welded workpieces. This decreases the metallurgical changes when welding hardenable and high carbon content steels.

Experimental techniques used to map the temperature distribution in the HAZ of a weld are thermocouples and infrared technology; cameras, sensors, pyrometers. An infrared camera is used in the current investigation to collect thermal images of the temperature distribution at and surrounding the HAZ. Isotherms form by the dispersion of heat into the base metal as the weld is produced. An infrared camera is used to measure the temperature distribution as isotherms form during the welding of two pipes. An analytical solution uses essentially the same parameters of the experimental process to calculate the temperature isotherms and compare the results.

Infrared cameras were developed based on the discovery of infrared radiation by Fredrik William Herschel in 1800. The infrared spectrum gives radiation wave lengths which fall into three separate categories;

1. Subatomic particles, such as electrons, whose energy shift levels supply most of the radiation in the near infrared region,
2. Atomic particles whose movements produce intermediate (Mid) infrared Region, and
3. Molecules whose vibrations and rotations generate radiation in the far infrared region.

Each of the above infrared radiation spectrum descriptions are labeled as near infrared radiation (0.7 - 1.5 μm), middle infrared radiation (3 - 5.5 μm), and thermal infrared radiation (5.5 - 10^3 μm), respectively. The levels of infrared radiation are given by the electromagnetic radiation wave lengths and identified on regions, as shown in Figure 1.1. γ-rays, X-rays, ultra-violet, and visible light have been labeled by their respective wave length regions preceding the infrared spectrum, all consisting of smaller wave lengths. Microwaves and radiowaves fall after the infrared spectrum, consisting of larger wave lengths than infrared wave lengths, i.e. > 10^3 μm.

Infrared cameras utilize the infrared wave length regions when recording images of objects viewed. Prior to the discovery of infrared data collecting techniques, thermal experimental data relied on thermal modeling and various experimental procedures, such as (1) thermocouples, (2) thermal paints, and (3) metallographic techniques. High temperatures involved in welding limited prior techniques to thermocouples and

metallographic techniques, such as low temperature thermal paints which are ineffective for most HAZ temperatures.

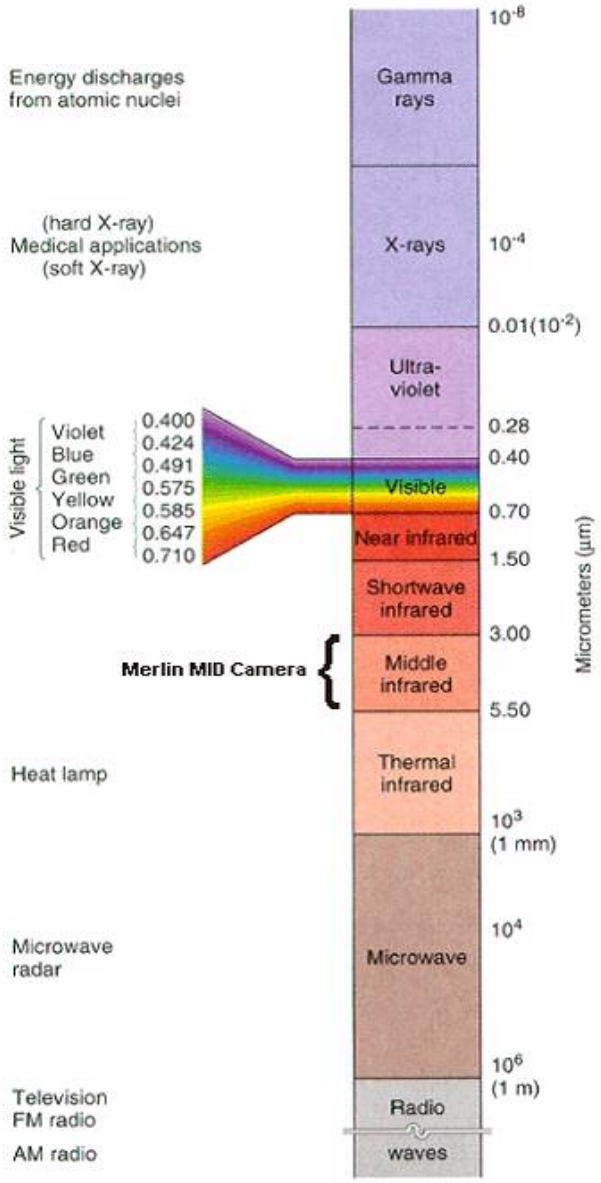

Figure 1.1: Electromagnet radiation wave lengths and regions [22]

Radiation energy is emitted by any body at any temperature varies continuously over the wavelength range. Stefan (1879) and Boltzmann (1884) showed that a blackbody surface emits radiant energy at a rate proportional to the fourth power of the absolute

temperature of the surface, given by Eqn. 1.1. Planck (1901) introduced a blackbody spectral distribution explanation with the development of quantum theory. A blackbody is a perfect emitter and a perfect absorber of radiant energy; no radiation is reflected because all radiation is absorbed. To define the emissivity of a non-blackbody, the ability of a surface to emit and absorb radiant energy, requires the comparison of the non-blackbody to a blackbody at identical temperatures and environmental conditions. A blackbody is the reference against which all radiating surfaces can be compared for accurate calculation and identification of results. A blackbody is characterized by the following:

1. It has unit emissivity and absorbs all incident radiation, regardless of wavelength and direction
2. For a given wavelength and temperature no surface can emit more energy than a blackbody
3. Radiation emitted by a blackbody is a function of wavelength and temperature; it is independent of direction

Radiant energy, E_b (W) of a blackbody surface is calculated using Eqn. 1.1 involving an area, A (m^2), the absolute temperature of the surface, T (K), and the Stefan-Boltzmann constant, σ (5.67051 x 10-8 W/m^2K^4).

$$E_b = \sigma A T^4 \qquad 1.1$$

Real surfaces are not perfect radiation emitters or absorbers. Eqn. 1.2 is used to find the radiant energy of a non-blackbody. To account for a body that is not a perfect

$$E = \varepsilon E_b = \varepsilon \sigma A T^4 \qquad 1.2$$

emitter or a perfect absorber a dimensionless parameter called the emissivity value, ε is multiplied by the blackbody radiating energy for exactly the same conditions. The emissivity value of a non-blackbody surface is a pre-determined value found by comparing surface emission and absorption of the non-blackbody to that of a blackbody. It must be a value between 0 and 1. Studies have shown that emissivity values vary with temperature and the characteristics of the selected surfaces, namely, roughness, texture, color, degree of oxidation, wavelength, and presence of coatings [32].

The present experimental procedure involves measurement of temperature distributions during welding using emitted and absorbed infrared radiation of pipe surfaces. Temperatures recorded by the infrared camera are different from the actual temperatures because of required emissivity and calibration corrections. The relationship between the emissivity of the viewed object, ε_{object}, ambient temperature (room temperature), $T_{background}$ (K), real temperature, T_{object} (K), and recorded temperature, T_{camera} (K), is given by Eqn. 1.3.

$$T_{camera} = \varepsilon_{object}.T_{object} + (1-\varepsilon_{object}).T_{background} \qquad 1.3$$

The temperature recorded by the infrared camera is assumed to be higher than the actual object temperatures because of data collected during calibration. To prevent incorrect temperature data it is necessary to recalculate recorded temperatures using Eqn. 1.4 to calculate the actual temperatures of the pipe surface.

$$T_{object} = \frac{T_{camera} - (1-\varepsilon_{object}).T_{background}}{\varepsilon_{object}} \qquad 1.4$$

In the present investigation, recorded temperatures are corrected with a VBA code using Eqn. 1.4. After recalculation, the data is then plotted using TecPlot software for visual

comparison to analytically calculated and plotted images. In the present investigation, the pipe is painted with a high heat, black paint with a known emissivity value of 0.95. Therefore an emissivity value of 0.95 is assumed within VBA calculations.

1.2 Thesis Overview

In this investigation, the temperature distribution of a fusion welding process (MIG welding) joining two ASTM A500 Grade B steel pipes is monitored using an infrared camera to collect thermal images. An analytical method calculates the temperature isotherms for essentially the same parameters as the experimental work. Analytical and experimental results are compared. Chapter 1 is an introduction of the MIG welding process, a summary of welding problems, procedures developed to reduce thermal shock induced failure, the benefits of post-weld and pre-weld micro-structural analysis, and a brief introduction of radiation and emissivity.

Chapter 2 is a literature review of the experimental, analytical, and simulated thermal weld analyses. The literature review covers work published from 1986 through 2005. Mackerle [5] covers non-destructive testing methods, including infrared techniques, for manufacturing processes of 1976 through 1997. Lin *et al.* [7], Khan *et al.* [8], Belanger and Patchett [9], and Wikle *et al.* [10] investigate welding of in-service workpieces. They commonly investigate the temperature distributions using infrared technology; sensors, cameras, pyrometers. Wilke *et al.* [10] compared temperature distributions of welds in different liquid media, recorded with infrared sensors, to finite element method (FEM) to simulate temperature distributions. Parameters investigated in the literature review address the effects of welding on material hardness, temperature distribution geometry, and microstructural changes. Prior to the use of infrared camera

techniques, thermocouples were used to model temperature distributions of welding. Infrared camera techniques collect surface temperature data whereas thermocouples are used to record surface and depth temperature data. Infrared thermal imaging techniques are still being developed. Emphasis has been placed on simulated methods because of the absence of wasted material, health concerns, and advancement of computer technology. A comparison of experimental results is required to assure the accuracy of the simulated results. Current simulation programs include finite difference methods and finite element analysis (FEA).

Chapter 3 lists experimental objectives in the problem statement.

Chapter 4 describes the equipment used in the experimental work. Important equipment information includes technical information for the Merlin^{TM} Mid infrared camera, Lincoln Electric MIG/Flux-Cored welder, and pipe welding machine. Chapter 4 also lists detailed steps used in the experimental procedure.

An analytical solution is provided in Chapter 5 based on the work reported by Komanduri and Hou [20]. The analytical solution was provided in the form of a Visual BASIC for Applications (VBA) code to calculate the temperatures at specific points, spot temperatures throughout the pipe surface area. Spot temperatures are calculated relative to the heat source location during welding. A thermal image is produced with multiple spot temperatures of a specified area in TecPlot software, Version 9.2.

Analytical and experimental results, temperature isotherm distributions, are compared in Chapter 6 Results and Discussion. Concluding remarks and future recommendations that would extend the current investigation are listed in Chapter 7.

CHAPTER 2

LITERATURE REVIEW

2.1 Infrared Technology

MIG welding is one of over forty types of welding processes used in the manufacturing industry in the United States of America (USA). [3] Welding is an economical process that produces a strong bonding between two identical materials, especially carbon steels.

The elements of a welding process can be classified into four categories - welding materials, heat sources, performance, and evaluation of weld reliability or weld life. Multiple parameters of the welding process, namely, the heat input parameters, number of welding passes, material properties, welding torch parameters, influence the quality of the weld. Welding can unintentionally aid in developing corrosive conditions leading to fatigue, creep, stress corrosion cracking, and fracture [4]. Many experimental investigations have focused on specific parameters, namely, microstructure, temperature distribution, corrosion, effects on material properties, stress and strain behavior, cooling rates, and final weld material properties with the objective of a better understanding of the welding process through set parameters and experimental results. This review presents experimental, analytical, and/or simulated techniques presented in the literature. Few reports of a comparison between experimental and analytical or simulated

temperature distributions in welded materials. A better understanding of the welding process improves the efficiency of the welds and reliability of the weld life.

Infrared camera technology introduces the ability to view and record surface temperature distributions during the production of welds. It is a non-destructive alternative method that can contribute towards a better understanding of thermal aspects of various manufacturing processes. Continuous advancements in infrared camera technology are being made in the cooling mechanisms, resolution, accuracy, and size. Mackerle [5] reviewed the development of non-destructive testing (NDT) methods and how the methods are integrated into experimentation between the years 1976 through 1997. These methods are listed in the following order:

- Electrical, magnetic, and electromagnetic methods,
- Sonic methods,
- Mechanical methods,
- Optical methods,
- Condition monitoring, and
- Other methods.

Infrared camera sensing techniques are included in Mackerle's [5] list of NDT methods under the title, other methods. Figure 2.1 is the convection-diffusion equation prediction showing an ideal visual representation of isothermal temperature distributions developed from temperature data collected by an infrared camera. Calibration of infrared cameras is required to assure no drift and the ability to record different temperatures (signal recognition) occurring in the welding process. Correctional equations are used whenever drift in the recorded thermal images is observed.

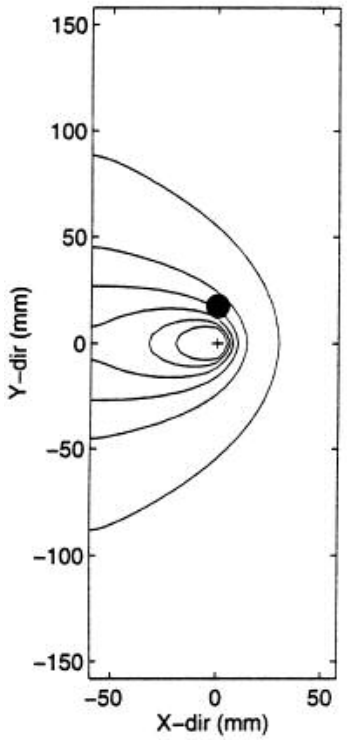

Figure 2.1: Convection-diffusion equation prediction showing a projection of the field of view of the IR sensor onto a contour plot of a solution [5]

Another NDT method used to simulate isothermal temperature distribution during the production of a weld as listed by Mackerle [5] is the finite element method (FEM). FEM is used to simulate welds based on mesh analysis and does not directly record or measure temperatures as in an experimental manner. Experimental data collection and verification are necessary to justify the assumptions and results of FEM weld simulations.

2.2 In-Service Weld Examples

Infrared camera imaging is used to view the temperature distribution during a weld under different conditions to enable an understanding of the process as it would be applied to in-service components. In-service infrared technology monitors welding temperature distribution to predict weld quality and failure. Monitoring of in-service weld repairs or welding production processes can be incorporated into the manufacturing

cycle, such as in assembly lines to monitor weld quality during production. Lin *et al.* [7] uses infrared sensors to monitor welds produced by an automatic robotic welding machine in an assembly process. Important conclusions that relate to the present study, taken from the Lin *et al.* [7] experiments are, (1) infrared thermography can accurately monitor temperature plate distributions in aluminum, steel, and stainless steel plates during the welding process, (2) infrared sensing systems are capable of detecting arc misalignment, plate mismatch, surface contamination, and geometric defects, such as plate gap and plate offset in a wide variety of materials, (3) thermal distributions seen in the welding of aluminum and stainless steel are very similar to those measured in steel and only the magnitude of the thermal distributions are different due to thermal conductivity and melting point differences, (4) infrared sensors are applicable for monitoring AC/DC gas tungsten arc welding and gas-metal arc welding operations, and (5) an intelligent real-time video interface can be used to transfer information from the infrared camera to the computer at a speed consistent with the on-line control.

Khan *et al.* [8] used an infrared camera to detect defect formation during an arc welding process. The objectives of Khan *et al.* [8] experiments include (1) determining the sensitivity of the thermal field and infrared detector to geometric variations, arc position, contaminants, penetration depth, and weld parameters, and (2) determining the time required to identify changes in the weld status. The monitoring of the temperature distributions with an infrared camera is proceeded by an investigation of the macrostructure of the cooled weld. The macrostructure analysis enabled examination of the quality of the weld. They concluded that an infrared camera can be used to detect welding defects as the weld is produced in an assembly process.

Belanger and Patchett [9] used an infrared pyrometer to monitor surface temperatures during in-service welding of two pressure pipes to determine the residual stresses produced. Figure 2.2 shows their experimental setup. It shows the position of the optical infrared pyrometer in reference to the welding torch and other experimental equipment; GTAW torch, coupon/head assembly, chart recorder, pressure gauge, regulator, outlet, inlet. They found that water, as the working fluid, produced no boiling transition even at high temperatures and the cooling rate could not be controlled using pressure variations. Alternative surrounding media were used to focus on property changes involved in the working fluid. They demonstrated that infrared sensor systems are useful in multiple media. Calibration of the temperature sensors in each medium is required before experimentation in that medium to assure accuracy of the viewed temperature distribution.

Wikle *et al.* [10] considered production of welds in corrosive environments during an experimental investigation of submerged arc welding. Tests showed that perturbations affected the collected temperature distribution data in an arc welding process with fixed parameters. An example of different FEM predictions of temperature distributions are shown in Figure 2.3 to demonstrate welding of separated and fitted plates. An infrared sensor showed constant temperature penetration depth control in submerged arc welded plates with and without gaps in their fittings.

2.3 Experimental Welding Preparation

Pipe welding is an important field for research to avoid premature failures in welded pipes at the weld seams during transportation of various media, many harmful

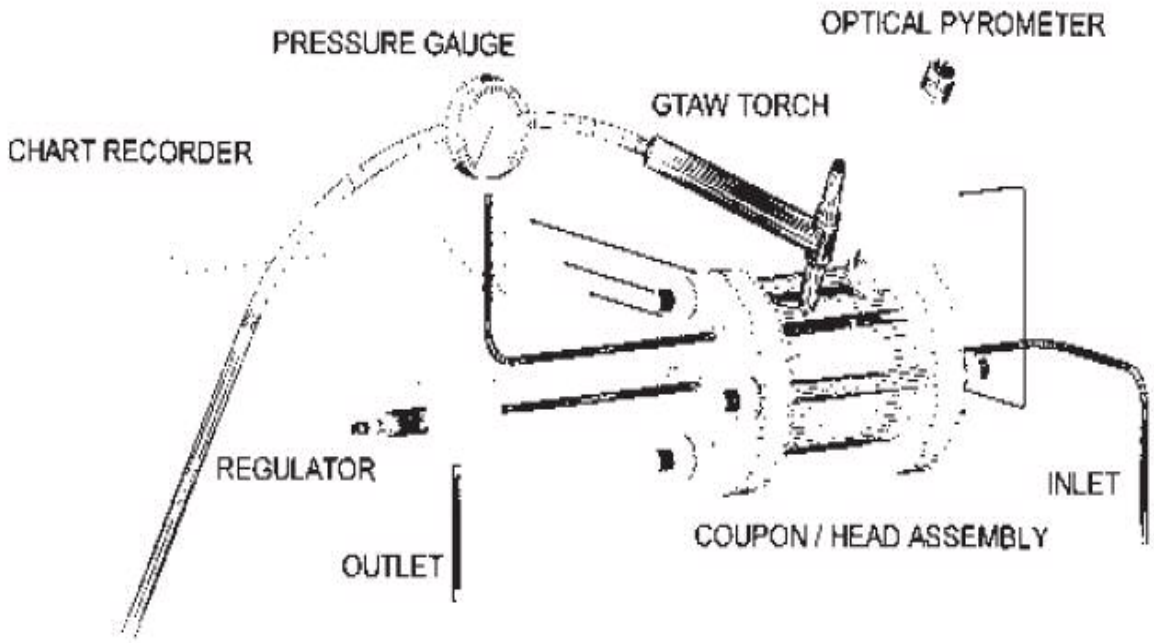

Figure 2.2: Experimental pressurized pipe test assembly showing position of the chart recorder, pressure gauge, GTAW torch, optical pyrometer, inlet, coupon/head assembly, outlet, and regulator [9]

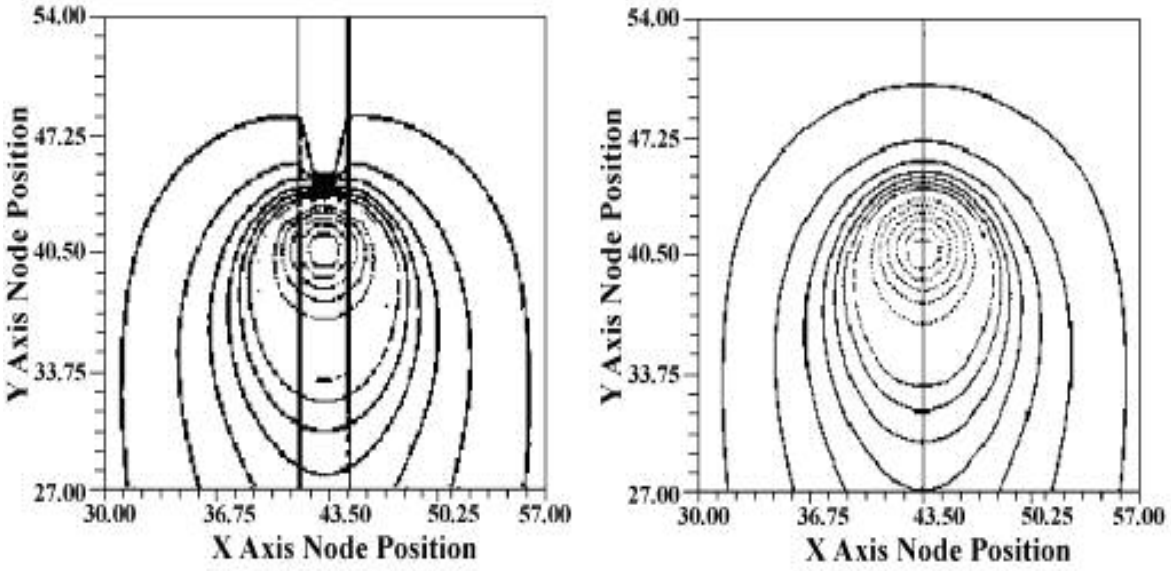

Figure 2.3: (right) Predicted temperature distribution of two plates without a separating gap in the plate fittings and (left) two plates with a 3 mm separating gap between the plate fittings [10]

to the environment. Experimental work is carried out in manufacturing industries under controlled conditions to provide thermal data in the hope of better understanding of the welding process. Figures 2.4 and 2.5 show two pipes welded using a single and a double-sided V-groove (showing dimensions) connection, respectively. Figure 2.4 (a) shows a single V-groove formed to weld two pipes from experiments carried out by Shehata [3]. He focused on recording hardness distribution across a multiple pass weld. Figure 2.4 (c) shows the completed multi-layered weld. A direct relation between the hardness, input heat, and cooling rate of the weld was investigated. To collect hardness data in the horizontal and vertical directions across the weld HAZ, the Charpy V-notch test was used. Figure 2.4 (b) shows details of the method reported for the collection of hardness data. The current experiment monitors the thermal effects produced by a single V-groove weld; although to completely fill the V-groove multiple weld passes are required, as shown in Figure 2.4 (c).

Olabi and Hashmi [11] focused on the weld post-heat treatment, hardness, and microstructural changes throughout the weld metal and base metal. They investigated the relation of each parameter to the temperature distribution during welding. Experimental data was collected for the welding of two flat rectangular pieces of steel using a double sided V-groove geometry. Dimensions of the double sided V-groove are shown in Figure 2.5. Olabi and Hashmi [11] investigated microstructural transitions involving ferrite and pearlite in the base metal to martensite and bainite after welded. For analysis of the steel microstructure they used transverse sections of the welded components by first mounting the sample in Bakelite, polishing, etching, and viewing the sample under a microscope. The transverse sections are observed with an optical microscope to view the

microstructure of the HAZ and the microstructure of the original base metal for comparison.

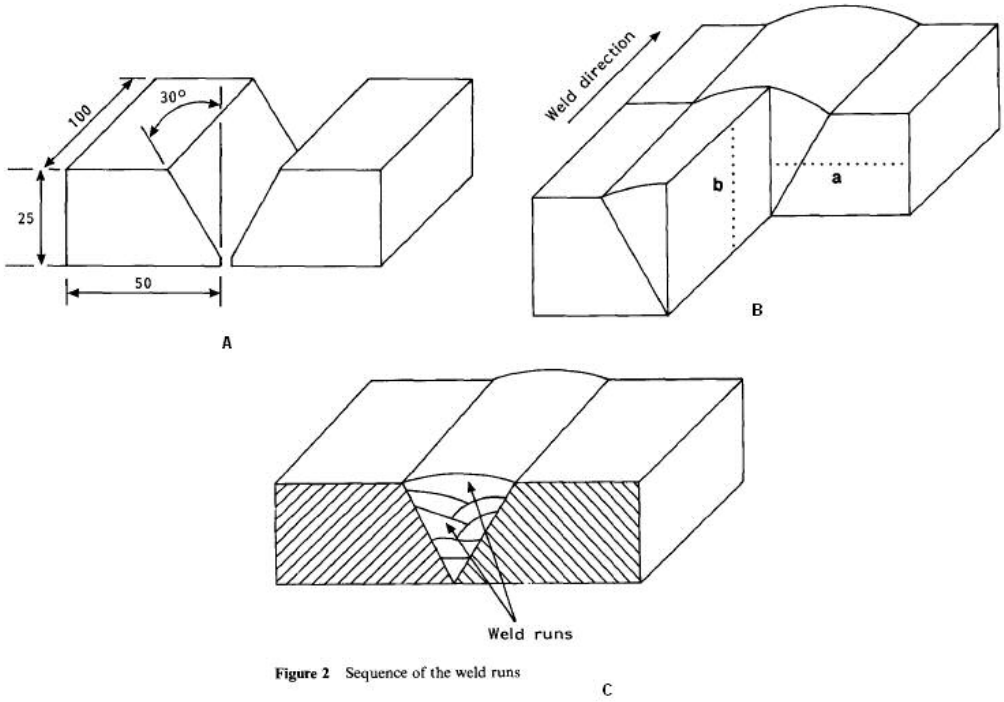

Figure 2 Sequence of the weld runs

Figure 2.4: Connections used in welded pipe joints a) V-groove geometry b) cross-sectional hardness data point locations in the vertical (b) and horizontal directions (a) c) multiple weld passes as created to fill the V-groove connection [3]

Both Olabi and Hashmi [11] and Shehata [3] monitored the power input during experimentation and concluded that power has a direct effect on the microstructual changes, HAZ and surrounding effected area, which occur in welded steel joints. The higher the power output the greater is the heat penetration and larger is the thermally altered area. Olabi and Hashmi [11] monitored the heat input rate as it changed and Shehata [3] monitored the voltage by maintaining a consistent 80 V as the control power parameter. Multiple options to prevent corrosion of pipe welds have been discussed and used in the experiments. One such method is the aluminum enrichment of carbon steels to prevent oxidation after welding is complete.

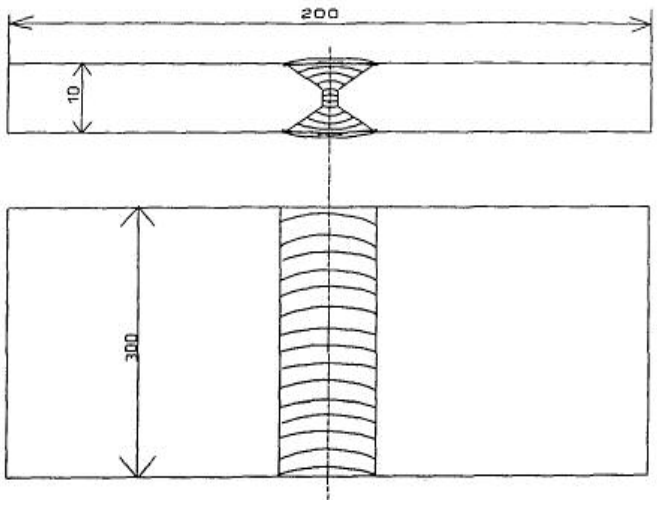

Figure 2.5: Schematic of the double sided V-groove workpiece with the predicted weld [11]

Bhambri *et al.* [1] conducted an experimental study to improve oxidation resistance of the workpiece surface after welded. They focused on the effects of varying the welding filler wire feed rate and power consumption. An aluminum electrode was added during the welding process and is fed at the same time as the welding filler wire. Figure 2.6 shows effects during the addition of aluminum to the carbon steel weld and the effect of power input during the welding process. Regardless of the type of the workpiece material (metal) used, the power input has a direct effect on the melt pool and HAZ size. Burn-through is complete melting of any connecting material with a gap in which molten material passes through. It occurs instead of the joining of two base materials when an excess amount of power is used to produce the weld. Figure 2.7 shows multiple welding passes required to fill larger dimensioned connecting geometries, V-groove pads of 6, 8, and 12 mm widths and the number of welding passes to fill each. The weld pad V-groove width is measured at the widest part of the V-groove. In Figure 2.7, the width is measured as the distance between the two top surfaces. The root weld or first welding pass provides the initial thermal shock and penetration to the base material,

determining that sufficient fusion has or has not occurred. During a weld pass, the temperature is highest at the contact point where the filler wire contacts the workpiece. Many simulations and analytical solutions produce models consisting of temperatures

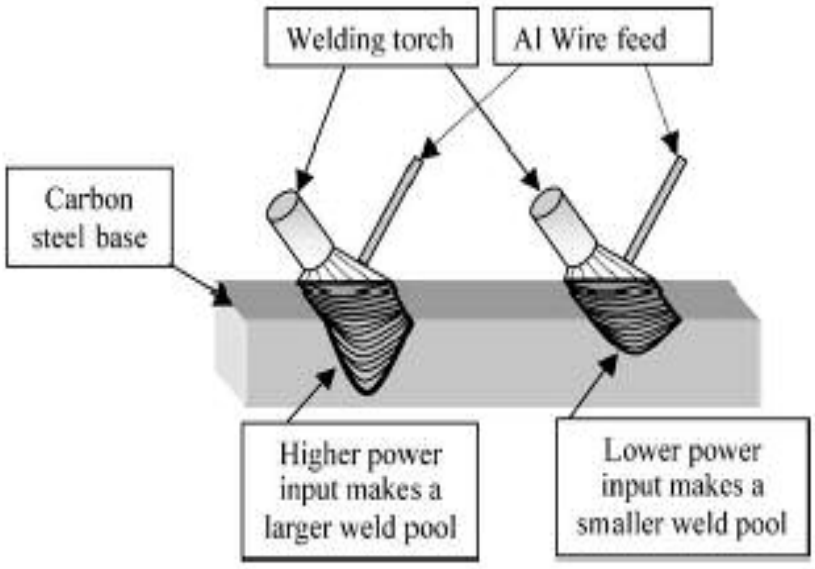

Figure 2.6: Effect of power input on the size of the steel weld pool [1]

distributions that disperse heat in a symmetrical manner, on the axis of the weld motion relative to the contact point. The symmetrical temperature distributions of simulations do not match with the current experimental results. Simulations predict temperature distributions to the side of the weld and behind the weld to be spaced further apart than the isothermal temperatures located in front of the weld.

Mohandas *et al.* [13] investigated the composition of the steel and the softening of the HAZ based on the post-weld heat treatment in shielded metal arc welding (SMAW), gas tungsten arc welding (GTAW), and gas metal arc welding (GMAW). The experimental process involved the use of high-strength, low-alloy steel but an equivalent comparison is made to a carbon steel, as shown in Table 2.1. After a weld is completed a post-weld heat treatment exposes the weld coupon to a temperature of ~ 900°C for 30

minutes and then the weld coupon is quenched in oil. Figure 2.8 shows the welding coupons used for data collection in the experimental work reported by Mohandas *et al.* [13].

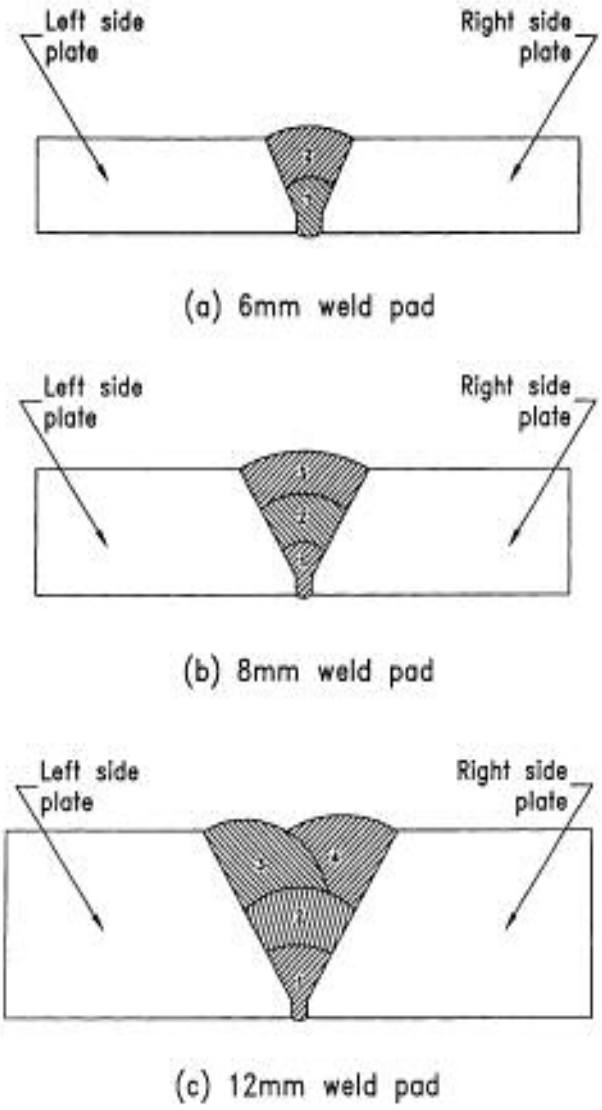

Figure 2.7: Multiple welding passes in weld sequences involving 6, 8, and 12 mm weld pad V-grooves [12]

Table 2.1: Carbon steel compositional equivalent of the high-strength low-alloy steel weld coupon material used in experiments [13]

Steel	C.E.(IIW) Ref. [4] $= C + \frac{Mn}{6} + \frac{Cu+Ni}{15} + \frac{CR+Mo+V}{5}$	C.E.(Graville) Ref. [5] $= C + \frac{Mn}{16} - \frac{Ni}{50} + \frac{CR}{23} + \frac{Mo}{7} + \frac{Nb}{8} + \frac{V}{9}$
P	1.1333	0.5051
S	0.8799	0.4369
J	0.7008	0.457

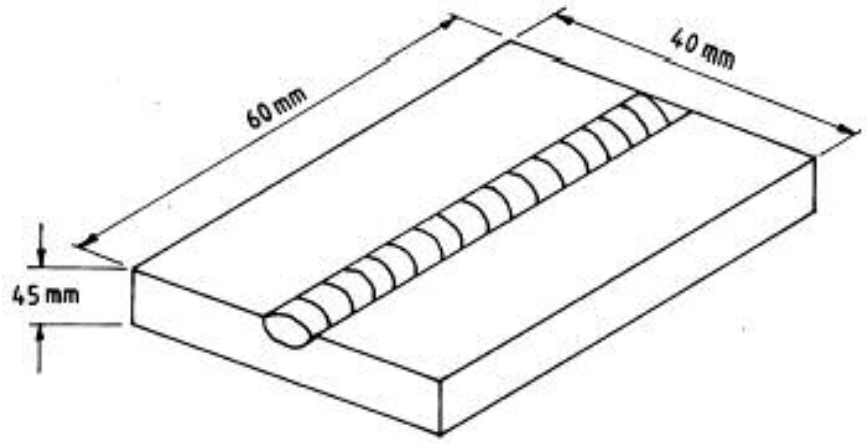

Figure 2.8: Dimensioned schematic of a high-strength, low-alloy steel weld coupon used in experiments [13]

The specific welding parameters considered are the material hardness of the thermally altered regions, fusion zone, and HAZ according to preset distances relative to the contact point of the filler wire and workpiece. Mohandas *et al.* [13] showed the distance relationships in which the thermal alteration affects the base metal hardness. Figure 2.9 shows a schematic of the cross-section of a weld coupon marking the locations where

hardness readings were recorded perpendicular to the axis the weld. External cooling was found to minimize HAZ softening. The specified post-weld heat treatment eliminated the soft zone formed during welding. The softening zone was found to be dependent of the composition of the steel.

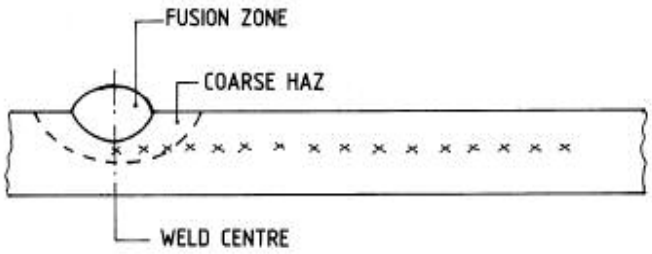

Figure 2.9: Schematic of the hardness readings across the fusion zone of the weld coupon cross section, HAZ and base metal [13]

2.4 Experimental Techniques

In-service welding, in many circumstances, requires welding under unconventional welding conditions. Infrared camera techniques were not the first method of recording temperature data in the welding of pipes. Other methods include infrared pyrometers and thermocouples.

Extremely high temperature gradients generated in a weld limits the thermocouple temperature data collection ability. To measure the peak temperatures at locations in the base metal Murugan *et al.* [12] located thermocouples that on either side of the weld. Figure 2.10 shows the positioning of the thermocouples. Thermocouple temperature data collection in a welded workpiece over a specified area requires thermocouples to be distributed in the depth at or near the surface of the workpiece. Placement of thermocouples requires drilling into the workpiece and placing them in the holes before the workpiece is welded. Thermocouple temperature data collection is limited by

unmeasured material temperatures between thermocouples. Calculations involving temperatures collected are used to fill in the temperature gaps for the material inbetween the thermocouples. Drilling holes for thermocouple placement in the workpiece does not accurately represent welding conditions because removed material produces air pockets in the material.

Experimental temperature collection in the HAZ can be extended to determine the residual stresses and strain distributions in a weld. They can be compared with the thermal data to determine the weld life and physical limitations of the weld. Recorded peak temperatures and their positions relative to the centerline of the weld, reported by Murugan *et al.* [12], are given in Table 2.2 with the corresponding welding pass number and specified weld pad. Maximum temperatures were recorded by thermocouples in the temperature range of 698°C to 837°C in a 6 mm weld pad during the second weld pass. The maximum peak temperature recorded in a carbon steel weld was 950°C for the 6 mm welding pad. Thermocouples have a limited temperature range when collecting experimental temperature data because of their material properties as compared with the properties of the workpiece material. Figure 2.11 shows residual stresses in 6, 8, and 12 mm weld pads in stainless steels and carbon steels relative to the peak temperatures associated with the location of a specified point. They reported that the peak temperatures involved in carbon steel welding in weld pads to be consistently lower when compared to the temperatures obtained in the current investigation. Lower temperatures can be attributed to the unfavorable thermal properties of the workpiece material in the case of stainless steel. Residual stresses were higher in the carbon steel than in stainless steels using similar welding conditions. Infrared cameras record temperature

distributions on the surface of the workpiece during the welding process. Bicknell *et al.* [14] used an infrared sensor to determine the size of the weld bead and

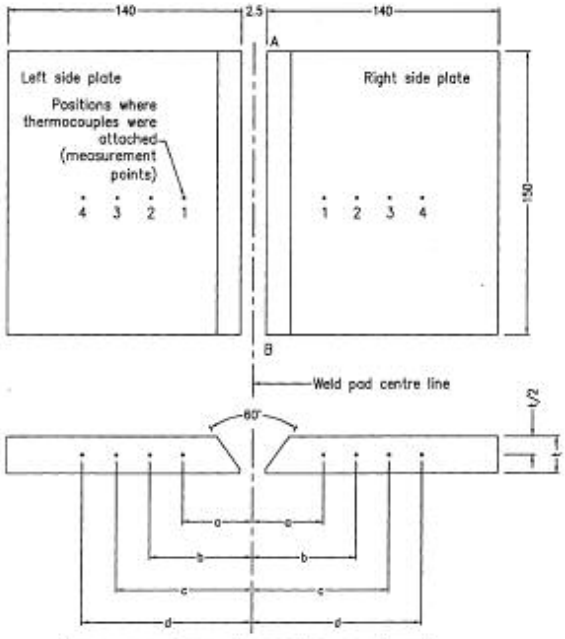

Thickness of plate 't'	a	b	c	d
6	11.5	16.5	21.5	26.5
8	11.5	16.5	21.5	26.5
12	13.5	18.5	23.5	28.5

All dimensions are in mm

Figure 2.10: Thermocouple distribution in the base metal during single and multi-pass welds during experiments [12]

Table 2.2: Thermocouple recorded welding temperatures during deposition of weld beads in low carbon steel weld pools [12]

Plate thickness (nominal) (mm)	Pass number	Measurement point											
		Left side plate				Right side plate				Average value			
		1	2	3	4	1	2	3	4	1	2	3	4
6 (first pad)	1	494	381	324	266	523	410	340	285	509	396	332	276
	2	763	566	466	419	698	513	419	380	731	540	443	400
8	1	532	400	362	295	551	419	352	305	542	410	357	300
	2	598	466	410	350	616	466	370	324	607	466	390	337
	3	635	498	410	339	584	470	390	333	610	484	400	336
12	1	324	240	200	175	314	246	210	190	319	243	205	183
	2	333	260	210	186	303	244	211	200	318	255	211	193
	3	491	381	310	256	299	248	210	192	–	–	–	–
	4	385	330	279	234	481	381	305	276	–	–	–	–
6 (second pad)	1	532	400	333	280	536	402	324	265	534	401	329	273
	2	837	569	494	460	698	524	428	390	768	547	461	425

temperature difference between the HAZ and weld pool. This study provided three identified control loops for welding, namely, (1) control of the weld torch position and altitude over the weld seam, (2) control of weld bead dimensions, and (3) a posteriori quality assurance control performed online. Emphasis is placed on the importance of viewing a properly penetrated weld without the use of an external light source.

Figure 2.12 shows various stages for weld penetration modeled by Bicknell *et al.* [14]; (a) unpenetrated, (b) penetrated, (c) overpenetrated, and (d) burn through. The infrared camera technology is used to improve collection of thermal data in a specified area, namely, the weld pool of the weld region. Thermal data is collected with an infrared camera, redefined for use in a computer with filters, and then stored for viewing on a computer. Figure 2.13 shows the location of various components of the experimental apparatus, and parameters used by Bicknell *et al.* [14]. The camera used was an Electrophysics 7292 Vidicon connected to an IBM PC AT computer with an Intel 80286 microprocessor. Computer software monitored thermal penetration with an image analysis code, stepper motor interface code, welding power supply interface code, and file handling utilities. Stainless steel workpieces were welded using a pulsed tungsten inert gas (TIG) welding process. Figures 2.14 (a) and (b) show the thermal data collected by the infrared camera and data filtered for further use, respectively. They concluded that the use of thermal imaging and image processing techniques enables measurements of the weld bead size for both continuous and pulsed TIG welding. Infrared technology enables the determination of the temperature distribution in the weld pool and near the melt zone during laser welding.

Multiple simulations are available for the weld-pool and surrounding melt zone but few experimental procedures have addressed the high temperatures of laser welding. Lhospitalier [15] used a calibrated camera sensor and image processing equipment with tungsten-based (W5 type) thermocouples for measurement of temperatures between 1000°C and 1800°C because of the laser welded base material, UNS N08904, whose melting point is 1380°C. Figure 2.15 shows the thermocouple locations at various depths in the material used by Lhospitalier [15]. Temperatures recorded were plotted to show the temperature evolution over a 31 s time period. Thermocouple separations are based on distances measured from the center of the weld, as shown in Figure 2.15. Figure 2.16 shows images of the thermal distribution recorded with a CCD infrared camera and converted into a thermal map. The thermal maps were compared with the recorded thermal images from the thermal camera, as shown in Figure 2.17. The thermal map is then compared to the finished weld geometry, as shown in Figure 2.18. A prediction of

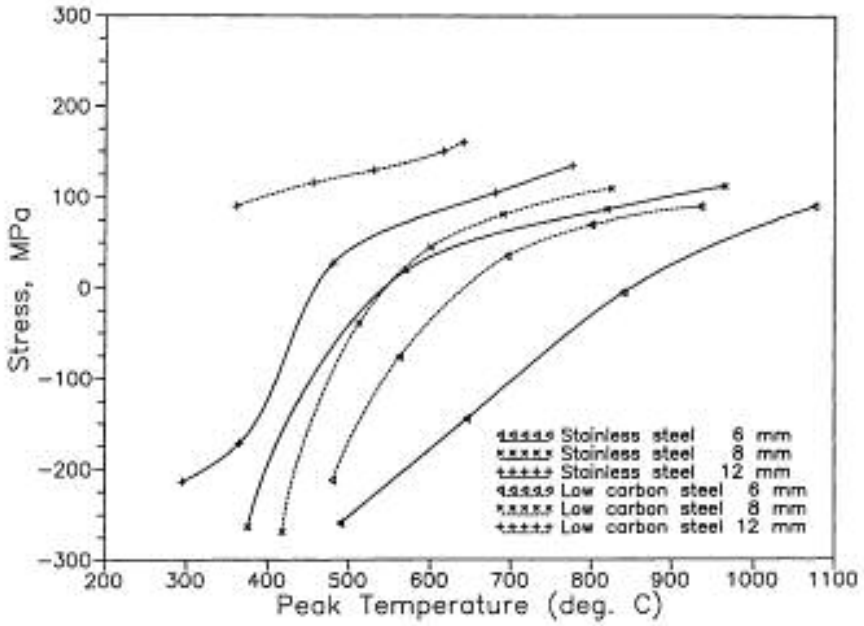

Figure 2.11: Residual stresses versus peak temperatures for 6, 8, and 12 mm weld pads of stainless steel and carbon steel [12]

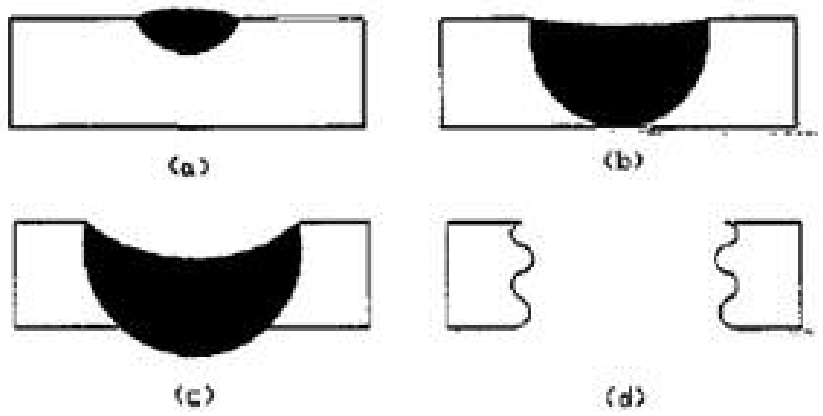

Figure 2.12: Weld depth penetration as modeled (a) unpenetrated (b) penetrated (c) overpenetrated (d) burn-through [14]

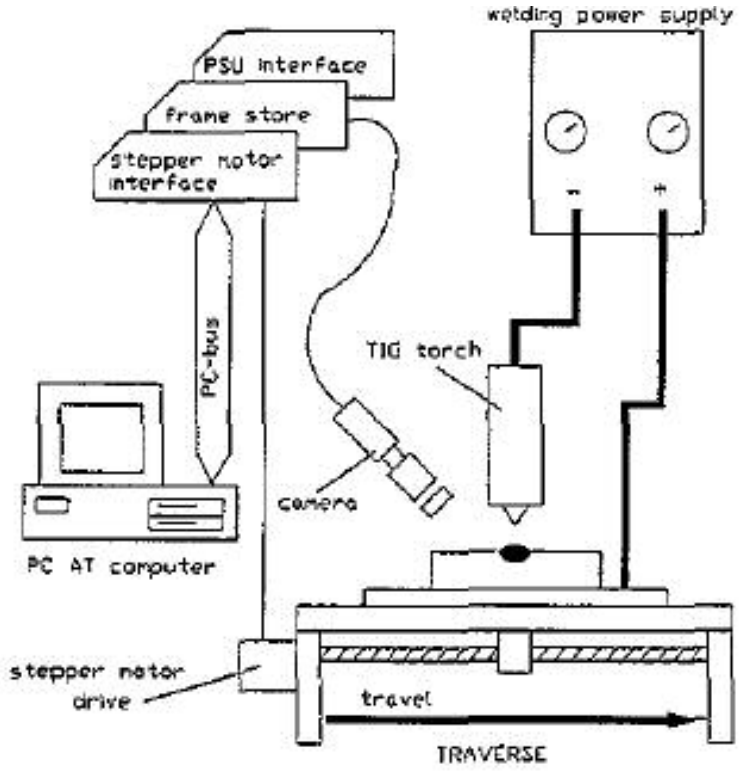

Figure 2.13: Front face vision system including an Electrophysics 7292 Vidicon type connected to an IBM PC AT computer with an Intel 80286 microprocessor [14]

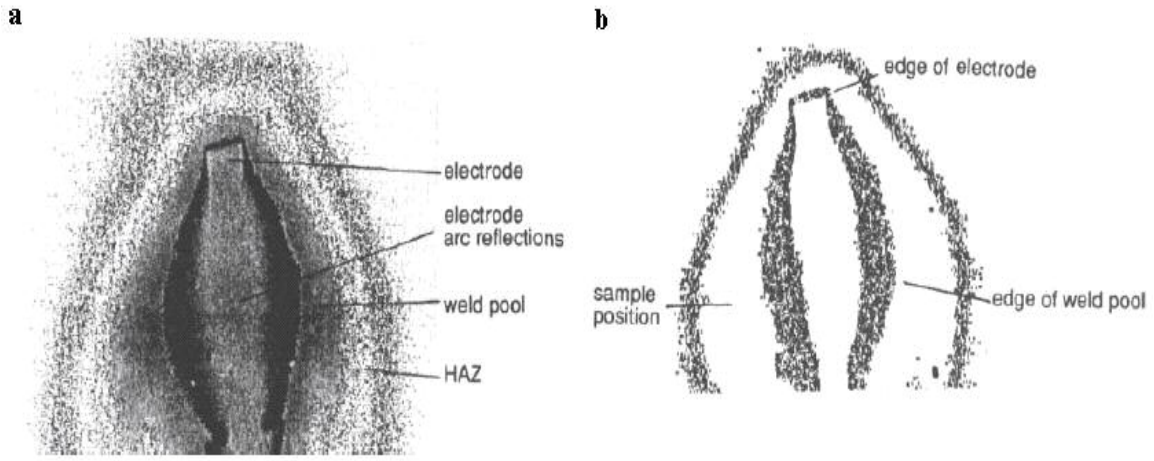

Figure 2.14: (a) Front face image of a pulsed TIG weld on 3 mm stainless steel from an infrared camera (b) Filtered and threshold image of a 3 mm pulsed TIG weld [14]

10 % final experimental error for the recorded data is assumed in the experimental research. The infrared sensors differ from those used in previous experiments because the surrounding temperatures were incorporated as welding temperatures. Maximum temperatures viewed were recorded to be > 1700°C and were not recorded by the infrared camera because of saturation of the image, as in the current experiment. It was recommended that similar experiments be conducted for other welding techniques.

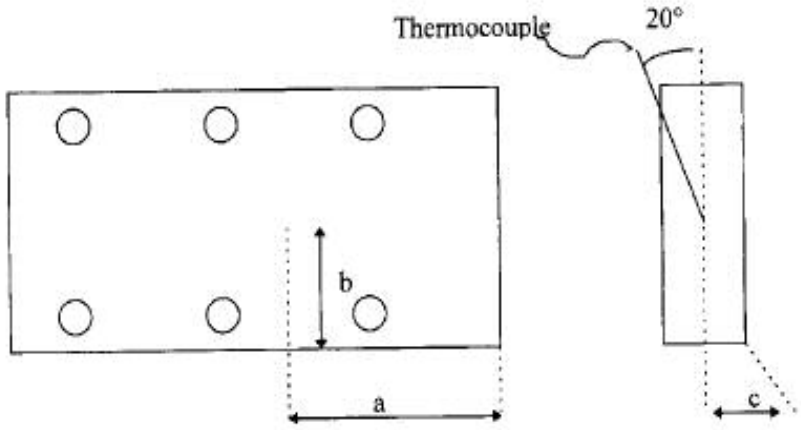

Figure 2.15: Thermocouple locations in the workpiece (a) = 85 mm with a deviation of 1 mm (b) = 40, 39, 38, 37 mm with a deviation of 0.1 mm (c) = 4 mm with a deviation of 0.1 mm [15]

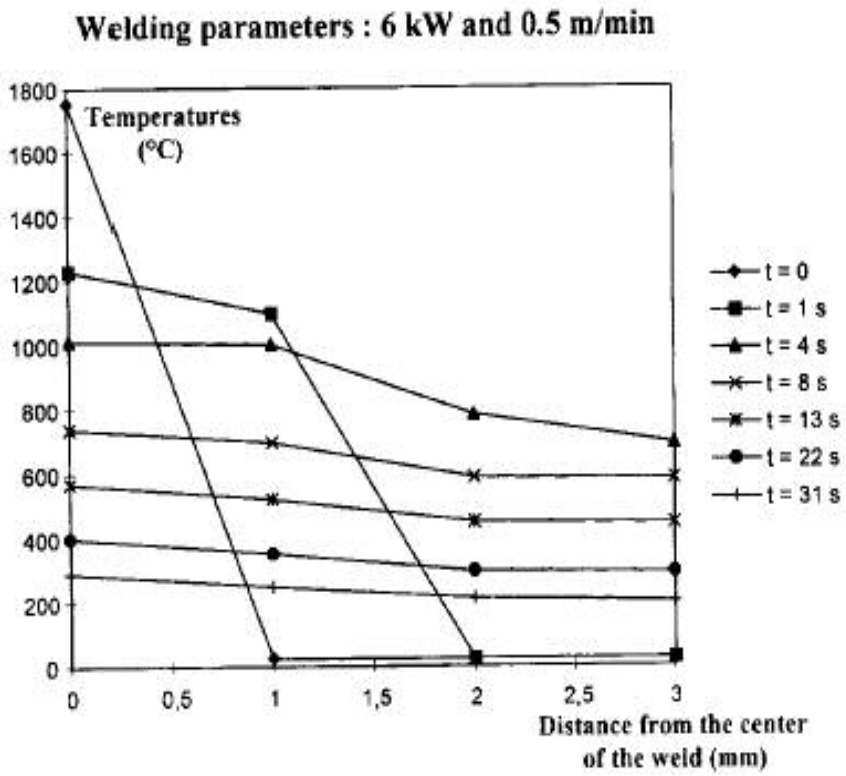

Figure 2.16: Temperature measurements were made with thermocouples to show the thermal gradient evolution versus time for samples [15]

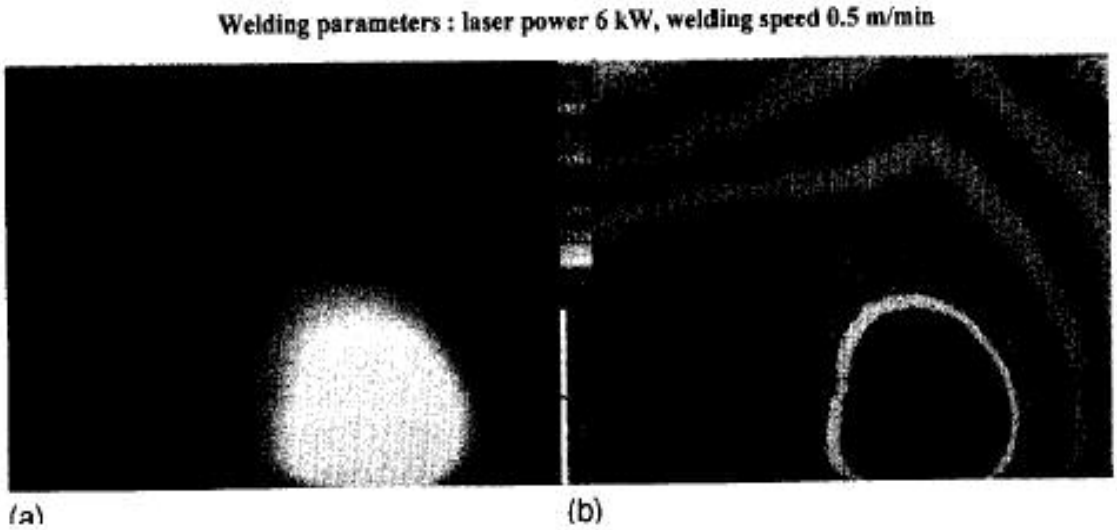

Figure 2.17: Comparison between a recorded laser weld image and its conversion into a thermal map (a) gray levels image (b) thermal conversion [15]

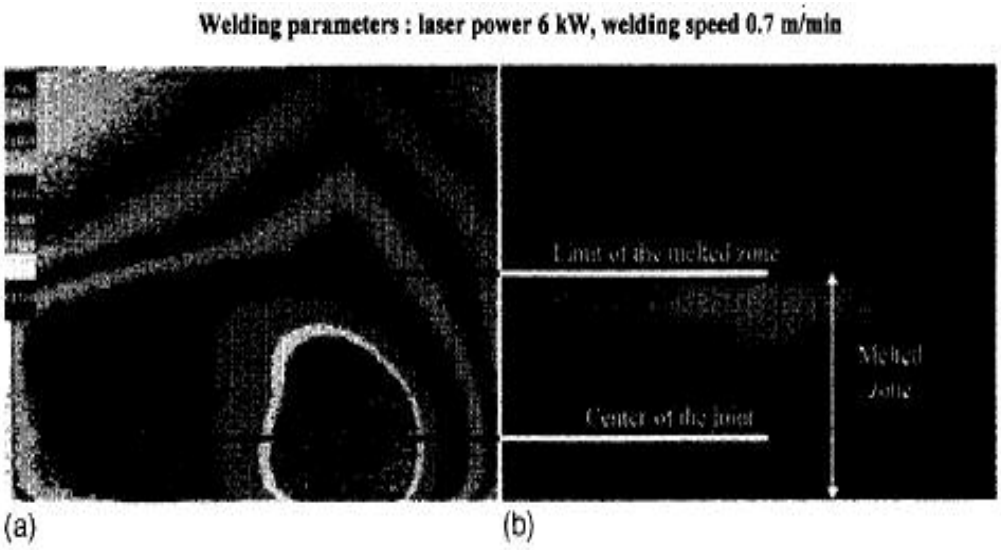

Figure 2.18: Comparison between a laser weld thermal image and laser weld geometry after cooling (a) thermal card of a welding operation.(b) welded joint after cooling [15]

2.5 Analytical Techniques

Rosenthal's moving heat source equations for welding are used as a basis for the analytical solutions of the temperature isotherms of arc welding of pipes. The analytical solutions (with various assumptions) are used primarily to create visual images for comparison with the experimental results. Usually, the images are created and subsequently modified for accuracy after the experimental data is collected. Thus the analytical results are brought closer to the experimental values. Likewise, the validity of the experimental values are checked and verified with the analytical results. The two way process guides in the development of better models for the thermal analysis of arc welding.

Akselsen *et al.* [16] used an Arrhenius-type relationship to predict changes in the average grain size caused by thermal change. To predict this, a known peak temperature is required. They simulated it using a commercial Weld Thermal Simulator and Rosenthal's equation toward developing a linear-type relationship. The peak

temperatures for a single cycle weld simulation experiment are shown in Table 2.3. The highest temperature recorded was 1376°C. Austenitic grain coarsening of steel for different peak temperatures is shown in Figure 2.19. Grain size is different when analyzed after welding with a 1200°C peak temperature compared to welding at a peak temperature of 1350°C.

Table 2.3: Data from the single cycle weld simulation experiments [16]

Steel	T_p (°C)	$\Delta t_{8/5}$ (s)	$D\gamma$ (μm)
A[a]	1372	4	60 ± 7
	1352	8	64 ± 7
	1356	14	66 ± 6
	1374	25	96 ± 26
	1376	49	166 ± 11
B[a]	1346	6	62 ± 3
	1359	9	57 ± 7
	1361	13	62 ± 4
	1368	24	65 ± 9
	1364	50	78 ± 8

[a]Average heating rate: ~200°C/s.

Infrared technology has advanced significantly in the last couple of decades or so but the accuracy of the recorded temperature, especially high temperatures, limits its use in industrial procedures. It is ideal to model the welding process with a computer simulation or analytical model to predict the impending failure or success of a weld to limit wasted material. Computer simulations conserve money, material, time, and energy while maintaining safe conditions for workers and the environment. Akselsen *et al.* [16] studied data for niobium microalloyed steels and those steels containing an excess amount of phosphorus and nitrogen. They concluded that the results of the experimentation were qualitatively consistent with the classic impurity drag theories for grain boundary motion.

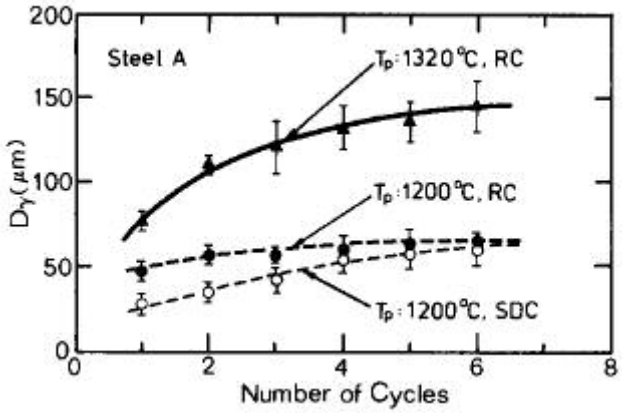

Figure 2.19: Grain diameter versus number of cycles for differing peak temperatures during the experiment [16]

Zhang *et al.* [17] investigated double-sided V-groove plate welding of austenitic stainless steel (Type 304). Figure 2.20 shows the weld after it was cooled and cut into cross sectional pieces for microstructural analysis. Visual images were recorded during the welding process and an analytical approach was used to calculate the temperature distributions over specified areas. A plasma arc was used to weld one side and simultaneously a GTAW arc was used on the other side. A microstructural analysis was completed for both types of welds. Conclusions of the Zhang *et al.* [17] experimental work focused on improving keyhole double sided arc welding (DSAW) and understanding the effects of varying keyhole DSAW parameters.

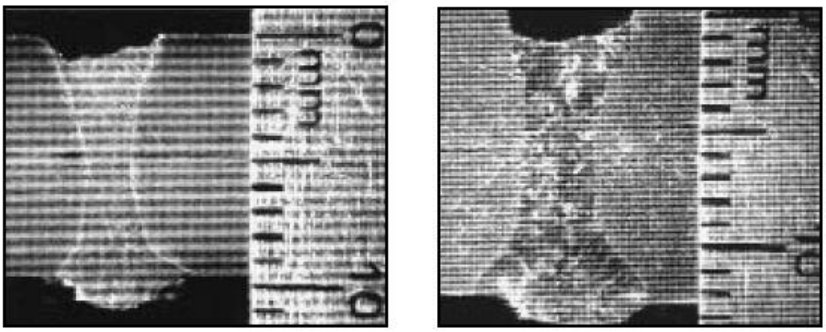

Figure 2.20: Keyhole double-sided arc butt joint weld traveling at 80 mm/min with 70 A on a (right) 12.7 mm thick plate welding upwards (left) 9.5 mm thick plate welding flat [17]

2.6 Welding Simulation

Modeling the welding of pipes is difficult in industrial situations because of numerous parameter affecting the welding process. FEM is a popular computer simulation technique used to model various manufacturing processes. Distortions caused by extreme thermal changes are a problem in welding. Bachorski *et al.* [18] has reported the results of FEM simulations to model the distortion of welded material using a shrinkage volume approach. Figure 2.21 shows curves representing models of three different shrinkage volumes and the experimental results. Figure 2.22 is a cross sectional view showing a comparison of the deformation, shrinkage, and the predicted shrinkage surrounding the weld. The actual shrinkage is larger with an unpredictable shape and irregular boundaries than the predicted shrinkage. Finite element analysis (FEA) is used to model temperature distributions throughout the weld as shown in Figure 2.23. Although the FEM technique is widely used in industry its application is somewhat limited when simulating high temperatures and high temperature gradient applications because of unpredictable accuracy. Bachorski *et al.* [18] study concluded that a split heat source with a Gaussian distribution is an effective heat source for welding analysis. Figure 2.24 shows a schematic of the split heat source after Bachorski *et al.* [18]. This method is accurate for V-grooves with angles > 50°; V-grooves of < 50° require a more accurate means of calculating shrinkage volume because the shrinkage area becomes process dependent. As the V-groove angle increases, the resulting angular distortion also increases. The shrinkage volume approach accurately accounts for the magnitude of distortion and has potential to develop into a useful tool for more complex welded structures.

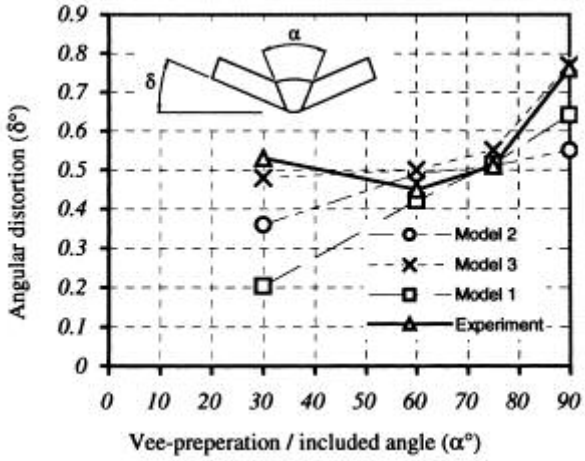

Figure 2.21: Comparison of three shrinkage volume FEM models. Model 1 represents joint preparation geometry as the shrinkage volume. Model 2 represents thermal modeling data to calculate shrinkage volume. Model 3 represents the actual weld fusion zone from welded samples determined by macro-sections [18]

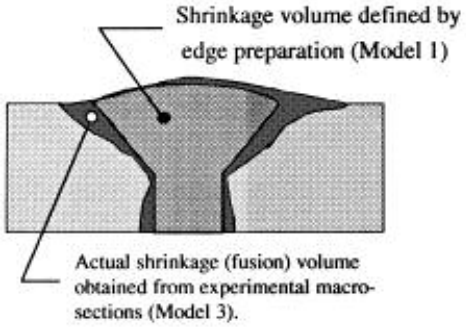

Figure 2.22: Schematic showing the differences between assumed shrinkage volume for Model 1 and the actual fusion zone determined from macrographs in Model 3 [18]

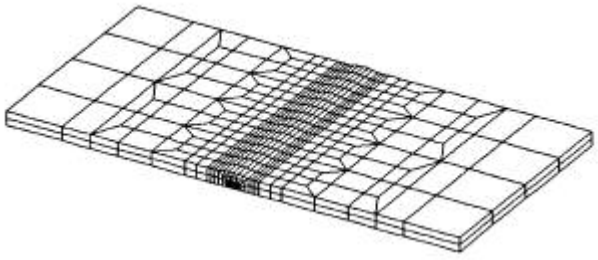

Figure 2.23: Finite-element mesh for a 90^{o} included angle single-V butt joint [18]

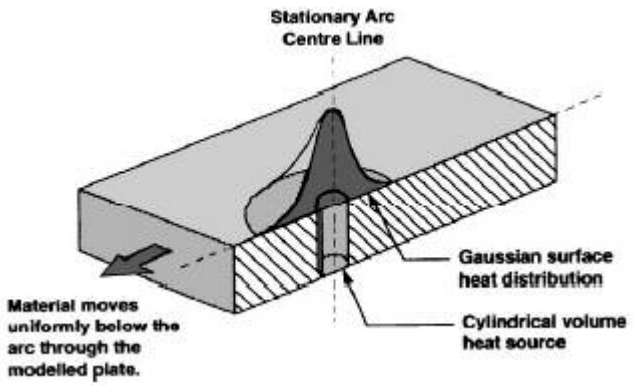

Figure 2.24: Split heat source with a Gaussian distribution [18]

Oddy and McDill [19] investigated the use of FEA to select welding parameters for in-service pressurized gas lines, and to prevent burn-through during welding as well as to prevent hydrogen assisted cold cracking. The finalized thermo-mechanical FEA for pressurized vessels is presented and compared with experimental data. Figure 2.25 shows the FEA temperature distribution in a mesh form during welding. Predictions of the heat generation and temperature distributions in a weld are shown in Figure 2.25 for a cross-sectional view. The cross-sectional area, shown in Figure 2.25, does not provide a geometrical scale for the heat penetration into the workpiece. Figure 2.26 shows refined areas as they are viewed using FEM. Increased heat penetration is represented by smaller rectangular meshes. They represent that FEA simulation predicted failure in areas that failed during experimentation. However, the FEA also predicted failure in welded areas that did not fail during experiments leading to the conclusion that FEA is overly conservative in predicting failure of welds.

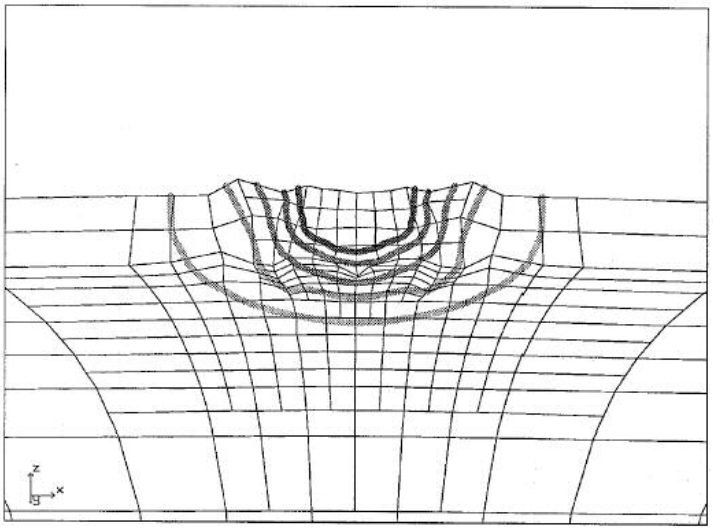

Figure 2.25: Melt-through instability in external spot heating of a pipe. Contours from inner surface to spot centre at 500°C, 750°C, 1000°C, 1250°C, and 1500°C. Displacements is magnified 3x [19]

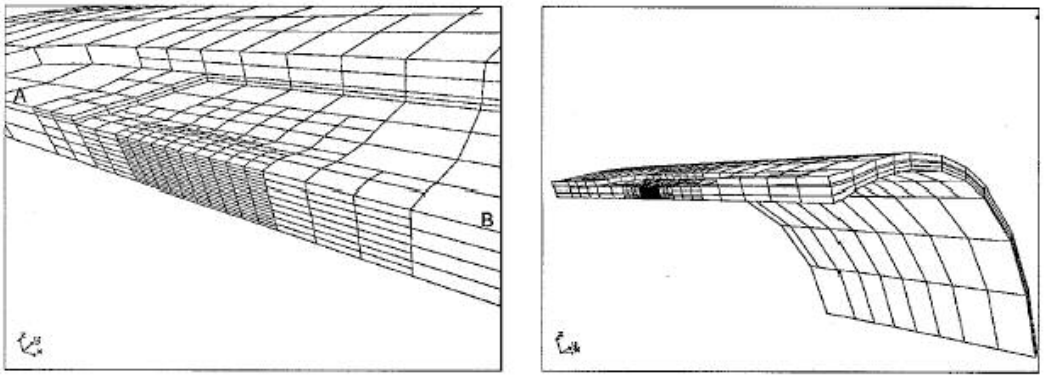

Figure 2.26: (right) Pipe mesh and (left) close-up of a refined region. Direction of source motion is from A to B. [19]

CHAPTER 3

PROBLEM STATEMENT

The literature review presented here addresses the analytical, simulated (FEM), and experimental aspects of welding. The experimental work involves the use of infrared technology and thermocouple techniques. However, advancements in the infrared sensing techniques and lack of experimental investigations of pipe welding primarily led to this investigation.

The first objective of this investigation is to design and build an apparatus for welding of pipes and record the temperature contours using an infrared camera.

The second objective of this study is to use an infrared camera to collect, record, and analyze the experimental temperature gradients produced in welding of ASTM A500 Grade B steel pipes. Welding of pipes was considered in two stages - transient and quasi-steady state. An experimental procedure was developed to collect the temperature distribution data, produce temperature contours, and compare the experimentally produced temperature contours with analytically produced temperature contours.

The third objective is to calculate temperature contours using an analytical thermal model, and represent them in the form of a Visual BASIC for Application (VBA) code, using essentially the same parameters as the experimental procedure. The analytical model used was based on an analytical model developed by Komanduri and Hou [20, 21] for welding of two plates.

The fourth objective of this report is to provide a comparison of experimental and analytical temperature contours for the welding of ASTM A500 Grade B steel pipes.

CHAPTER 4

EXPERIMENTAL SETUP AND TEST PROCEDURE

4.1 Introduction

The collection and recording of experimental temperature distributions for comparison with analytically calculated temperature distributions are difficult due to high temperatures involved comparative studies. Consequently, very few are available in the literature. Experimentally collected infrared thermal data is recorded and corrected according to emissivity requirements in correctional calculations for the current investigation; to assure the accuracy of the data.

A workpiece prepared with a V-groove connection between two ASTM A500 Grade B steel pipes is secured and rotated in the chuck of a pipe welding machine. An infrared camera records the temperature distributions in a pixel format. The computer software Dynamite® and Version 2.4.11 of ThermaGram Pro were used for data analysis during continuous pipe welding. The data recorded is transferred to a Microsoft Excel spreadsheet for emissivity and calibration related corrections. The corrected data is then plotted using Version 9.2 of TecPlot. The following are the steps used in sequential order for the experimental work:

1. Workpiece preparation
2. Setup of the Lincoln Electric welding machine
3. Workpiece positioning

4. Determination of the Workpiece rotational velocity

5. Setup of the Computer and television

6. Setup of the Infrared camera

7. Setup of the Safety equipment

8. Temperature data collection

10. Post experiment weld analysis

11. Analytical thermal modeling

12. Compare analytical and experimental results

13. Microscopic analysis

4.2 Pipe Welding Machine

A pipe welding machine was designed and built according to the required parameters for welding pipes and to record temperatures using an infrared camera. Figure 4.1 shows a photograph of the completed pipe welding machine. Parameters that were

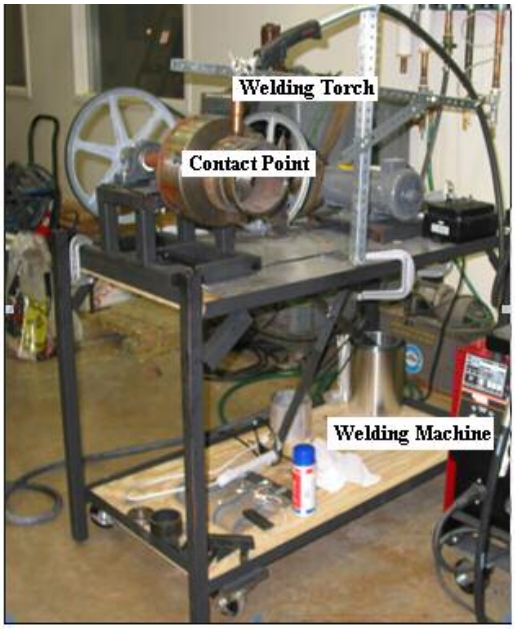

Figure 4.1: View of the complete pipe welding machine as positioned on a steel cart

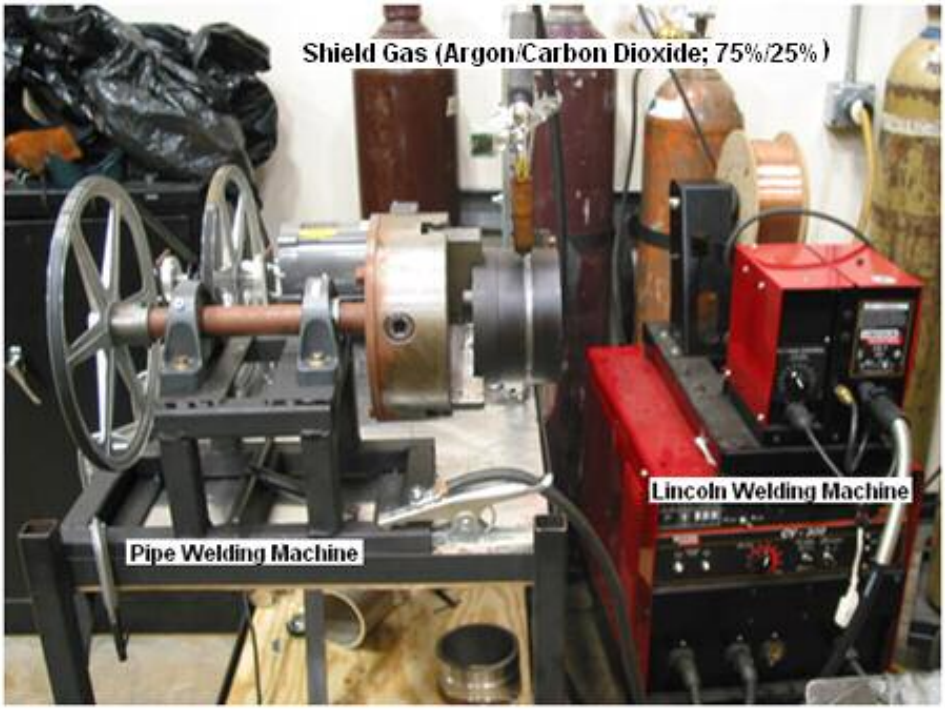

Figure 4.2: Complete pipe welding machine and Lincoln Electric welding machine setup

met included a 5 ft distance from the contact of the filler wire with the pipe to the front face of the infrared camera, variable rotational speeds, pipe holding device for variable diameters, a safety power switch, and maintaining a mobile setup. The pipe welding machine consists of a speed control, a motor, pulley and belt system, a shaft connecting the pulley and belt system to the chuck, a chuck, and a stainless steel welding torch holder. The completed pipe welding machine was mounted onto a steel frame cart allowing the experimental setup to be moved easily. The motor used is a Baldor CD3450 and is controlled and connected to a BC154 adjustable speed DC control drive. Technical specifications for the Baldor motor and speed drive are given in Appendix I.

The pulley and belt system is designed for welding of pipes with a maximum outer diameter of < 12". The pulleys within the system are replaceable to allow multiple rotational velocities. Figure 4.3 shows the pulley and belt system used in the current

investigation. Two 14” diameter and two 1 ½” diameter pulleys are rotated using two 22” diameter belts.

A chuck is connected to a machined, circular, flat base plate that is welded to a shaft connected to the belt and pulley system. The shaft fits through two 1 ½” pillow block bearings that hold the system in place. Figure 4.4 shows the chuck, back plate, pillow block bearings, pulley system, and shaft setup. Figure 4.5 shows two pieces of stainless steel square tubing setup that allows multiple welding torch positions with reference to the V-groove on the workpiece. Figure 4.6 shows the 5 ft required distance (from the calibration conditions) between the front face of the infrared camera and the welding contact point.

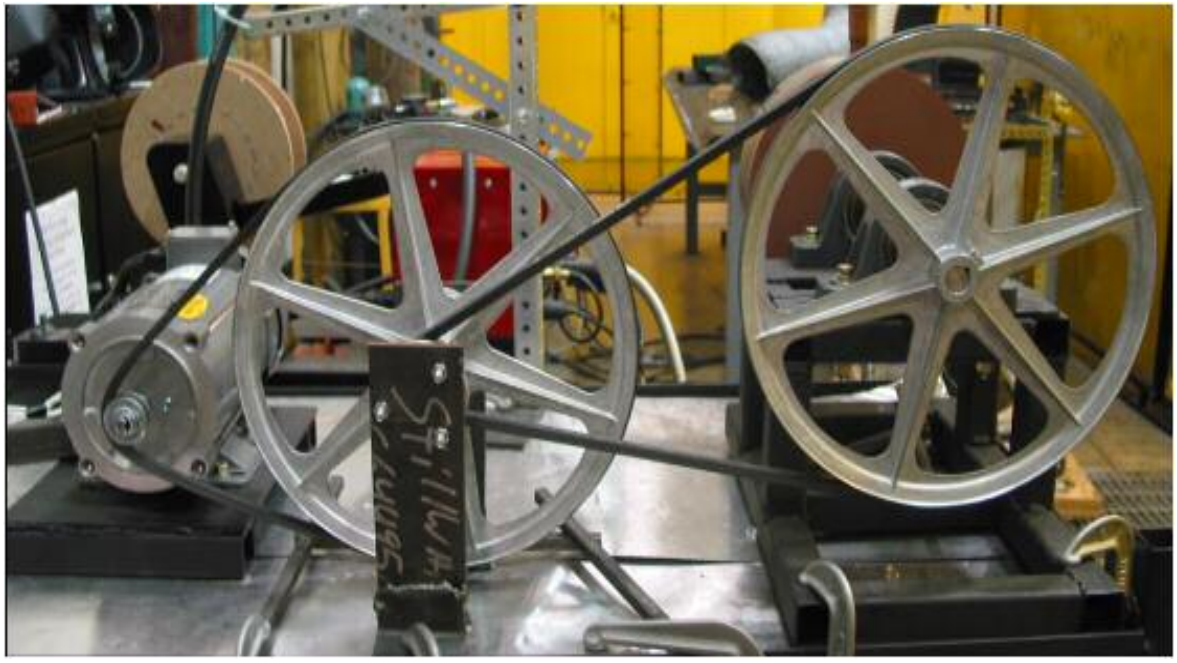

Figure 4.3: The motor as connected to the belt and pulley system on the pipe welding machine

The welder is positioned in front of the welding machine with an exit from the welding area directly behind them. The welder operates the pipe-welding machine while an assistant operates the computer, camera, and data collection system.

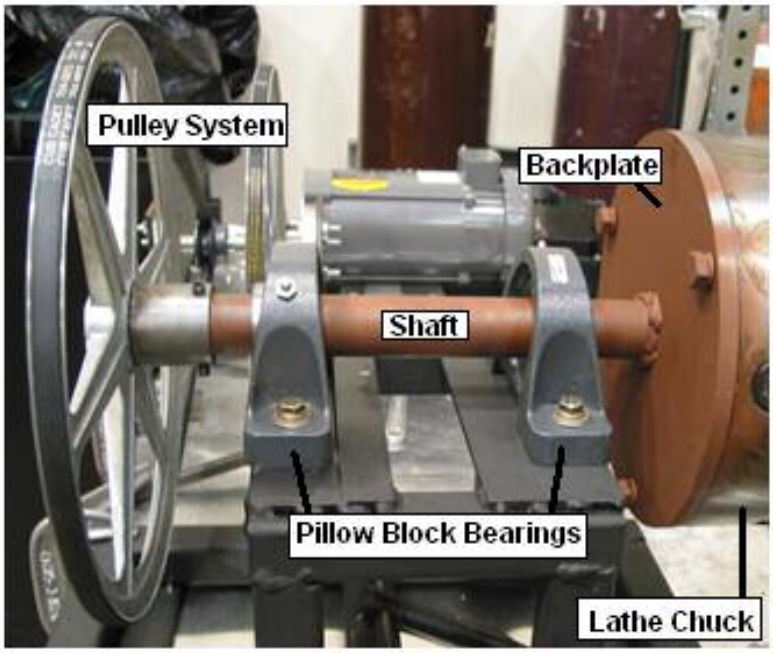

Figure 4.4: Pulley system shaft, and backplate setup connected through two 1 ½" pillow block bearings

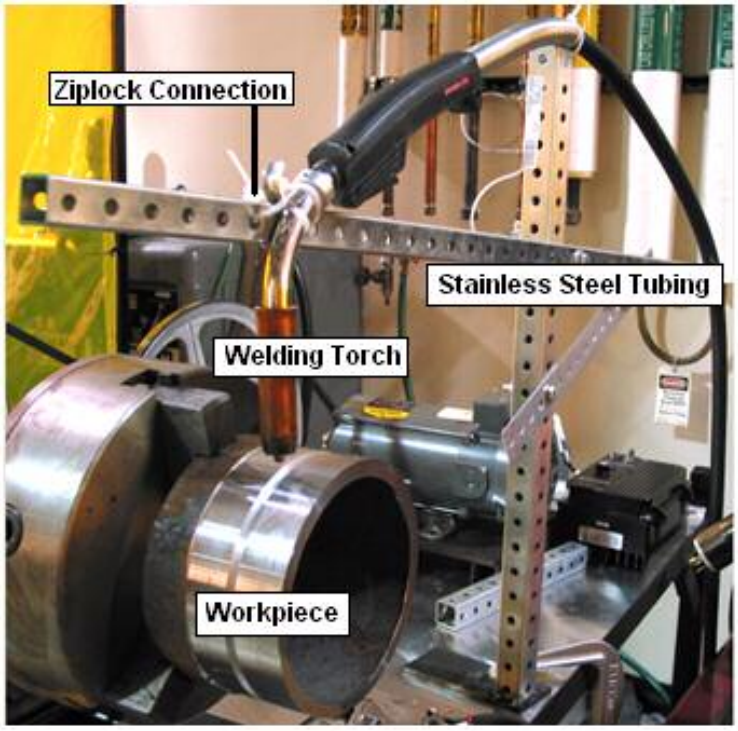

Figure 4.5: Welding torch holder made of stainless steel tubing: ziplock connection, welding torch, stainless steel tubing, workpiece

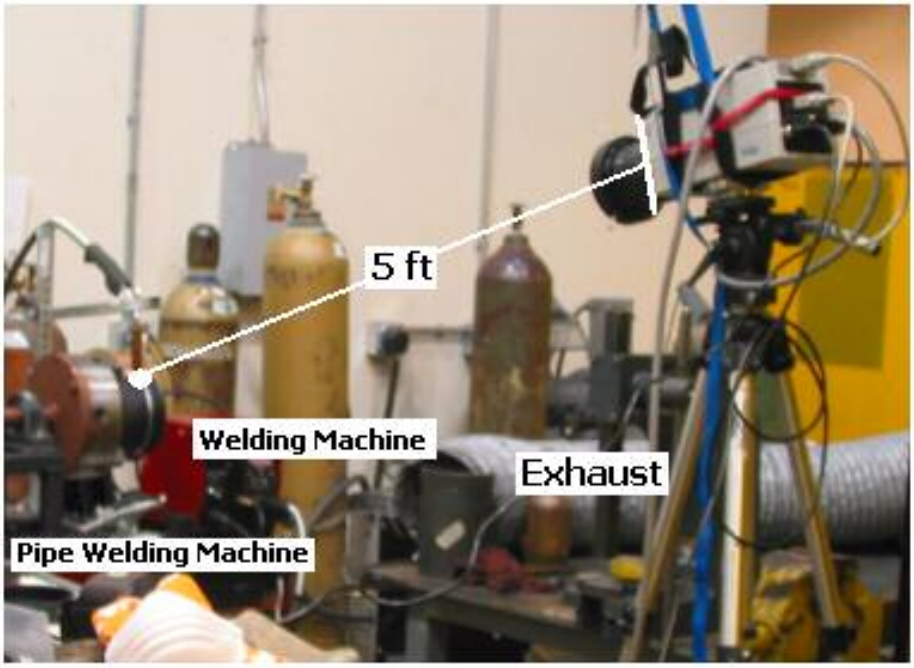

Figure 4.6: Infrared camera setup during welding, in reference to the pipe welding machine

4.3 Workpiece Preparation

The ASTM A500 Grade B steel (also known as UNS K03000) has carbon content and composition similar to AISI 1030 steel. The material properties used in the calculations for the analytical solutions are those of AISI 1030 steel.

Dimensions of the steel pipe as received include a diameter of 6.5", thickness of 0.5", and length of 2 ft. A lathe is used to machine the pipe to a required inner diameter, outer diameter, and length to create measurements in the X-, Y-, and Z- planes of the workpiece. The final dimensions of the completed round steel pipe are an outer diameter of 6.5" (+/- 0.15"), a thickness of 0.3" (+/- 0.02"), and a length of 3.9" (+/- 0.3"). To prevent corrosion on the workpiece surface and assure an emissivity value of 0.95 for calculations, the workpiece is coated with a single layer of high temperature, black paint. The paint undergoes heat damage only above 1200°C.

To simulate welding of two separate pipes a single piece of pipe is welded in a V-groove that has a depth of 0.2” or less. A V-groove is machined into the center of the machined length, i.e. 1 ½” from the outer edge and 1 ½” from the inner machined edge. The HAZ is < 1” on either side of the contact point between the filler wire and pipe. Therefore, the length of the pipe was disregarded and approximately 1 ½” (+/- 0.1”) was provided from the center of the V-groove in the outward direction on either side. Figure 4.7 shows the positioning of the V-groove on the pipe. The V-groove has an approximate depth of 0.2” leaving 0.1” or less of material connecting the two pipe pieces. High temperatures produce burn-through when initial contact occurs between the filler wire and bottom of the V-groove. Because of minimal material connecting the two base metals at the center of the V-groove, it will not significantly effect the welding isothermal temperature distribution. A complete dimensioned workpiece with black paint is shown in Figure 4.7. A 90° groove, 45° from the center to each side of the V-groove was generated. Recommended groove dimensions are given in ASM standards for pipe welding. Figure 4.8 shows V-groove dimensions used in the current investigation.

Figure 4.7: Machined and painted workpiece with a finished V-groove

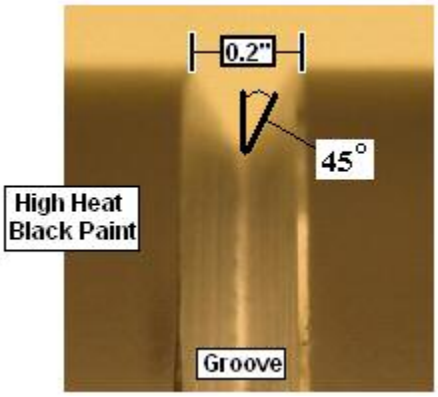

Figure 4.8: Pipe workpiece V-groove dimensions

4.4 Workpiece Positioning

The pipe is secured onto a chuck on the pipe welding machine. The position of the filler wire in the V-groove directly affects the temperature distribution. The welding torch is held in place and the welder has control over the activation of the power switch. Figure 4.9 shows the positioning of the welding nozzle and insert. To simulate good welding practice the filler wire is positioned in the center of the V-groove. The end of the insert is placed approximately ¼" above the welded material.

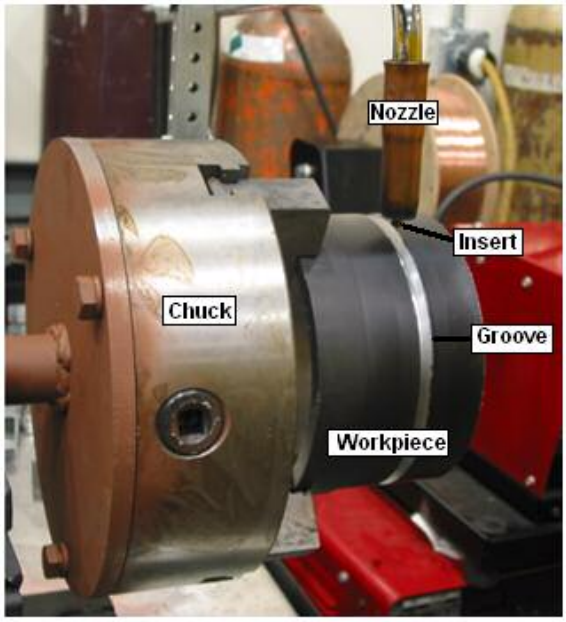

Figure 4.9: Welding nozzle and insert positions relative to the V-groove

4.5 Merlin™ Mid Infrared Camera

Figure 4.10 shows a photograph of a Merlin™ Mid InSb infrared camera (a mid-wavelength infrared (MWIR) high-performance camera) from Indigo Systems. It is used to collect infrared thermal data during pipe welding. The technical specifications for the infrared camera are given in Appendix I. Two threaded holes, located on the bottom of the camera are provided to mount the camera on a tripod. This infrared camera does not require cryogenic fluid refills to cool the camera and provide a reference temperature. The camera is operated with a button remote panel located on the top of the camera, a rectangular grey area with blue buttons. A menu is provided on a television and used as a reference when camera settings are changed. The visual output menu must be used when changing non-uniformity correction (NUC) tables and other important camera

Figure 4.10: Merlin™ Mid InSb MWIR Camera [24]

parameters, namely, integration time and one point corrections. Details of the infrared camera integration time, neutral density filter, and protective sapphire lens are provided in Appendix I. One point and two point corrections for all NUC tables are available to maintain the accuracy of recorded temperatures, according to the calibration of the camera. One point corrections are required to prevent the accuracy of the infrared camera from shifting from a uniform to non-uniform state, drifting.

4.6 Optical Interfaces

Figures 4.11 (a) through (c) show three exterior lenses, namely, namely, optical, filter, and protective, used in the current investigation. The external protective lens is made of sapphire and is placed on the camera using a machined delrin holder, held together with nylon screws, as shown in Figures 4.11 (b) and (c). The completely assembled optical setup is shown in Figure 4.11 (c). Infrared optical lens materials are limited because of their size infrared wave lengths (see Appendix I for details). The infrared camera lens is primarily composed of silicon with a magnesium fluoride and alumina coating because of the 3 – 5 μm wavelengths viewed by the infrared camera. The conductive properties of silicon limit the lens viewing conditions because when the lens is heated it will become opaque. Therefore, it is important that the lens be maintained at room temperature, approximately 21 – 25°C. A silicon/germanium doublet is utilized for the Merlin^{TM} Mid infrared camera lens.

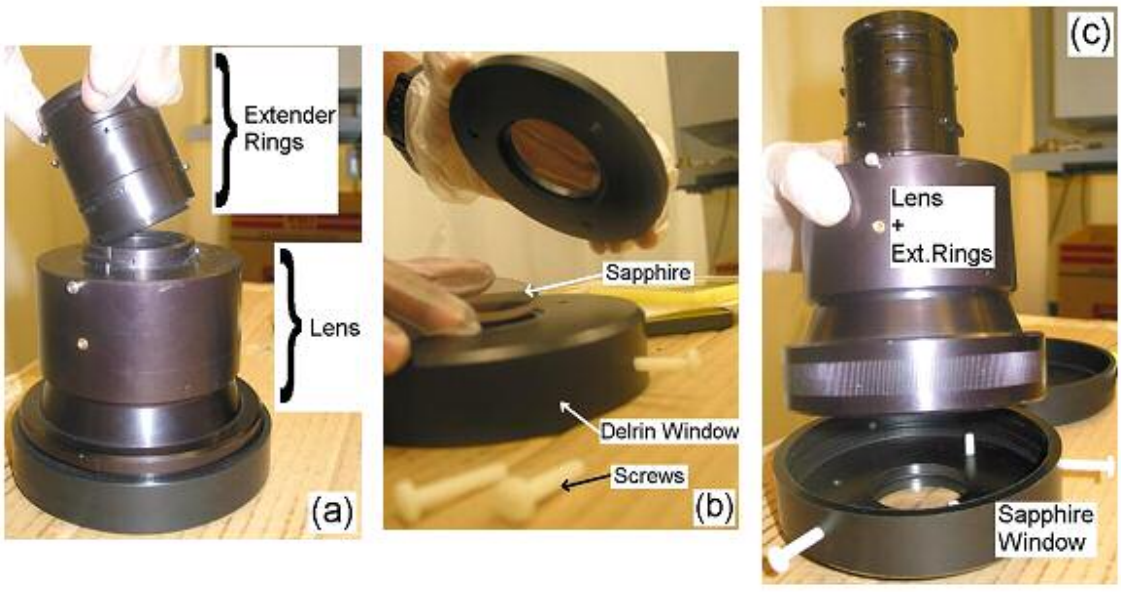

Figure 4.11: Lens layering of the Merlin^{TM} Mid MWIR high-performance infrared camera [25]

4.7 Non-Uniformity Correction Tables (NUC)

Infrared sensors in the infrared camera vary in their individual response to thermal or photon energy, otherwise referred to as the non-uniformity of an infrared detector. Non-uniformity in infrared detectors causes grainy or unclear images with incorrect pixels data located randomly in recorded images. Six preset NUC tables, referred to as manufacture calibration tables, are provided to record thermal images within temperature ranges. NUC 0, NUC 1, NUC 2, NUC 3, NUC 4, and NUC 5 tables represent temperature ranges in the camera of 2 to 68°C, 44 to 123°C, 111 to 231°C, 221 to 425°C, 380 to 765°C, and 600 to 1600°C, respectively. A neutral density filter (NDF) is required when using the NUC 4 and NUC 5 tables. A clear image of the focal plane area on the workpiece and geometrical distances are established using the NUC 0 table before the camera is switched to the NUC 4 or NUC 5 tables to record data. A one point correction is required whenever a NUC table setting is changed.

4.8 Calibration

Before using the camera for the present investigation it was necessary to assure the calibration of the camera remained accurate, without any drift and within the range of temperatures recorded by the camera in pipe welding. We were rather fortunate to have a calibration facility accessible to us. The calibration of the infrared camera was performed at the National Institute of Standards and Technology (NIST) in Gaithersburg, MD in cooperation with Dr. Robert Ivester.

A graybody with a known emissivity value of 0.99 was heated in incremental steps from 30 and 1050 °C. The camera was setup 5 ft from the graybody to the front face of the infrared camera to record temperatures. Both the infrared camera and graybody

remained stationary throughout the temperature measurement and data recording. The graybody was heated until a steady temperature was reached. Then the temperature was measured with the infrared camera. This was done multiple times to check the accuracy and reproducibility of the temperatures recorded by the camera. Figure 4.12 shows the plot of actual graybody temperature versus the temperature recorded by the infrared camera. It can be seen that temperatures measured by the camera are in close agreement to the actual graybody temperatures until the temperature of ~ 575°C. As the graybody temperatures are increased past 575°C, the temperatures recorded by the infrared camera are observed to be higher than the actual graybody temperatures. Higher temperatures were recorded using the NDF according to the

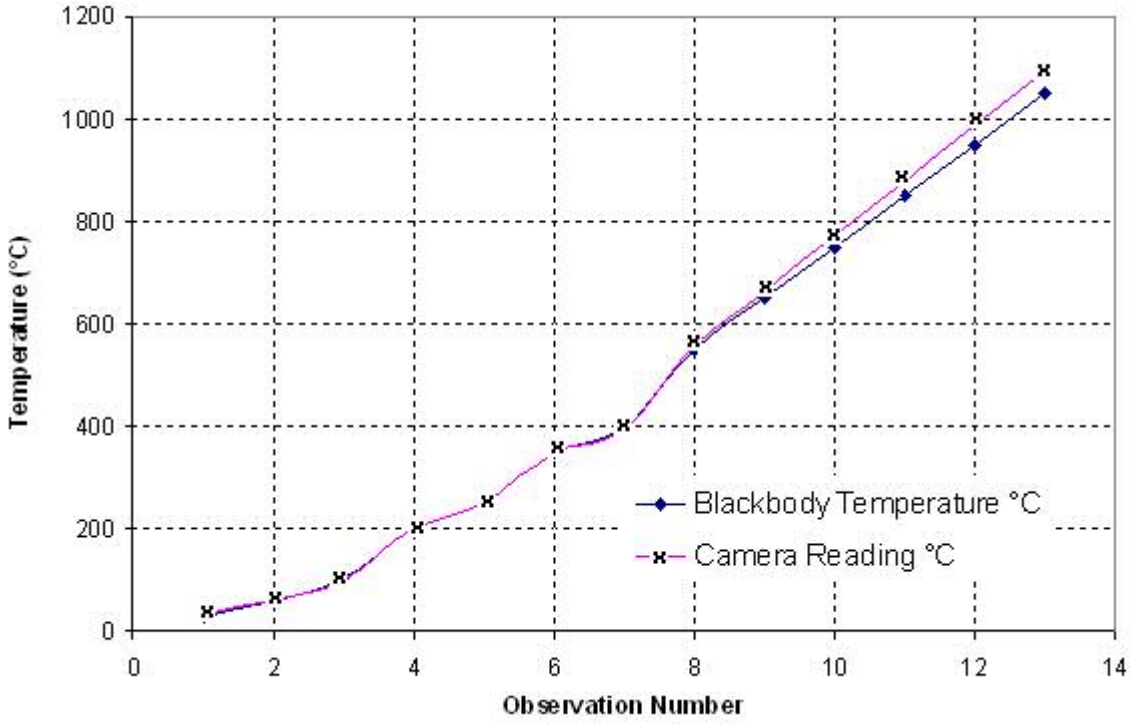

Figure 4.12: Camera calibration plot using 100 mm lens, NDF, and sapphire protective window (the graybody is represented by temperatures labeled for the blackbody) [25]

camera specifications outlined for the infrared camera in the manufacturer's manual [24]. For temperatures > 575°C, a separate calibration curve was created using the camera signal recorded during the calibration process. The equation generated uses the best fit line form the temperature > 575°C and < 1050°C is provided in the equation and plotted in Figure 4.13. The temperatures involved in the welding processes were observed to be higher and the best fit calibration curve to be used in the analysis of recorded temperatures was extended up to ~ 1450°C.

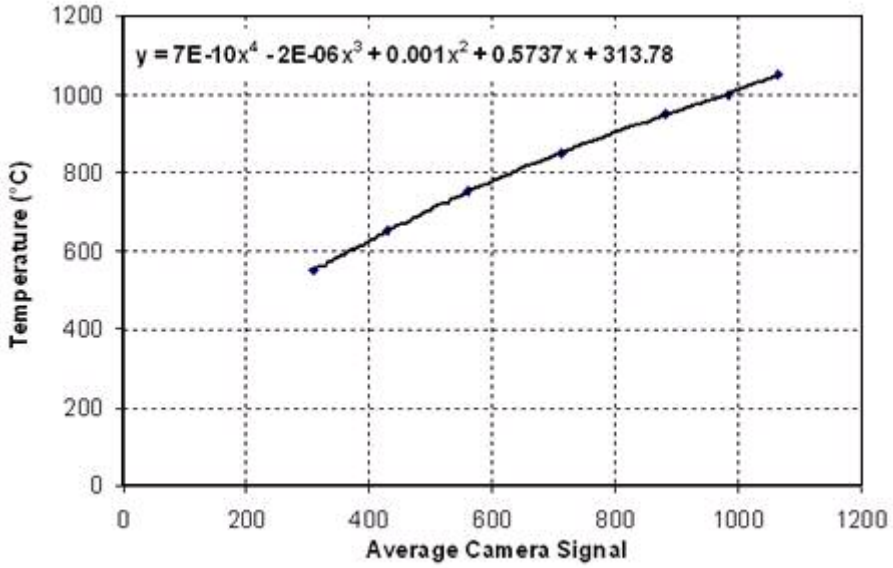

Figure 4.13: Camera calibration and correctional equation using 100 mm lens, NDF, and sapphire protective window at a 100 μs integration time [25]

4.9 Lincoln Electric MIG/Flux-Cored Welder

Figure 4.15 shows a Lincoln Electric MIG/Flux-Cored Idealarc CV-300 welder with LN-7 GMA wire feeder. It was used to produce a MIG weld within a V-groove connection between two ASTM A500 Grade B steel pipes. Figure 4.14 is a schematic of the MIG welding process [27]. Technical specifications for the Lincoln Electric welder

are given in Appendix I. The LN-7 GMA semiautomatic constant speed wire feeder is positioned on top of the Idealarc CV-300 welding machine, as shown in Figure 4.15.

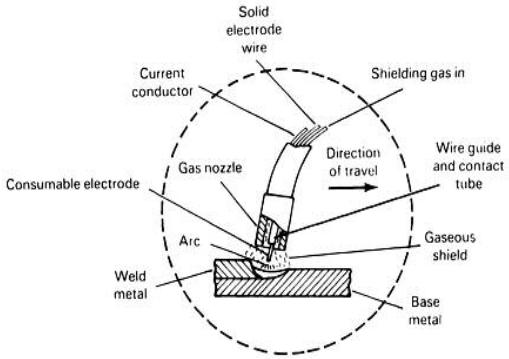

Figure 4.14: Schematic of MIG welding [27]

Figure 4.15: Lincoln Electric Idealarc CV-300 welder with LN-7 GMA wire feeder [29]

Technical specifications for the LN-7 GMA wire feeder magnum gas-shielded gun and cable assembly for the LN-7 GMA wire feeder are given in Appendix I.

4.10 Computer and Television Setup

The computer and television were setup for easy visibility. Accessibility of the computer keyboard is required. A separate cart provides shelving for the computer and television, as shown in Figure 4.16. Protective shields surround the computer and television cart but are not positioned in front of the camera.

After the infrared camera has sufficiently warmed up, it is focused on the contact point in the NUC 0 table setting. The NDF2 is attached to the 100 mm lens and the NUC table is changed to the NUC 5 setting for experimental data collection.

Figure 4.16: Computer, television, and camera setup with surrounding safety shields

4.11 Safety Equipment Setup

The welder and the assistant are required to wear proper safety equipment and use proper procedures. A lab coat, safety dark hood, protective glasses, fire resistant boots, gloves, respirator, hat, ear protection, and a handkerchief are recommended while welding. These items are shown in Appendix I. UV radiation preventative safety panels surround the welding area. Exhaust piping is provided for proper ventilation of the welding area.

4.12 Welding Coupons

The weld was cut into multiple cross sections called weld coupons. The weld coupons have a height of 1", width of 1.5", and a thickness of 0.75". After the weld coupon is ground and etched the weld was viewed using an optical microscope and viewed under a hand held magnification glass, 3x. Figures 4.17 (a) and (b) show photographs taken using a digital camera and hand held magnification lens. Observations

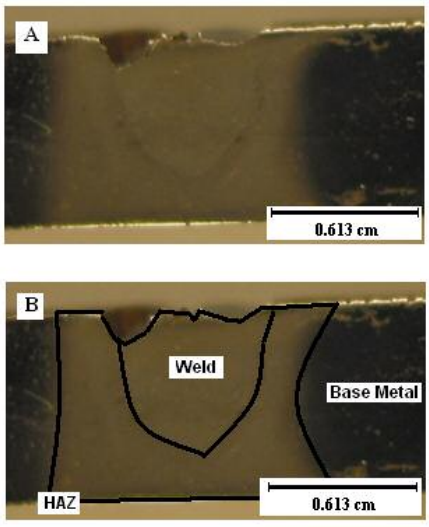

Figure 4.17: (a) Polished and etched welding coupon, 3x (b) labeled base metal, HAZ, and weld metal polished and etched welding coupon, 3x

made when viewing the HAZ show microstructual changes and confirm fusion of the materials. Microstructure within a weld determines the quality and longevity of the weld.

4.13 Temperature Data Acquisition

Dynamite® is a computer software program used to capture thermal images, frame by frame sequences, taken with the infrared camera. The Dynamite® program directly records, stores, and views thermal images through the infrared camera. Recorded thermal image sequences are cropped, saved, and transferred to a second computer. Images are converted from a Dynamite® format to a ThermaGram format for temperature data extraction. ThermaGram allows extraction of temperatures and pixel data at a specified time. The Dynamite® and ThermaGram software compliment the use of one another.

ThermaGram allows the export of temperature data for individual pixels to other computer programs, such as Microsoft Excel, in the form of an ASCII file. The ASCII file creates a thermal map for the area selected in the ThermaGram. Thermal images of the lateral and vertical ruler images provide length measurements of individual pixels later used in the measurement of the recorded temperature distributions.

Microsoft Excel temperature data is corrected using calculations in a VBA code. Emissivity and calibration correction equations alter temperature values that are output and plotted with Version 9.2 TecPlot software. TecPlot software provides a plotted image of the temperature distribution produced during welding.

Figure 4.18 shows a Dynamite® software computer screen 17 s after the weld was initiated. The individual 17 s frame is extracted using alternative software, ThermaGram. Figure 4.19 shows the ThermaGram computer screen for 17 s after the weld is initiated.

Three of the commonly used thermal data extraction techniques of ThermaGram are shown in Figure 4.19, a spot temperature, temperature distribution over a line, and temperature pixel data over a specified area (box). When correctional calculations are complete, the temperature distribution is plotted on the X- and Y-plane using TecPlot, Version 9.2 software. Figure 4.20 shows a TecPlot plotted screen example.

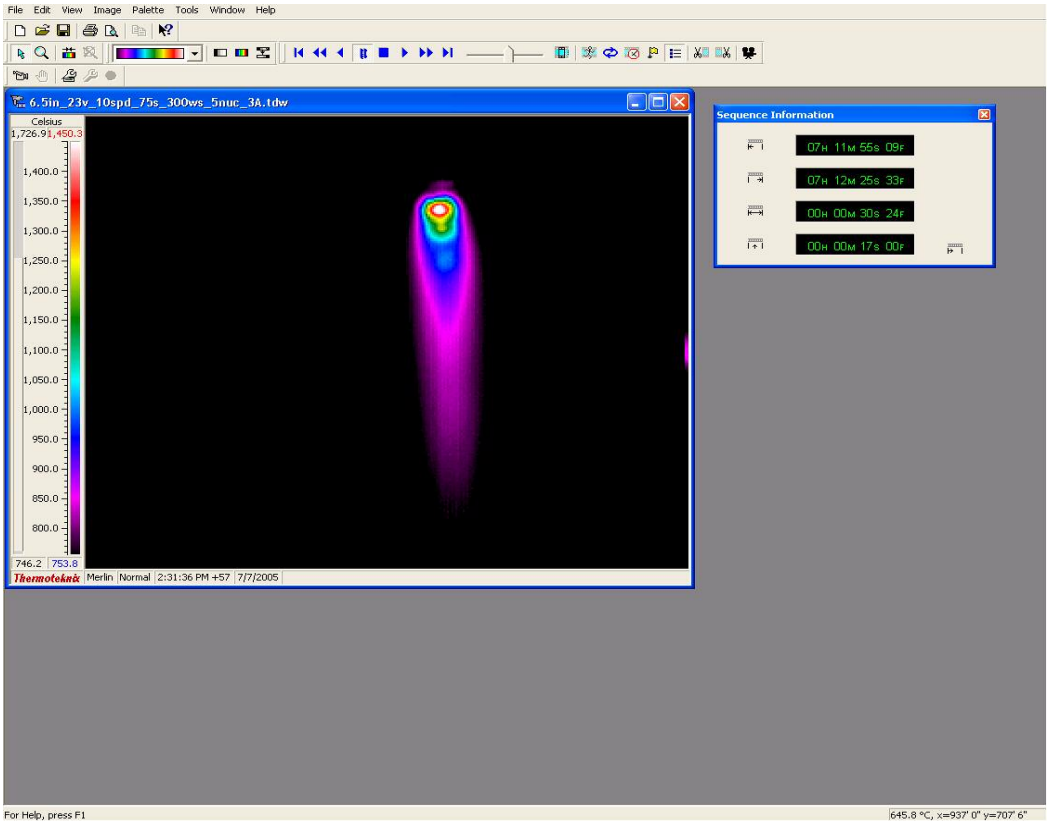

Figure 4.18: Dynamite® computer screen for the 17 s after the weld is initiated

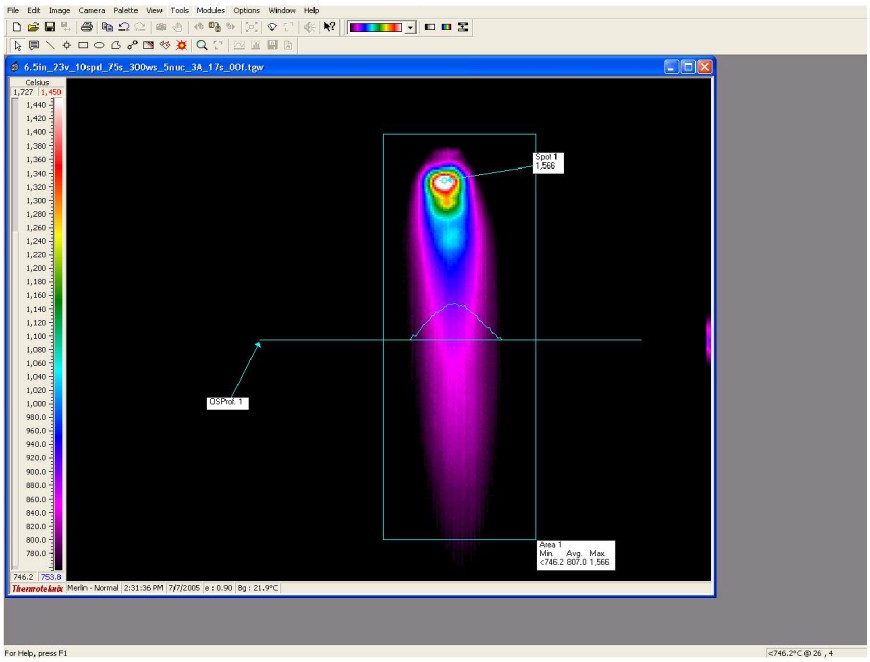

Figure 4.19: TheramGram computer screen for the 17 s after the weld is initiated with the demonstration of three thermal data collecting techniques; a spot temperature, temperature distribution on a line, temperature pixel data over a specified area

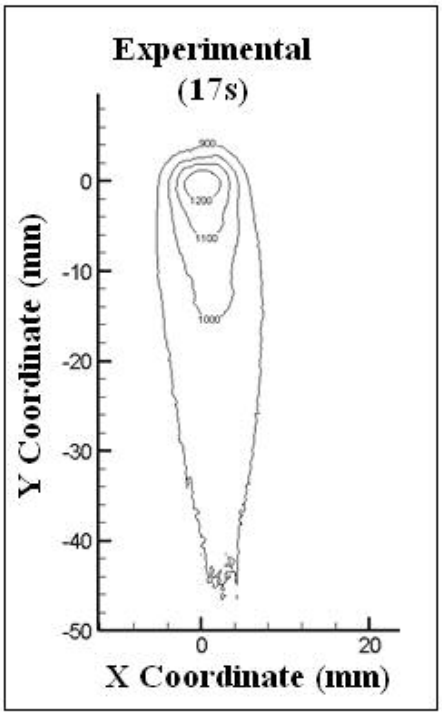

Figure 4.20: TecPlot isothermal plot for 17 s after the weld is initiated

CHAPTER 5

ANALYTICAL SOLUTION

5.1 Analytical Procedure

As mentioned earlier the experimental results obtained using an infrared camera are compared with the analytical results. Both are presented in a graphical X-Y form. The analytical solution calculates spot temperatures with respect to distances using parameters essentially similar to those used for the experimental results. Plots provide experimental and analytical temperature isotherms for comparison and are given in Chapter 7 Results and Discussion. The analytical solution models the welding arc as a moving circular disc heat source. In the present investigation, the parameters used for analytical calculations are essentially the same as those used in the experiments. The analytical model predicts temperatures in the solid phase of the welded material. However, welding involves multiple phases, namely, solid, liquid, and vapor. The welding process includes a state change from solid to liquid and vapor during welding. The liquid state then transforms to a solid state as the weld cools. The actual welding process is more complex than some of the simplifications of the analytical model.

5.2 Analytical Modeling

Much of the material presented in this chapter is based on Jaeger's moving heat source theory developed by Komanduri and Hou [20]. The analytical solution model is obtained by using a moving disc heat source as the welding arc (heat source). The

diameter of the welding arc is assumed to be the diameter of the filler wire. The welding arc is larger but the exact size is unknown. The moving disc heat source consists of multiple concentric ring heat sources of varying radii. Each ring heat source consists of multiple arc segment heat sources. Each arc segmental heat sources is assumed to consist of multiple point heat sources.

The fundamental heat source equation used to develop the analytical model is the instantaneous point heat source equation, given by Eqn. 5.1. Figure 5.1 is a schematic of an instantaneous point heat source.

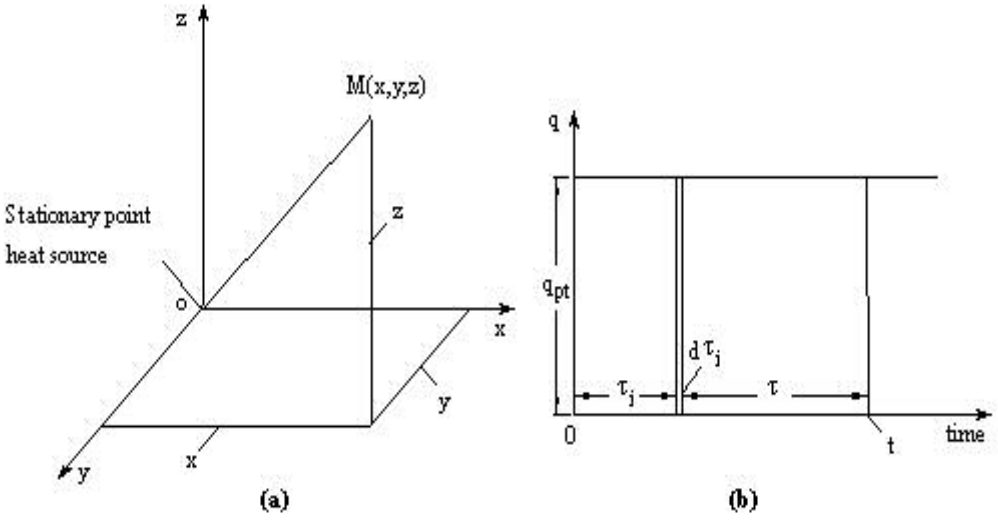

Figure 5.1: Schematic of an instantaneous point heat source [20]

$$\theta = \frac{Q_{pt}}{c\rho\left(4\pi a\tau\right)^{\left(3/2\right)}} e^{-\left(R^2/4a\tau\right)} \qquad 5.1$$

Q_{pt} is the heat liberated by an instantaneous point heat source (Joule), ρ is the density of the medium (g/cm^3), a is the thermal diffusivity of the medium (cm^2/s), τ is the time (s), R is the distance between the center of the point heat source and the point at which the

temperature rise at time τ (cm), and *c* is specific heat of the medium (J/(g.^{o}C)). Heat liberated by the instantaneous point heat source per unit length is calculated using Eqn. 5.2.

$$Q_{pt} = \frac{Q_{Rg}}{2\pi R_o} d\alpha \qquad 5.2$$

Q_{pt} is the heat liberated by a point heat source (Joules), Q_{Rg} is the heat liberation by a ring heat source (Joules), and R_o is the radius from the center of the heat source to the spot temperature of interest (cm). The equations for *r, R',* and *R* are given by Eqns. 5.3 to 5.5, respectively based on the relationships between the heat source geometry and location of the heat source.

$$r = \sqrt{(x^2 + y^2)} \qquad 5.3$$

$$R' = \sqrt{r_o^2 + r^2 - 2rr_o \cos\alpha} \qquad 5.4$$

$$R = \sqrt{z^2 + R'^2} \qquad 5.5$$

The variable *r* is the X-Y distance from the instantaneous heat source to the point where the temperature of interest is concerned (cm), *R'* is the distance from the edge of the instantaneous point heat source to the location of the X-Y coordinates of the instantaneous point heat source (cm), and *R* is the distance from the edge of the heat source to the point where the temperature of interest is concerned (cm). The relationship (Eqn. 5.2) involving heat liberation by an instantaneous point heat source, Q_{pt} and the ring heat source heat liberation, Q_{Rg}, is substituted into Eqn. 5.1 to derive Eqn. 5.6. After substitution of the heat liberated per unit length, the primary heat source equation becomes the instantaneous circular ring heat source (Eqn. 5.6). The integral limits used

to calculate the temperature at any point in the coordinate system (using the equation of an instantaneous point heat source equation) are 0 to 2π. Thus, the instantaneous circular ring heat source equation is given by (Eqn. 5.6).

$$\theta = \frac{Q_{Rg}}{c\rho(4\pi a\tau)^{3/2}} e^{\frac{r+r_o^2+z^2}{4a\tau}} \frac{1}{2\pi} \int_0^{2\pi} e^{\frac{rr_o}{2a\tau}\cos\alpha} d\alpha \qquad 5.6$$

Figure 5.2 is a schematic of an instantaneous circular ring heat source. To simplify Eqn., 5.6 the Bessel function relationship within the instantaneous ring heat source equation can be written as Eqn. 5.7. The value of the Bessel function can, therefore, be found in mathematical handbooks [20, 21].

$$I_o(p) = I_o\left(\frac{rr_o}{2a\tau}\right) \qquad 5.7$$

The instantaneous circular ring heat source equation is used to calculate spot temperatures (as given in Eqn. 5.8) which is a simplified version of Eqn. 5.6.

$$\theta = \frac{Q_{Rg}}{c\rho(4\pi a\tau)^{(3/2)}} e^{-\left(\frac{r^2+r_o^2+z^2}{4a\tau}\right)} I_o\left(\frac{rr_o}{2a\tau}\right) \qquad 5.8$$

Since a welding arc continuously joins two pieces of base material, in this case two rotating circular pipes, by the moving disc heat source at high temperatures, it is necessary to incorporate this into the analytical equation. To account for the arc movement an equation (Eqn. 5.9) for a moving instantaneous circular ring heat source is derived. The amount of heat sources and mirror heat sources differs from welding two flat plates. To model welding of two rotating pipes, two moving heat sources and two image heat sources, one for each moving heat source, are considered. Eqns. 5.3 through 5.5 are substituted into the

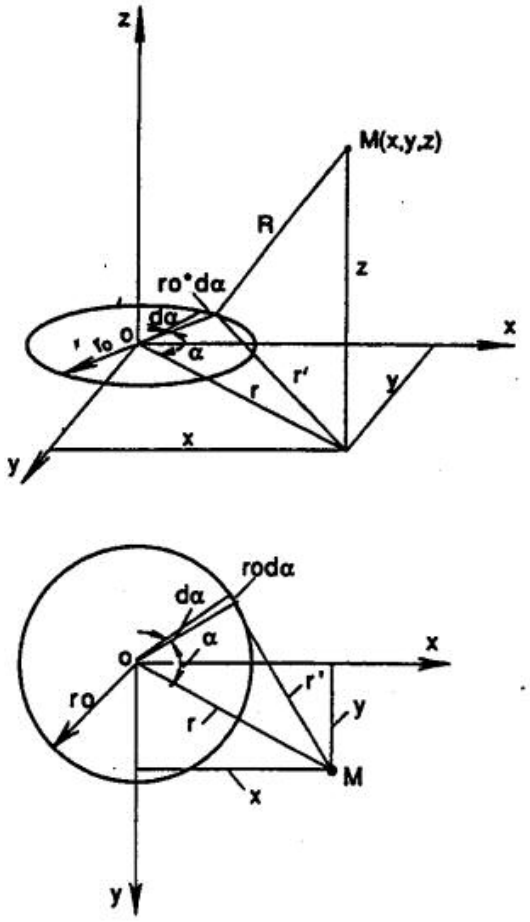

Figure 5.2: Schematic of an instantaneous circular ring heat source [35]

instantaneous circular ring heat source equation (Eqn. 5.8) resulting in Eqn. 5.9. To simplify Eqn. 5.9 and create a non-dimensional equation, the variable ω, a non-dimensional parameter is defined (Eqn. 5.10) and substituted into Eqn. 5.9. Other geometric and relevant equations are given in Eqns. 5.11 through 5.14.

$$\theta = \frac{q_{Rg}}{c\rho(4\pi a)^{3/2}} \int_{\tau_{i=0}}^{\tau_{i=t}} \frac{d\tau_i}{\tau} e^{\frac{-[(x-v\tau_i)^2+y^2+z^2+r_o^2]}{4a\tau}} I_o\left(\frac{\sqrt{\left((x-v\tau_i)^2+y^2\right)r_o^2}}{2a\tau}\right) \quad 5.9$$

$$\omega = \left(\frac{v^2 t}{4a}\right) \quad 5.10$$

$$R_h^2 = r_o^2 + x^2 + y^2 + z^2 \quad 5.11$$

$$V = \frac{v}{2a} \tag{5.12}$$

$$u = R_h V \tag{5.13}$$

$$v\tau = \frac{2\omega}{V} \tag{5.14}$$

After substitution of these relations (Eqns. 5.10 through 5.14) into the instantaneous circular ring heat source equation (Eqn. 5.8) the moving ring heat source in a semi-infinite medium Eqn 5.14 is obtained.

$$\theta = \frac{q_{Rg} v}{16\lambda a \pi^{3/2}} e^{-XV} \int_{\omega=0}^{\omega=\frac{v^2 t}{4a}} \frac{d\omega}{\omega^{3/2}} e^{-\omega} e^{-\frac{u^2}{4\omega}} I\left(\frac{r_o V^2}{2\omega}\sqrt{\left(x+\frac{2\omega}{V}\right)^2 + y^2}\right) \tag{5.14}$$

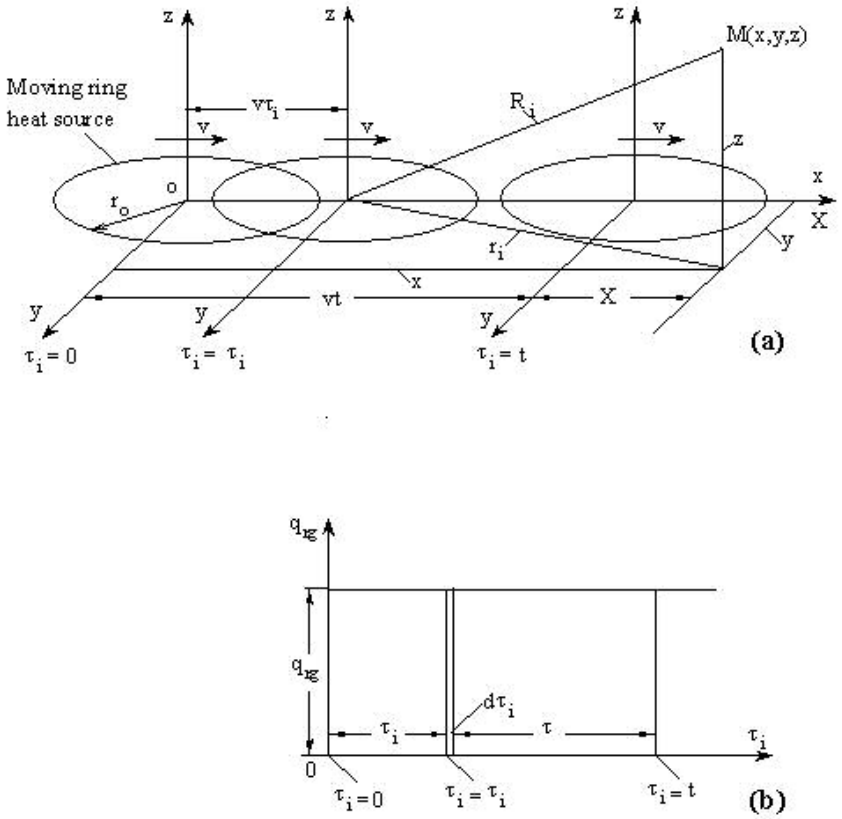

Figure 5.3: Schematic of a moving ring heat source [20]

Figure 5.3 is a schematic of a moving ring heat source in a semi-infinite medium. A welding arc heat source in motion is modeled as a moving disc heat source consisting of multiple ring heat sources of varying radii. The source of the heat liberation rate for multiple ring heat sources of varying radii is different for the two modeled heat sources. Integration limits for a disc heat source are ~ 0 and the outermost diameter of the included ring heat sources. In the current investigation the outermost diameter is ~ 0.9 mm. Figure 5.4 is a the schematic of a moving disc heat source.

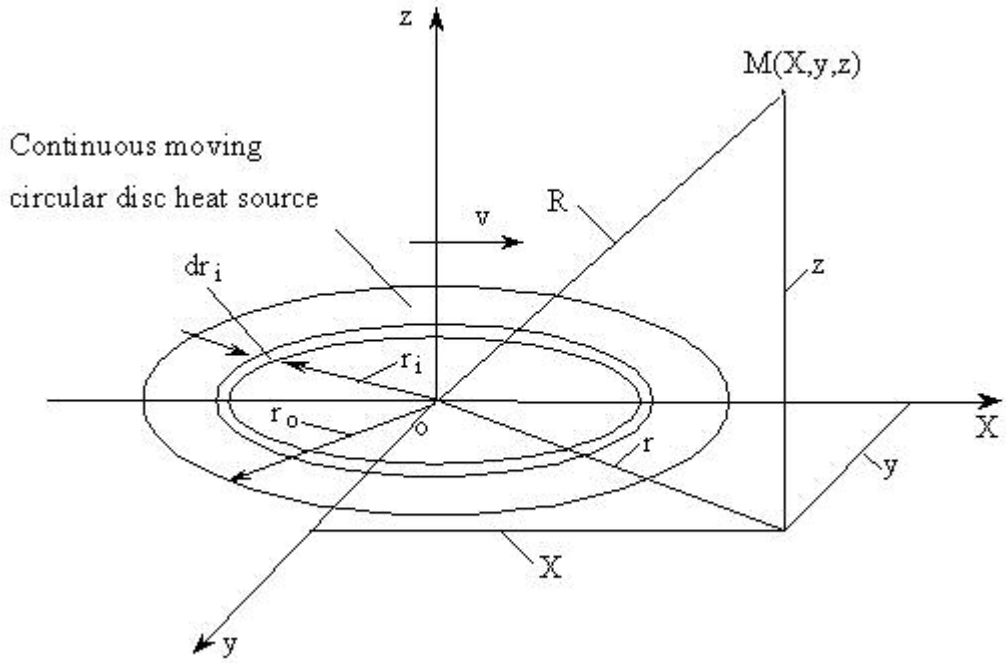

Figure 5.4: Schematic of a moving disc heat source [20]

Eqn. 5.11 gives the heat liberation rate of multiple ring heat sources as they vary in radii values. A pseudo-Gaussian distribution of the heat liberation rate is given in Eqn. 5.12. The constant, *C*, is calculated using Eqn. 5.12. It incorporates multiple radii representing a disc heat source made of multiple ring heat sources. A numerical value precedes the

$$q_{Rg} = q_o 2\pi r_i dr_i \qquad 5.11$$

radius ratio in the exponential with a value that varies between 0 and 9 to provide an accurate Gaussian type distribution. A perfect Gaussian distribution curve is represented by the value of 9. The value used in the current analytical solution to define the Gaussian shape of the temperature isotherms is 3, as shown in the exponent of Eqn. 5.12. The number 3 is best thought to represent the Gaussian-like heat distribution produced during welding.

$$q_o = Ce^{-3\left(\frac{r_i}{r_o}\right)2} \qquad 5.12$$

Eqn. 5.12 is substituted into Eqn. 5.11 to obtain Eqn. 5.13.

$$q_{pl} = \int_{r_i=0}^{r_i=r_o} dq = \int_{r_i=0}^{r_i=r_o} Ce^{-3\left(\frac{r_i}{r_o}\right)2} 2\pi\, r_i\, dr_i \qquad 5.13$$

A non-dimensional equation is formed by substituting Eqns. 5.14 and 5.15 into Eqn. 5.13.

$$z = \left(\frac{r_i}{r_o}\right)^2 \qquad 5.14$$

$$2r_i dr_i = d\left(r_i^2\right) = r_o^2 d\left(r_i^2\right)/r_o^2 = r_o^2 d\left(\frac{r_i}{r_o}\right)^2 = r_o^2 dz \qquad 5.15$$

The finalized equation becomes Eqn. 5.16.

$$q_{pl} = \int_{z=0}^{z=1} Ce^{-6z^2} \pi\, r_o^2 dz \qquad 5.16$$

The integral limits of Eqn. 5.13 are changed to non-dimensional values based on previous integral limits. Which are the maximum and minimum radii of the ring heat source involved. The only time Eqn. 5.14 is true is when the relationship $r_i = r_o$ is true, i.e. when z =1. Therefore, it is assumed that the upper integral limit is z =1 and the lower integral

limit is z =0. Eqn. 5.16 shows the final form of Eqn. 5.13 after the non-dimensional integral limits have been substituted. Taking the constants out of the integral and solving Eqn. 5.16 results in Eqn. 5.17 which is the equation for the heat liberation rate, q_{pl}, of a moving circular disc heat source.

$$q_{pl} = 0.3167C\pi\ r_o^2 \qquad 5.17$$

Eqn. 5.17 is rearranged to solve for C by substituting for the heat liberation and radius (Eqn. 5.11).

$$C = \frac{q_{pl}}{0.3167\pi\ r_o^2} \qquad 5.18$$

Eqn. 5.18 is substituted into Eqn. 5.12 to provide Eqn. 5.19, representing the relationship between the heat liberation rate for a moving disc source and the radii of a circular disc heat source.

$$q_o = \frac{q_{pl}}{0.3167\pi\ r_o^2} e^{-3\left(\frac{r_i}{r_o}\right)^2} \qquad 5.19$$

Eqn. 5.19 is substituted into Eqn. 5.11 to obtain an equation for a moving circular heat source (Eqn. 5.20) accountable for multiple radii of a moving ring heat sources.

$$q_{Rg} = \left[\frac{q_{pl}}{0.3167\pi\ r_o^2} e^{-3\left(\frac{r_i}{r_o}\right)^2}\right] 2\pi\ r_i dr_i \qquad 5.20$$

Eqn. 5.20 is substituted into Eqn. 5.14 (the moving ring heat source in a semi-infinite medium) to obtain an equation for a circular disc heat source with a pseudo-Gaussian distribution of a specified heat intensity moving on the surface of a semi-infinite conduction medium equation (Eqn. 5.21).

$$\theta = \frac{q_{pl} v e^{-XV}}{4\lambda a (0.3167)\pi^{3/2} r_o^2} e^{-XV} \int e^{-3\left(\frac{r_i}{r_o}\right)^2} dr_i \int_{\omega=0}^{\omega=\frac{v^2 t}{4a}} \frac{d\omega}{\omega^{3/2}} e^{-\omega} e^{-\frac{u^2}{4\omega}} I\left(\frac{r_o V^2}{2\omega}\sqrt{\left(x+\frac{2\omega}{V}\right)^2 + y^2}\right) \quad 5.21$$

This equation is used to calculate temperatures for locations relative to the center of the heat source, where the filler wire contacts the welding arc. To simplify the model for welded pipes, the heat sources are modeled as welding a continuous flat plate. The plate is modeled such that the beginning point is also the end point. The heat sources are therefore modeled as on two plates one at the point of contact and the other as the trailing edge of the heat source by the pipe. The heat sources and their images account for the heat addition to the pipe material behind the primary heat source as it moves. The actual length of the modeled flat plate is the circumference of the pipe. Therefore, Figure 5.5 shows that the length of the pipe is added before and after the primary heat source to model the movement of the heat source on the material. As the heat source moves it affects the entire pipe. A secondary heat source is modeled trailing the primary heat source to provide a rise in temperature at the point of interest according to the effect of the heat source on the entire pipe. Figure 5.5 shows the analytical model for the current welding investigation. It shows the movement of the welding heat sources relative to the pipe at the beginning point, an intermediate point, and the end point of the weld. The intermediate point is used to label distance parameters. Figure 5.5 also shows two primary heat sources and two image heat sources moving material with adiabatic boundaries. The primary and secondary heat sources and their image coordinates are

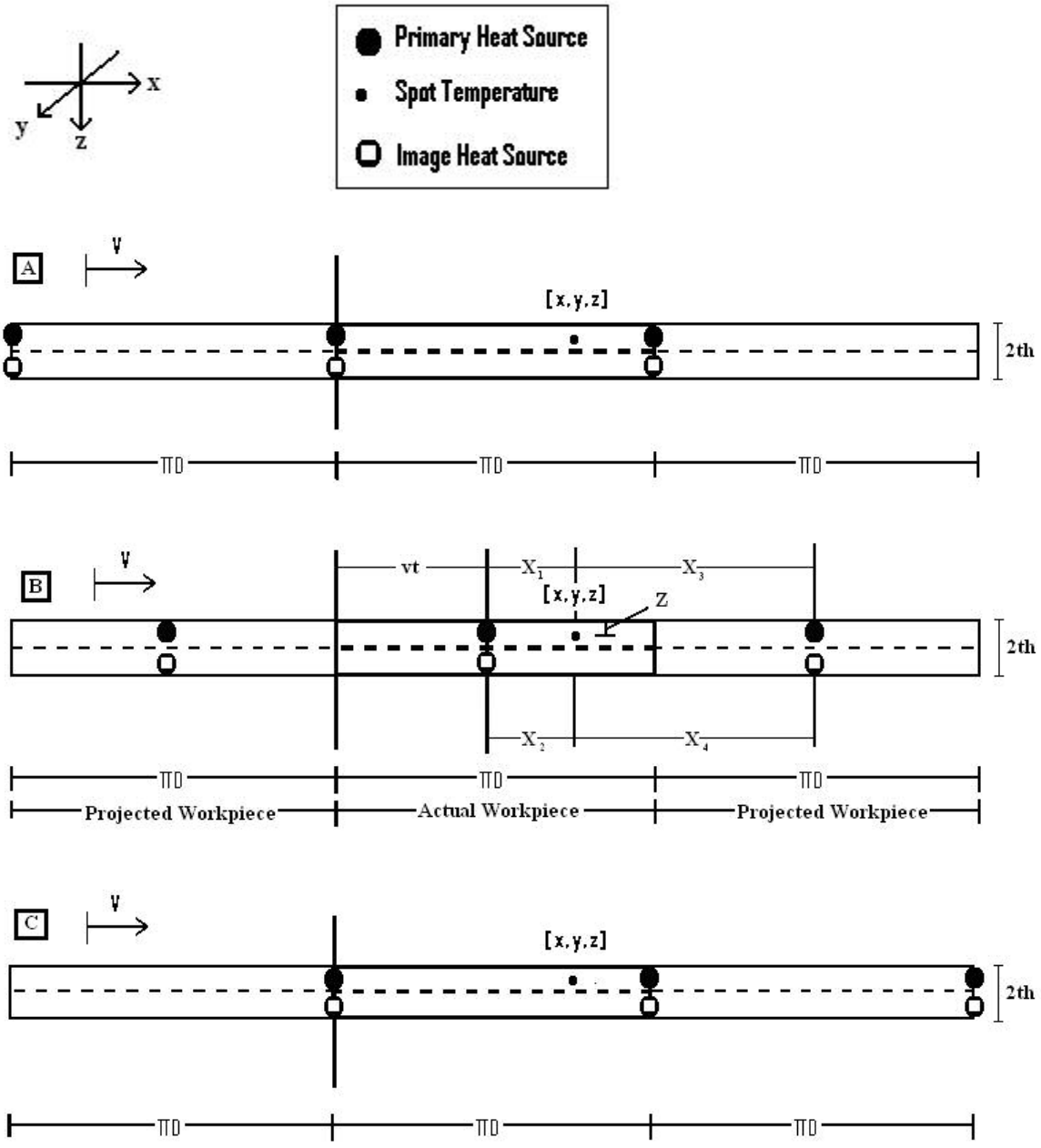

Figure 5.5: Schematic of a moving welding torch modeled on the pipe welding schematic heat source (a) at the beginning point during welding (b) heat source at an intermediate point during welding (with labeled nomenclature) and (c) heat source at the end point during welding

given by Eqns. 5.22 through 5.29. The secondary heat source is actually at the same spot as the primary heat source but modeled as a trailing heat source as shown in Figure 5.5. *X* is the distance from the heat source to the spot temperature in the X-direction (cm) and *D*

is the diameter of the welded pipes (cm). X_1 and Z_1 represent the primary heat source coordinates, X_2 and Z_2 represent the coordinates of the image of the primary heat source, X_3 and Z_3 represent the coordinates of the secondary heat source, and X_4 and Z_4 represent the coordinates of the image of the secondary heat source.

$$X_1 = X_1 \quad (5.22)$$

$$X_2 = X_2 \quad (5.23)$$

$$X_3 = \pi D - X_1 \quad (5.24)$$

$$X_4 = \pi D - X_2 \quad (5.25)$$

The *Z* variables represent the distance from the heat source to the primary and secondary heat sources and respective heat source images by their location in the Z direction (cm) and *th* is the thickness of the pipe (cm).

$$Z_1 = Z \quad (5.26)$$

$$Z_2 = 2(th) - Z \quad (5.27)$$

$$Z_3 = Z \quad (5.28)$$

$$Z_4 = 2(th) - Z \quad (5.29)$$

Substitution of Eqns. 5.22 through 5.29 into Eqn. 5.11 results in Eqns. 5.30 through 5.33, representing the distance from the heat source to the spot temperature (cm).

$$u_o^2 = r_o^2 + x^2 + y^2 + z^2 \quad (5.30)$$

$$u_1^2 = r_o^2 + (\pi D - X)^2 + y^2 + Z^2 \quad (5.31)$$

$$u_2^2 = r_o^2 + X^2 + y^2 + (2th - Z)^2 \quad (5.32)$$

$$u_3^2 = r_o^2 + (\pi D - X)^2 + y^2 + (2th - Z)^2 \quad (5.33)$$

Substituting distance relationships (Eqns. 5.30 through 5.33) into Eqn. 5.21 results in an equation that determines the temperatures at specified distances within the X-, Y-, Z-coordinate system for welding.

The VBA code representing the analytical solution is given in Appendix III and the VBA code used for calculations involving experimentally collected data is given in Appendix II. Within the two VBA codes, distance measurements are provided in mm and converted into cm within the program for calculations, as labeled in the analytical solution.

5.3 Analytical Plotting

The analytical solution provided in this chapter is provided in the form of a VBA code in Appendix III. The VBA code is used to calculate temperatures with essentially the same parameters as that used in the experiments. They are entered into a prepared user data interface and the results are plotted in the X-Y plane to produce comparable temperature distribution images. Figure 5.6 shows the temperature distribution for the 17s of the weld as predicted by the analytical solution. A millimeter scale for the X and Y coordinates are used for comparison of the analytical and experimental images at the same time instance in Chapter 6 Results and Discussion.

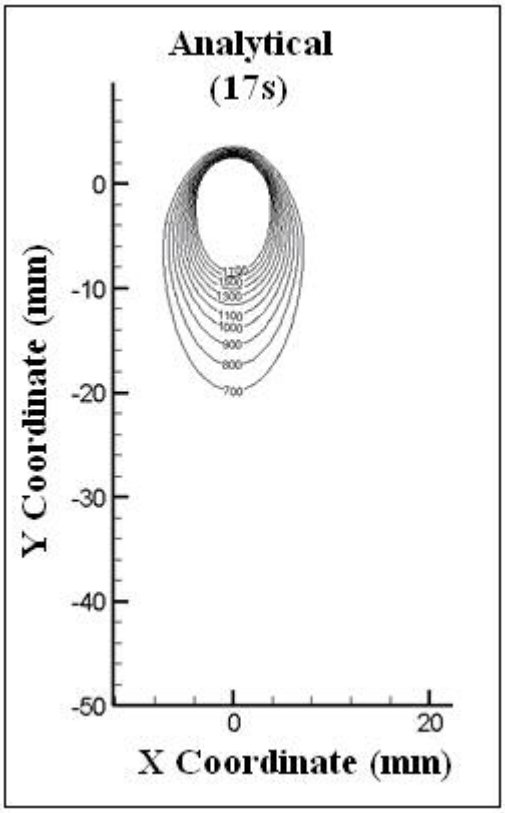

Figure 5.6: Analytical TecPlot plotted temperature isotherm distribution 17 s after welding was initiated

CHAPTER 6

RESULTS AND DISCUSSION

6.1 MIG Welding

Welding parameters used and the weld pipe dimensions in this investigation are given in Table 6.1. The weld velocities used are 0.514, 0.545, and 0.656 cm/s. Temperature data chosen in the current investigation was obtained for each weld velocity. Dimensions of the V-groove, workpiece, and experimental setup were kept constant for this investigation. Only the velocity of the workpiece is varied. The images collected at a weld velocity of 0.545 cm/s were included to show that the infrared camera can determine the sensitivity of the thermal field by detecting geometric isotherm variations, namely, arc position, penetration depth, and weld parameters, as concluded by Khan *et al.* [8]. Experimental and analytical results obtained for the weld velocities of 0.545 cm/s and 0.514 cm/s are given in Appendix IV and V, respectively. Three sequential velocities are chosen to demonstrate geometrical changes in the temperature isotherms relative to weld velocity.

Experimental parameters are recorded and entered into the analytical model interface by the user for each experimental test, as shown in Table 6.2. Arc velocity, arc beam radius, pipe thickness, thermal diffusivity, outer pipe diameter, elapsed time, heat

liberation, number of data points (number of required spot temperatures according to x-y coordinates), thermal conductivity are parameters of interest. Data entry by the user

Table 6.1: Welding and workpiece parameters

Workpiece Material	A500/UNS K03000
Workpiece Outer Diameter, cm	2.56
Workpiece Inner Diameter, cm	2.44
Wall Thickness, cm	0.12
Welding Filler Wire Material	Mild Steel
Workpiece Hardness HRB (BHN)	74 (131)
Groove Angle, degrees	45
Tip Distance from the Workpiece, cm	0.1
Shield Gas, %	Argon 75% Carbon Dioxide 25%

(in the user interface) assures that the analytical solution is adaptable for multiple experimental parameters. Parameters used in the analytical work have similar values to those used in the experimental work. Assumptions made in the analysis are required for the arc beam radius, thermal diffusivity, and effective heat liberation values. The arc beam radius is assumed to have the same diameter as the filler wire feed, namely, 0.9 mm. The actual welding arc beam diameter is larger but the exact diameter was not known. Thermal diffusivity and material properties are required to calculate the effective heat liberation rate for welding. The material properties are assumed to be the same as those for AISI 1030 steel because the material property information was not available for ASTM A500 Grade B steel. The carbon content is similar, max of 0.30 by weight, for the two chosen steel materials. Overall composition for the two materials was found to be similar.

The effective heat liberation, q_{pl}, was calculated using Eqn 6.1 [20]. Variables

$$q_{pl} = (P - Lh_{total}) \qquad 6.1$$

present in Eqn. 6.1 include P, the effective power of the arc (W) and Lh_{total}, the total heat for fusion of the filler wire per unit of time (J/s). Eqn. 6.2 [20] is used to calculate the

effective power of the arc. The variables involved in Eqn. 6.2 include the voltage, V, (v), the current, I, (A), and the efficiency, η. The total heat for fusion of the filler wire per unit time is calculated using Eqn. 6.3 [20].

$$P = V\ I\ \eta \qquad 6.2$$

$$Lh_{total} = \left(\frac{\pi d_{fw}^{2}}{4}\right) \upsilon_{feed} \rho L \qquad 6.3$$

The variables involved in Eqn 6.3 include the diameter of the filler wire, $d_{fw,}$ (cm), the feed velocity of the wire, v_{feed}, (cm/s), the density of the workpiece, ρ, (g/cm^3), and the total heat of fusion, *L*, (J/g).

The weld velocity is not involved in the calculation of the effective heat liberation rate. So, the effective heat liberation rate remains the same for all weld velocities during the current investigation. Table 6.2 gives the parameters required to calculate (using Eqns. 6.1 through 6.3) the effective heat liberation rate. All values for the parameters in Table 6.1 are kept constant during the current experiment except for the welding current for which an average value was used. Large fluctuation in the current was observed using a digital output on the front of the arc welding machine.

Table 6.2: Effective heat liberation rate parameters

Welding voltage (V)	23
Welding current (A)	170
Arc efficiency	0.67
Filler wire diameter (cm)	0.09
Filler wire feed velocity (cm/s)	12.7
Latent heat of fusion (J/g)	276.3
Density of steel (g/cm^3)	7.85

The current differs in a range of 90 A through 325 A, the majority of the current readings being 170 A +/- 15 A during welding. For analytical calculations a welding current of 170 A was used as listed in Table 6.1.

6.2 Temperature Measurements

Isothermal temperature data collected with the infrared camera is converted from initial captured pixel temperature data into accurate dimensioned (mm) spot temperature data; according to recorded camera calibration specific data. During the current experimental setup proper NUC tables are used to capture pixel temperature data. The NUC 5 table was used to capture thermal images within the temperature range of 700°C to 1725°C. Each NUC table allows the capture of thermal images within a specified temperature range, as given in Table 6.3. NUC 4 and NUC 5 tables require the use of an NDF2 to prevent damage to the camera lenses while viewing temperatures greater than 400 °C. The steel pipes have an inconsistent surface emissivity. To create a constant and

Table 6.3: Non-uniform correctional (NUC) temperature range table [24]

Non-Uniformity Correction Table	Temperature Range (°C)
NUC0	0 to 60
NUC1	20 to 125
NUC2	70 to 220
NUC3	140 to 350
NUC4**	300 to 700
NUC5**	600 to 1745
**Temperature range requires an ND2 filter	

known emissivity on the steel pipe surface a high heat black paint with an emissivity of 0.95 is used to coat the pipe surface. This assures the accuracy required by calibration calculations involving the infrared camera data and computer analysis of temperatures. Calibration of the camera was accomplished at NIST using a calibrated gray body. The calibration curve generated with the recorded data from NIST is shown in Figure 4.12

(Chaper 4). A difference in the recorded temperature and actual temperatures being viewed by the camera was observed for temperatures above ~ 575 ^{o}C. A correctional equation is generated to correct temperatures based on the NIST calibration curve presented.

6.3 Infrared Camera Imaging; Transient and Quasi-Steady State

The initial contact between the filler wire and the workpiece creates thermal shock in the workpiece because of the rapid increase in temperature from the workpiece temperature (room temperature of ~ 23 °C) to a temperature of 1100 °C, or higher, in less than 1 s, as shown in the first temperature frame of Figure 6.1. Pre-heating and post-heating techniques are suggested to prevent temperature shock in the workpiece.

Post heating methods were investigated by Mohandas *et al.* [13] and Olabi and Hashmi [11] to reduce the negative effects of thermal shock induced by welding. In the current investigation no post-heating or pre-heating techniques were used. Isothermal temperature distributions begin at the contact point and increase in radial size as the distance from the contact point increases. Observation of the isothermal temperature distribution geometries in recorded images is used to determine if the weld has reached a quasi-steady state. In the present investigation, a quasi-steady state is found to be reached at different time periods depending on the weld velocity. Changes in the geometry of isotherms during the transitional time between the transient state and the quasi-steady state conditions were observed using multiple images. The images were taken over the period of 1 s thru 20 s in 1 s intervals in sequential order for the weld velocities of 0.656, 0.545, and 0.514 cm/s as shown in Figure 6.1, Appendix IV, and Appendix V, respectively. To demonstrate that a quasi-steady state was maintained after

it is identified through observation, three later thermal images were taken at time intervals of 21 s, 25 s, and 29 s. The later images are shown for the weld velocities of 0.656, 0.545, and 0.514 cm/s in Figure 6.2 and Appendix IV and V, respectively.

Table 6.4 gives the welding parameters entered by the user for the analytical model of the current investigation for the weld velocity of 0.656 cm/s. The user must enter the time elapsed, as provided by sequential Dynamite® frames, and the number of experimental points, as provided by the experimental calibration corrective interface. Figure 6.1 shows experimentally produced temperature isotherms for the first 20 s of the weld intervals in intervals of 1 s. Figure 6.2 shows experimental temperature isotherms at 21 s, 25 s, and 29 s. Parameters are taken from the ASME Material Property books, and measurements taken directly from the workpiece. Temperature data is input to a VBA code to calculate corrected temperatures with distances (mm) relative to the center of the isotherms. The user must enter a positive numerical value for the time elapsed (s) and the number of experimental data points. Temperature isotherms, as recorded by the infrared camera, and corrected temperature plots of experimental images are compared in Figure 6.1.

Table 6.4: Analytical solution interface at weld velocity of 0.656 cm/s

Given Parameters	Value (Entered by User)	Units
Welding Speed (Arc Velocity)	6.560	mm/s
Arc Beam Radius	0.900	mm
Thickness of Steel Pipe	0.762	mm
Thermal Diffusivity	0.136	cm^2/s
Pipe (outer) diameter	165	mm
Time Elapsed		s
No of Experimental Data Points		
Heat Liberation Qpl	2444.46	W
Thermal Conductivity	0.52	J/(cm.s.K)
Z-Coordinate	0	cm

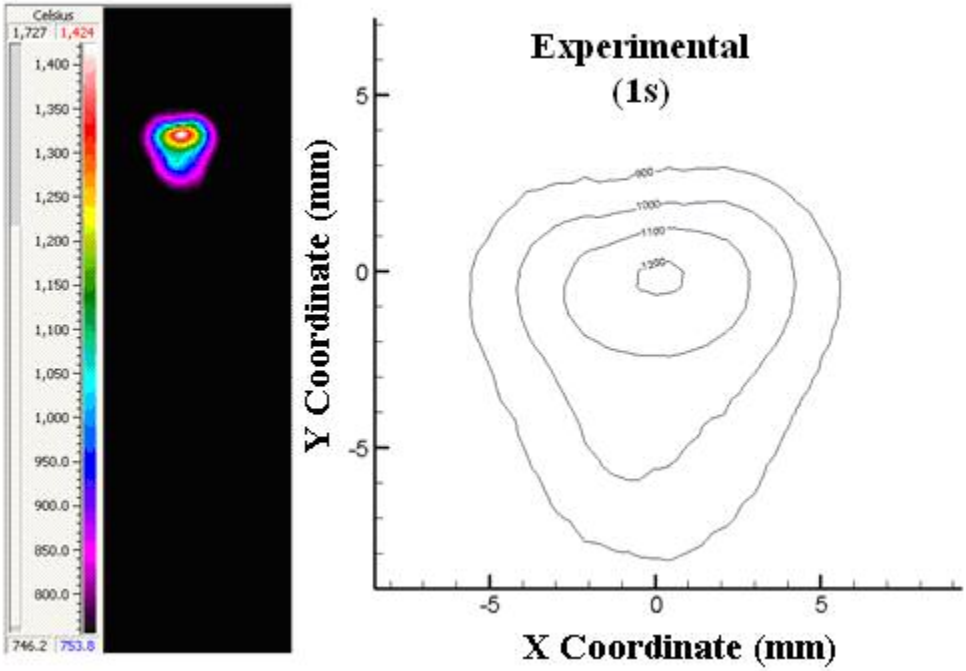
Celsius
1,727
1,424
1,400
1,350
1,300
1,250
1,200
1,150
1,100
1,050
1,000
950.0
900.0
850.0
800.0
746.2
753.8
Experimental
(1s)
Y Coordinate (mm)
X Coordinate (mm)
5
0
-5
-5
0
5

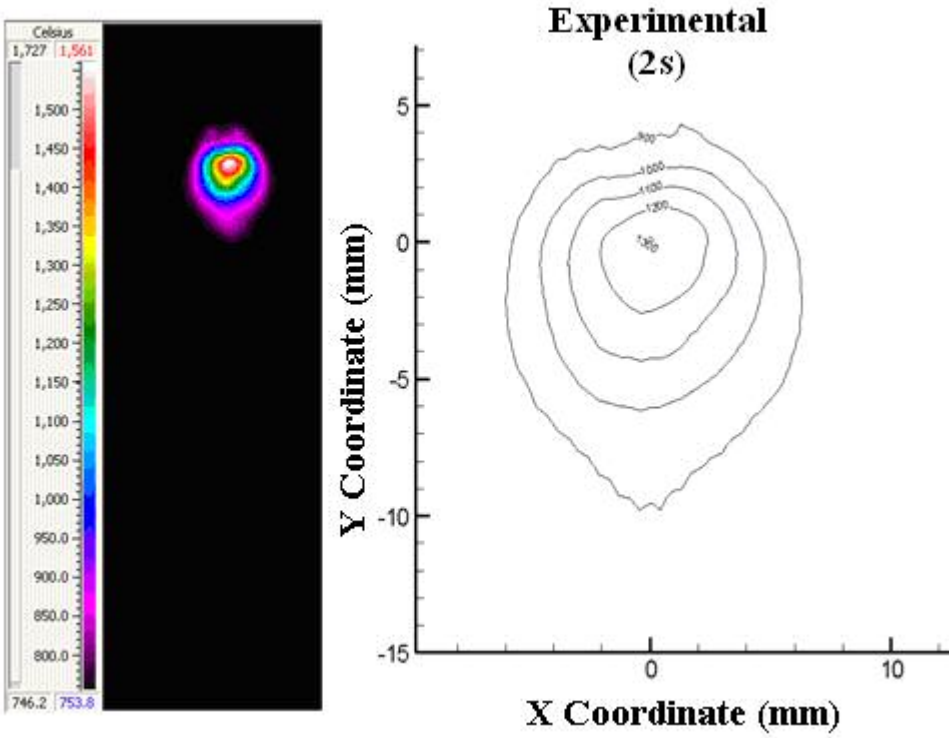
Celsius
1,727
1,561
1,500
1,450
1,400
1,350
1,300
1,250
1,200
1,150
1,100
1,050
1,000
950.0
900.0
850.0
800.0
746.2
753.8
Experimental
(2s)
Y Coordinate (mm)
X Coordinate (mm)
5
0
-5
-10
-15
0
10

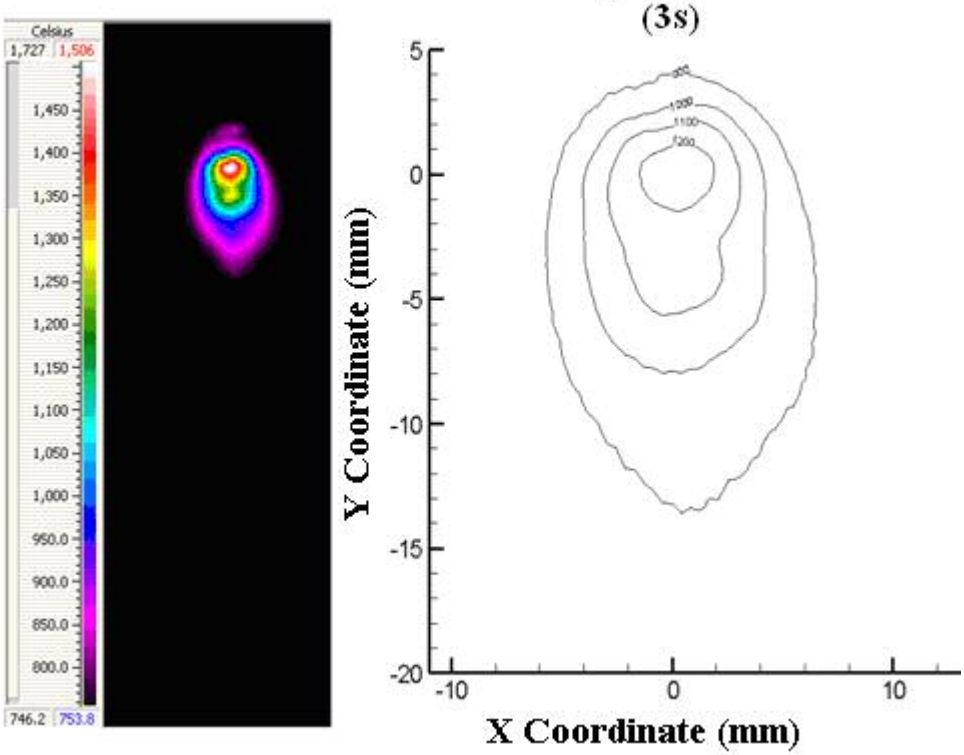
Celsius
1,727
1,506
1,450
1,400
1,350
1,300
1,250
1,200
1,150
1,100
1,050
1,000
950.0
900.0
850.0
800.0
746.2
753.8
Experimental
(3s)
Y Coordinate (mm)
X Coordinate (mm)
5
0
-5
-10
-15
-20
-10
0
10

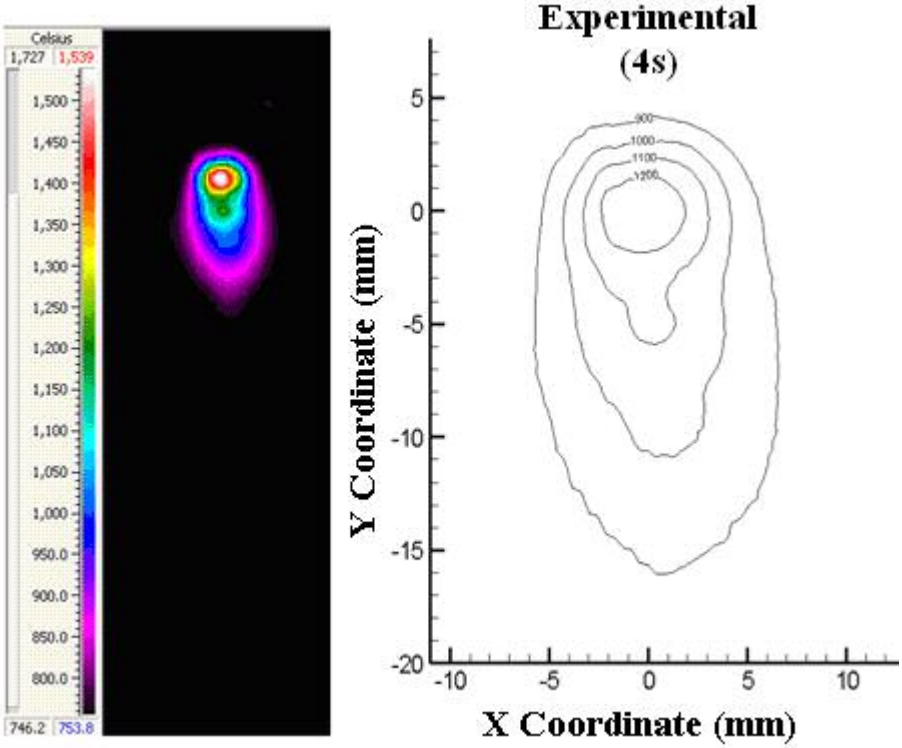
Celsius
1,727
1,539
1,500
1,450
1,400
1,350
1,300
1,250
1,200
1,150
1,100
1,050
1,000
950.0
900.0
850.0
800.0
746.2
753.8
Experimental
(4s)
Y Coordinate (mm)
X Coordinate (mm)
5
0
-5
-10
-15
-20
-10
-5
0
5
10

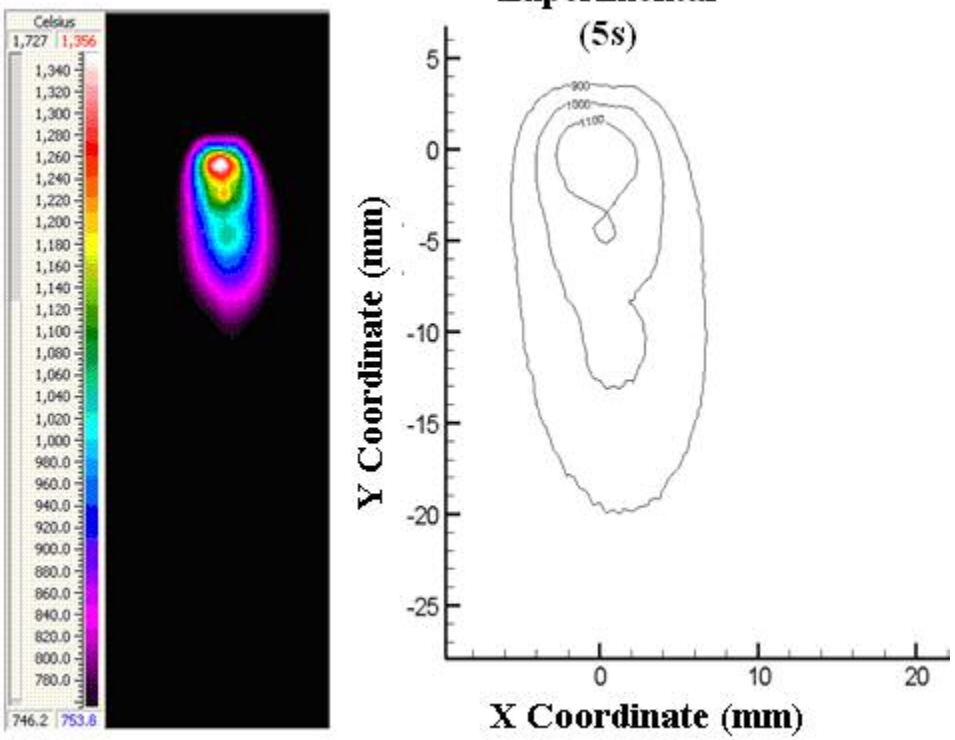
Celsius
1,727
1,356
1,340
1,320
1,300
1,280
1,260
1,240
1,220
1,200
1,180
1,160
1,140
1,120
1,100
1,080
1,060
1,040
1,020
1,000
980.0
960.0
940.0
920.0
900.0
880.0
860.0
840.0
820.0
800.0
780.0
746.2
753.8
Experimental
(5s)
Y Coordinate (mm)
X Coordinate (mm)
5
0
-5
-10
-15
-20
-25
0
10
20
900
1000
1100

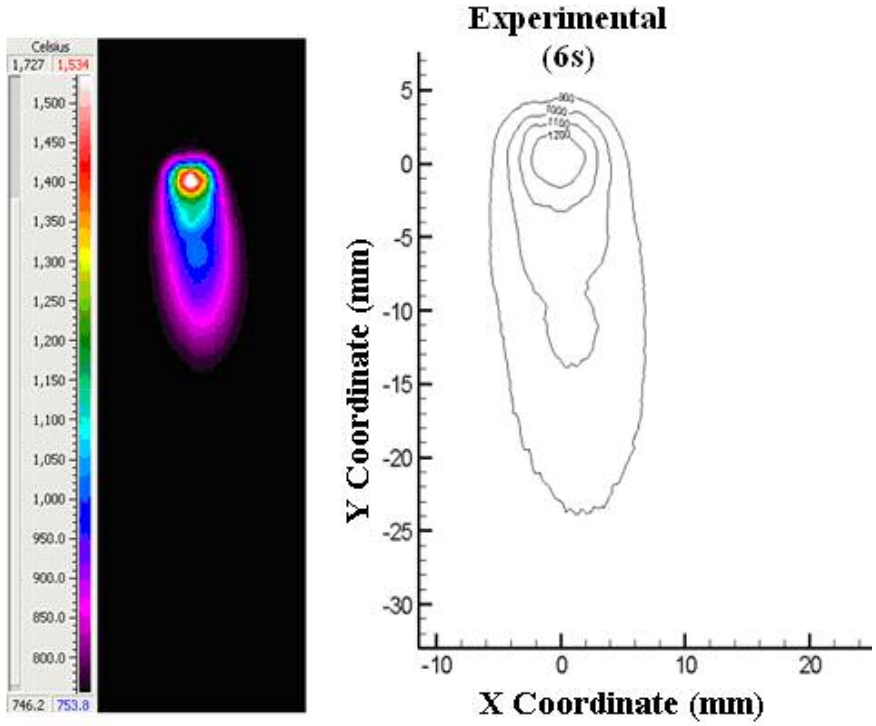
Celsius
1,727
1,534
1,500
1,450
1,400
1,350
1,300
1,250
1,200
1,150
1,100
1,050
1,000
950.0
900.0
850.0
800.0
746.2
753.8
Experimental
(6s)
Y Coordinate (mm)
X Coordinate (mm)
5
0
-5
-10
-15
-20
-25
-30
-10
0
10
20
900
1000
1100
1200

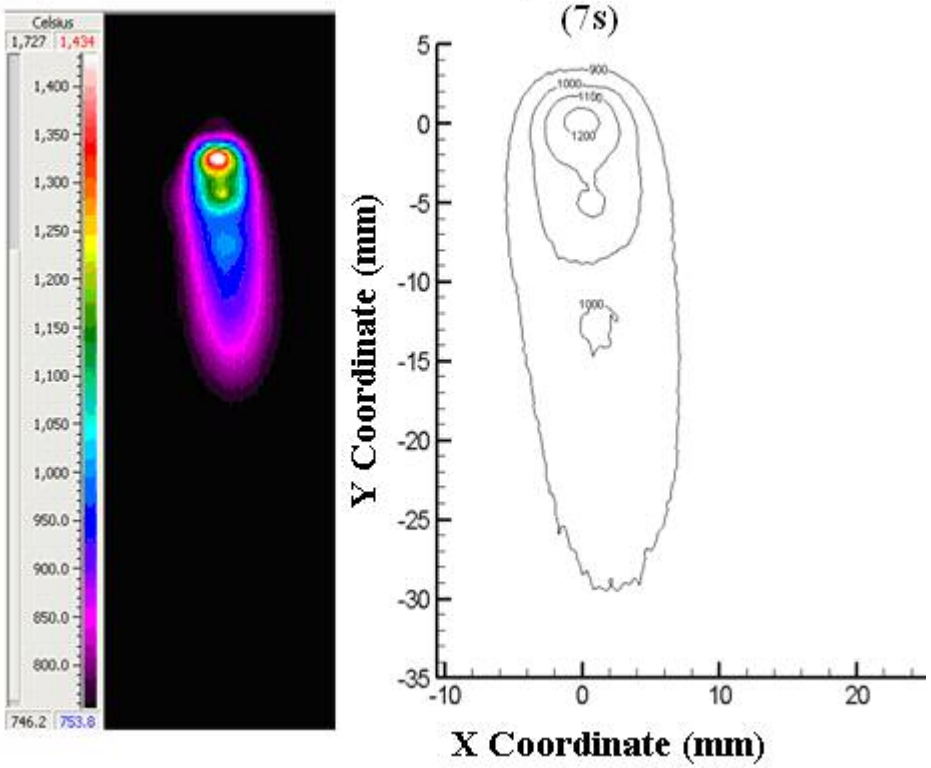
Celsius
1,727
1,434
1,400
1,350
1,300
1,250
1,200
1,150
1,100
1,050
1,000
950.0
900.0
850.0
800.0
746.2
753.8
Experimental
(7s)
Y Coordinate (mm)
X Coordinate (mm)
5
0
-5
-10
-15
-20
-25
-30
-35
-10
0
10
20
900
1000
1100
1200
1000

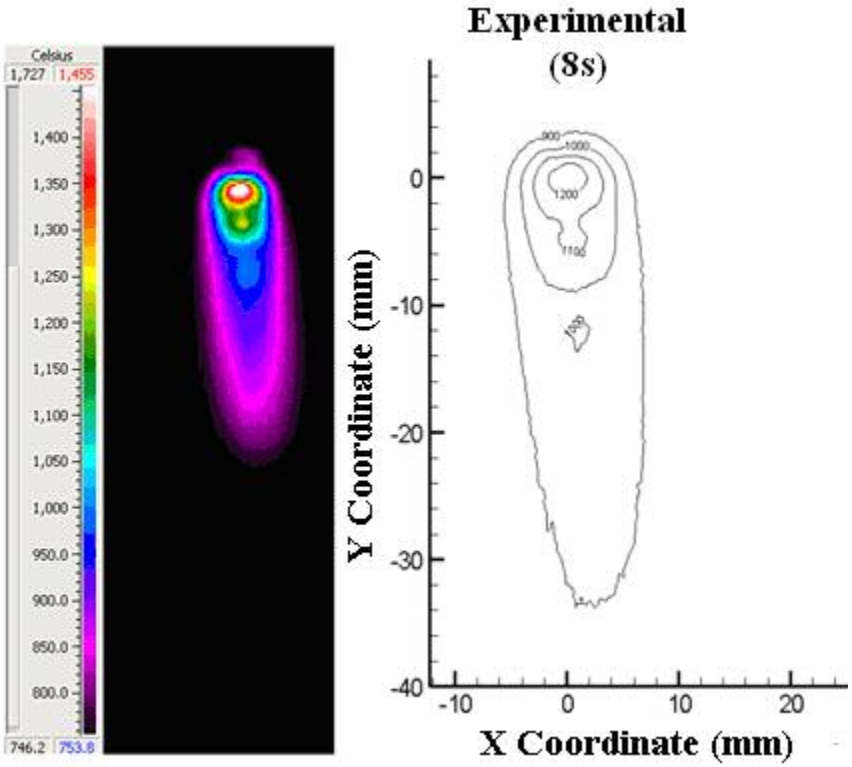
Celsius
1,727
1,455
1,400
1,350
1,300
1,250
1,200
1,150
1,100
1,050
1,000
950.0
900.0
850.0
800.0
746.2
753.8
Experimental
(8s)
Y Coordinate (mm)
X Coordinate (mm)
0
-10
-20
-30
-40
-10
0
10
20
900
1000
1200
1100

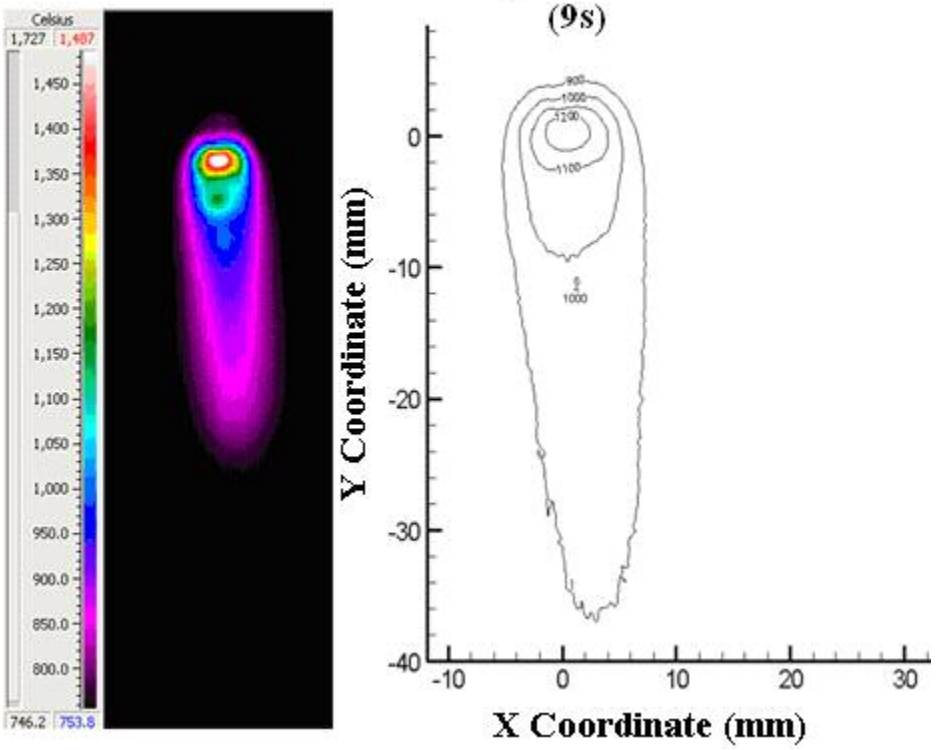
Celsius
1,727 1,487
1,450
1,400
1,350
1,300
1,250
1,200
1,150
1,100
1,050
1,000
950.0
900.0
850.0
800.0
746.2 753.8
Experimental
(9s)
Y Coordinate (mm)
X Coordinate (mm)
0
-10
-20
-30
-40
-10
0
10
20
30

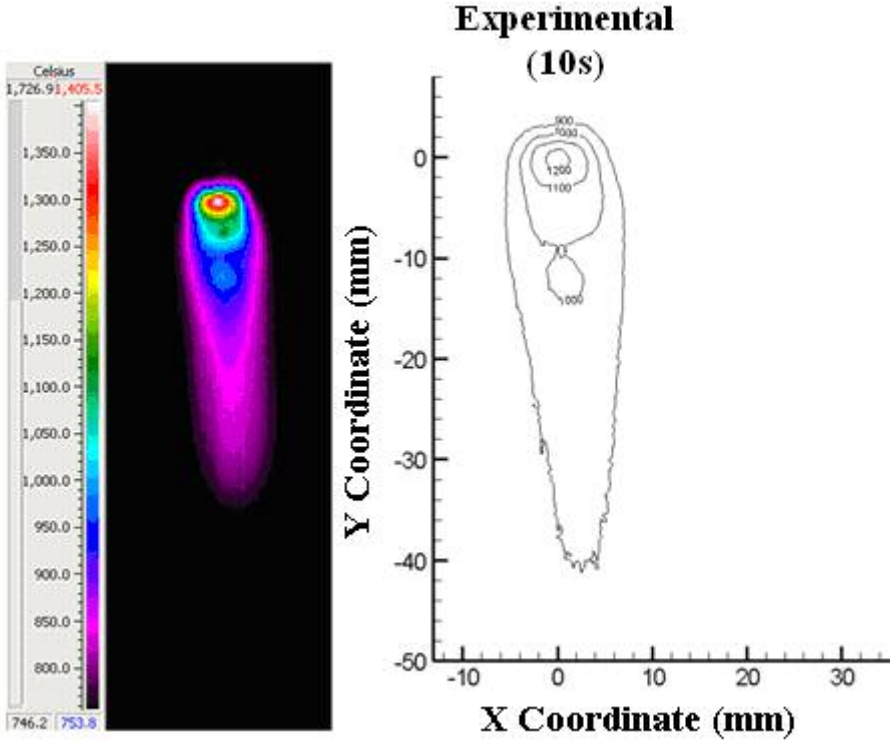
Celsius
1,726.91,405.5
1,350.0
1,300.0
1,250.0
1,200.0
1,150.0
1,100.0
1,050.0
1,000.0
950.0
900.0
850.0
800.0
746.2 753.8
Experimental
(10s)
Y Coordinate (mm)
X Coordinate (mm)
0
-10
-20
-30
-40
-50
-10
0
10
20
30

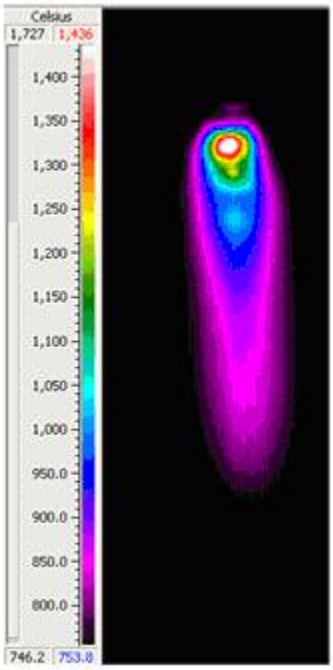
Celsius
1,727
1,436
1,400
1,350
1,300
1,250
1,200
1,150
1,100
1,050
1,000
950.0
900.0
850.0
800.0
746.2
753.8

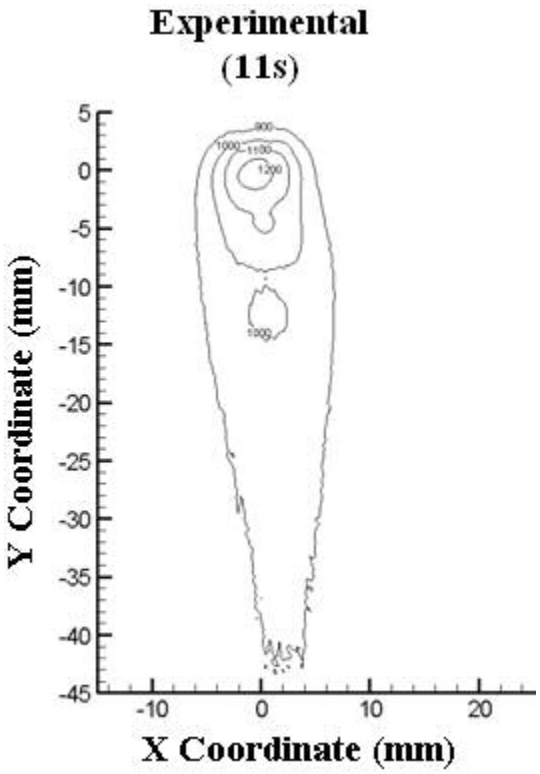
Experimental
(11s)
Y Coordinate (mm)
X Coordinate (mm)
5
0
-5
-10
-15
-20
-25
-30
-35
-40
-45
-10
0
10
20
900
1000
1100
1200
1300

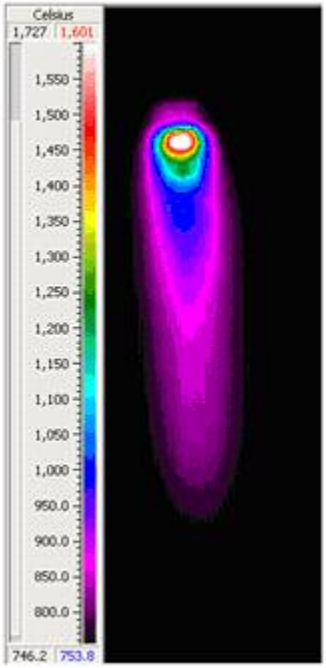
Celsius
1,727
1,601
1,550
1,500
1,450
1,400
1,350
1,300
1,250
1,200
1,150
1,100
1,050
1,000
950.0
900.0
850.0
800.0
746.2
753.8

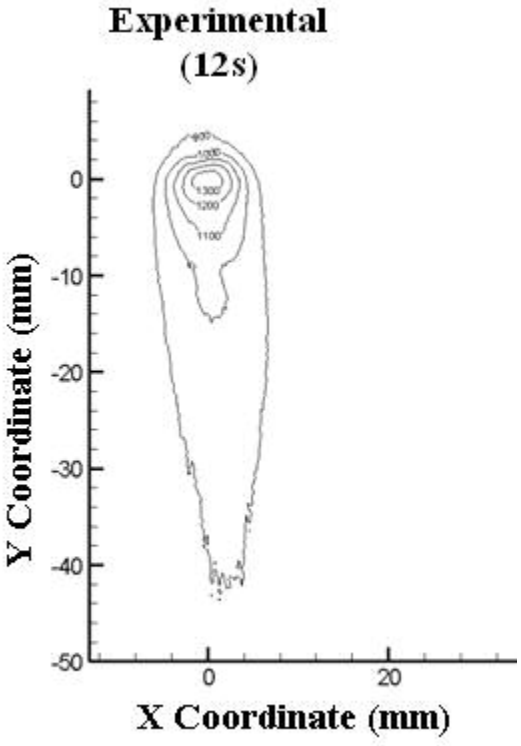
Experimental
(12s)
Y Coordinate (mm)
X Coordinate (mm)
0
-10
-20
-30
-40
-50
0
20
900
1000
1100
1200
1300

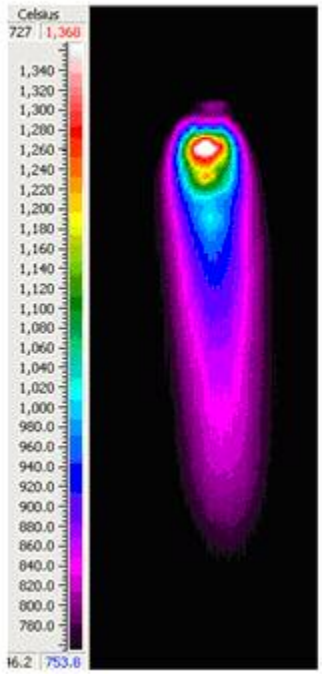
Celsius
727 1,360
1,340
1,320
1,300
1,280
1,260
1,240
1,220
1,200
1,180
1,160
1,140
1,120
1,100
1,080
1,060
1,040
1,020
1,000
980.0
960.0
940.0
920.0
900.0
880.0
860.0
840.0
820.0
800.0
780.0
16.2 753.8

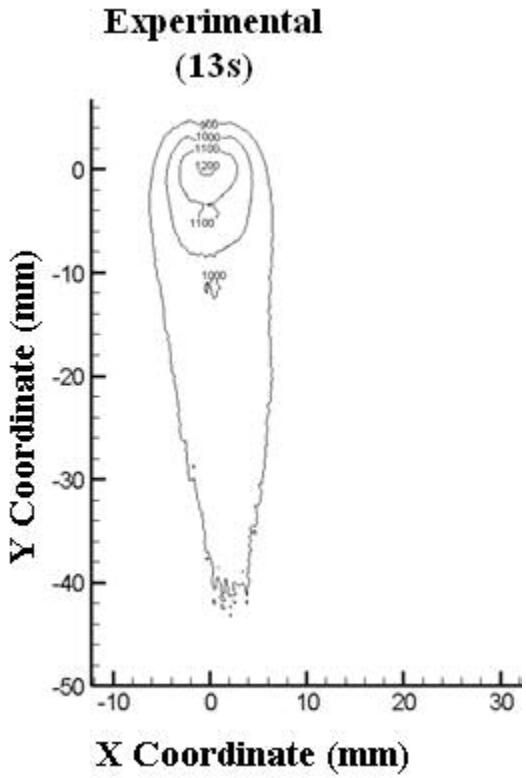
Experimental
(13s)
Y Coordinate (mm)
X Coordinate (mm)
0
-10
-20
-30
-40
-50
-10
0
10
20
30
900
1000
1100
1200
1100
1000

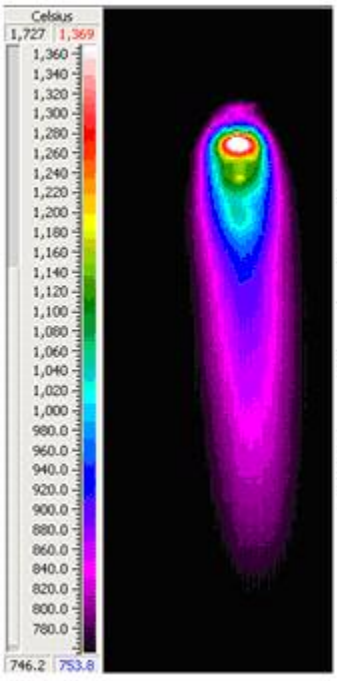
Celsius
1,727 1,369
1,360
1,340
1,320
1,300
1,280
1,260
1,240
1,220
1,200
1,180
1,160
1,140
1,120
1,100
1,080
1,060
1,040
1,020
1,000
980.0
960.0
940.0
920.0
900.0
880.0
860.0
840.0
820.0
800.0
780.0
746.2 753.8

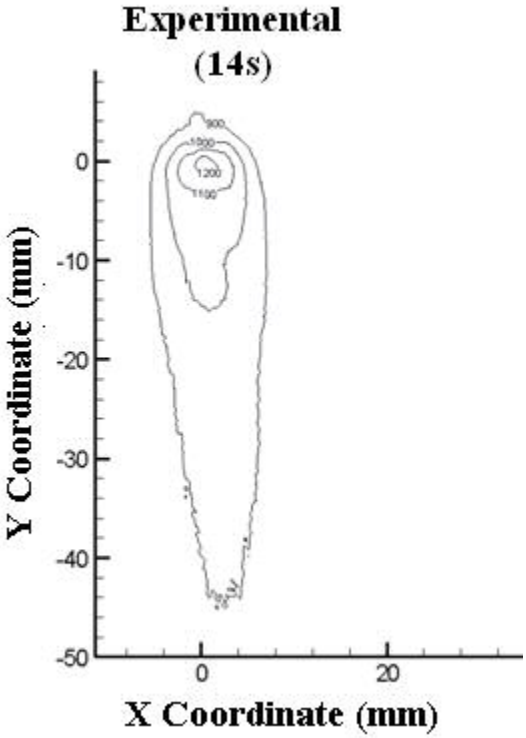
Experimental
(14s)
Y Coordinate (mm)
X Coordinate (mm)
0
-10
-20
-30
-40
-50
0
20
900
1000
1200
1100

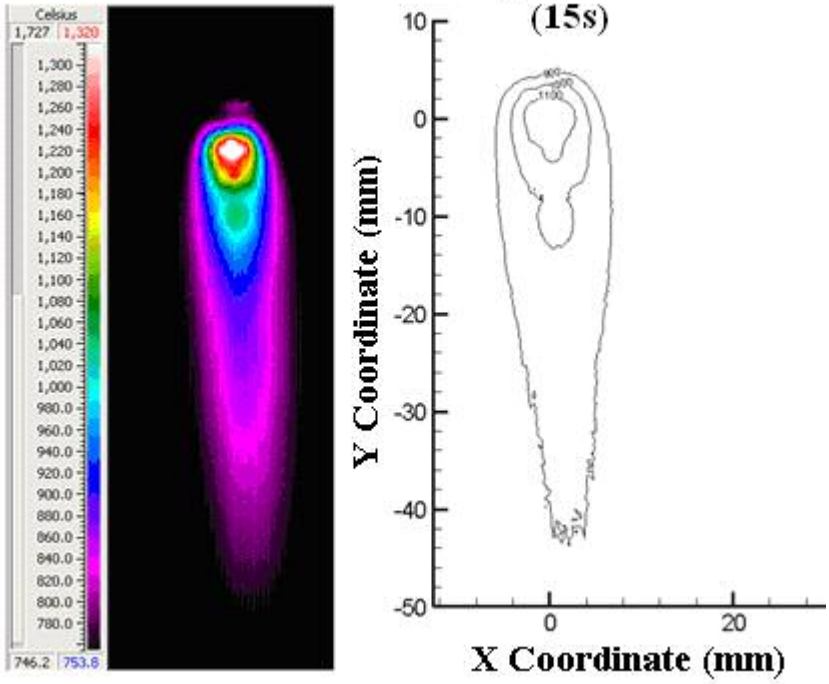
Celsius
1,727
1,320
1,300
1,280
1,260
1,240
1,220
1,200
1,180
1,160
1,140
1,120
1,100
1,080
1,060
1,040
1,020
1,000
980.0
960.0
940.0
920.0
900.0
880.0
860.0
840.0
820.0
800.0
780.0
746.2
753.8
Experimental
(15s)
Y Coordinate (mm)
X Coordinate (mm)
10
0
-10
-20
-30
-40
-50
0
20

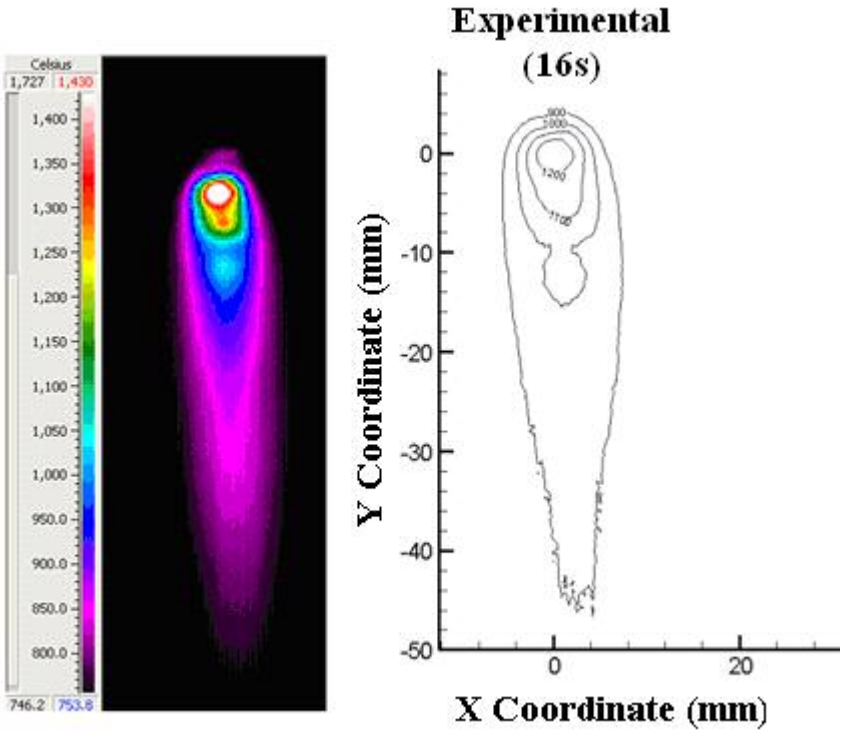
Celsius
1,727
1,430
1,400
1,350
1,300
1,250
1,200
1,150
1,100
1,050
1,000
950.0
900.0
850.0
800.0
746.2
753.8
Experimental
(16s)
Y Coordinate (mm)
X Coordinate (mm)
0
-10
-20
-30
-40
-50
0
20

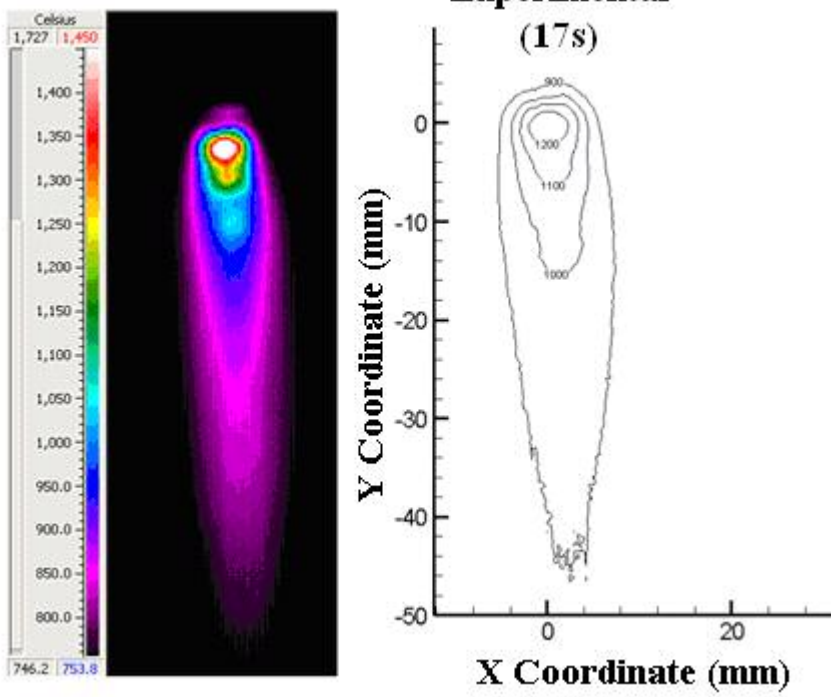
Celsius
1,727
1,450
1,400
1,350
1,300
1,250
1,200
1,150
1,100
1,050
1,000
950.0
900.0
850.0
800.0
746.2
753.8
Experimental
(17s)
900
1000
1100
1200
0
-10
-20
-30
-40
-50
Y Coordinate (mm)
0
20
X Coordinate (mm)

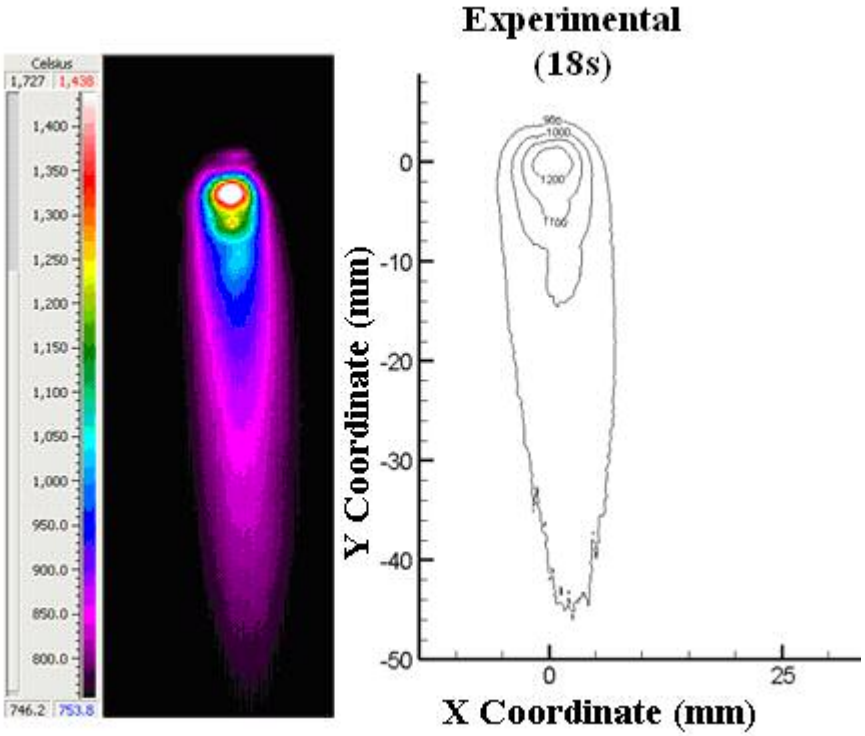
Celsius
1,727
1,438
1,400
1,350
1,300
1,250
1,200
1,150
1,100
1,050
1,000
950.0
900.0
850.0
800.0
746.2
753.8
Experimental
(18s)
900
1000
1100
1200
0
-10
-20
-30
-40
-50
Y Coordinate (mm)
0
25
X Coordinate (mm)

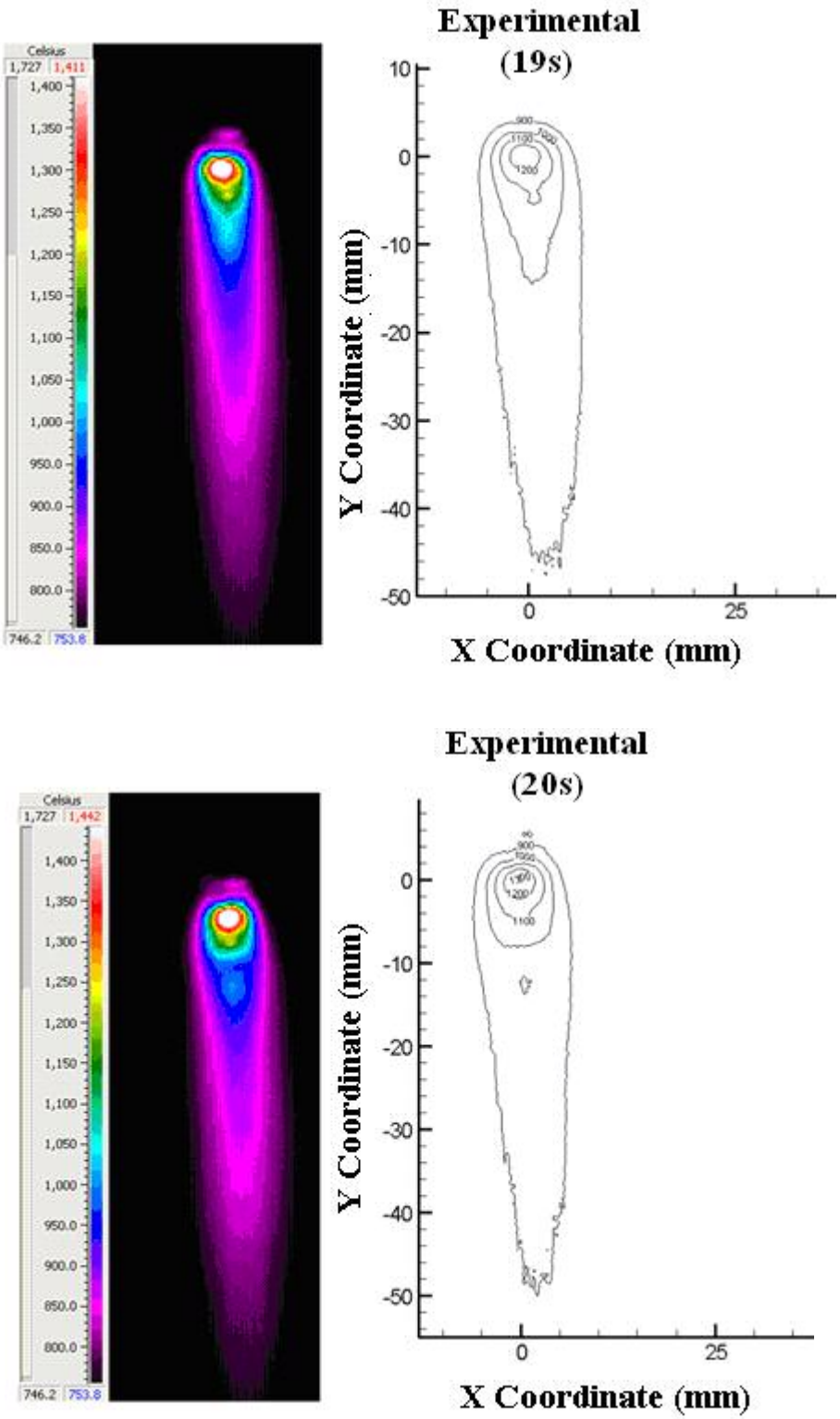

Figure 6.1: Transient to quasi-steady state temperature distributions for the experimental data at 1 s to 20 s in 1 s intervals for a welding velocity of 0.656 cm/s

It is shown that isotherms reach a quasi-steady state, for a weld velocity of 0.656 cm/s, at ~ 14 s. Isothermal temperature distribution geometry becomes semi-constant, although fluctuation of the isotherm geometry, length, width, and borders occur during the welding process as shown at 1 s intervals (Figure 6.1). It is observed that the 1000°C isotherm is approximately 18 mm in length after the quasi-steady state has been reached. The 1000°C isotherm sometimes splits into two separate isotherms; this is acknowledged by welders to be a molten slag pool and is watched to determine the quality of a weld. To demonstrate the consistency or inconsistency of the temperature distribution during the entire welding procedure after quasi-steady state is identified, Figure 6.2 provides three later images at 19 s, 25 s, and 29 s. It is noted that the 900°C isotherm (the outermost isotherm) varies in length along the y axis from 48 mm to 55 mm after the quasi-steady state has been reached. The connection point temperature (greatest spot temperature) varies from 1200 to 1400°C for the weld velocity of 0.656 cm/s. The geometry of the temperature isotherms is not symmetric about any axis and the borders are jagged (not smooth). Spatter is visible in the recorded images and is represented by temperature distributions in the form of small isotherms outside of the 900°C isotherm. There is no scale measurement for the images recorded directly from the camera using Dynamite®. A millimeter scale is used to plot temperature isotherms after emissivity correction calculations are complete. The temperatures collected with the infrared camera are within the NUC 5 temperature range.

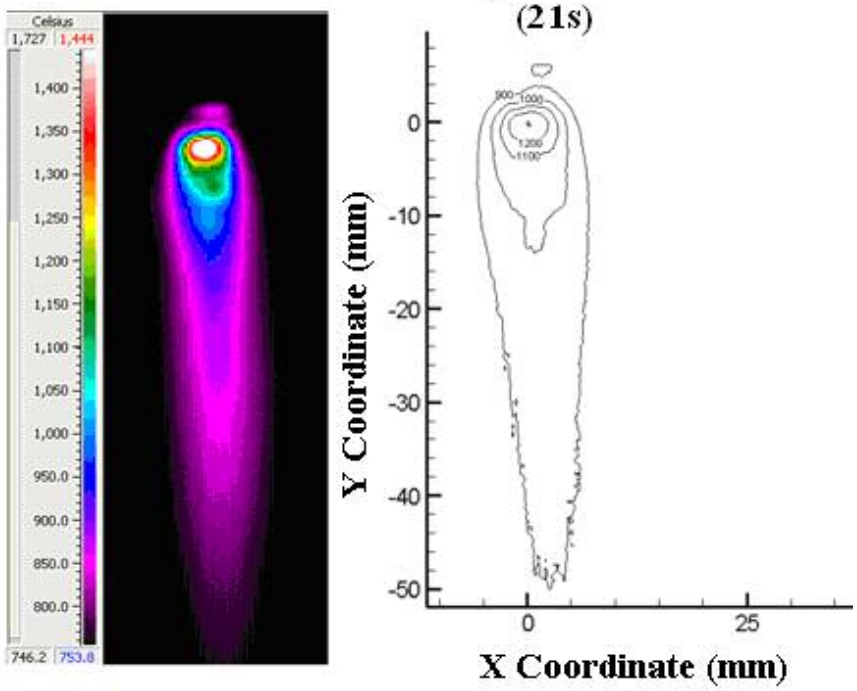
Celsius
1,727
1,444
1,400
1,350
1,300
1,250
1,200
1,150
1,100
1,050
1,000
950.0
900.0
850.0
800.0
746.2
753.8
Experimental
(21s)
0
-10
-20
-30
-40
-50
Y Coordinate (mm)
0
25
X Coordinate (mm)

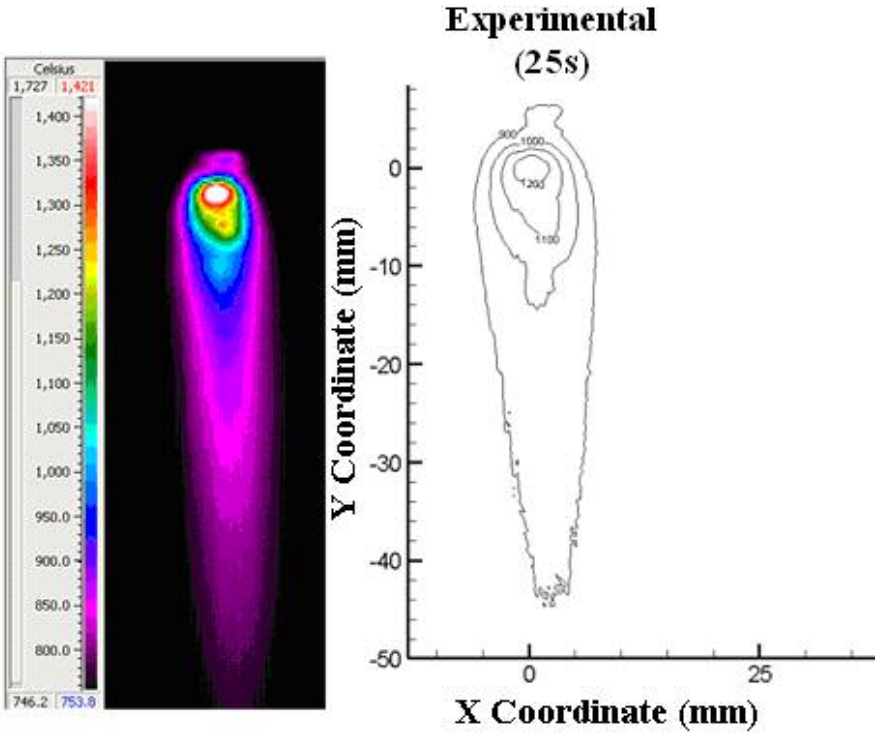
Celsius
1,727
1,421
1,400
1,350
1,300
1,250
1,200
1,150
1,100
1,050
1,000
950.0
900.0
850.0
800.0
746.2
753.8
Experimental
(25s)
0
-10
-20
-30
-40
-50
Y Coordinate (mm)
0
25
X Coordinate (mm)

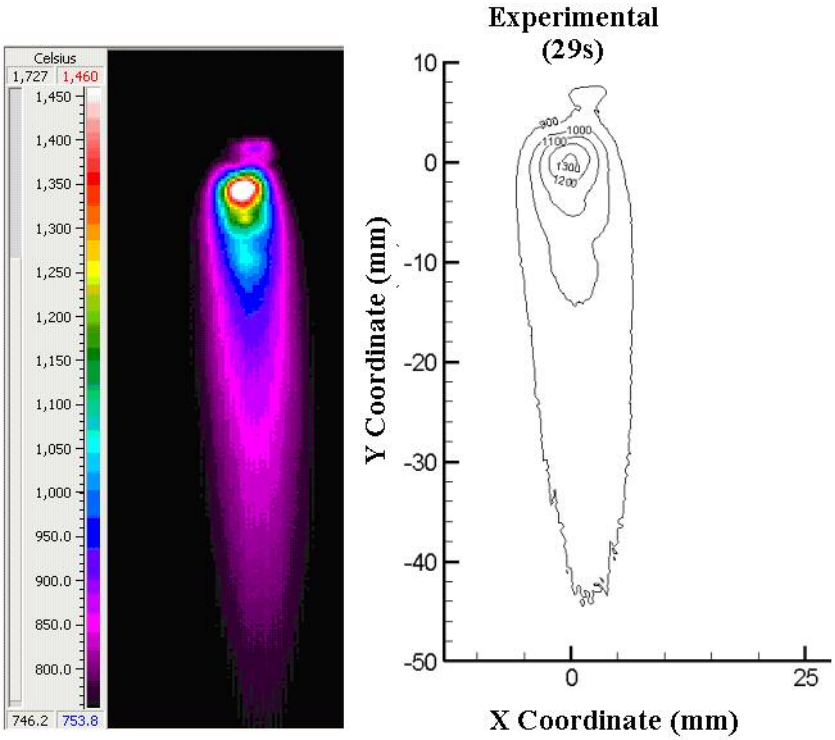

Figure 6.2: Quasi-steady state temperature distributions for the experimental data at 21 s, 25 s, and 29 s for a weld velocity of 0.656 cm/s

It is noted that the length of every isotherm varies during experimentation or each frame (60 frames per second were taken) but are reported per second. There is no explanation for this but it is assumed that ideal welding parameters (as assumed in the analytical model by Komanduri and Hou [20]) are not present and multiple welding parameters have a direct effect the temperature distribution. Other reasons for inconsistent isothermal temperature distribution geometry include unpredictable spot composition, material properties, and weld process quality.

Another significant difference is the placement of the welding wire with respect to the center of the V-groove. The weld isothermal temperature distribution is identified to reach a quasi-steady state at ~ 12 s for a weld velocity of 0.545 cm/s. It is noted that the weld made at a weld velocity of 0.545 cm/s was generated with a wire positioning

slightly right, as viewed by the camera, of the V-groove, effecting the isotherm length and width. Appendix IV gives thermal images as captured by the infrared camera, for the weld velocity of 0.545 cm/s, by the infrared camera and corrected with the emissivity and calibration calculations for the first 20 s of welding in 1s intervals and at 21 s, 25 s, and 29 s time intervals. The isotherms for the weld velocity of 0.545 cm/s are significantly shorter and wider than the isotherms produced by weld velocities of 0.656 and 0.514 cm/s. It is found through multiple experiments that when the filler wire is centered in the V-groove; the isotherm geometry is consistent with the weld velocities of 0.656 and 0.514 cm/s. Properly positioned filler wire produces isotherms that are shorter and wider than the isotherms produced at 0.656 cm/s but longer and thinner than the isotherms produced using a weld velocity of 0.514 cm/s. The variation in length and width of the isotherms with respect to the placement of the filler wire (s viewed by the infrared camera) is consistent with the conclusions of Khan *et al.* [8]. After reviewing the welding conditions it was observed that the welding filler wire was offset to the right of the center of the V-groove. It is assumed that this altered the way the heat was dissipated into the workpiece at the contact point in the connecting V-groove geometry. The outermost isotherm (900°C) length is 32 mm +/- 2 mm and the higher temperature isotherms are consistently shorter than those produced for weld velocities of 0.656 and 0.514 cm/s. The maximum temperature recorded during the weld velocity of 0.545 cm/s was over 1300°C, higher than the maximum temperature in either of the other weld velocities.

The third and final weld velocity reported for the current experiment is 0.514 cm/s. Appendix V provides experimentally captured thermal images by the infrared

camera for the weld velocity of 0.514 cm/s, by the infrared camera and corrected for the emissivity and calibration calculations for the first 20 s of welding in 1s intervals and at 21 s, 25 s, and 29 s time intervals. The isotherms are visibly shorter and wider than the isotherms produced during the weld velocity of 0.656 cm/s. There is no symmetry about an axis and the boundaries remain irregular as was found for all three weld velocities, namely, 0.656, 0.545, 0.514 cm/s, regardless of the filler wire positioning. For the weld velocity of 0.514 cm/s a quasi-steady state is reached at approximately 14 s.

6.4 Analytical Imaging; Transient and Quasi-Steady State

To determine when quasi-steady state conditions are reached for images produced by the analytical program, for each weld velocity, a temperature versus time graph is plotted. The coordinates provided are the same as those used in the experimental emissivity and calibration correctional calculations for spot temperatures. Table 6.4 shows the user interface of the analytical program for entry of parameters used for the spot temperature data for a weld velocity of 0.656 cm/s. Figures 6.3 and 6.4 show the first 20 s in 1 s intervals and at time instances of 21 s, 25 s, and 29 s, respectively for a weld velocity of 0.656 cm/s.

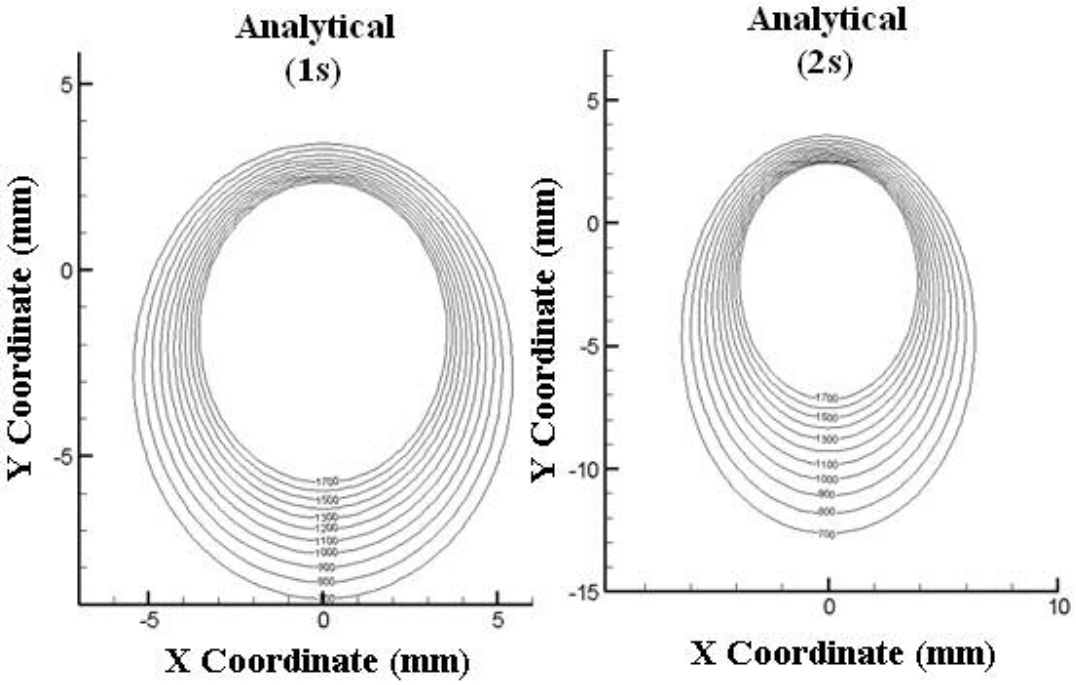
Analytical
(1s)
Y Coordinate (mm)
X Coordinate (mm)
Analytical
(2s)
Y Coordinate (mm)
X Coordinate (mm)

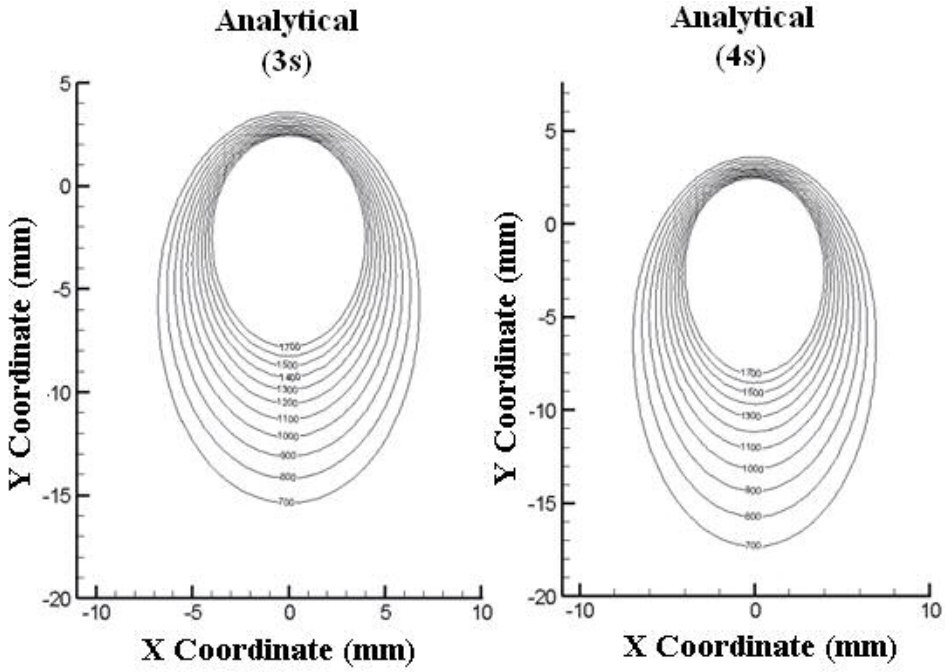
Analytical
(3s)
Y Coordinate (mm)
X Coordinate (mm)
Analytical
(4s)
Y Coordinate (mm)
X Coordinate (mm)

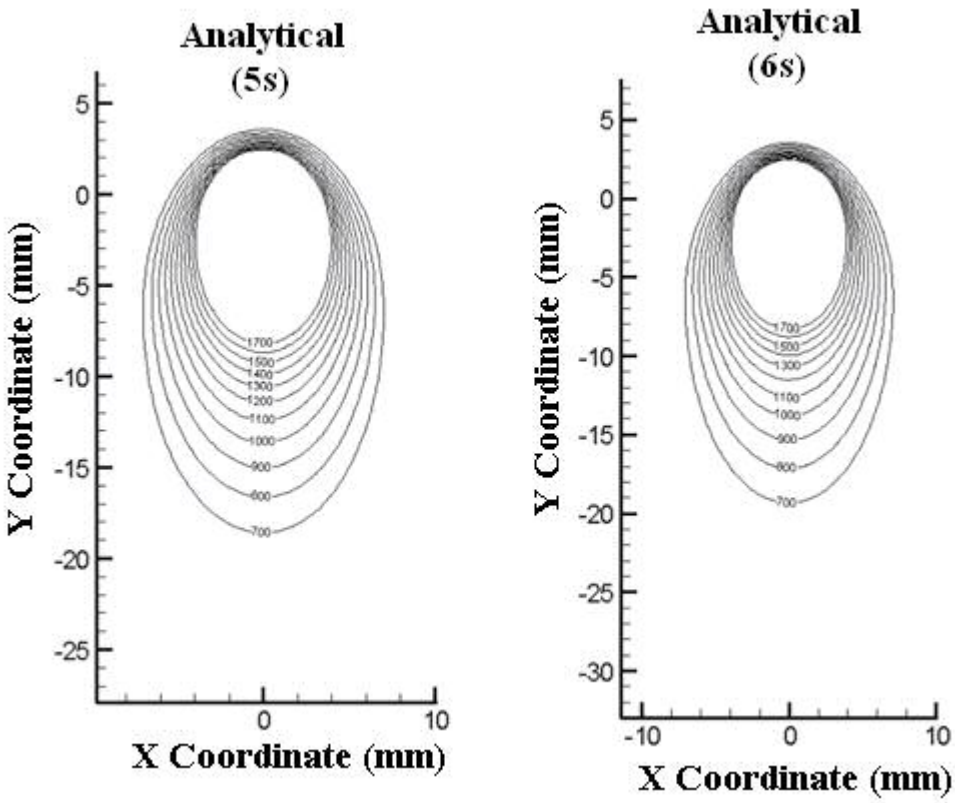
Analytical
(5s)
Y Coordinate (mm)
X Coordinate (mm)
Analytical
(6s)
Y Coordinate (mm)
X Coordinate (mm)

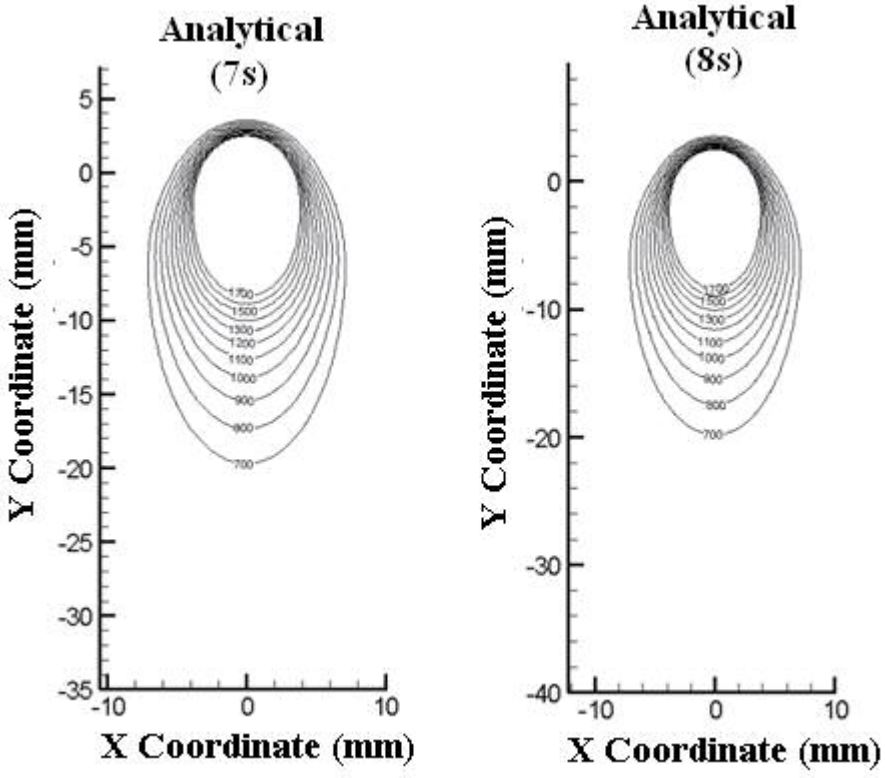
Analytical
(7s)
Y Coordinate (mm)
X Coordinate (mm)
Analytical
(8s)
Y Coordinate (mm)
X Coordinate (mm)

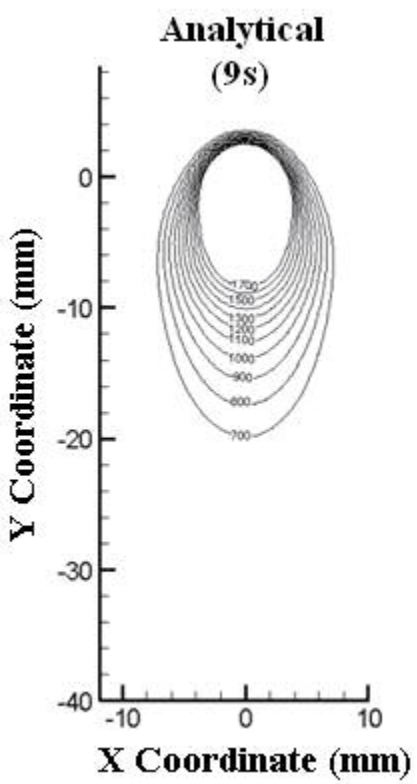
Analytical
(9s)
Y Coordinate (mm)
X Coordinate (mm)
0
-10
-20
-30
-40
-10
0
10
1700
1500
1300
1200
1100
1000
900
800
700

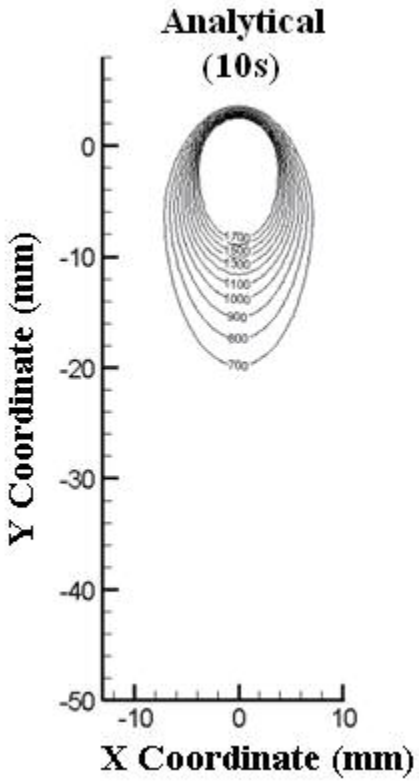
Analytical
(10s)
Y Coordinate (mm)
X Coordinate (mm)
0
-10
-20
-30
-40
-50
-10
0
10
1700
1500
1300
1100
1000
900
800
700

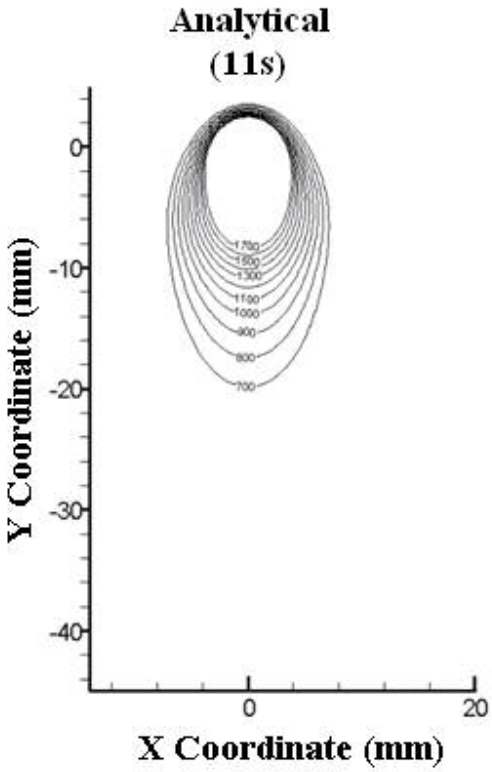
Analytical
(11s)
Y Coordinate (mm)
X Coordinate (mm)
0
-10
-20
-30
-40
0
20
1700
1500
1300
1100
1000
900
800
700

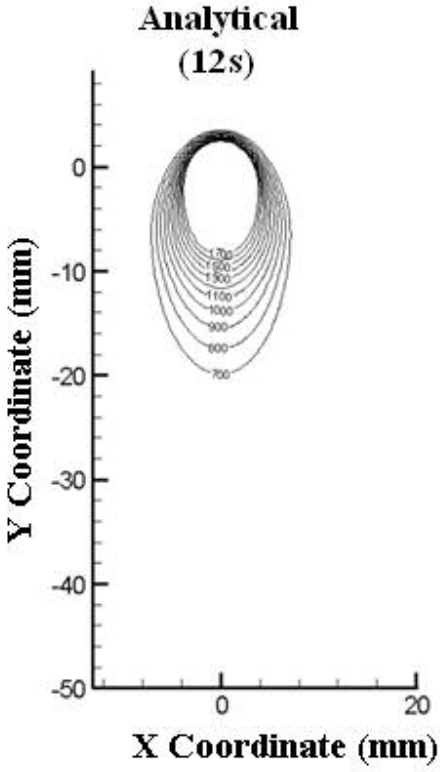
Analytical
(12s)
Y Coordinate (mm)
X Coordinate (mm)
0
-10
-20
-30
-40
-50
0
20
1700
1500
1300
1100
1000
900
800
700

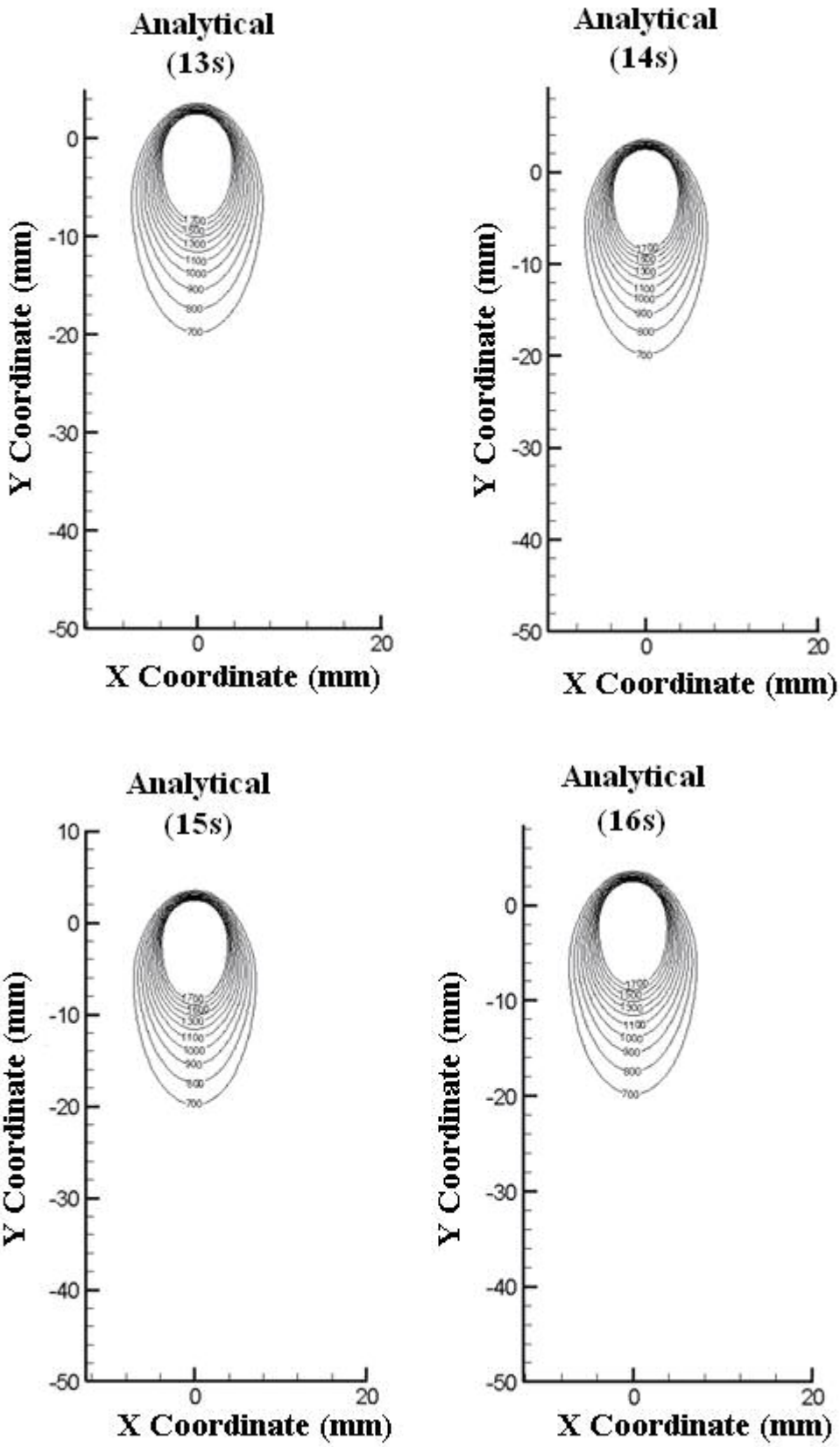
Analytical
(13s)
Analytical
(14s)
Analytical
(15s)
Analytical
(16s)
Y Coordinate (mm)
X Coordinate (mm)
0
-10
-20
-30
-40
-50
20
10
1700
1500
1300
1100
1000
900
800
700

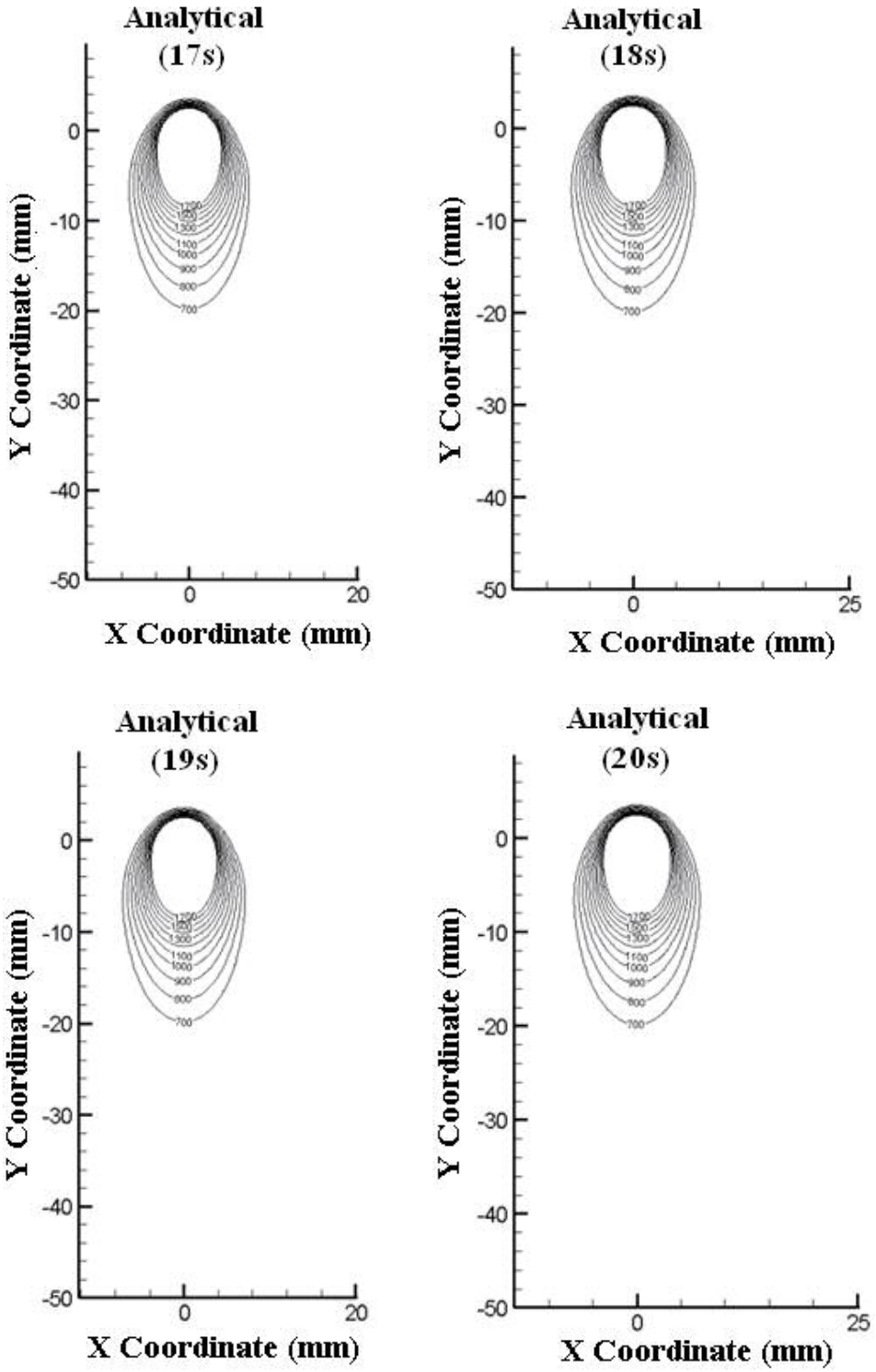

Figure 6.3: Analytically derived transient to quasi-steady state temperature distributions at 1 s to 20 s in 1 s intervals for a welding velocity of 0.656 cm/s

The analytically calculated (experimentally equivalent) temperature distribution images are provided for comparison with the corrected experimentally produced images for a weld velocity of 0.656 cm/s.

Quasi-steady state is calculated and observed to begin at 11 s after the welding contact is initiated. To demonstrate minor differences in temperature, once a quasi-steady state is reached, the analytical solution images at 21 s, 25 s, and 29 s for a weld speed of 0.656 cm/s are shown in Figure 6.4. The calculated isothermal temperature distribution for the analytical solution varies greatly from the experimentally produced isotherms. The isotherms are closer, symmetric about the Y axis (when positioned through the center of the contact point), and the length of the isotherms are shorter. Analytical and experimental isotherms to the front and to the sides of the heat source are closer together. As the distance from the contact point increases the spacing between the isotherms increases, especially behind the heat source. The maximum temperature occurs at the contact point and is predicted to be > 2000°C. It may be noted that analytical model is not applicable to molten materials but only to solid materials. So, the maximum temperature given in the experimental data was to be lower than the melting point of the material. The experimental method does not output dimensions for the molten area during welding. The outermost isotherm (700°C) of the analytical predications begins in a transient state with a length of ~ 12 mm and ends in a quasi-steady state with a length of ~ 25 mm. It is approximately double in length. The isotherm dimensions remain constant after the predicted quasi-steady state time interval of 11 s.

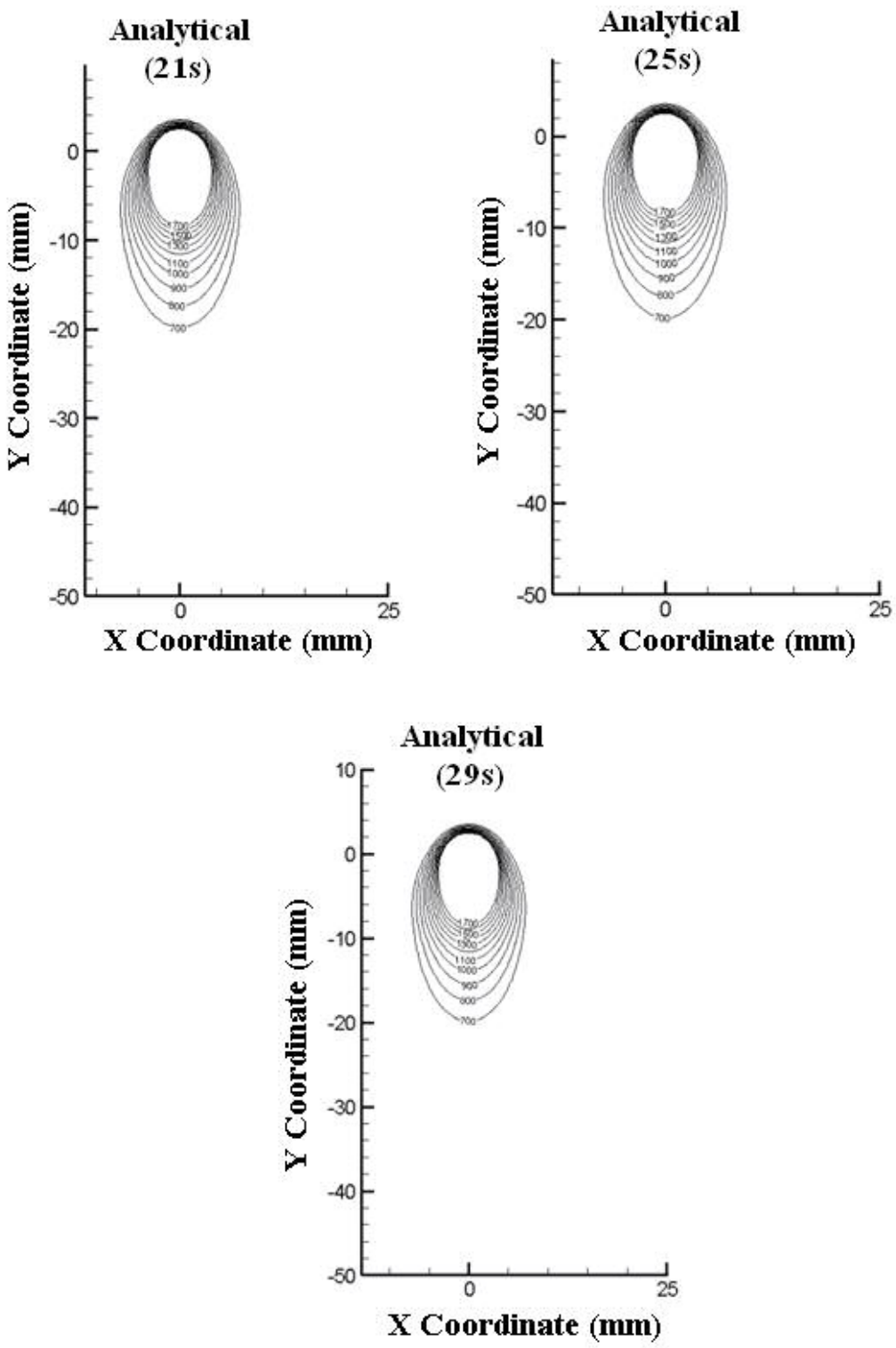

Figure 6.4: Analytical quasi-steady state, after 11 s, temperature distributions at 21 s, 25 s, and 29 s for a weld velocity of 0.656 cm/s

Analytical solution images produced in TecPlot for a velocity of 0.545 cm/s are given as in Appendix IV for the first 20 s in 1 s intervals and at 21 s, 25 s, and 29 s. The initial length of the isotherm at 1 s is 12 mm and the length after a quasi-steady state is reached in the 11 s; 25 mm

The analytical solution TecPlot images for a velocity of 0.514 cm/s are given as Appendix V for the first 20 s in 1 s intervals and at 21 s, 25 s, and 29 s. The initial length of the isotherm, at 1 s, is 12 mm and the length of 25 mm after a quasi-steady state is reached in the 11 s.

It is observed that the shape and size of the images obtained with the analytical solution do not differ sufficiently when plotted for each of the three different weld velocities. The outer isotherm, 700°C, has a consistent length of ~ 25 mm and a consistent width of ~ 30 mm after the quasi-steady state is observed. Each isotherm of a temperature > 700°C is shorter and thinner but has a similar symmetrical shape. The highest isotherm plotted because of experimental camera limitations is the 1700°C isotherm with an approximate length of 10 mm and a width of 10 mm. The 1700°C isotherm incorporates all temperatures at and above 1700°C. Thermal images taken at the 1 s time intervals of the weld demonstrate that the 700°C isotherm has an initial length of ~ 10 mm and a width of ~ 12 mm while the 1700°C isotherm has an approximate length of ~ 10 mm and a width of ~ 8 mm. The isotherms are in sequential order and are slightly smaller as they increase in temperature. This is true for all three weld velocities when calculated and plotted using the analytical solution.

6.5 Results of Analytical and Experimental Comparison

Figure 6.5 shows a comparison of the experimental and analytical temperature

distribution images for a weld velocity of 0.656 cm/s. Figure 6.6 compares the experimental and analytical temperature distribution images for the weld velocity of 0.656 cm/s at 21 s, 25 s, and 29 s time intervals. Appendix IV compares the experimental and analytical temperature distribution images for the weld velocity of 0.545 cm/s and at 21 s, 25 s, and 29 s time intervals. Appendix V compares the experimental and analytical isotherm temperature distribution images for the welding speed of 0.514 cm/s and at 21 s, 25 s, and 29 s time intervals. The assumed experimental parameters and analytical user interface are provided for the weld velocities of 0.545 and 0.514 cm/s in Appendix IV and V, respectively.

Comparison of the experimental and analytical isotherm temperature distribution images show significant differences. The isotherms of the experimentally produced images are longer than the isotherms in the analytical images. It is assumed that the experimental isotherms are longer because of the V-groove geometry and that the V-groove is not completely filled. The analytical solution assumes that the weld is created on the surface under ideal conditions; centered, without current fluctuation, consistent wire feed, ideal material properties, etc. These and other assumptions can partially explain the closer spacing of higher temperature isotherms in the analytical results. The experimental temperature isotherms show that the variation in the length of the isotherms is not dependent on the weld velocity. They vary within ~ 10 length range. The maximum length of the experimental 900°C isotherm varied but did not vary in a consistent manner relative to the weld velocity. The length of the 900°C isotherms varied from ~ 50 to 55 mm, 35 to 40 mm, and 40 to 45 mm for the weld velocities of 0.656, 0.545, and 0.514 cm/s, respectively.

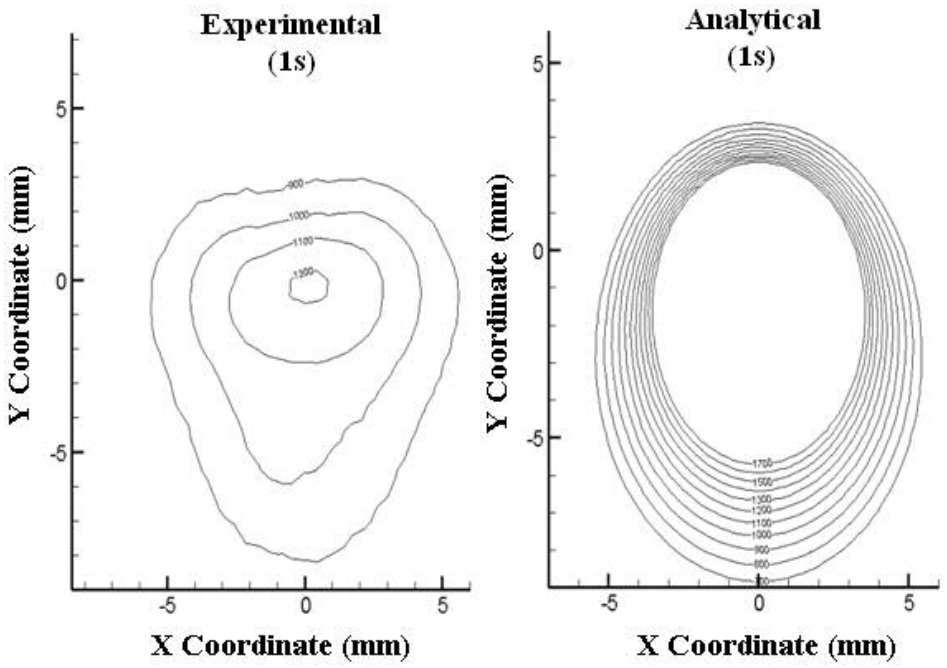
Experimental
(1s)
Analytical
(1s)
Y Coordinate (mm)
X Coordinate (mm)
5
0
-5

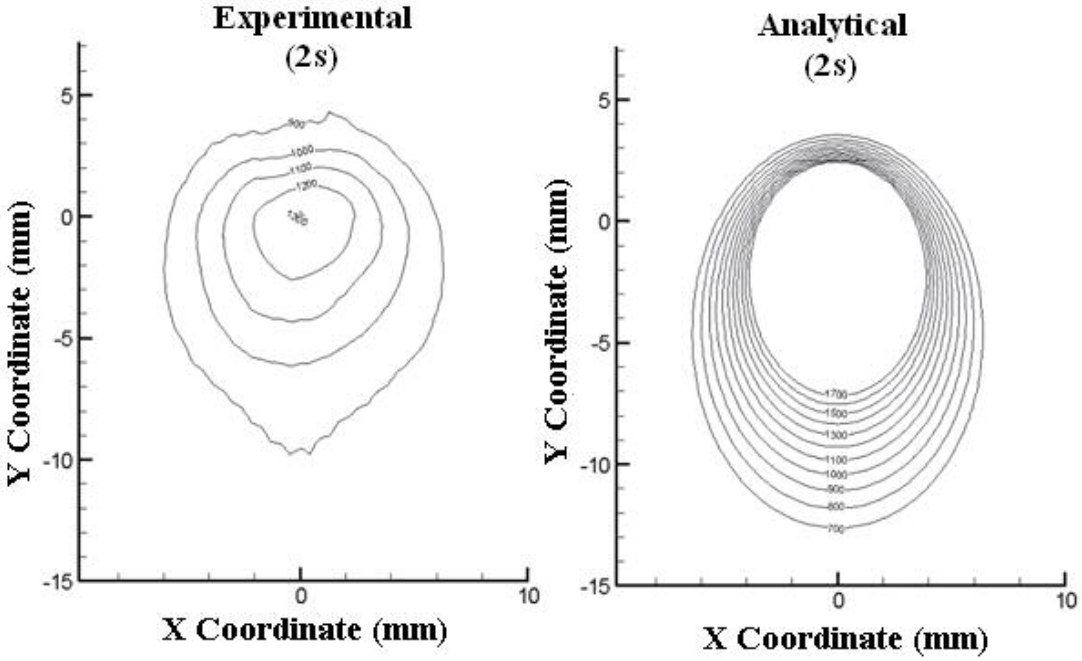
Experimental
(2s)
Analytical
(2s)
Y Coordinate (mm)
X Coordinate (mm)
5
0
-5
-10
-15
10

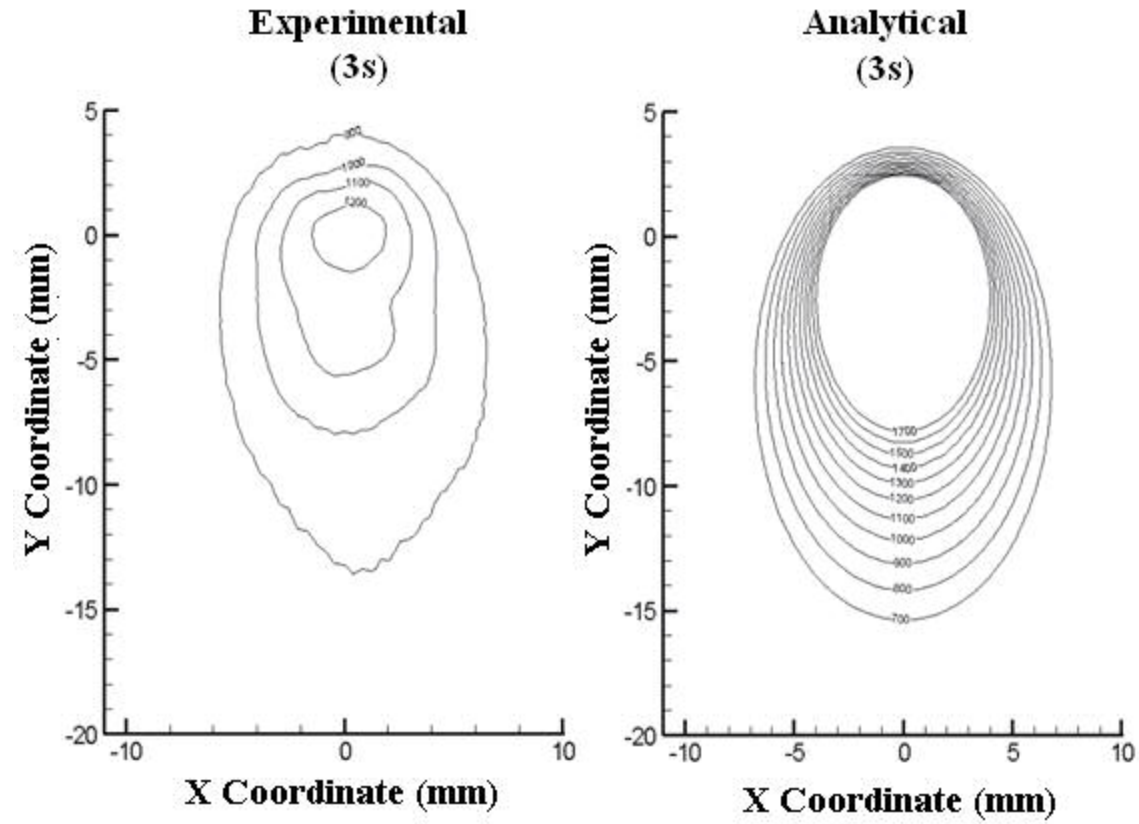
Experimental
(3s)
Analytical
(3s)
Y Coordinate (mm)
X Coordinate (mm)
5
0
-5
-10
-15
-20
-10
0
10
1700
1500
1400
1300
1200
1100
1000
900
800
700

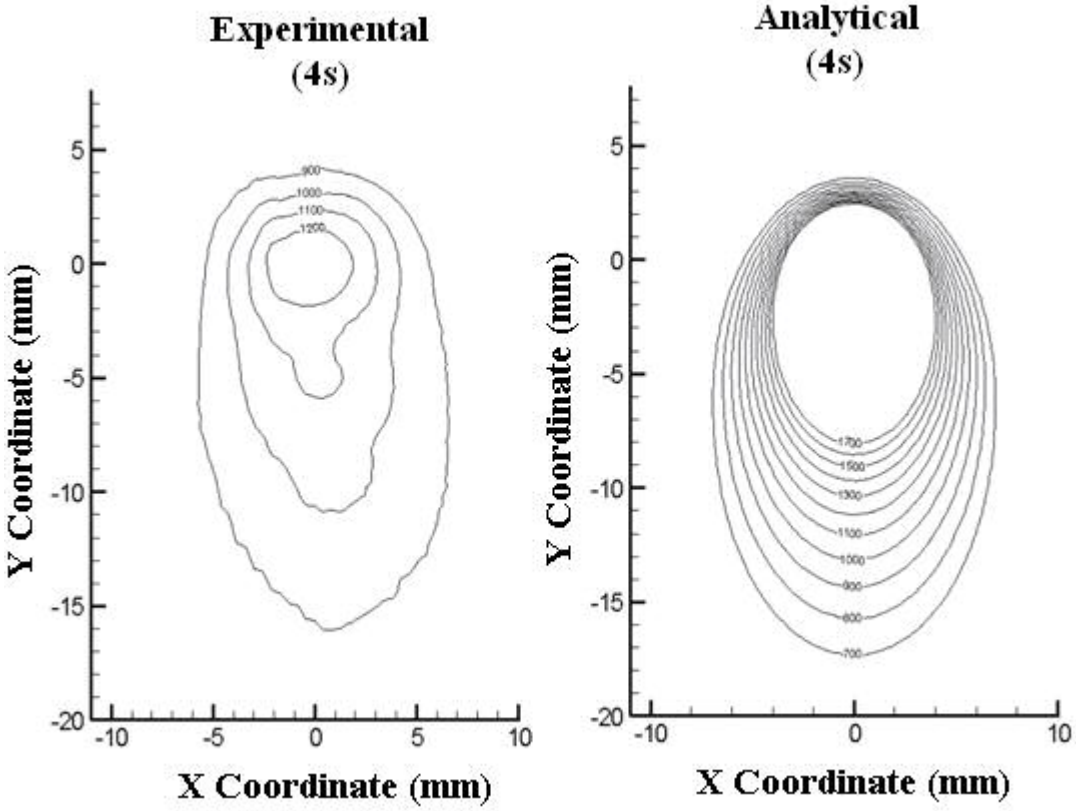
Experimental
(4s)
Analytical
(4s)
Y Coordinate (mm)
X Coordinate (mm)
5
0
-5
-10
-15
-20
-10
-5
0
5
10
900
1000
1100
1200
1700
1500
1300
1100
1000
900
800
700

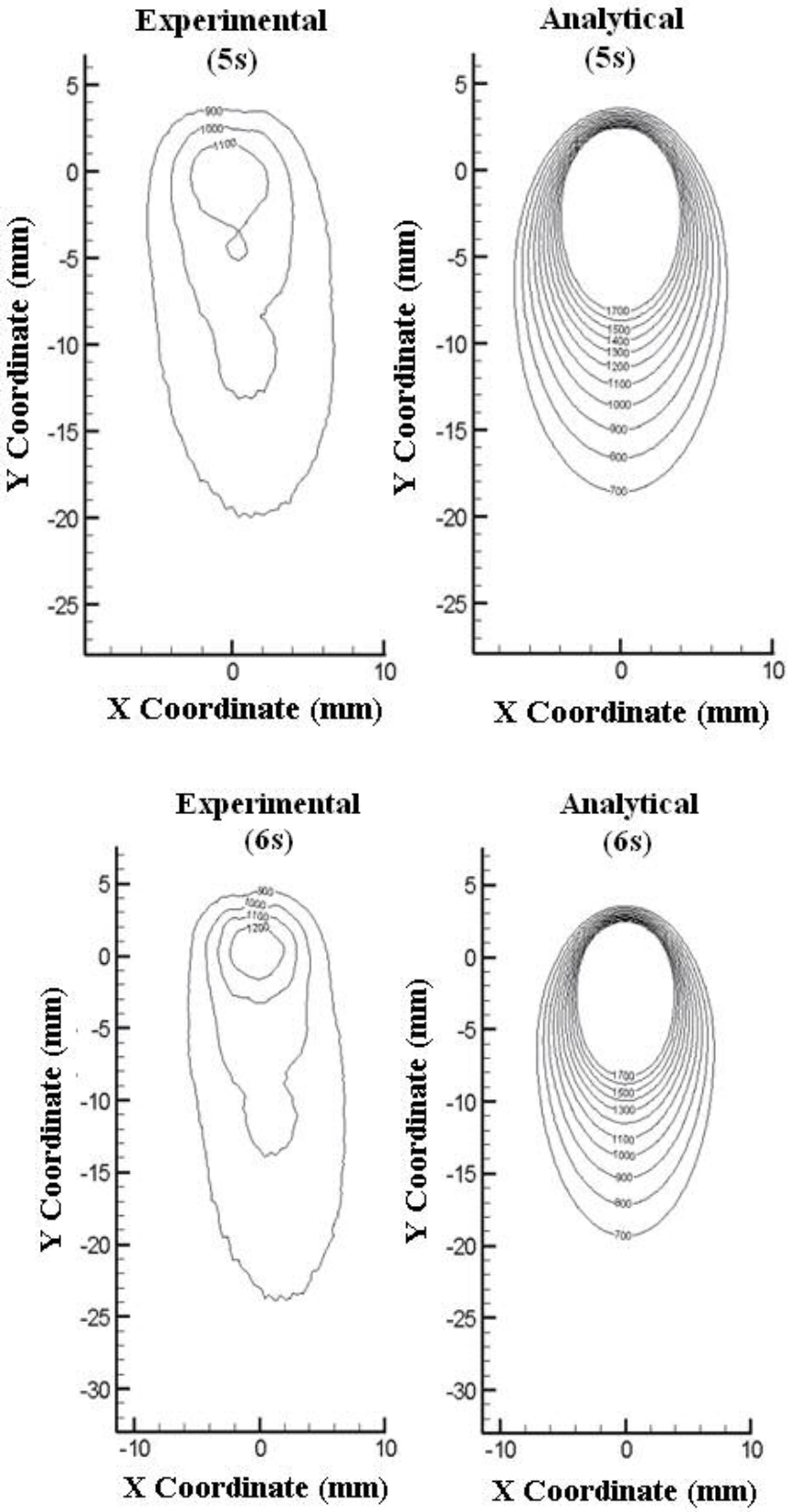
Experimental
(5s)
Analytical
(5s)
Y Coordinate (mm)
X Coordinate (mm)
Experimental
(6s)
Analytical
(6s)
Y Coordinate (mm)
X Coordinate (mm)

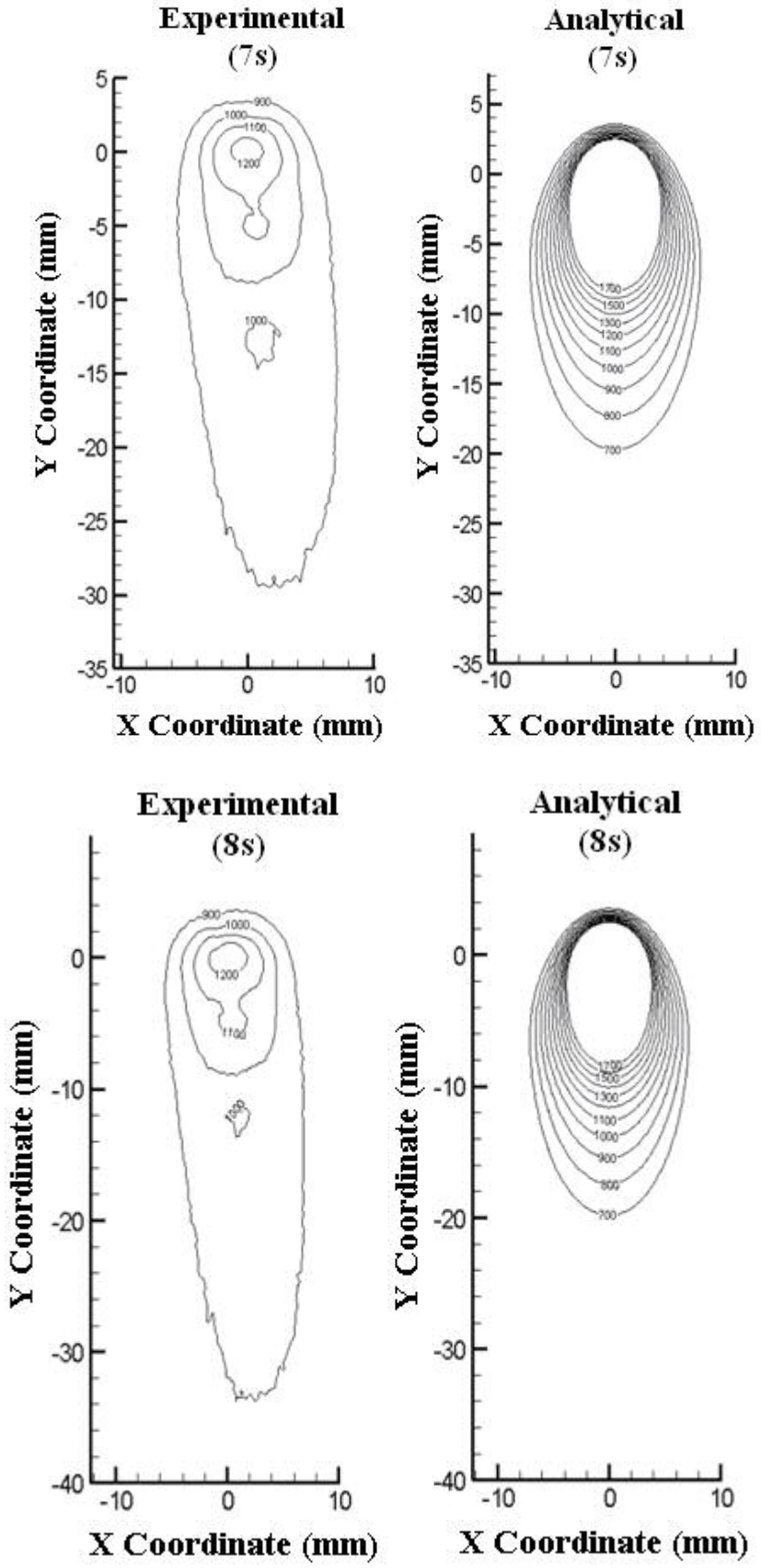
Experimental
(7s)
Analytical
(7s)
Y Coordinate (mm)
X Coordinate (mm)
Experimental
(8s)
Analytical
(8s)
Y Coordinate (mm)
X Coordinate (mm)

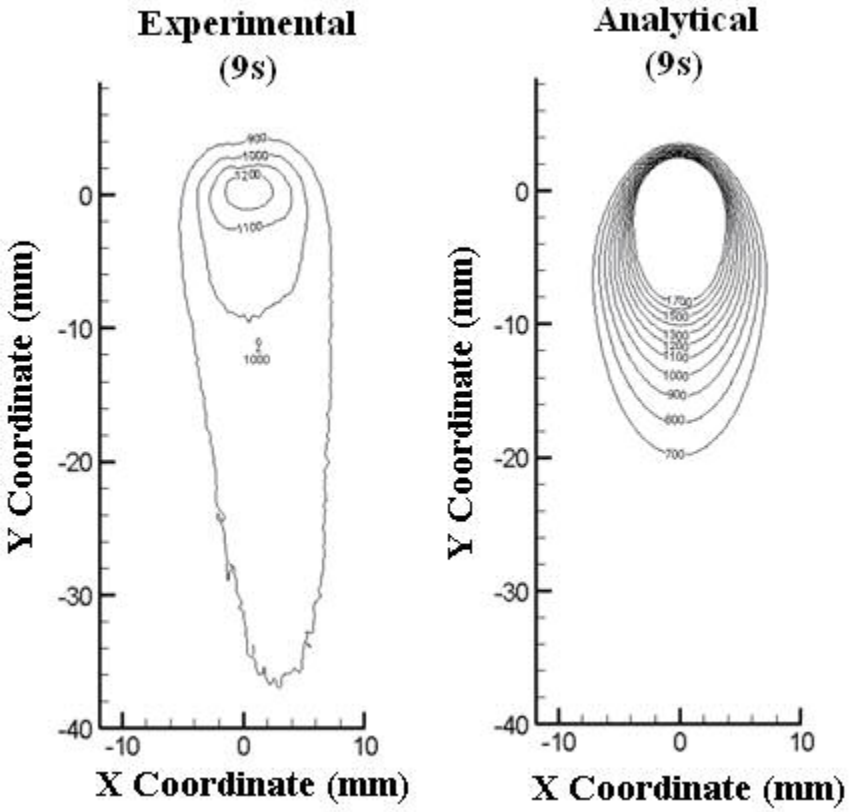
Experimental
(9s)
Analytical
(9s)
Y Coordinate (mm)
X Coordinate (mm)
0
-10
-20
-30
-40
-10
0
10
900
1000
1200
1100
1000
1700
1500
1300
1200
1100
1000
900
800
700

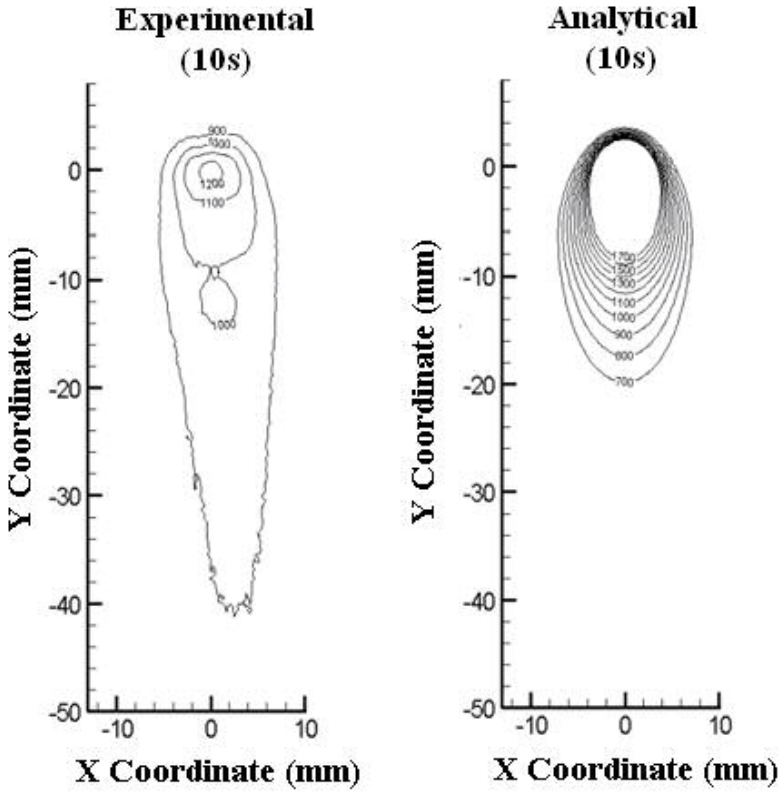
Experimental
(10s)
Analytical
(10s)
Y Coordinate (mm)
X Coordinate (mm)
0
-10
-20
-30
-40
-50
-10
0
10
900
1000
1200
1100
1000
1700
1500
1300
1100
1000
900
800
700

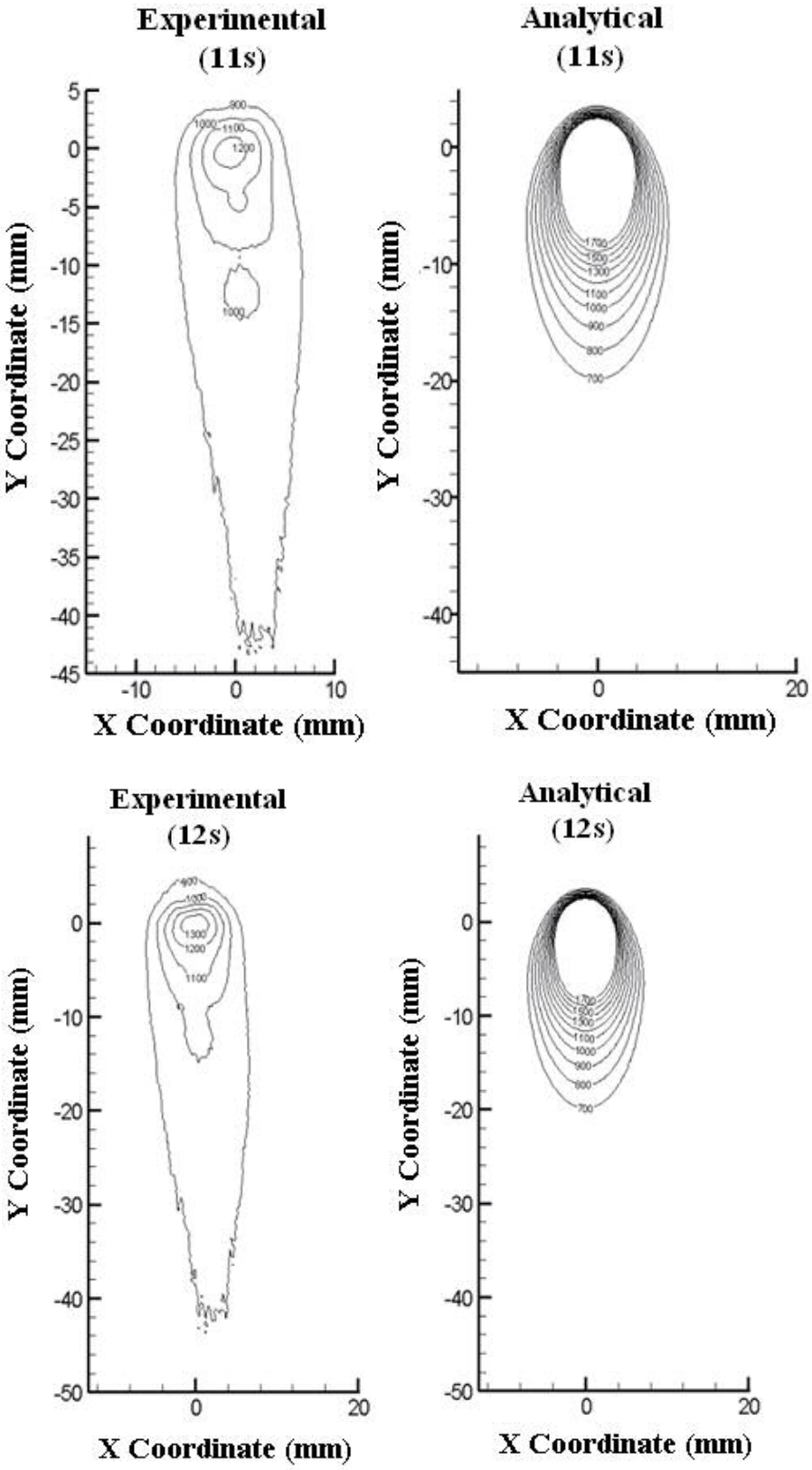
Experimental
(11s)
Analytical
(11s)
Y Coordinate (mm)
X Coordinate (mm)
Experimental
(12s)
Analytical
(12s)
Y Coordinate (mm)
X Coordinate (mm)

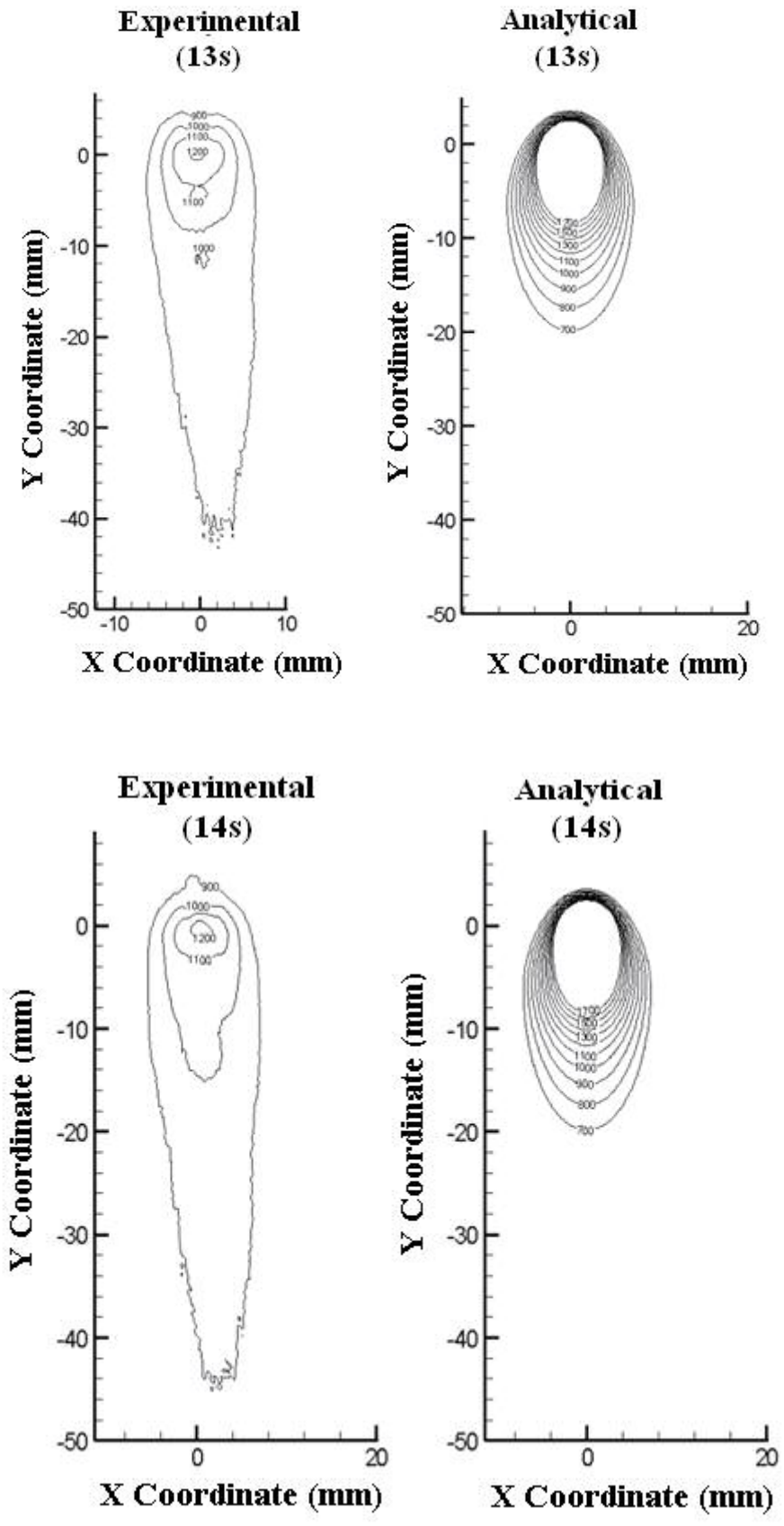
Experimental
(13s)
Analytical
(13s)
Y Coordinate (mm)
X Coordinate (mm)
Experimental
(14s)
Analytical
(14s)
Y Coordinate (mm)
X Coordinate (mm)

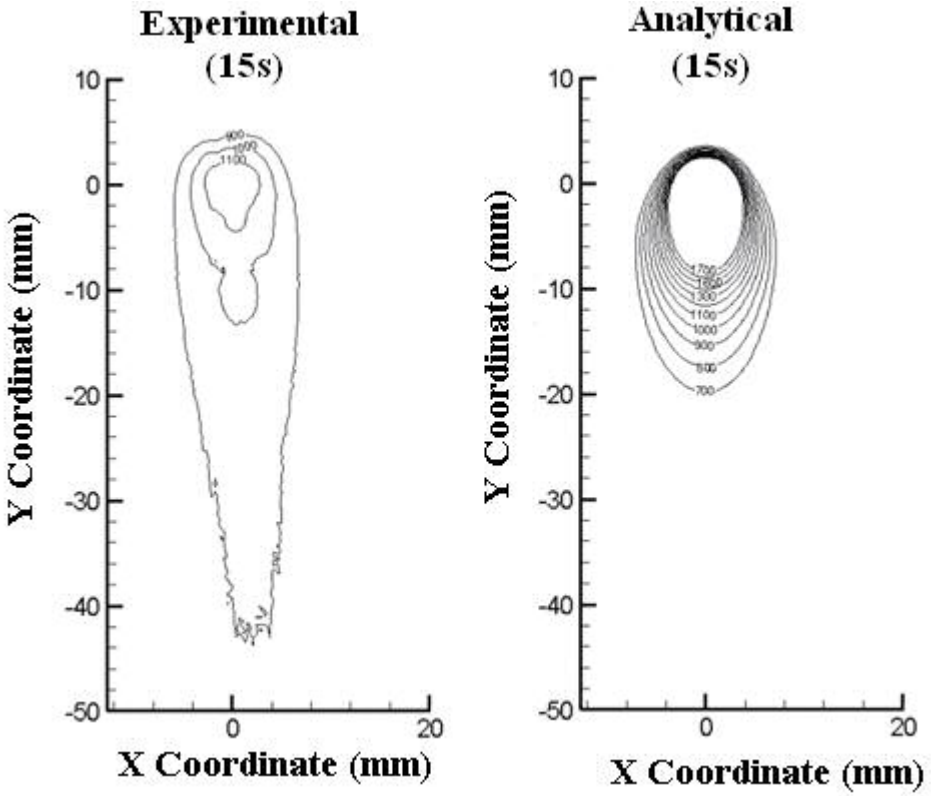
Experimental
(15s)
Analytical
(15s)
Y Coordinate (mm)
X Coordinate (mm)
10
0
-10
-20
-30
-40
-50
0
20

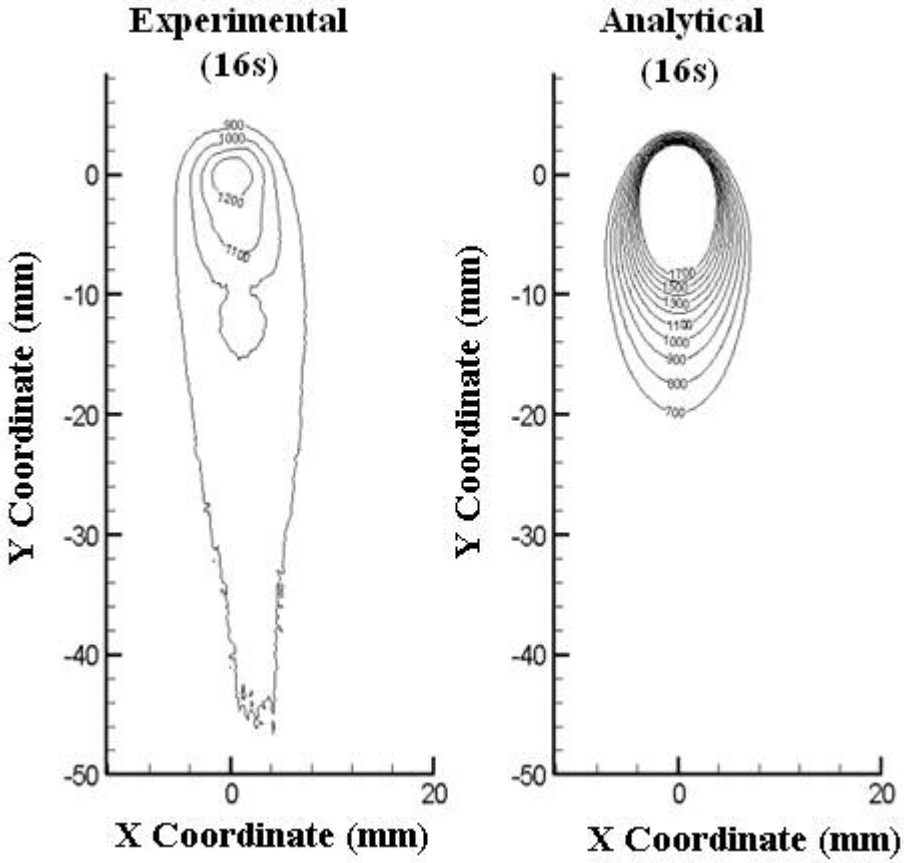
Experimental
(16s)
Analytical
(16s)
Y Coordinate (mm)
X Coordinate (mm)
0
-10
-20
-30
-40
-50
0
20

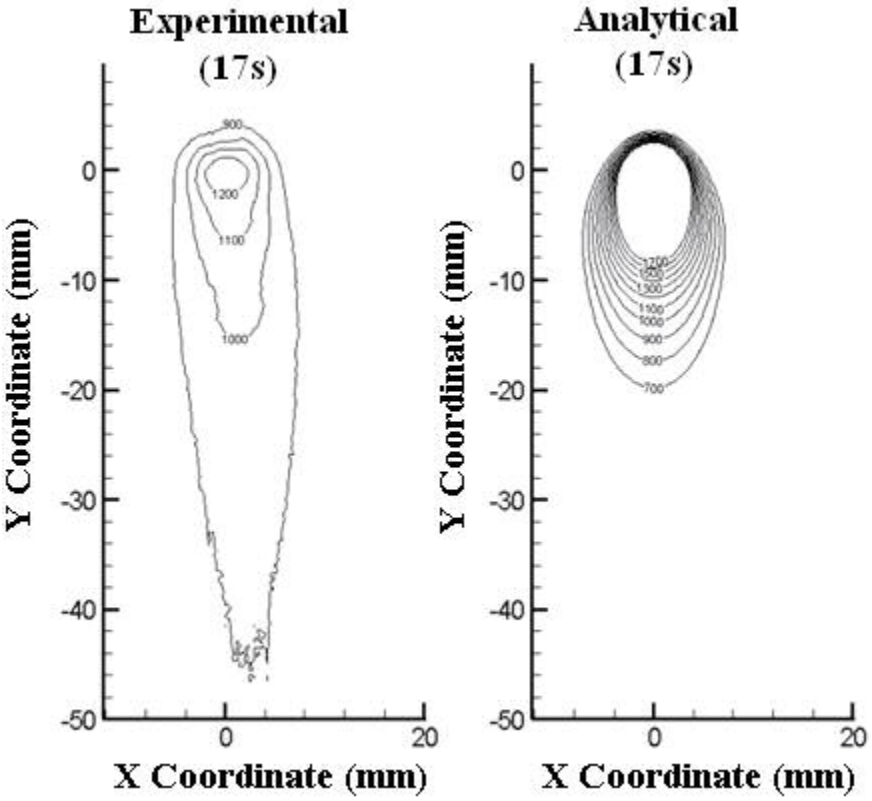
Experimental
(17s)
Analytical
(17s)
Y Coordinate (mm)
X Coordinate (mm)
0
-10
-20
-30
-40
-50
20
900
1000
1100
1200
1300
1400
1500
700
800

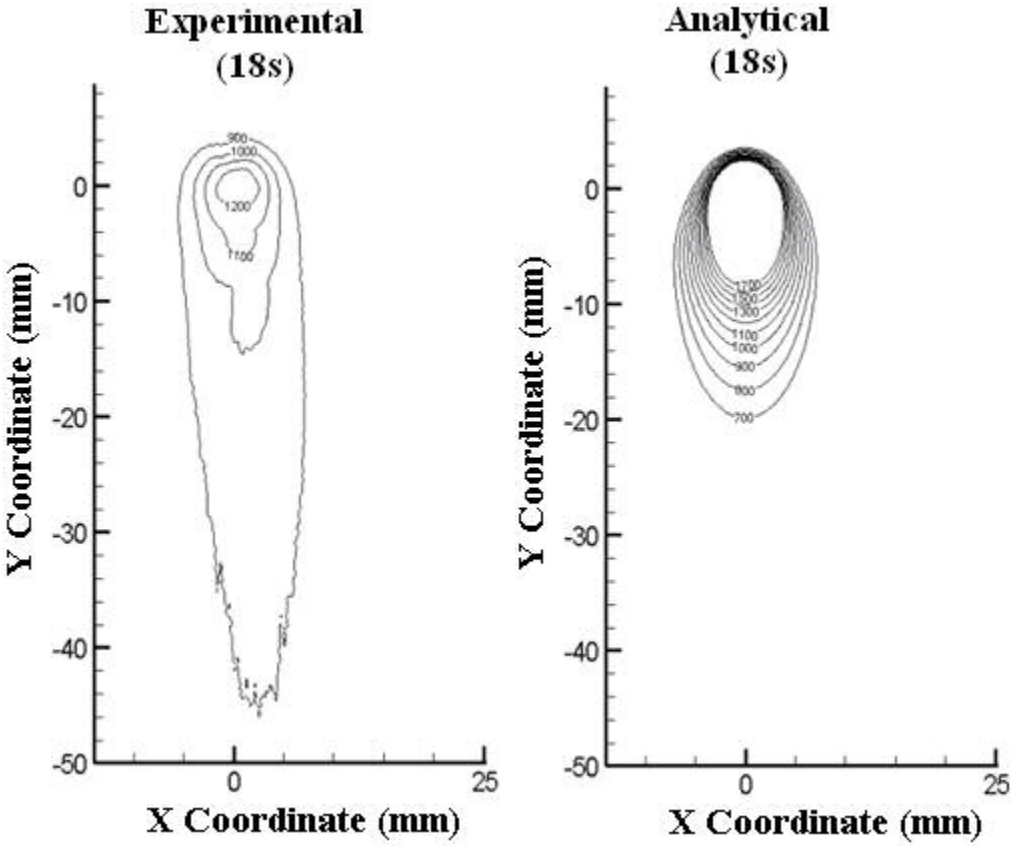
Experimental
(18s)
Analytical
(18s)
Y Coordinate (mm)
X Coordinate (mm)
0
-10
-20
-30
-40
-50
25
900
1000
1100
1200
1300
1400
1500
700
800

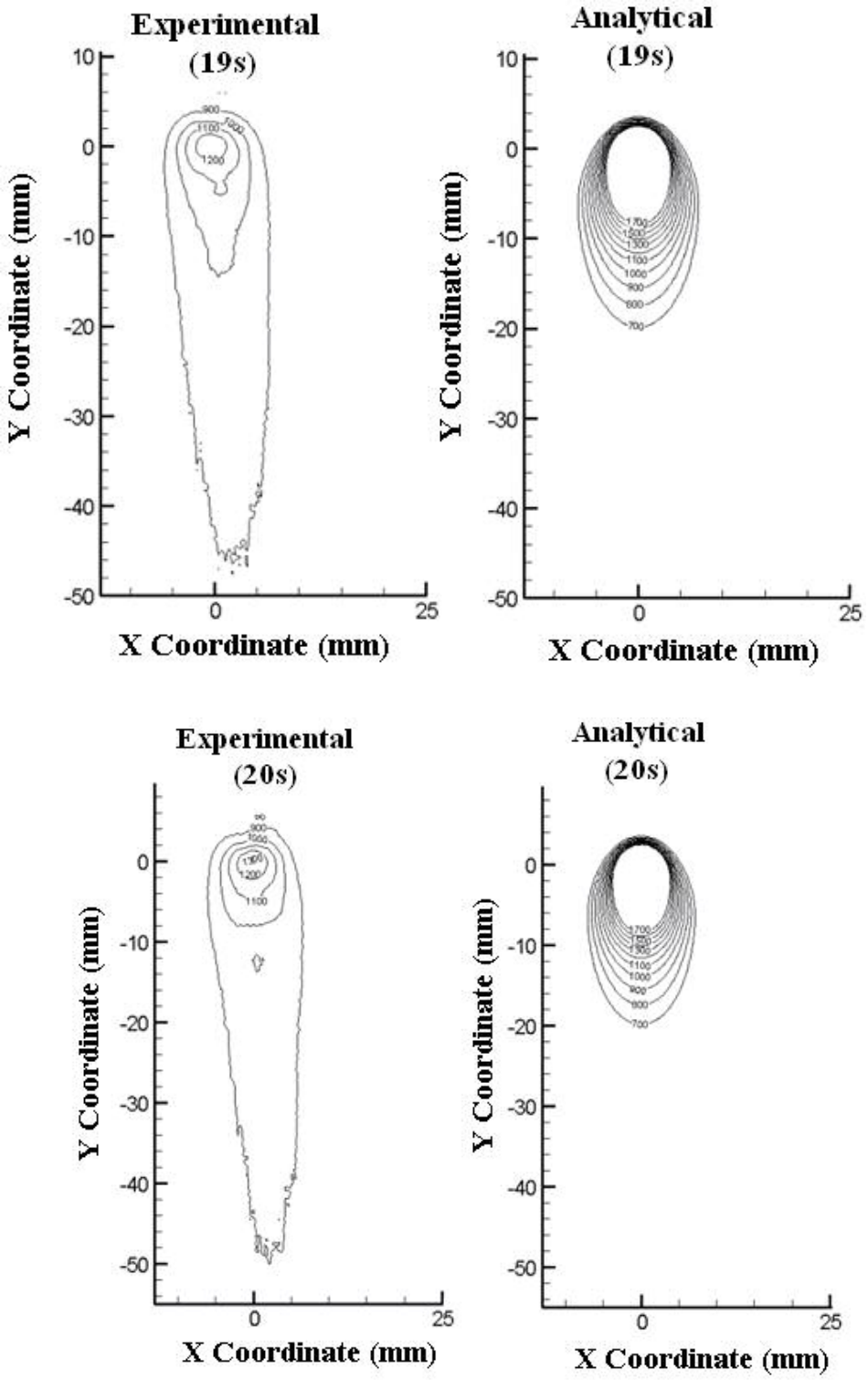

Figure 6.5: Experimental data compared with analytical data during transient to quasi-steady state temperature distributions for 1 s to 20 s in 1 s intervals collected for a weld velocity of 0.656 cm/s

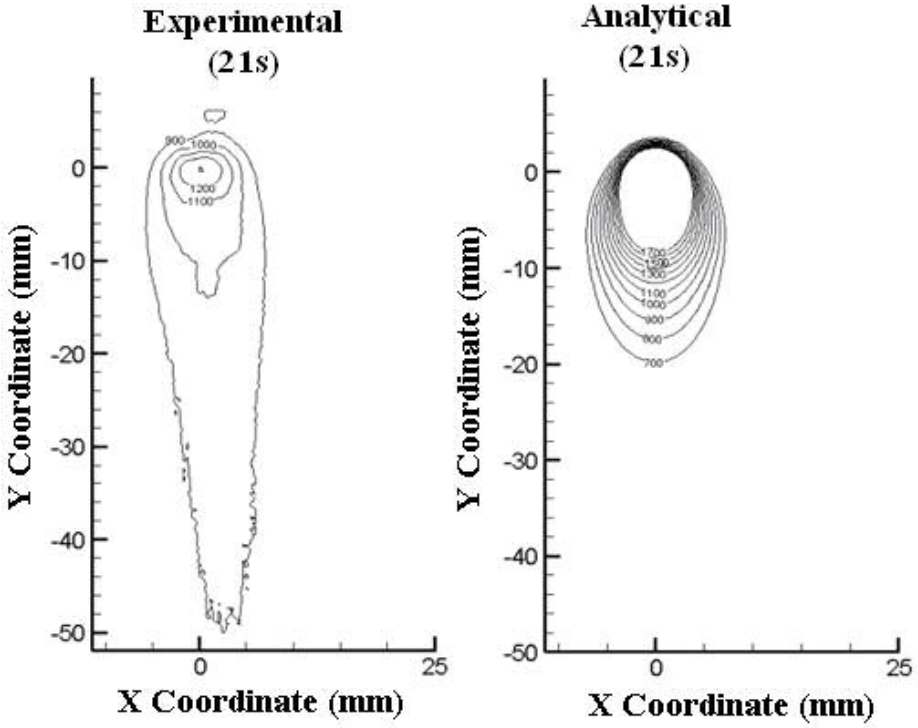
Experimental
(21s)
Analytical
(21s)
Y Coordinate (mm)
X Coordinate (mm)
0
-10
-20
-30
-40
-50
25
900
1000
1200
1100
700

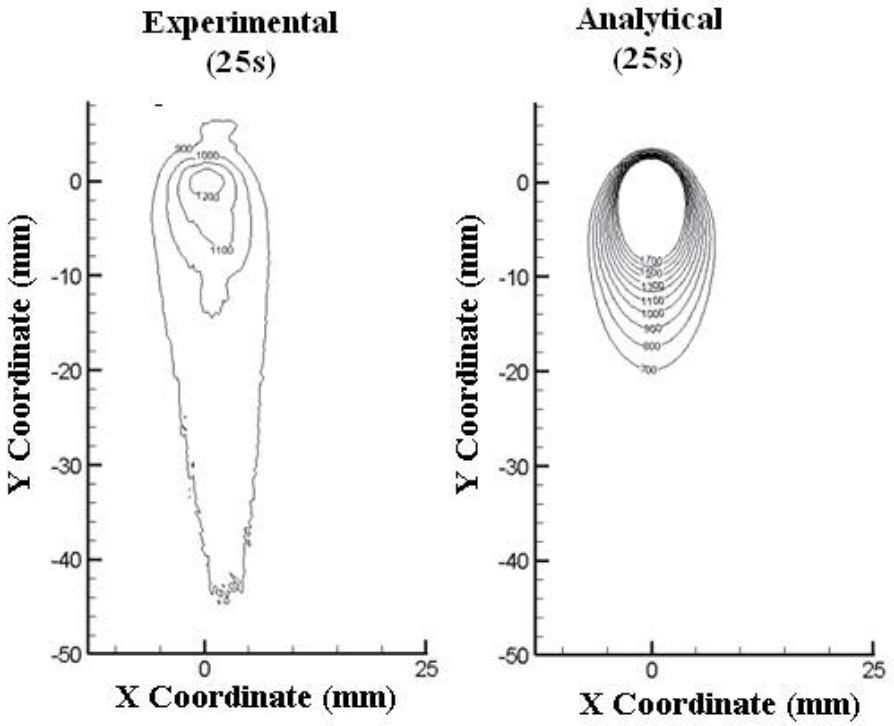
Experimental
(25s)
Analytical
(25s)
Y Coordinate (mm)
X Coordinate (mm)
0
-10
-20
-30
-40
-50
25
900
1000
1200
1100
700

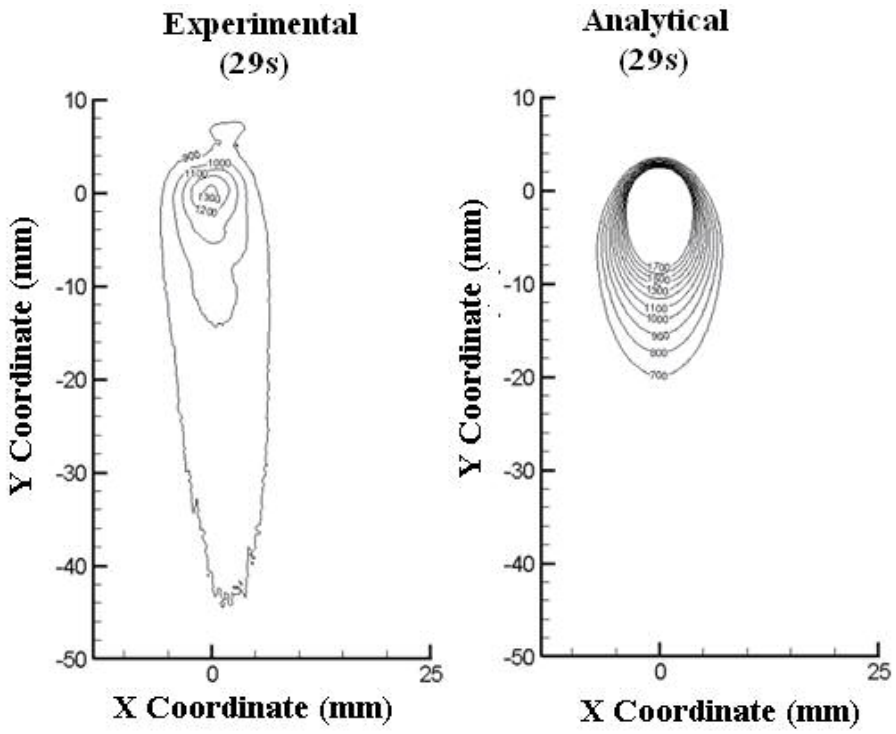

Figure 6.6: Experimental data compared with analytical data during transient to quasi-steady state temperature distributions for 21 s, 25 s, and 29 s for a weld velocity of 0.656 cm/s

It is assumed that wire placement in the groove effects the temperature distribution in the workpiece similar to the conclusions made by Khan *et al.* [8] and reported in the conclusions of the current experiment. This is true for the higher temperature isotherms but is predominately noticed in the outermost experimental isotherm (900 °C). Uniformity of the material composition is assumed in the analytical solution but this is not known for the experimental material.

It is noted from the results of the analytical and experimental temperature isotherms that the analytical solution is somewhat simplified because of the assumptions. Some of the assumptions can be modified when comparisons are made with the experimental procedure and outcome. Analytical assumptions have allowed for a basic data calculation that can be further built upon modified assumptions in the connecting

geometry, material properties, alternating current, dissipation of heat to the surroundings, physical state change, etc. An assumption that directly effects the heat dissipation into the workpiece is the location of the weld; assumed to be on the surface of the pipe for the analytical solution and in a V-groove connection for the experimental solution. The shape and amount of filled V-groove will allow different heat dissipations than just welding on the top surface of the pipe.

6.6 Welding Contact Area

An area that is not fully analyzed or accounted for in the analytical or experimental techniques is the contact area. Extremely high temperatures are present because of the latent heat effect, once a molten state is reached less heat is required to maintain the state. The welding arc diameter is not accurately accounted for in the analytical method and could not be measured in the experimental procedure.

CHAPTER 7

CONCLUSIONS

7.1 Conclusions

The following conclusions are reached based on the current experimental investigation of welding of pipes.

1. A reproducible experimental technique for welding of pipes using a MIG welder together with an infrared camera was developed to view the temperature distributions in the weld area. A temperature range between 900°C to 1700°C was recordable within the specifications of the infrared camera. Welding of two ASTM A500 Grade B steel pipes with a V-groove connection was accomplished and temperature distributions were recorded using the infrared camera.

2. A calibration technique was used at NIST to check the accuracy of temperatures recorded by the infrared camera. A correctional equation was developed using the data obtained during calibration of the camera.

3. Transient and quasi-steady state temperature distributions were obtained in experimentally collected images. Approximate transitional times observed during pipe welding for weld velocities of 0.656, 0.545, and 0.514 cm/s were 14 s, 12 s, and 14 s, respectively.

4. Three weld velocities were used in experiments, namely, 0.656, 0.545, and 0.514 cm/s to observe forany differences in the temperature isotherms produced. The variation in weld velocities showed somewhat unpredictable nature of weld isotherm geometry and boundary dimensions. Temperature isotherms varied within a 10 mm range regardless of the weld velocity. It is noted that a change in the position of the welding filler wire within the V-groove were the cause for shortened and widened isotherms produced at the weld velocity of 0.514 cm/s.

5. Weld velocity variation had a distinct effect on the bead size and heat penetration, shown by the size variation of the isotherms for the various weld velocities, as similar to that reported by Finch *et al.* [3]

6. The maximum temperature involved in the welding of ASTM A500 Grade B steel was produced at the filler wire and workpiece contact point. Varying the weld velocities produced temperatures > 1100°C but < 1400°C as registered by the infrared camera. The maximum temperature was reached in the 1 s and a spread within a 200°C range during the experimental process. This was observed after quasi-steady state was reached for the weld velocities of 0.656, 0.545, and 0.514 cm/s.

7. An analytical solution was obtained under the assumption that rotational movement can be translated into linear coordinates, based on the analytical model of Komanduri and Hou [20]. The analytically calculated spot temperatures were plotted and compared with the experimentally collected temperature distributions.

8. Comparison of experimental and analytically obtained temperature distribution images showed geometrical differences for images collected at three weld velocities (0.656, 0.545, and 0.514 cm/s). Experimentally produced isotherms were longer,

spaced further apart, and consisted of lower temperature isotherms when compared to shorter, spaced close together, and at higher temperature isotherms obtained analytically.

9. Differences between experimental and analytical temperature isotherms are partially attributed to assumptions made in the analytical model. The experimentally produced weld is created in a V-groove and the analytical weld assumes the weld is created on the top surface of the pipe. The experimentally produced weld is underfilled leaving V-shapes between the base metal and weld metal on either side of the center of the weld. The analytical weld assumes that the weld is ideally filled. The experimentally produced weld is created using a non-uniform ASTM A500 Grade B steel which may consist of a non-uniform composition and microstructure while the analytical solution assumes a uniform or homogeneous material (with properties of AISI 1030).

10. The analytical solution predicts quasi-steady state to occur at 11 s and the isotherms do not change after that time in the welding process, for the three weld velocities. The analytical solution predicts temperature isotherms of a similar geometry and spacing for all three weld velocities. Experimental data demonstrates constant variation in the temperature isotherm boundaries; although the range is observed to be smaller after reaching quasi-steady state.

11. The slower the weld velocity, the shorter the isotherms and deeper the heat penetration in the welded material. The inconsistency of the lengths and widths of the isotherms for the weld velocity of 0.545 cm/s (when compared to those of the other two weld velocities) can probably be due to the filler wire position. Thus the slower the

weld velocity, the longer is the HAZ. The effects of the filler wire position for the middle weld velcitey (0.545 cm/s) are similar to the conclusions of Khan *et al.* [8]

12. The experimental process shows that fluctuation in the temperature isotherms does not stop after the quasi-steady state has reached and maintained. Experimental parameters that are not included in the analytical solution and have a direct effect, as shown for the weld velocity of 0.545 cm/s, include the position of the welding filler wire.

13. Initial thermal shock, is produced by an extreme change of temperature, from 23 to 1100°C or greater, in 1 s or less. At the end of 1 s 900, 1000, 1100, and 1200°C have formed for all three weld velocities a 1300°C isotherms has formed for the weld velocity of 0.545 cm/s which is attributed to a misplaced filler wire weld.

14. The high heat, black paint provides a known emmisivity for calculations and provides a visual of the damage caused by the heat dissipation from the weld in an outward motion. The analytical solution assumes adiabatic boundaries dismissing heat liberation into the surroundings but the welder can feel the heat being dissipated to the surroundings.

15. Temperature isotherms were produced for three experimental weld velocities. The weld velocities demonstrate a predictable temperature distribution pattern. They show a predictable temperature distribution pattern. The mid-weld velocity results diverged somewhat from the predicted temperature distribution. This is explained by the filler wire position due to perhaps the movement of the filler wire position. These findings are similar to the conclusions of Khan *et al.* [8].

7.2 Future Work

The following are recommendations for future experimental work for a better understanding of the process and implications to the welding industry in general.

1. Experimentation using different workpiece materials, such as stainless steel.

2. Experimental investigation of multiple welding connection geometries for pipes. For example extend the investigation to double V-groove, fillet, square, J-groove, U-groove, and bevel groove.

3. Experimental investigations of individual parameters without variation in the experimental process, namely, feed wire position, surrounding temperature, preheating, post heating, current, voltage, latent heat of fusion, arc efficiency, arc beam radius, feed wire velocity, etc.

4. Comparison of the microstructual analysis to the infrared recorded temperatures to better understand the welding process and to investigate if thermal damage to welds can be controlled.

5. Derivation of an analytical model that accounts for various geometrical factors.

6. An accurate method of measurement for the welding arc diameter.

7. Extend the current investigation to include temperature isotherms including a larger temperature range, i.e. 0°C to 2000°C (limited to 2000°C by the infrared camera viewing specifications) using another infrared camera or multiple Merlin^{TM} Mid infrared cameras.

REFERENCES

1. Bhambri, Y., Sikka, V.K., Walker, L.R., Santella, M.L., Muralidharan, G., Hales, J.W., "Al enrichment of carbon steel through weld overlay process for improved oxidation resistance," Materials Science and Engineering 394 (2004) 249-255
2. Finch, Richard, Welder's Handbook; A Complete Guide to MIG, TIG, ARC & Oxyacetylene Welding The Berkley Publishing Group New York (1997)
3. Shehata, F., "Effect of plate thickness on mechanical properties of steel arc welded joints," 15 (1994) 105-110
4. Basavaraju, C., "Simplified analysis of shrinkage in pipe to pipe butt welds," Nuclear Engineering and Design 197 (2000) 239-247
5. Mackerle, J., "Finite-element modeling of non-destructive material evaluation: a bibliography (1976-1997)," Modelling Simulation Material Science Engineering 7 (1998) 107-145
6. Wikle, H.C., Zee, R.H., Chin, B.A., "A sensing system for weld process control," Journal of Materials Processing Technology (1999) 254-259
7. Lin, T.T., Groom, K., Madsen, N.H., Chin, B.A., "Infrared sensing techniques for adaptive robotic welding conference on modeling of casting and welding processes: proceedings of the third conference on modeling of casting and welding processes," AIME-TMS (1986) 19-31
8. Khan, M.A., Madsen, N.H.,Goodling, J.S., Chin, B.A., "Infrared thermography as a control for the welding process," Optical Engineering 25 (1986) 799-805

9. Belanger, R.J., Patchett, B.M., "The Influence of working fluid physical properties on weld qualification for in-service pipelines," Welding Journal (2000) 209-214
10. Wikle, H.C. Kottilingam, S., Zee, R.H., Chin, B.A., "Infrared sensing techniques for penetration depth control of the submerged arc welding process," Journal of Materials Processing Technology 113 (2001) 228-233
11. Olabi, A.G., and Hashmi, M.S.J., "The microstructure and mechanical properties of low carbon steel welded components after the application of PWHTs," Journal of Material Processing Technology 56 (1996) 88-97
12. Murugan, S., Rai, S.K., Kumar, P.V., Jayakumar, T., Raj B., Bose, M.S.C., "Temperature distribution and residual stresses due to multipass welding in type 304 stainless steeel and low carbon steel weld pads," International Journal of Pressure Vessels and Piping 78 (2001) 307-317
13. Mohandas, T., Madhusudan, R., Kumar, B.S., "Heat-affected zone softening in high-strength low-alloy steels," Journal of Materials Processing Technology 88 (1999) 284-294
14. Bicknell, J., A Smith, J., Lucas, "Infrared sensor for top face monitoring of weld pools," Measurement Science Technology 5 (1993) 371-378
15. Lhospitalier, S., "Temperature measurement inside and near the weld pool during laser welding," Journal of Laser Applications 11 (1999) 32-37
16. Akselsen, O.M., Grong, O., Ryum, N., Christensen, N., "HAZ grain growth mechanisms in welding of low carbon microalloyed steels," Acia Metall 34 (1986) 1807-1815

17. Zhang, Y.M., Zhang, S.B., Jiang, M., "Keyhole double-sided arc welding process," Welding Journal (2002) 249-255
18. Bachorski, A., Painter, M.J., Smailes, A.J., Wahab, M.A., "Finite-element prediction of distortion during gas metal arc welding using the shrinkage volume approach," Journal of Materials Processing Technology (1999) 405-409
19. Oddy, A.S., McDill, J.M.J., "Burnthrough prediction in pipeline welding," International Journal of Fracture 97 (1999) 249-261
20. Komanduri, R., and Hou, Z.B., "Thermal analysis of the arc welding process: part I general solutions," Metallurgical and Materials Transactions B 31B (2000) 1353-1369
21. Komanduri, R., and Hou, Z.B., "Thermal analysis of the arc welding process: part II effect of variation of thermophysical properties with temperature," Metallurgical and Materials Transactions B 32B (2001) 483-499
22. Vanzetti, R., Practical Applications of Infrared Techniques, John Wiley and Sons, New York (1972)
23. http://www.ccohs.ca/oshanswers/safety_haz/welding/ppe.html
24. Merlin™ Mid InSb MWIR Camera User Manual
25. Bhome, A., "Temperature measurement in orthogonal machining of SAE 1015 steel using an infrared camera," M.S. Thesis, Oklahoma State University Stillwater, OK (2004)
26. Chandrasekar, S., Narayanan V., Krishnamurthy, K., Hwang, J., Madhavan, V., and Farris, T. N., "Measurement of temperature field at the tool-chip interface in machining," Proceedings of NSF workshop on Research Needs in Thermal

Aspects of Material Removal Processes, Oklahoma State University, Stillwater, (2003) 63-69

27. ASM Handbook Online Volume 6; Welding, Brazing, and Soldering 2002 Fusion Welding, Gas-Metal Inert Welding, Process Fundamentals
28. http://www.lincolnelectric.com
29. Idealarc CV-300 welder Operator's Manual
30. http://www.baldor.com
31. BC154 and BCWD140 Adjustable Speed DC Control "Installation and operating manual," Baldor Motors and Drives
32. Belanger, R.J., Patchett, B.M., "The influence of working fluid physical properties on weld qualification for in-service pipelines," Welding Journal (2000) 209-214
33. Kehl The Principles of Metalographic Laboratory Practices First Edition McGraw-Hill Book Company, Inc. New York (1939)
34. http://www.matweb.com
35. Komanduri, R., and Hou, Z.B., "Magnetic field assisted finishing of ceramics-part I: thermal model," Trans ASME Journal of Tribology 120 (1998) 645-651

APPENDIX I

Safety equipment for welding [23]

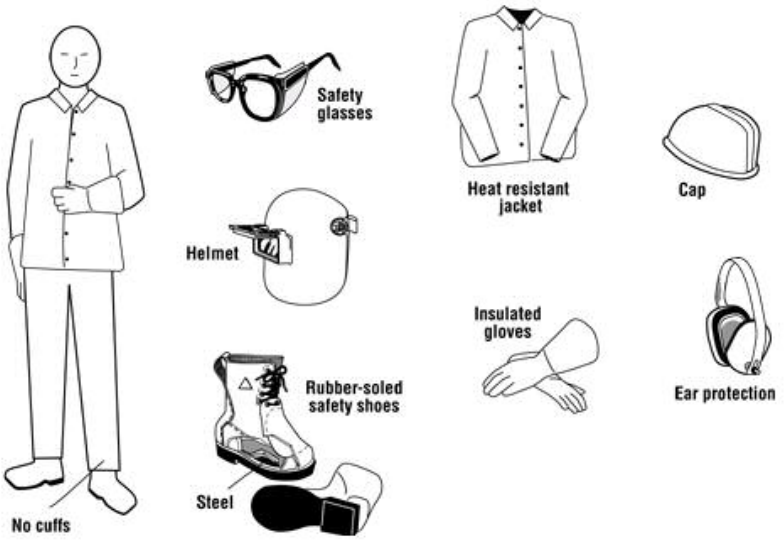

An exploded view of a welding safety hood [23]

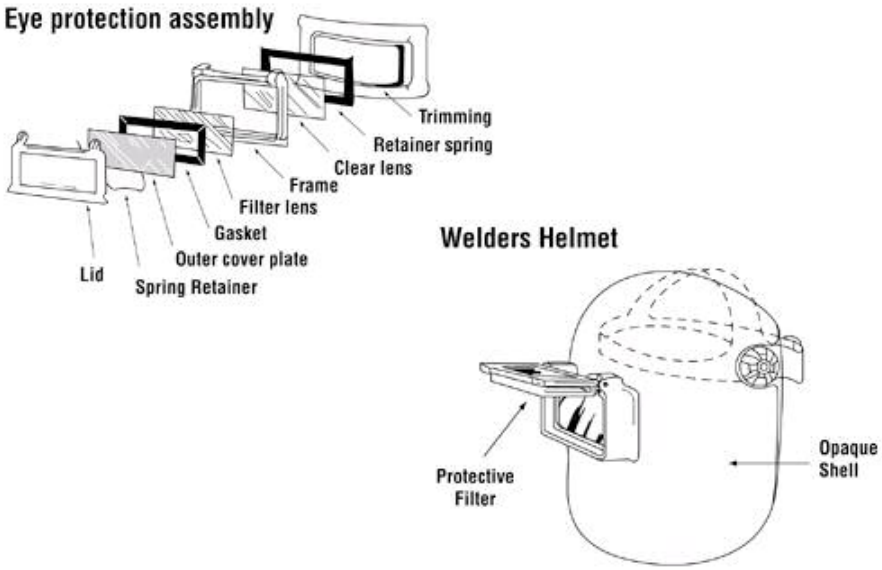

Table of required darkness shades for safety hoods [23]

Process	Electrode Diameter (mm)	Current (Amperes)	Minimum Shade	Suggested Shade
SMAW	< 2.5 2.5 - 4 4 - 6.4 > 6.4	< 60 60 - 160 160 -250 250 - 550	7 8 10 11	- 10 12 14
GMAW and FCAW		< 60 60 -160 160 -250 250 -500	7 10 10 10	- 11 12 14
Air Carbon Arc Cutting light heavy		 < 500 500 -1000	 10 11	 12 14

14 mil. yellow transparent safety shields surrounding the welding area

Merlin™ Mid MWIR Infrared Camera Specifications [24]

Detector Type	InSb (Indium Antimonide)	
Spectral Range	1 - 5.4 µm (3 - 5 µm set by cold filter)	
Detector Size	30 x 30 µm	
Array Format	320 x 256	
Integration Time	5 µs - 16.5 ms	
Camera f/#	2.5 or 4.1	
Cooling Type	Integral Stirling	
Analog Video	NTSC @ 30 Hz (PAL @ 25 Hz optional) S-Video	
Digital Video	60Hz (50 Hz PAL), 12-bit	
Remote Control	Button Panel & RS-232	
Size	140mm H x 125mm W x 250mm L	
Weight	4Kg	
Temperature Measurement		
Standard	0-350°C	
Extended	300-2000°C	
Accuracy	2°C or 2%	
	Temperature Range (°C)	Integration Time (µs)
NUC 0	2 to 68	2000
NUC 1	44 to 123	400
NUC 2	111 to 231	80
NUC 3	221 to 425	10
NUC 4 (ND2)	380 to 765	200
NUC 5 (ND2)	600 to 1600	20

Infrared Camera Neutral Density Filter

A neutral density filter (NDF) is designed to decrease the light intensity input without affecting the spectral distribution, otherwise referred to as the color distribution. The NDF allows a specified amount of light to pass through preventing saturation of recorded thermal images. This particular NDF is neutral and does not alter the spectral distribution as light passes through it. The transmission value of the NDF can be calculated using the optical density (OD) equation given as Eqn 1.

$$T=10^{-OD} \qquad 1$$

An OD of 2 is used in the present investigation, referred to as a neutral density filter of 2 (NDF2). Thus by using the above equation the transmission value is calculated to be 0.01, 1%. For a NDF2 with a 1% transmission value the filter blocks 99% of the incident radiation created by the viewed heated object and allows 1% of the incident radiation from the heat object viewed to pass through.

The NDF in the current experimental work is used to protect the FPA from the excessive intensity of radiation produced in welding as temperatures greater than 400 °C, as specified in the camera's manufacturing manual [24]. This NDF is fixed by a threaded mount at the connection point of the lens to the camera.

Infrared Protective Sapphire Window

It is necessary to protect the camera lens from flying particles that might damage it; spatter, dust, smoke. A sapphire protective window was used as a protective lens.

The use of sapphire in infrared applications is confirmed by previous applications such as experimentation by Chandrasekar *et al.* [26]. A 50 mm diameter sapphire window, with commercial optical finish on both sides, is used. The casing and mounting mechanism for the protective sapphire window in the present experimentation is machined from delrin to form a frontal ring that is connected to a backing with nylon screws. The sapphire lens setup fits over the 100 mm lens secured with nylon screws.

Lens materials used for wavelength ranges of 3-5 μm and 8-13 μm [25]

Type of material	**3-5μm**	**8-13μm**
Alkali halides	-	KCl, NaCl, CsI
Other Halides	BaF_2, LiF, MgF_2	KRS_5, PbF_2, ThF_4
Semiconductors	Si	Ge, GaAs, InP, GaP
Chalcogenides	-	ZnS, ZnSe, CdS, CaLaS
Others	Al_2O_3, SiN, SiC, ZrO, Y_2O_3	-

Infrared Integration Time

Focal place array (FPA) integration time varies from 5 μs to 16.6 ms, provided by a built in integration time (INTG_TIME) function. Integration time is not permanently stored unless a one-point or two-point correction is performed after the power of camera is turned on and sufficient warm-up time is allowed (15 to 30 minutes). Every time the INTG_TIME is changed a one-point correction is required.

The infrared camera used is a microbolometer type camera. Other cameras, such as picture cameras, detect individual photons using a photovoltaic or photoconductive method. A photoconductive or photovoltaic camera generates current through the integration of absorbed photons over a length of time on an integration capacitor. The photon sensor in a microbolometer camera always receives input power from the viewed thermal radiations, even as it is integrated over a length of time, making it a rolling-mode device. The bolometer camera therefore integrates the current for a full frame time when referencing the integration method for photoconductive or photovoltaic camera. A microbolometer camera receives different amounts of thermal radiation from a viewed scene and records the differences in the varying thermal radiation with respect to the bolometer array substrate for individual pixels. Pixel measurements are taken in alternating rows, not like a snapshot as in a photoconductive or photovoltaic camera. Each part of the bolometer heats up and is thermally isolated from the substrate allowing a small input of infrared (IR) power resulting in a measurable change in the bolometer temperature. The amount of heat detected for each pixel, the intensity of the IR scene, is determined by passing a known current or known voltage through a resistive element in the thermally isolated section of the bolometer. The resistive element changes resistance

significantly with change in temperature. Since a known voltage is applied across the bolometer's resistor for a short time the current generated is related to the resistance of the resistor. The resistance of the resistor is then related to the bolometer temperature, a direct measurement of the incident IR radiation.

The length of time that the current is allowed to flow through the bolometer before being collected on an integrating mechanism, such as an integration capacitor, is considered the camera's integration time. The amount of collected signal in an integration capacitor is proportional to the length of the integration time and the amount of passing current. Since higher currents passing through the resistor result from viewing higher temperatures a shorter integration time will allow the higher temperatures to be imaged without allowing saturation of the integration capacitor. Similarly, a lower temperature will generate a larger signal on the integration capacitor if the passing currents are integrated longer.

BC154 adjustable DC control speed drive technical specifications [27]

Parameter	Specification	Factory Setting
AC Line Input Voltage (VAC +/- 10%,50/60 Hz)	115 or 230	230
AC Line Frequency (Hz), # of Phases	50/60, 1	-
Arm Voltage Range at 115VAC Line (VDC)	0-90	-
Arm Voltage Range at 230VAC Line (VDC)	0-180, 0-90	0-180
Field Voltage at 115VAC Line (VDC)	100/50	-
Field Voltage at 230VAC Line (VDC)	200/100	-
Horsepower Range at 115 VAC HP, (KW)	1/50-1, (0.015-0.75)	-
Horsepower Range at 230 VAC HP, (KW)	1/50-2, (0.03-1.5)	-
Ambient Temperature Range (°C)	0-50	-
Speed Range (Ratio)	50:01:00	-
Arm Feedback Load Regulation (% Base Speed)	+/-1	-
Tach Feedback Load Regulation (% Set Speed)	+/-1	-
Line Regulation (% Base Speed)	+/-0.5	-
Current Ranges (ADC)	2.5, 5.0,7.5, 10	10
ACCEL and DECEL Ranges (Sec.)	0.1-15	1
MIN Speed Range (% Base Speed)	0-30	0
MAX Speed Range (% Base Speed)	60-140	100
IR Comp Range at 115VAC Line (VDC)	0-15	4
IR Comp Range at 230VAC Line (VDC)	0-30	8
CL Range (% Range Setting)	0-200	150
Timed CL Range (Sec.)	0.5-15	7
Voltage Following Linearity (% Base Speed)	+/-0.5	-

Technical Specification for LN-7 GMA wire feeder technical specifiations [29]

INPUT VOLTAGE		
Supplied by power source: 115 VAC, 50/60 Hz, 2.5 Amps		
WIRE FEED SPEED		
LN-7 GMA	75 to 700 in. per minute (1.90 to 17.8 m/min)	
WIRE DIAMETERS		
LN-7 GMA	0.023 in. through 1/16 in. (0.6 through 1.6 mm)	Solid Electrode
	0.045 in. through 5/64 in. (1.2 through 2.0 mm)	Cored Electrode

Magnum Gas-Shielded Gun and Cable Assembly technical specifications [29]

Gun Tube Angle	Duty Cycle at Rated Amperage	Wire Diameter in (mm)	Cable Length	Rated Amperage
60	0.6	.035-.045 (0.9-1.2)	12 ft.	300

Baldor CD3450 motor technical specifications [26]

Catalog Number:	CD3450
Specification Number:	34-6172-1909
Horsepower:	0.50
Armature Voltage:	90
Field Voltage:	100/50
Full Load Amps - Armature:	N/A
Full Load Amps - Field:	n/a
RPM:	1750
Frame Size:	56C
Service Factor:	n/a
Rating:	40C
Insulation Class:	F
Form Factor:	n/a
Enclosure:	TEFC
Baldor Type:	3420D
DE Bearing:	6203
ODE Bearing:	6203
Electrical Specification Number:	34WG1909
Mechanical Specification Number:	34LY6172
Base:	RG
Mounting:	F1
Tach Mounting Kit:	n/a
Blower Kit:	n/a
Filter Kit:	n/a
Recommended SCR Control:	n/a

Lincoln Electric Idealarc CV-300 welding machine technical specifications [29]

INPUT – THREE PHASE ONLY		
Standard Voltage 230/460/575/3/60	Input Current at Rated Output 100% Duty Cycle 60/30/24 60% Duty Cycle 61/31/25	Code Number 10181
RATED OUTPUT		
Duty Cycle 100% Duty Cycle	Amps 300	Volts at Rated Output 32
MISC INFORMATION		
Efficiency at 100% Load See Appendix B for Plot Idle Power 800W	Input kVA 60% Load – 24.1 100% Load – 23.8	Idle Current - Amps 11/10/5

APPENDIX II

TecPlot and Visual BASIC for Application (VBA) code

```
Sub Fetch()
Dim imax, jmax, kmax, max_temp_col, max_temp_row As Integer
Dim x, y, signal, temp, camera_scale As Double
Dim camera_y_factor, spec_wavelength, const_c2 As Double
Dim emm_plate, emm_weld, x_shift, y_shift, pipe_dia, fn As Double

const_c2 = 14387 ' universal constant, never changes
spec_wavelength = 0.004 ' constant for our camera

camera_y_factor = 1.36667878884876 'depends on cmaera distances and angles
camera_scale = 1 / 60 'in

camera_scale = 25.4 * camera_scale 'mm
camera_y_factor = camera_y_factor * camera_scale 'mm

emm_plate = 0.95 ' high heat paint
emm_weld = 0.85 ' oxidised steel

imax = ActiveSheet.Cells(2, 11)
jmax = ActiveSheet.Cells(3, 11)
max_temp_col = ActiveSheet.Cells(4, 11)
max_temp_row = ActiveSheet.Cells(5, 11)

pipe_dia = ActiveSheet.Cells(7, 11) * 25.4  'mm

x_shift = ActiveSheet.Cells(11, 11) ' shift of origin
y_shift = ActiveSheet.Cells(12, 11) ' shift of origin

kmax = imax * jmax

ActiveSheet.Cells(9, 9) = kmax

For i = 1 To imax
   For j = 1 To jmax

      x = x_shift + camera_scale * (j - max_temp_col) 'mm ' no geometry compensataion
      y = y_shift + camera_scale * (i - max_temp_row) 'mm 'geometry compensation
```

```
        'fn = 1 - (2 * y / pipe_dia)
        'y = 0.5 * pipe_dia * (Math.Atn(-fn / Math.Sqr(Math.Abs(-fn * fn + 1))) + 2 _
         * Math.Atn(1))


        ActiveSheet.Cells(18, 11) = y

        y = -y

        'Rotational to linear coordinates
        'If (y < 0) Then
           'y = (pipe_dia / 2) * ActiveSheet.Cells(19, 11)
        'Else
           'y = -(pipe_dia / 2) * ActiveSheet.Cells(19, 11)
        'End If

        signal = Sheet1.Cells(i, j)

        temp = 0.57128 * signal + 401.37567 'calibration curve

        temp = temp + 273.15 ' kelvin

        If (x > 7 & x < -7) Then
           emm = emm_plate ' painted plate
        Else
           emm = emm_weld ' unpainted weld
        End If

        temp = 1 / ((1 / temp) + ((spec_wavelength * Log(emm)) / const_c2)) 'kelvin

        temp = temp - 273.15 ' deg C

        ActiveSheet.Cells(((i - 1) * jmax + j), 1) = x 'mm
        ActiveSheet.Cells(((i - 1) * jmax + j), 2) = y 'mm
        ActiveSheet.Cells(((i - 1) * jmax + j), 3) = temp 'deg C
    Next j
Next i
Call SortRange1
'(ActiveSheet.Range("A1:C65536"),ActiveSheet.Range("A1:A65536"),ActiveSheet._
Range("B1:B65536"))
End Sub
Sub SortRange1()
   Worksheets("Sheet2").Range("A1:C65536").Sort _
        Key1:=Worksheets("Sheet2").Range("A1"), _
        Key2:=Worksheets("Sheet2").Range("B1")
```

```
End Sub
Sub Clear()
ActiveSheet.Range("A1:C65536").ClearContents
End Sub
Sub RunTecplot()
'Calls Tecplot
  Dim myappID As Variant
  Dim strEnv As String
  Dim strCommand As String
  Dim strTecpath As String
  Dim nLenv As Integer

  'Determine where to put the datafile
  strTecpath = Environ("TEMP")

  strEnv = ""
  strCommand = ""

  'Find Tecplot
  If Environ("TEC90HOME") <> "" Then
    strEnv = Environ("TEC90HOME")
  ElseIf Environ("TEC80HOME") <> "" Then
    strEnv = Environ("TEC80HOME")
  ElseIf Environ("TEC75HOME") <> "" Then
    strEnv = Environ("TEC75HOME")
  ElseIf Environ("TEC70HOME") <> "" Then
    strEnv = Environ("TEC70HOME")
  Else
    MsgBox ("Tecplot not found.  Please check system variables for correct path.")
  End If
  If strEnv <> "" Then
    'Check strEnv for excess quotemarks
    nLenv = Len(strEnv) - 2
    If Right(strEnv, 1) = """" Then
      strCommand = Mid(strEnv, 2, nLenv)
    Else
      strCommand = strEnv
    End If
    strCommand = strCommand + "\bin\tecplot"

    If Validrange(strTecpath) = True Then
      strCommand = strCommand + " " + strTecpath + "\" + "tecfile.dat"
      myappID = Shell(strCommand, 1)
      AppActivate myappID
    End If
```

```
  End If

End Sub

Function Validrange(strIn As String) As Boolean
'Determines appropriate range(s) and creates datafile from data in range.

   Dim rg1 As Range
   Dim nInd, nRow, nCol, nRows, nCols, nFnum As Integer
   Dim x, y, nFstat, nNumvars, nTop, yp As Integer
   Dim strFilename, strMacroname, strVars, strZone, strData As String
   Dim bNextblock As Boolean

   Set rg1 = Application.Selection
   strFilename = strIn + "\" + "tecfile.dat"
   nTop = ActiveCell.Row
   nCol = ActiveCell.Column
   nRow = nTop
   nFstat = 0
   nNumvars = 0
   nInd = nCol + 1

   If rg1.Cells.Count = 1 Then
   '*** one cell in range ****
     If ActiveCell.Value = "" Then
     'carpet format... determine block size
        Do While IsNumeric(CStr(Cells(nRow, nInd).Value)) = True
          nInd = nInd + 1
        Loop
        nCols = nInd - 1
        nInd = nRow + 1
        Do While IsNumeric(CStr(Cells(nInd, nCol).Value)) = True
          nInd = nInd + 1
        Loop
        nRows = nInd - 1

        'test the block
        If nCols = nCol Or nRows <= nRow + 1 Then
          MsgBox ("Not a valid selection.")
          Validrange = False
        Else
        'Write file header
          strVars = "VARIABLES = ""X"", ""Y"", ""V"""
          strZone = "ZONE I=" + CStr(nCols - nCol) + ", J=" + CStr(nRows - nRow) _
          + ", F=POINT"
          nFnum = FreeFile
```

```
        Open strFilename For Output As #nFnum
        Print #nFnum, strVars
        Print #nFnum, strZone

        'Write the data
        For y = nRow + 1 To nRows
          For x = nCol + 1 To nCols
            If IsNumeric(Cells(y, x).Value) = False Then
              Print #nFnum, CStr(Cells(nRow, x).Value); Tab; CStr(Cells_
              (y, nCol).Value); Tab; "0"
            Else
              Print #nFnum, CStr(Cells(nRow, x).Value); Tab; CStr(Cells_
              (y, nCol).Value); Tab; CStr(Cells(y, x).Value)
            End If
          Next x
        Next y
        Close #nFnum
        nFstat = nFstat + 1
      End If
Else
  'table format
    If IsNumeric(CStr(ActiveCell.Value)) = True Then
      'No variables listed . . .  determine block size
      Do While IsNumeric(CStr(Cells(nRow, nInd).Value)) = True
      nInd = nInd + 1
      Loop
      nCols = nInd - 1
      nInd = nRow + 1
      Do While IsNumeric(CStr(Cells(nInd, nCol).Value)) = True
        nInd = nInd + 1
      Loop
      nRows = nInd - 1
      'Test the range
      If nRows = nRow Then
        MsgBox ("Not a valid selection.")
        Validrange = False
      Else
      'Write file header
        strVars = "VARIABLES = ""X1"""
        If nCols > nCol Then
          For nInd = 2 To nCols - nCol + 1
            strVars = strVars + " , ""X" + CStr(nInd) + """"
          Next nInd
        End If
        strZone = "ZONE I=" + CStr(nRows - nRow + 1) + ", J = 1, F=POINT"
        nFnum = FreeFile
```

```
    Open strFilename For Output As #nFnum
    Print #nFnum, strVars
    Print #nFnum, strZone

    'Write the data
    For nInd = nRow To nRows
      strData = ""
      For x = nCol To nCols
        If IsNumeric(Cells(nInd, x).Value) = True Then
          strData = strData + CStr(Cells(nInd, x).Value) + " "
        Else
          strData = strData + "0" + " "
        End If
      Next x
      Print #nFnum, strData
    Next nInd
    Close #nFnum
    nFstat = nFstat + 1
  End If

Else
  'Table format ...  Variable names listed.
  Do While Cells(nRow, nInd).Value <> ""
  nInd = nInd + 1
  Loop
  nCols = nInd - 1
  nInd = nRow + 1
  Do While IsNumeric(CStr(Cells(nInd, nCol).Value)) = True
    nInd = nInd + 1
  Loop
  nRows = nInd - 1

  'Test the range
  If nRows > nRow + 1 Then
    'Write the file header
    strVars = "VARIABLES = """ + CStr(Cells(nRow, nCol).Value) + """"
    If nCols > nCol Then
      For nInd = nCol + 1 To nCols
        strVars = strVars + " , """ + CStr(Cells(nRow, nInd).Value) + """"
      Next nInd
    End If
    strZone = "ZONE I=" + CStr(nRows - nRow) + ", J = 1, F=POINT"
    nFnum = FreeFile
    Open strFilename For Output As #nFnum
    Print #nFnum, strVars
    Print #nFnum, strZone
```

```
            'Write the data
            For nInd = nRow + 1 To nRows
              strData = ""
              For x = nCol To nCols
                If IsNumeric(Cells(nInd, x).Value) = True Then
                  strData = strData + CStr(Cells(nInd, x).Value) + " "
                Else
                  strData = strData + "0" + " "
                End If
              Next x
              Print #nFnum, strData
            Next nInd
            Close #nFnum
            nFstat = nFstat + 1
          Else
            MsgBox ("Not a valid selection.")
          End If

        End If
    End If

Else
'************ More than one cell in range ************
  bNextblock = True
  nFstat = 0
  Do While bNextblock = True

   If Cells(nRow, nCol).Value = "" Then
   'carpet format...determine block size
      If nFstat = 0 Then
        nNumvars = 3
      End If
      nInd = nCol + 1
      Do While IsNumeric(CStr(Cells(nRow, nInd).Value)) = True And nInd < _
       nCol + rg1.Columns.Count
        nInd = nInd + 1
      Loop
      nCols = nInd - 1
      nInd = nRow + 1
      Do While IsNumeric(CStr(Cells(nInd, nCol).Value)) = True And nInd < _
       nTop + rg1.Rows.Count
        nInd = nInd + 1
      Loop
      nRows = nInd - 1
      'Test the range
```

```
  If nCols = nCol Or nRows <= nRow + 1 Or nNumvars <> 3 Then
    MsgBox ("Not a valid selection.")
    bNextblock = False
  Else
   'Write file header
    strVars = "VARIABLES = ""X"", ""Y"", ""V"""
    strZone = "ZONE I=" + CStr(nCols - nCol) + ", J=" + CStr(nRows - nRow) _
   + ", F=POINT"
    nFnum = FreeFile
    If nFstat = 0 Then
      Open strFilename For Output As #nFnum
      Print #nFnum, strVars
    Else
      Open strFilename For Append As #nFnum
      Print #nFnum,
    End If

    Print #nFnum, strZone

    'Write the data
    For y = nRow + 1 To nRows
       For x = nCol + 1 To nCols
          If IsNumeric(Cells(y, x).Value) = False Then
            Print #nFnum, CStr(Cells(nRow, x).Value); Tab; CStr(Cells_
            (y, nCol).Value); Tab; "0"
          Else
            Print #nFnum, CStr(Cells(nRow, x).Value); Tab; CStr(Cells_
            (y, nCol).Value); Tab; CStr(Cells(y, x).Value)
          End If
       Next x
     Next y
    Close #nFnum
    nFstat = nFstat + 1

  End If

Else
  'table format
  If IsNumeric(Cells(nRow, nCol).Value) = True Then
  'no variables listed
    nInd = nCol + 1
    Do While IsNumeric(CStr(Cells(nRow, nInd).Value)) = True And nInd < _
    nCol + rg1.Columns.Count
      nInd = nInd + 1
    Loop
    nCols = nInd - 1
```

```
If nFstat = 0 Then
  nNumvars = nCols
End If
nInd = nRow + 1
Do While IsNumeric(CStr(Cells(nInd, nCol).Value)) = True And nInd <_
nTop + rg1.Rows.Count
  nInd = nInd + 1
Loop
nRows = nInd - 1
'Test the range
If nRows = nRow Or nCols <> nNumvars Then
  MsgBox ("Not a valid selection.")
  bNextblock = False
Else
'Write file header
  strVars = "VARIABLES = ""X1"""
  If nCols > nCol Then
    For nInd = 2 To nCols - nCol + 1
      strVars = strVars + " , ""X" + CStr(nInd) + """"
    Next nInd
  End If
  strZone = "ZONE I=" + CStr(nRows - nRow + 1) + ", J = 1, F=POINT"
  nFnum = FreeFile
  If nFstat = 0 Then
    Open strFilename For Output As #nFnum
    Print #nFnum, strVars
  Else
    Open strFilename For Append As #nFnum
    Print #nFnum,
  End If
  Print #nFnum, strZone

  'Write the data
  For nInd = nRow To nRows
    strData = ""
    For x = nCol To nCols
      If IsNumeric(Cells(nInd, x).Value) = True Then
        strData = strData + CStr(Cells(nInd, x).Value) + " "
      Else
        strData = strData + "0" + " "
      End If
    Next x
    Print #nFnum, strData
  Next nInd
  Close #nFnum
  nFstat = nFstat + 1
```

```
  End If
Else
  'Table format...Variable names listed.
    nInd = nCol + 1
    Do While Cells(nRow, nInd).Value <> "" And nInd < nCol +_
            rg1.Columns.Count
      nInd = nInd + 1
    Loop
    nCols = nInd - 1
    If nFstat = 0 Then
      nNumvars = nCols
    End If
    nInd = nRow + 1
    Do While IsNumeric(CStr(Cells(nInd, nCol).Value)) = True And nInd < _
          nTop + rg1.Rows.Count
      nInd = nInd + 1
    Loop
    nRows = nInd - 1

    'Test the range
    If nRows > nRow + 1 And nCols = nNumvars Then
      'Write file header
      strVars = "VARIABLES = """ + CStr(Cells(nRow, nCol).Value) + """"
      If nCols > nCol Then
        For nInd = nCol + 1 To nCols
          strVars = strVars + " , """ + CStr(Cells(nRow, nInd).Value) + """"
        Next nInd
      End If
      strZone = "ZONE I=" + CStr(nRows - nRow) + ", J = 1, F=POINT"
      nFnum = FreeFile

      If nFstat = 0 Then
        Open strFilename For Output As #nFnum
        Print #nFnum, strVars
      Else
        Open strFilename For Append As #nFnum
        Print #nFnum,
      End If
      Print #nFnum, strZone

      'Write data
      For nInd = nRow + 1 To nRows
        strData = ""
        For x = nCol To nCols
          If IsNumeric(Cells(nInd, x).Value) = True Then
```

```
                    strData = strData + CStr(Cells(nInd, x).Value) + " "
                  Else
                    strData = strData + "0" + " "
                  End If
                Next x
                Print #nFnum, strData
              Next nInd
              Close #nFnum
              nFstat = nFstat + 1
            Else
              MsgBox ("Not a valid selection.")
              nNextBlock = False
            End If
          End If
        End If

        'Determine whether there is another block of data below
        nRow = nRows + 2

        If nRow > nTop + rg1.Rows.Count - 1 Or (Cells(nRow, nCol).Value = "" _
            And Cells(nRow, nCol + 1).Value = "") Then
          bNextblock = False
        End If

      Loop

    End If

    'Determine return value
    If nFstat > 0 Then
      Validrange = True
    Else
      Validrange = False
    End If

End Function
```

APPENDIX III

Analytical Calculation in Visual BASIC for Application (VBA) code

```
Option Explicit
Sub Pipe_Welding_Heat_Source()

Pi = 3.141592654
e = 2.718281828
arc_velocity = Worksheets("sheet1").Cells(2, 3) / 10
arc_beam_radius = Worksheets("sheet1").Cells(3, 3) / 10 / 2
thickness = Worksheets("sheet1").Cells(4, 3) / 10
a = Worksheets("sheet1").Cells(5, 3)
pipe_diameter = Worksheets("sheet1").Cells(6, 3) / 10
t = Worksheets("sheet1").Cells(7, 3)
max_row = Worksheets("sheet1").Cells(8, 3)
heat_liberation = Worksheets("sheet1").Cells(9, 3)
lambda = Worksheets("sheet1").Cells(10, 3)
k = 20
lower_limit_r = 0
upper_limit_r = arc_beam_radius
h = 30
delta_r = (upper_limit_r - lower_limit_r) / 30
Length = Pi * pipe_diameter
V = (arc_velocity) / (2 * a) '1/cm
distance_over_a_time = (arc_velocity) * t  'vt
integral_upper_limit = (V * distance_over_a_time / 2)
B = integral_upper_limit

Worksheets("sheet1").Cells(8, 4) = 0
For row = 0 To max_row

   theta = 0

   y_num = Worksheets("sheet1").Cells(row + 2, 8) / 10 'cm
   x_num = Worksheets("sheet1").Cells(row + 2, 9) / 10 'cm
   z_num = Worksheets("sheet1").Cells(11, 3)      'cm

   x1_num = x_num  '
   x2_num = Length - x_num
```

```
y0_num = y_num

z_heatsource_num = z_num
z_image_num = 2 * thickness - z_num

'Main equation loop for boundary conditions
For z = 1 To 2
   For jj = 1 To 30
      ri_num = jj * delta_r
      riv_num = ri_num * V

         If z = 1 Then
               eXV = e ^ (-x1_num * V)
               x_num = x1_num
               y_num = y0_num
               z_num = z_heatsource_num
               u_num = V * ((x1_num) ^ 2 + (y0_num) ^ 2 + (z_heatsource_num) ^ 2 +_
               ri_num ^ 2) ^ (1 / 2)
            ElseIf z = 2 Then
               eXV = e ^ (-x1_num * V)
               x_num = x1_num
               y_num = y0_num
               z_num = z_image_num
               u_num = V * ((x1_num) ^ 2 + (y0_num) ^ 2 + (z_image_num) ^ 2 + _
               ri_num ^ 2) ^ (1 / 2)
            ElseIf z = 3 Then
               eXV = e ^ (-x2_num * V)
               x_num = x2_num
               y_num = y0_num
               z_num = z_heatsource_num
               u_num = V * ((x2_num) ^ 2 + (y0_num) ^ 2 + (z_heatsource_num) ^ 2 +
               ri_num ^ 2) ^ (1 / 2)
            ElseIf z = 4 Then
               eXV = e ^ (-x2_num * V)
               x_num = x2_num
               y_num = y0_num
               z_num = z_image_num
               u_num = V * ((x2_num) ^ 2 + (y0_num) ^ 2 + (z_image_num) ^ 2 + _
               ri_num ^ 2) ^ (1 / 2)
         End If

      'Sum1 calculations
      sum1 = 0
      endsum = 0
      evensum = 0
      oddsum = 0
```

```
hh = 20
If B >= 6 Then
     upper_limit = 6
     lower_limit = 0.1
   ElseIf B < 6 And B >= 0.1 Then
     upper_limit = B
     lower_limit = 0.1
   ElseIf B < 0.1 Then
     delta_w = 0
End If
delta_w = (upper_limit - lower_limit) / hh
For ii = 0 To k
   ww_num = lower_limit + ii * delta_w
   pp_num = riv_num * (V / (2 * ww_num)) * ((x_num + (2 * ww_num / V)) ^ _
   2 + y_num ^ 2) ^ (1 / 2)
      If pp_num < 1.6 Then
         Fw_num(ii) = 0.935 * e ^ (0.352 * pp_num - ww_num - (u_num ^ 2 / _
         (4 * ww_num))) * (1 / ww_num ^ (3 / 2))
      ElseIf 1.6 < pp_num <= 3 Then
         Fw_num(ii) = 0.529 * e ^ (0.735 * pp_num - ww_num - (u_num ^ 2 / _
         (4 * ww_num))) * (1 / ww_num ^ (3 / 2))
      ElseIf pp_num > 3 Then
         Fw_num(ii) = (1 / (2 * Pi * pp_num) ^ (1 / 2)) * e ^ (pp_num - _
         ww_num - (u_num ^ 2 / (4 * ww_num))) * (1 / ww_num ^ (3 / 2))
   End If
Next ii
endsum = Fw_num(0) + Fw_num(k)
For kk = 1 To 19 Step 2 'k-1 must be an odd number
   oddsum = oddsum + Fw_num(kk)
Next kk
For kk = 2 To 18 Step 2 'k-2 must be an even number
   evensum = evensum + Fw_num(kk)
Next kk

sum1 = (endsum + 4 * oddsum + 2 * evensum) * delta_w / 3

'Sum2 calculations
sum2 = 0
endsum = 0
evensum = 0
oddsum = 0
If 0.1 > B And B > 0.001 Then
   upper_limit = B
   lower_limit = 0.001
ElseIf B > 0.1 Then
   upper_limit = 0.1
```

```
   lower_limit = 0.001
ElseIf B < 0.001 Then
   delta_w = 0
End If
delta_w = (upper_limit - lower_limit) / 20
For ii = 0 To 20
         'ii steps to solve integral
   ww_num = lower_limit + ii * delta_w 'divisions
         'Inside of the Bessel Function
   pp_num = riv_num * (V / (2 * ww_num)) * _
          ((x_num + (2 * ww_num / V)) ^ 2 + y_num ^ 2) ^ (1 / 2)

   'Bessel Function with radial integral attached
     If pp_num < 1.6 Then
         Fw_num1(ii) = 0.935 * e ^ (0.352 * pp_num - ww_num - (u_num ^ 2 / _
         (4 * ww_num))) * (1 / ww_num ^ (3 / 2))
      ElseIf 1.6 < pp_num <= 3 Then
         Fw_num1(ii) = 0.529 * e ^ (0.735 * pp_num - ww_num - (u_num ^ 2 / _
         (4 * ww_num))) * (1 / ww_num ^ (3 / 2))
      ElseIf pp_num > 3 Then
         Fw_num1(ii) = (1 / (2 * Pi * pp_num) ^ (1 / 2)) * e ^ (pp_num - _
         ww_num - (u_num ^ 2 / (4 * ww_num))) * (1 / ww_num ^ (3 / 2))
   End If
Next ii

'Integration including Bessel function
endsum = Fw_num1(0) + Fw_num1(k)

For kk = 1 To (k - 1) Step 2
   oddsum = oddsum + Fw_num1(kk)
Next kk

For kk = 2 To (k - 2) Step 2
   evensum = evensum + Fw_num1(kk)
Next kk

sum2 = (endsum + 4 * oddsum + 2 * evensum) * delta_w / 3

sum3 = 0
endsum = 0
evensum = 0
oddsum = 0
upper_limit = 0.001
lower_limit = 0.000001

'Start change for sum3
```

```
    hh = 20
    delta_w = (upper_limit - lower_limit) / hh
    For ii = 0 To k
            'ii steps to solve integral
       ww_num = lower_limit + ii * delta_w 'divisions
            'Inside of the Bessel Function
       pp_num = riv_num * (V / (2 * ww_num)) * _
             ((x_num + 2 * ww_num / V) ^ 2 + y_num ^ 2) ^ (1 / 2)
            'Bessel Function with radial integral attached
          If pp_num < 1.6 Then
            Fw_num2(ii) = 0.935 * e ^ (0.352 * pp_num - ww_num - (u_num ^ 2 / _
            (4 * ww_num))) * (1 / ww_num ^ (3 / 2))
          ElseIf 1.6 < pp_num <= 3 Then
            Fw_num2(ii) = 0.529 * e ^ (0.735 * pp_num - ww_num - (u_num ^ 2 / _
            (4 * ww_num))) * (1 / ww_num ^ (3 / 2))
          ElseIf pp_num > 3 Then
            Fw_num2(ii) = (1 / (2 * Pi * pp_num) ^ (1 / 2)) * e ^ (pp_num - _
            ww_num - (u_num ^ 2 / (4 * ww_num))) * (1 / ww_num ^ (3 / 2))
       End If
    Next ii

    'Integration including Bessel function
    endsum = Fw_num2(0) + Fw_num2(k)

    For kk = 1 To (k - 1) Step 2
       oddsum = oddsum + Fw_num2(kk)
    Next kk
    For kk = 2 To (k - 2) Step 2
       evensum = evensum + Fw_num2(kk)
    Next kk

    sum3 = (endsum + 4 * oddsum + 2 * evensum) * delta_w / 3

    'Sum of 3 exponential values 0-0.001, 0.001-0.1, and 0.1-5
    ssum = sum1 + sum2 + sum3

    'Integration of radius function
       Fr_num(jj) = ri_num * e ^ (-6 * (ri_num / arc_beam_radius) ^ 2) * ssum
    If ri_num = 0 Then
       Fr_num(jj) = 0
       ssum = 0
    End If
Next jj

'Integration of the r function
'rsum = 0
```

```
        roddsum = 0
        revensum = 0
        rendsum = Fr_num(0) + Fr_num(h)

        For ii = 1 To 29 Step 2 'h-1 must be an odd number
           roddsum = roddsum + Fr_num(ii)
        Next ii

        For ii = 2 To 28 Step 2 'h-2 must be an even number
           revensum = revensum + Fr_num(ii)
        Next ii

        rsum = (rendsum + 4 * roddsum + 2 * revensum) * delta_r / 3
        integral = (6.0132 * heat_liberation * arc_velocity * eXV * rsum) / (4 * lambda * _
        a * arc_beam_radius ^ 2 * Pi ^ (3 / 2))  'constant

        theta = theta + integral

        'Checking values within the program as they are calculated
        'Worksheets("sheet1").Cells(row + 2, 13 + z) = integral
        'Worksheets("sheet1").Cells(row + 2, 18 + z) = eXV
        'Worksheets("sheet1").Cells(row + 2, 23 + z) = ssum
        'Worksheets("sheet1").Cells(row + 2, 28 + z) = rsum

    Next z

    Worksheets("sheet1").Cells(row + 2, 10) = theta
    Worksheets("sheet1").Cells(8, 4) = row

Next row
Worksheets("sheet1").Cells(8, 4) = ""
End Sub
```

APPENDIX IV

Experimental and analytical images and comparison for a weld velocity of 0.545 cm/s.

Analytical solution interface for the weld velocity of 0.545 cm/s.

Given Parameters	Value (Entered by User)	Units
Welding Speed (Arc Velocity)	5.454	mm/s
Arc Beam diameter	0.900	cm
Thickness of Steel Pipe	0.762	mm
Thermal Diffusivity	0.136	cm^2/s
Pipe (outer) diameter	165	mm
Time Elapsed		s
No of Experimental Data Points		
Heat Liberation Qpl	2444.46	W
Thermal Conductivity	0.52	J/(cm.s.K)
Z-Coordinate	0	cm

Transient to quasi-steady state temperature distributions for 1 s to 20 s in 1 s increments for the comparison of experimental data and analytical data for a weld velocity of 0.545 mm/s

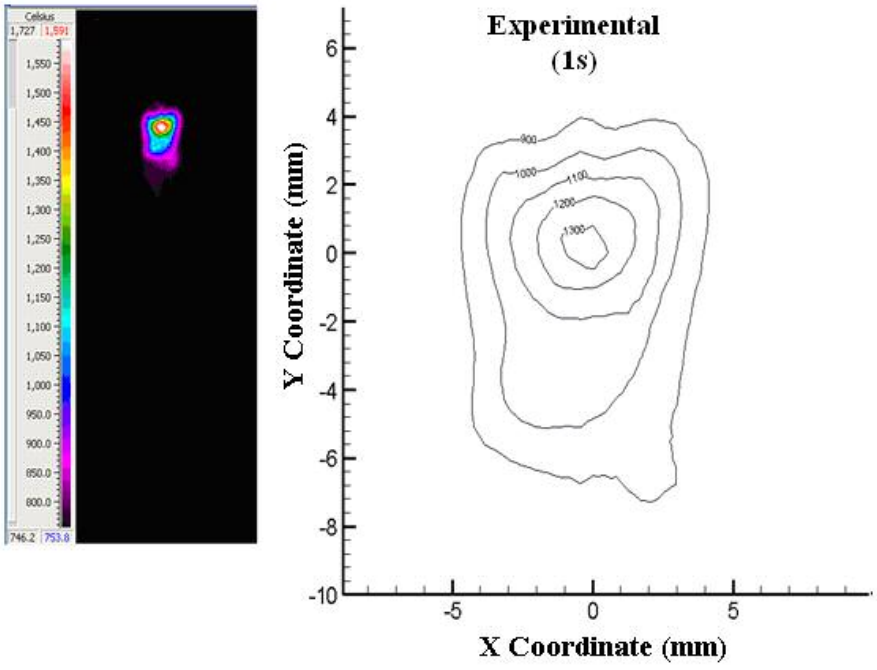

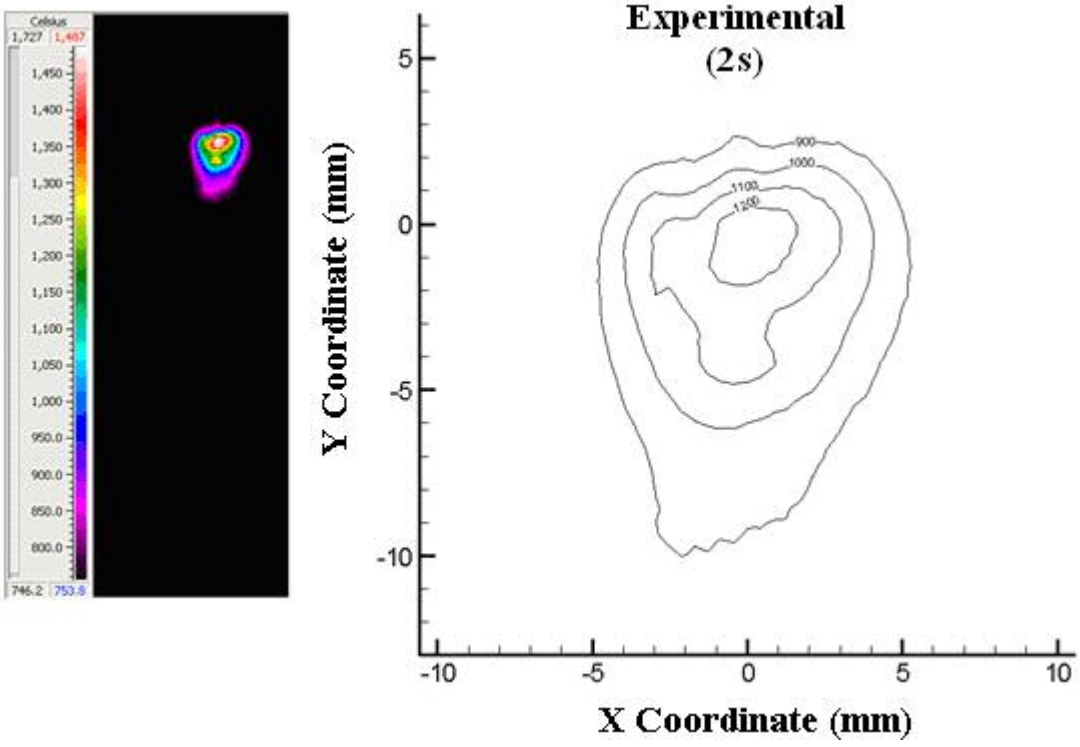
Celsius
1,727
1,467
1,450
1,400
1,350
1,300
1,250
1,200
1,150
1,100
1,050
1,000
950.0
900.0
850.0
800.0
746.2
753.8
Experimental
(2s)
900
1000
1100
1200
Y Coordinate (mm)
X Coordinate (mm)
5
0
-5
-10
-10
-5
0
5
10

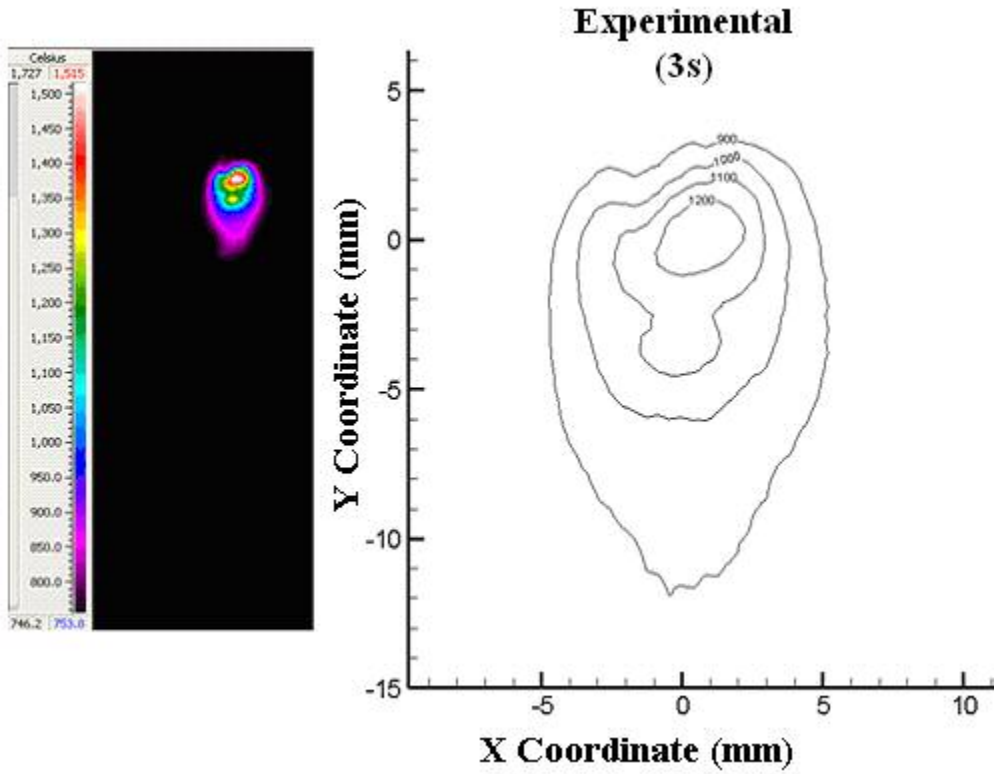
Celsius
1,727
1,515
1,500
1,450
1,400
1,350
1,300
1,250
1,200
1,150
1,100
1,050
1,000
950.0
900.0
850.0
800.0
746.2
753.0
Experimental
(3s)
900
1000
1100
1200
Y Coordinate (mm)
X Coordinate (mm)
5
0
-5
-10
-15
-5
0
5
10

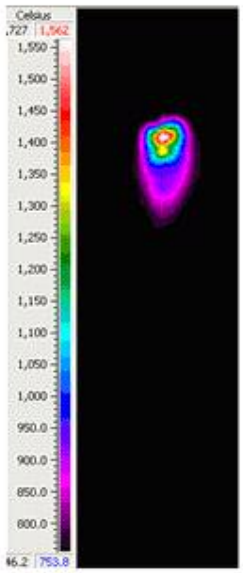
Celsius
1,727 1,562
1,550
1,500
1,450
1,400
1,350
1,300
1,250
1,200
1,150
1,100
1,050
1,000
950.0
900.0
850.0
800.0
746.2 753.8

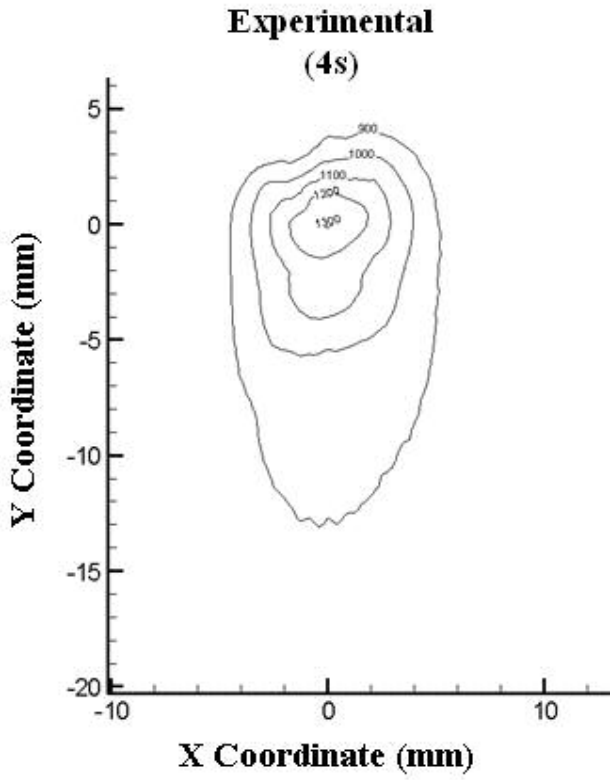
Experimental
(4s)
Y Coordinate (mm)
X Coordinate (mm)
5
0
-5
-10
-15
-20
-10
0
10
900
1000
1100
1200
1300

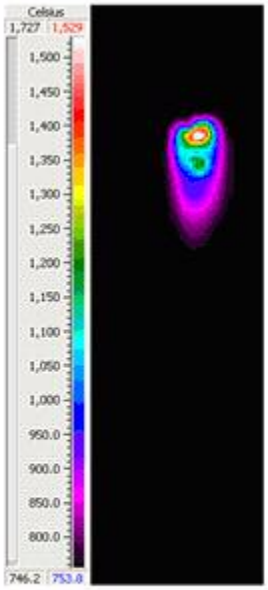
Celsius
1,727 1,529
1,500
1,450
1,400
1,350
1,300
1,250
1,200
1,150
1,100
1,050
1,000
950.0
900.0
850.0
800.0
746.2 753.8

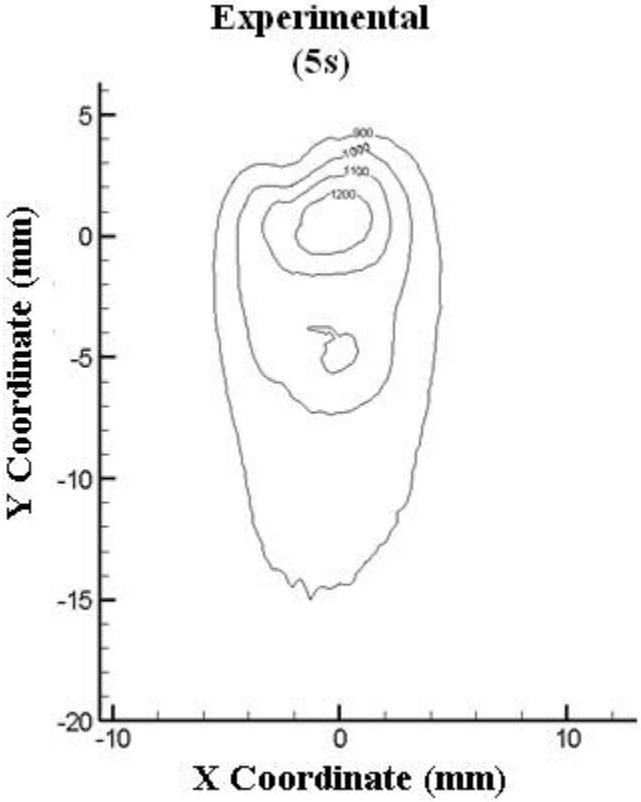
Experimental
(5s)
Y Coordinate (mm)
X Coordinate (mm)
5
0
-5
-10
-15
-20
-10
0
10
900
1000
1100
1200

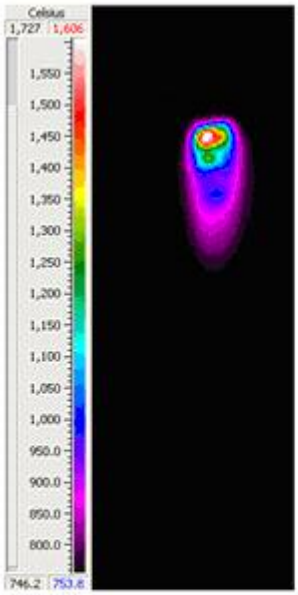
Celsius
1,727
1,606
1,550
1,500
1,450
1,400
1,350
1,300
1,250
1,200
1,150
1,100
1,050
1,000
950.0
900.0
850.0
800.0
746.2
753.8

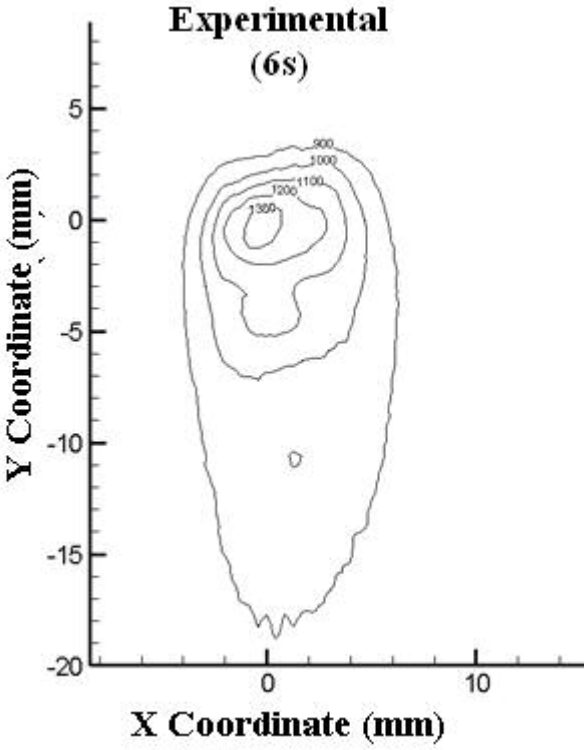
Experimental
(6s)
Y Coordinate (mm)
X Coordinate (mm)
5
0
-5
-10
-15
-20
0
10
900
1000
1100
1200
1300

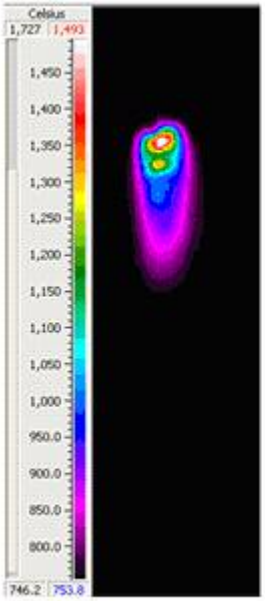
Celsius
1,727
1,493
1,450
1,400
1,350
1,300
1,250
1,200
1,150
1,100
1,050
1,000
950.0
900.0
850.0
800.0
746.2
753.8

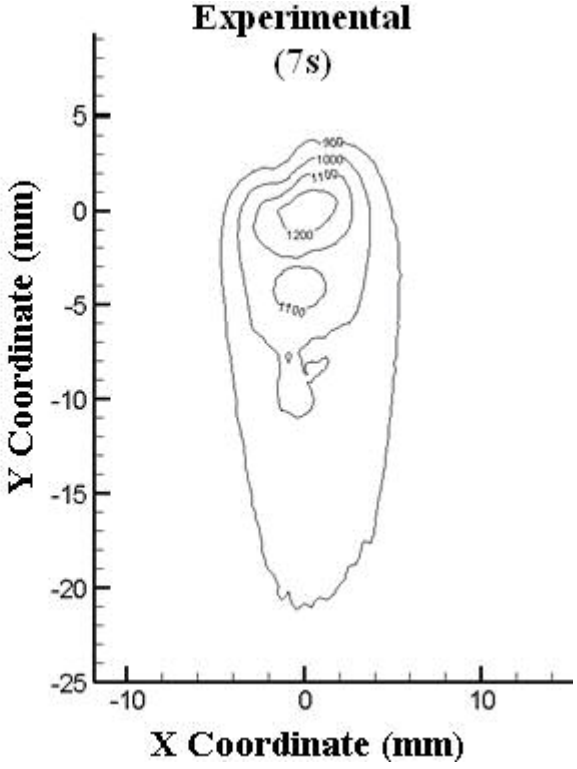
Experimental
(7s)
Y Coordinate (mm)
X Coordinate (mm)
5
0
-5
-10
-15
-20
-25
-10
0
10
900
1000
1100
1200
1700

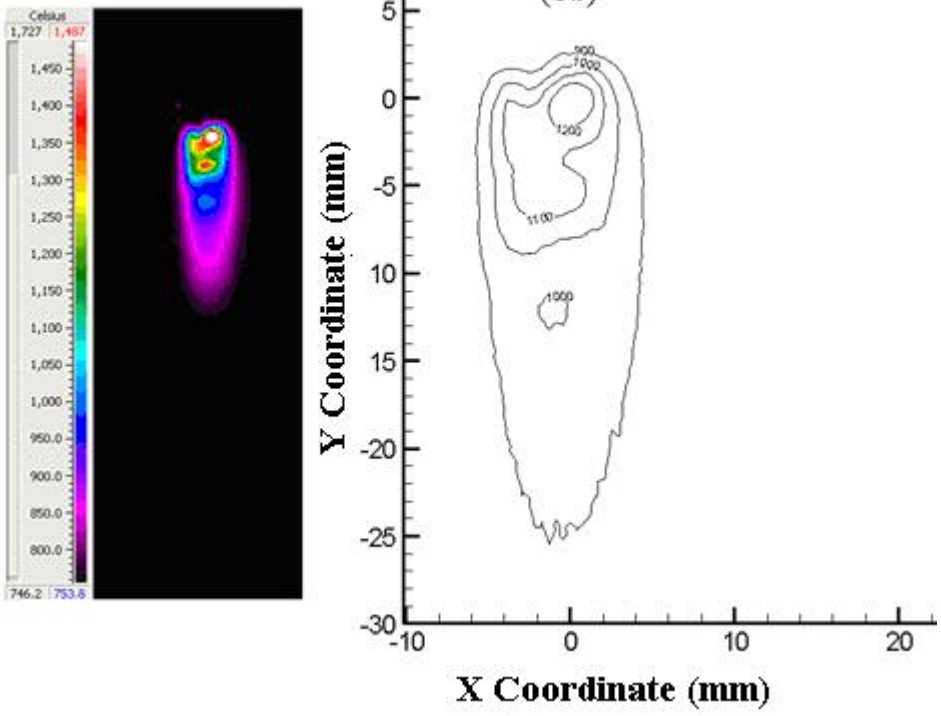
Celsius
1,727
1,487
1,450
1,400
1,350
1,300
1,250
1,200
1,150
1,100
1,050
1,000
950.0
900.0
850.0
800.0
746.2
753.8
Experimental
(8s)
Y Coordinate (mm)
X Coordinate (mm)
5
0
-5
-10
-15
-20
-25
-30
-10
0
10
20
900
1000
1100
1200

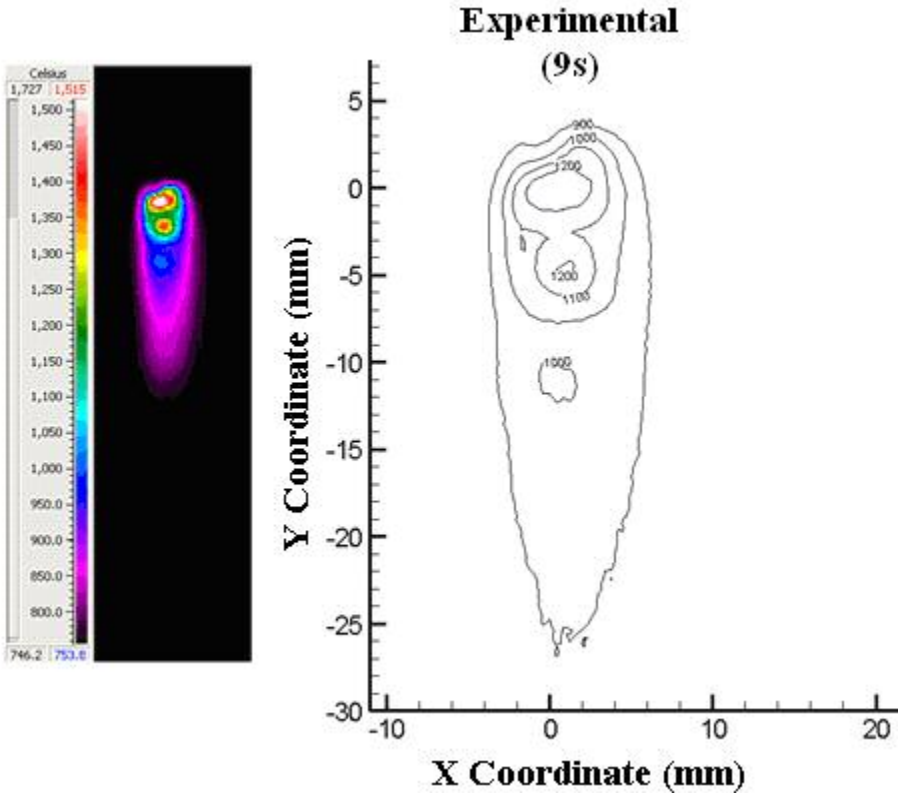
Celsius
1,727
1,515
1,500
1,450
1,400
1,350
1,300
1,250
1,200
1,150
1,100
1,050
1,000
950.0
900.0
850.0
800.0
746.2
753.8
Experimental
(9s)
Y Coordinate (mm)
X Coordinate (mm)
5
0
-5
-10
-15
-20
-25
-30
-10
0
10
20
900
1000
1100
1200

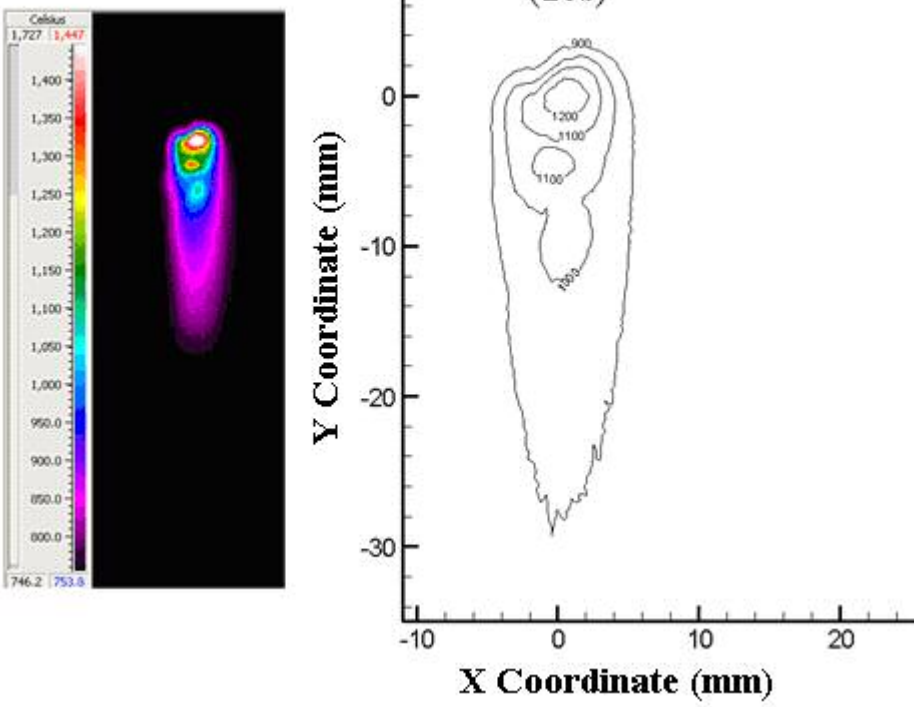
Experimental
(10s)
Celsius
1,727
1,447
1,400
1,350
1,300
1,250
1,200
1,150
1,100
1,050
1,000
950.0
900.0
850.0
800.0
746.2
753.8
900
1200
1100
1100
1000
0
-10
-20
-30
-10
0
10
20
Y Coordinate (mm)
X Coordinate (mm)

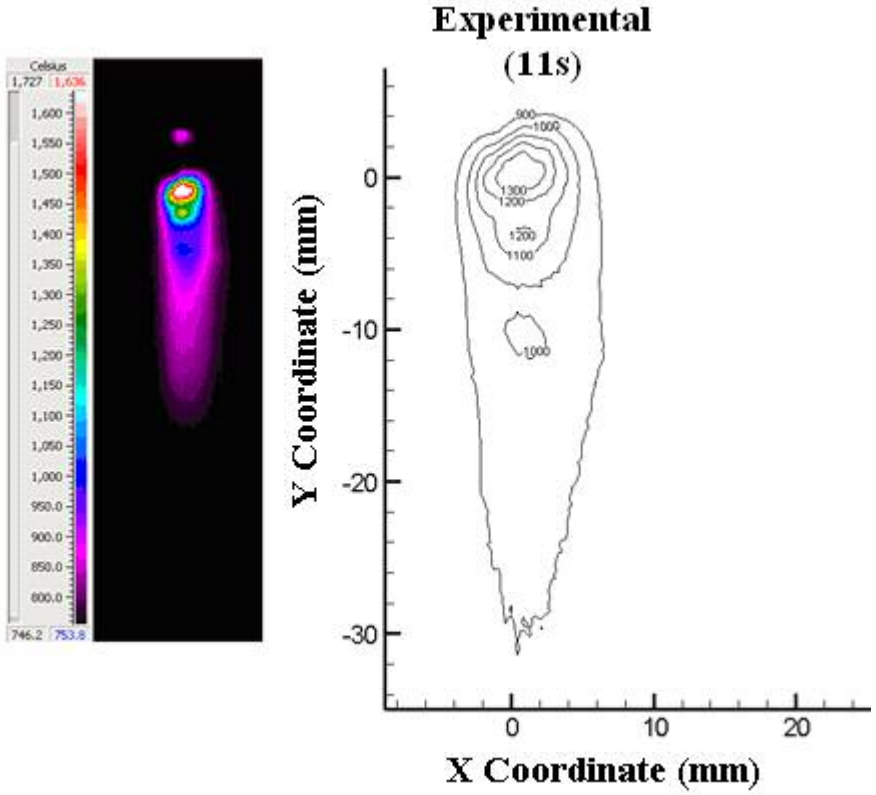
Experimental
(11s)
Celsius
1,727
1,636
1,600
1,550
1,500
1,450
1,400
1,350
1,300
1,250
1,200
1,150
1,100
1,050
1,000
950.0
900.0
850.0
800.0
746.2
753.8
900
1000
1300
1200
1200
1100
1000
0
-10
-20
-30
0
10
20
Y Coordinate (mm)
X Coordinate (mm)

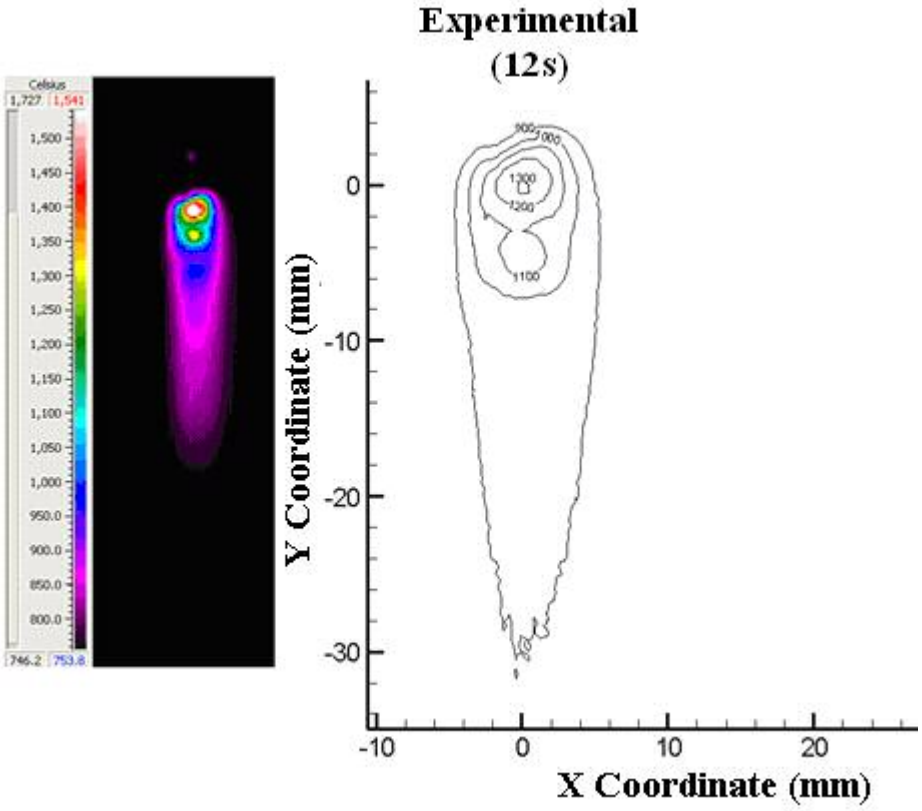
Experimental
(12s)
Celsius
1,727
1,541
1,500
1,450
1,400
1,350
1,300
1,250
1,200
1,150
1,100
1,050
1,000
950.0
900.0
850.0
800.0
746.2
753.8
900
1000
1200
1100
0
-10
-20
-30
Y Coordinate (mm)
-10
0
10
20
X Coordinate (mm)

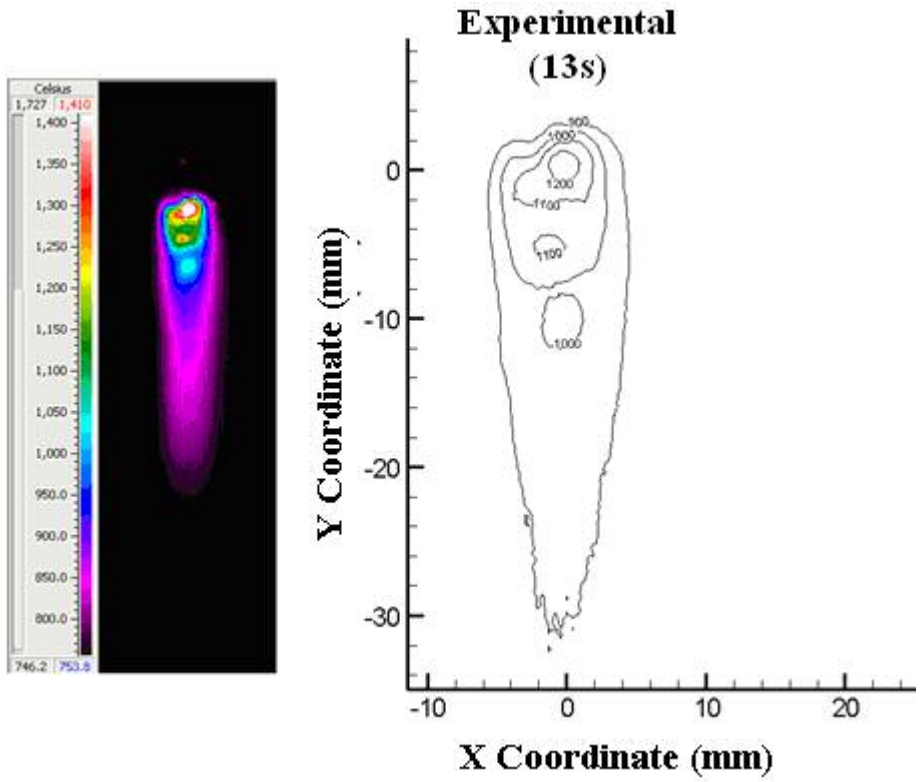
Experimental
(13s)
Celsius
1,727
1,410
1,400
1,350
1,300
1,250
1,200
1,150
1,100
1,050
1,000
950.0
900.0
850.0
800.0
746.2
753.8
900
1000
1200
1100
1100
1000
0
-10
-20
-30
Y Coordinate (mm)
-10
0
10
20
X Coordinate (mm)

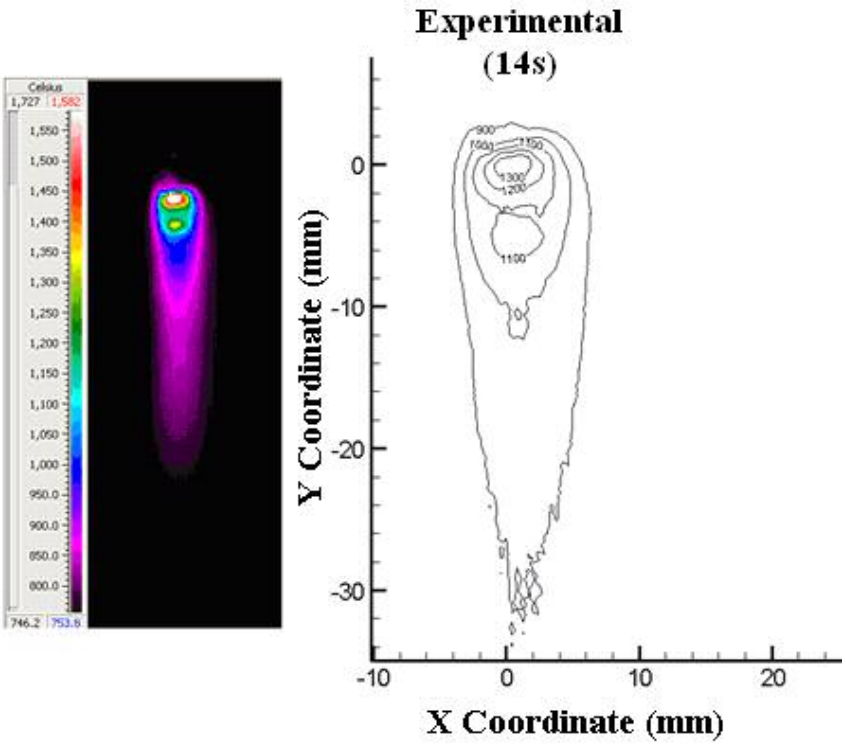
Experimental
(14s)
Celsius
1,727
1,582
1,550
1,500
1,450
1,400
1,350
1,300
1,250
1,200
1,150
1,100
1,050
1,000
950.0
900.0
850.0
800.0
746.2
753.8
900
1000
1100
1200
1300
0
-10
-20
-30
Y Coordinate (mm)
-10
0
10
20
X Coordinate (mm)

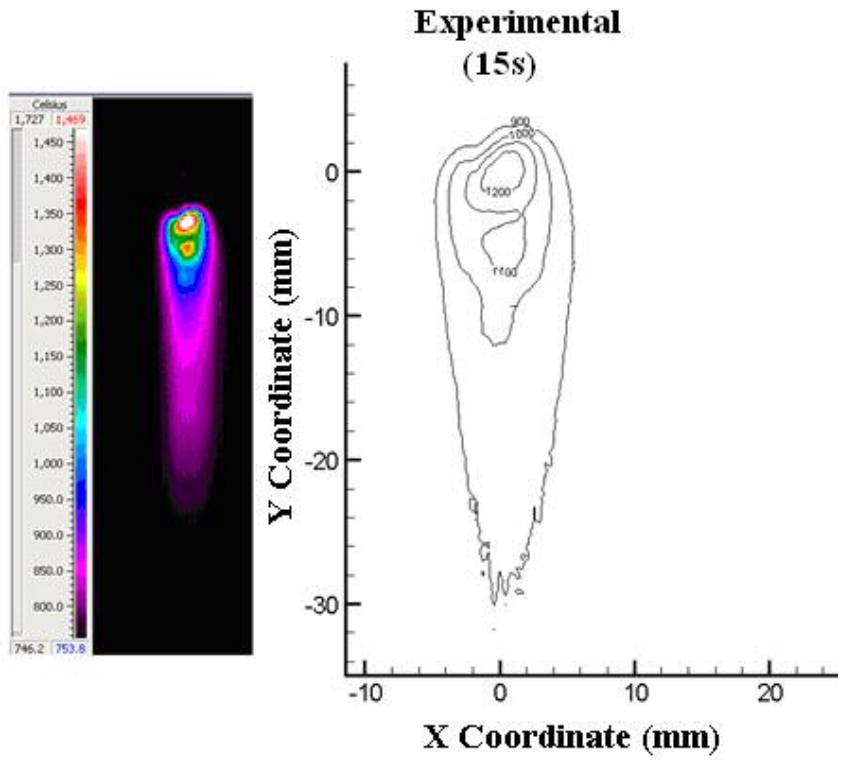
Experimental
(15s)
Celsius
1,727
1,469
1,450
1,400
1,350
1,300
1,250
1,200
1,150
1,100
1,050
1,000
950.0
900.0
850.0
800.0
746.2
753.8
900
1000
1200
1100
0
-10
-20
-30
Y Coordinate (mm)
-10
0
10
20
X Coordinate (mm)

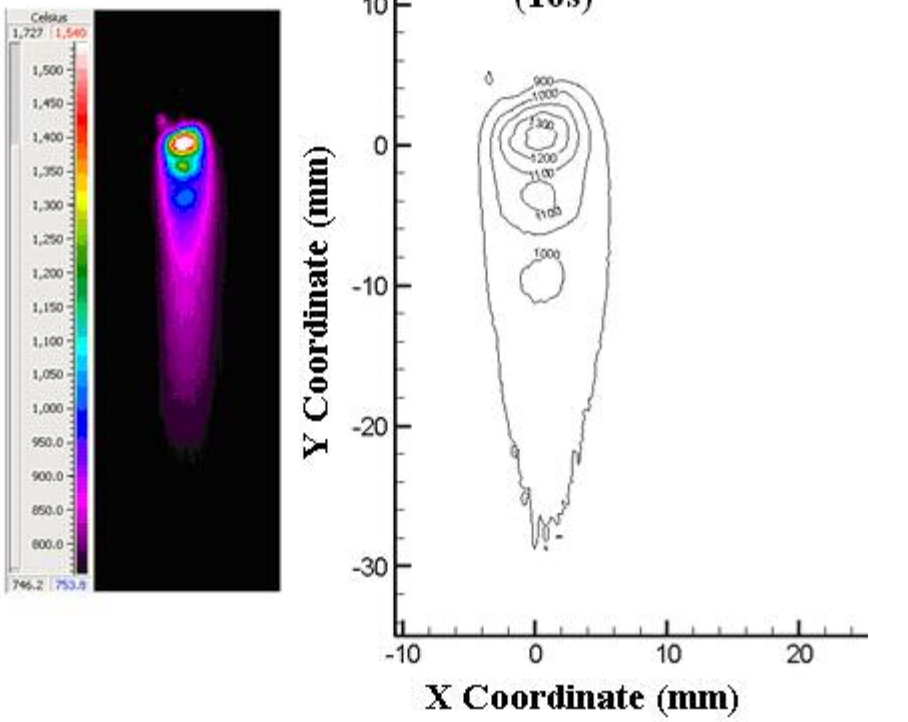
Experimental
(16s)
Celsius
1,727
1,540
1,500
1,450
1,400
1,350
1,300
1,250
1,200
1,150
1,100
1,050
1,000
950.0
900.0
850.0
800.0
746.2
753.0
Y Coordinate (mm)
10
0
-10
-20
-30
-10
0
10
20
X Coordinate (mm)
900
1000
1100
1200
1300
1000

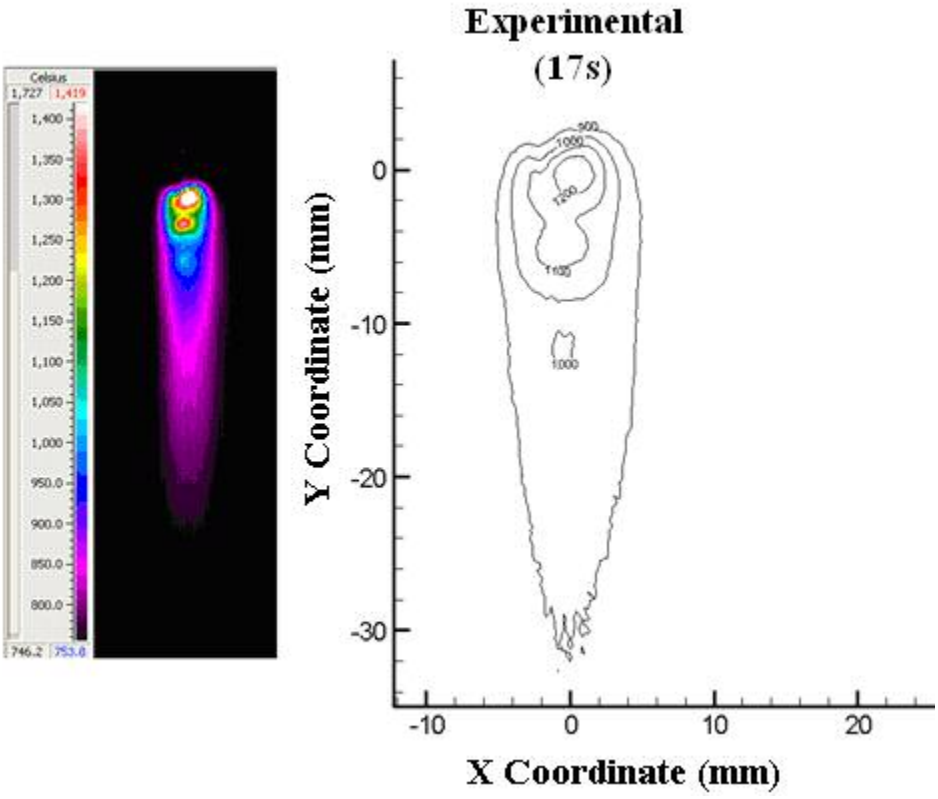
Experimental
(17s)
Celsius
1,727
1,419
1,400
1,350
1,300
1,250
1,200
1,150
1,100
1,050
1,000
950.0
900.0
850.0
800.0
746.2
753.0
Y Coordinate (mm)
0
-10
-20
-30
-10
0
10
20
X Coordinate (mm)
900
1000
1200
1100
1000

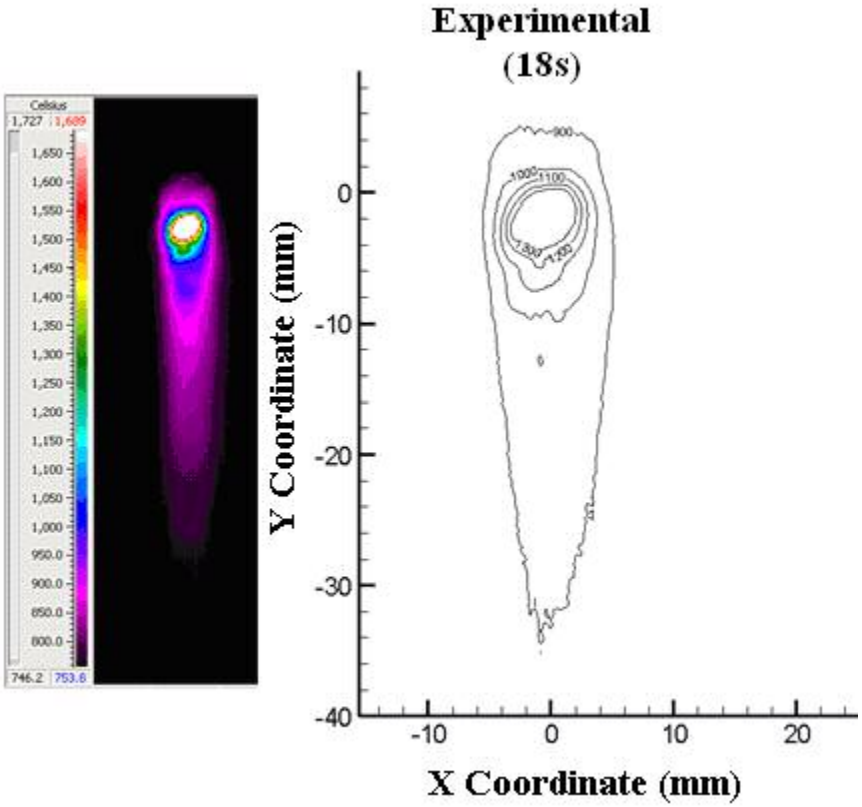
Experimental
(18s)
Celsius
1,727
1,689
1,650
1,600
1,550
1,500
1,450
1,400
1,350
1,300
1,250
1,200
1,150
1,100
1,050
1,000
950.0
900.0
850.0
800.0
746.2
753.8
900
1000
1100
1200
0
-10
-20
-30
-40
-10
0
10
20
Y Coordinate (mm)
X Coordinate (mm)

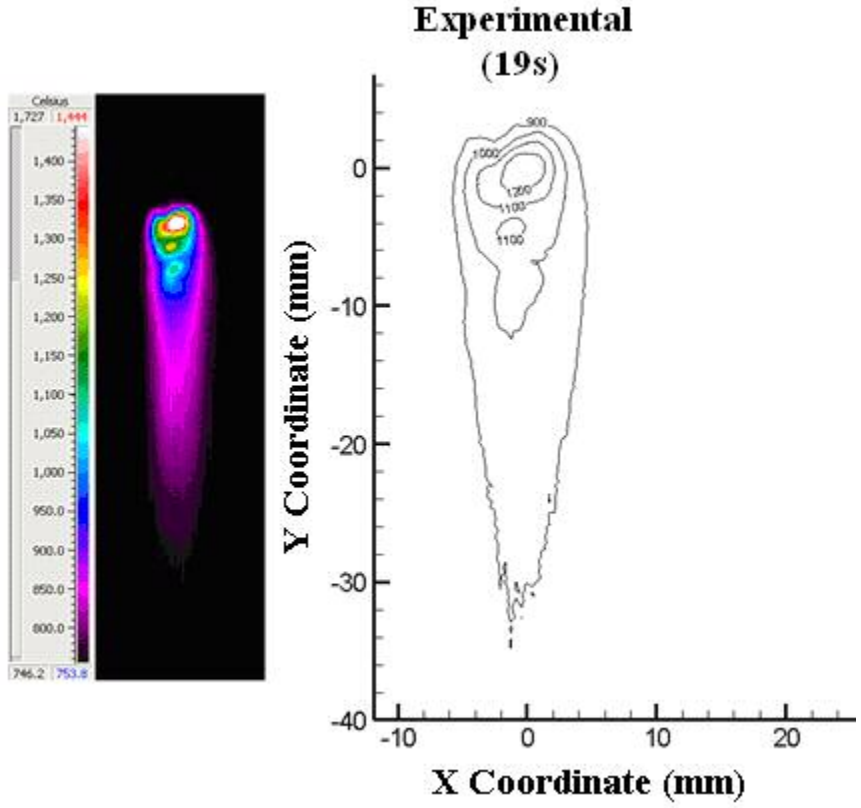
Experimental
(19s)
Celsius
1,727
1,444
1,400
1,350
1,300
1,250
1,200
1,150
1,100
1,050
1,000
950.0
900.0
850.0
800.0
746.2
753.8
900
1000
1200
1100
1100
0
-10
-20
-30
-40
-10
0
10
20
Y Coordinate (mm)
X Coordinate (mm)

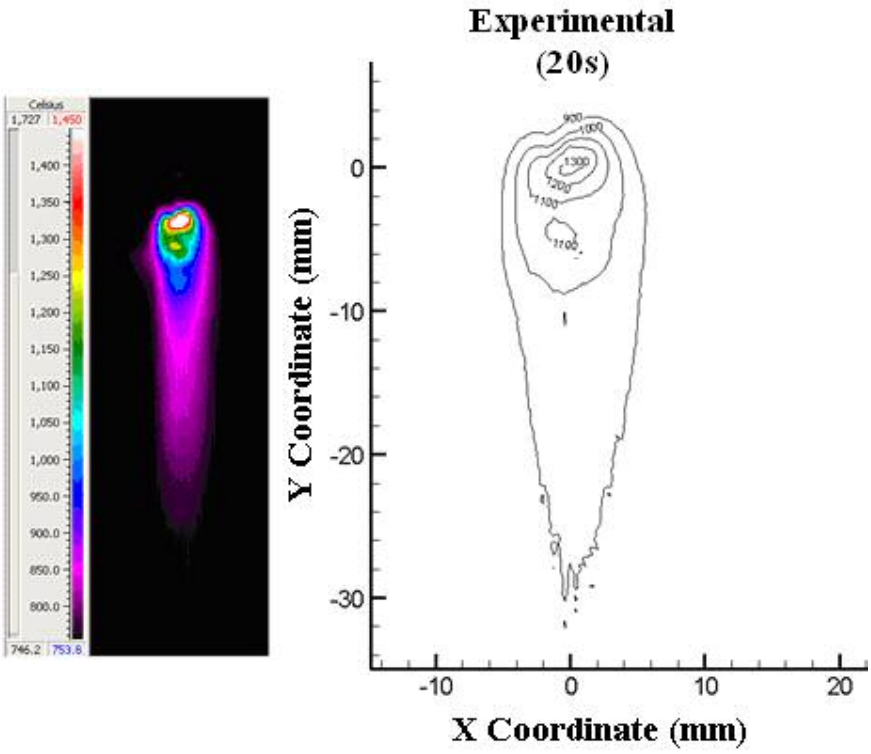

Quasi-steady state temperature distribution for experimental data at 21 s, 25 s, and 29 s for for a weld velocity of 0.545 mm/s

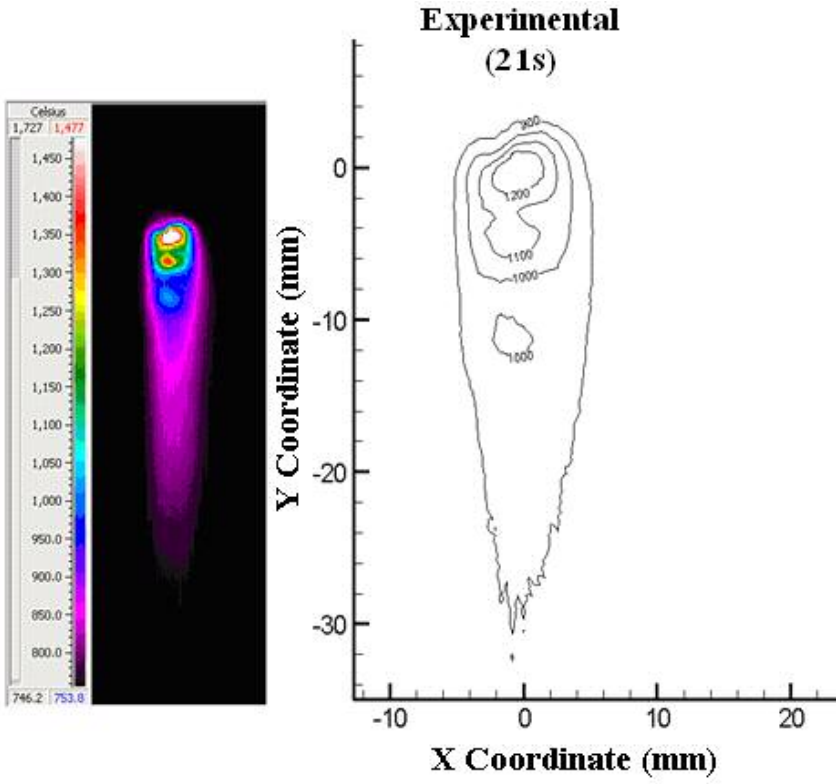

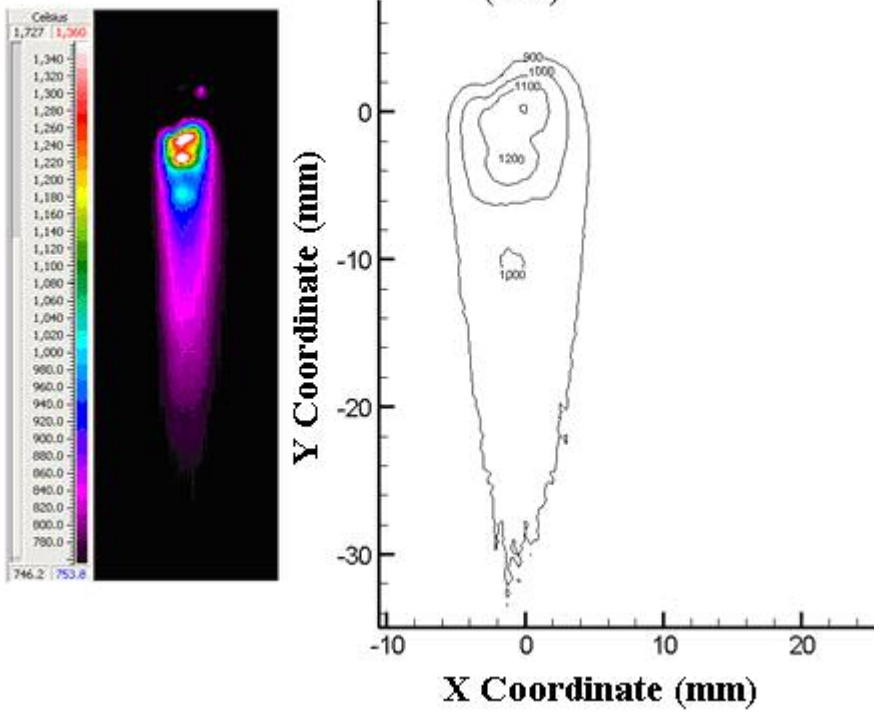
Experimental
(25s)
Celsius
1,727
1,360
746.2
753.8
900
1000
1100
1200
1000
Y Coordinate (mm)
X Coordinate (mm)
0
-10
-20
-30
-10
0
10
20

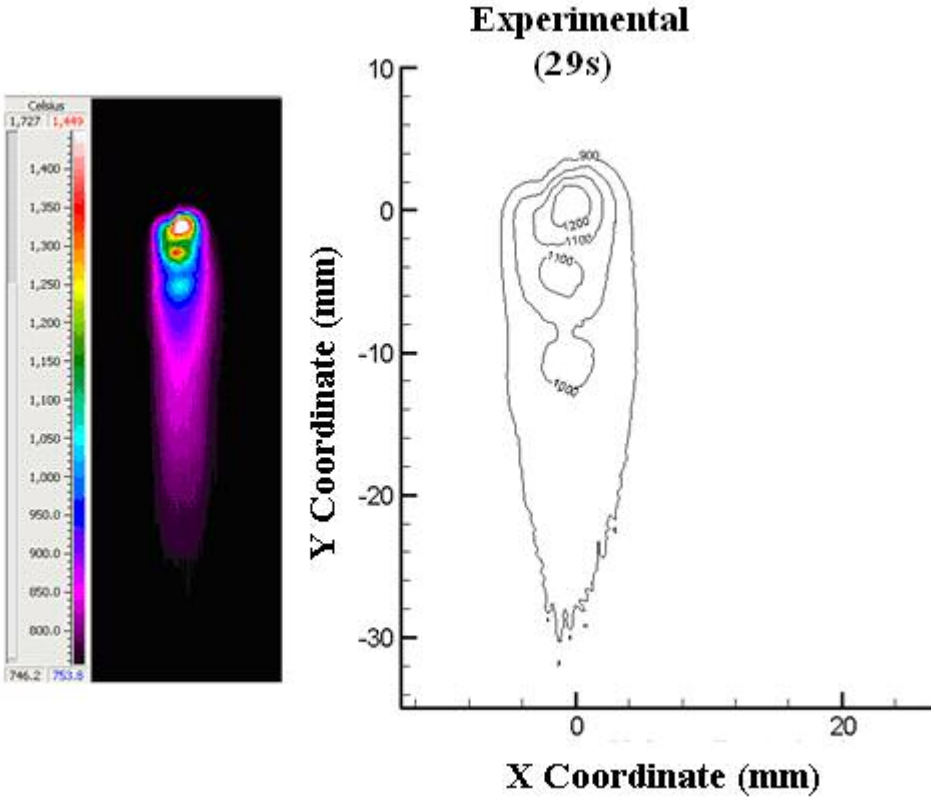
Experimental
(29s)
Celsius
1,727
1,449
746.2
753.8
900
1200
1100
1000
Y Coordinate (mm)
X Coordinate (mm)
10
0
-10
-20
-30
0
20

Transient to quasi-steady state temperature distributions for analytical data at 1 s to 20 s in 1 s increments for a weld velocity of 0.545 mm/s

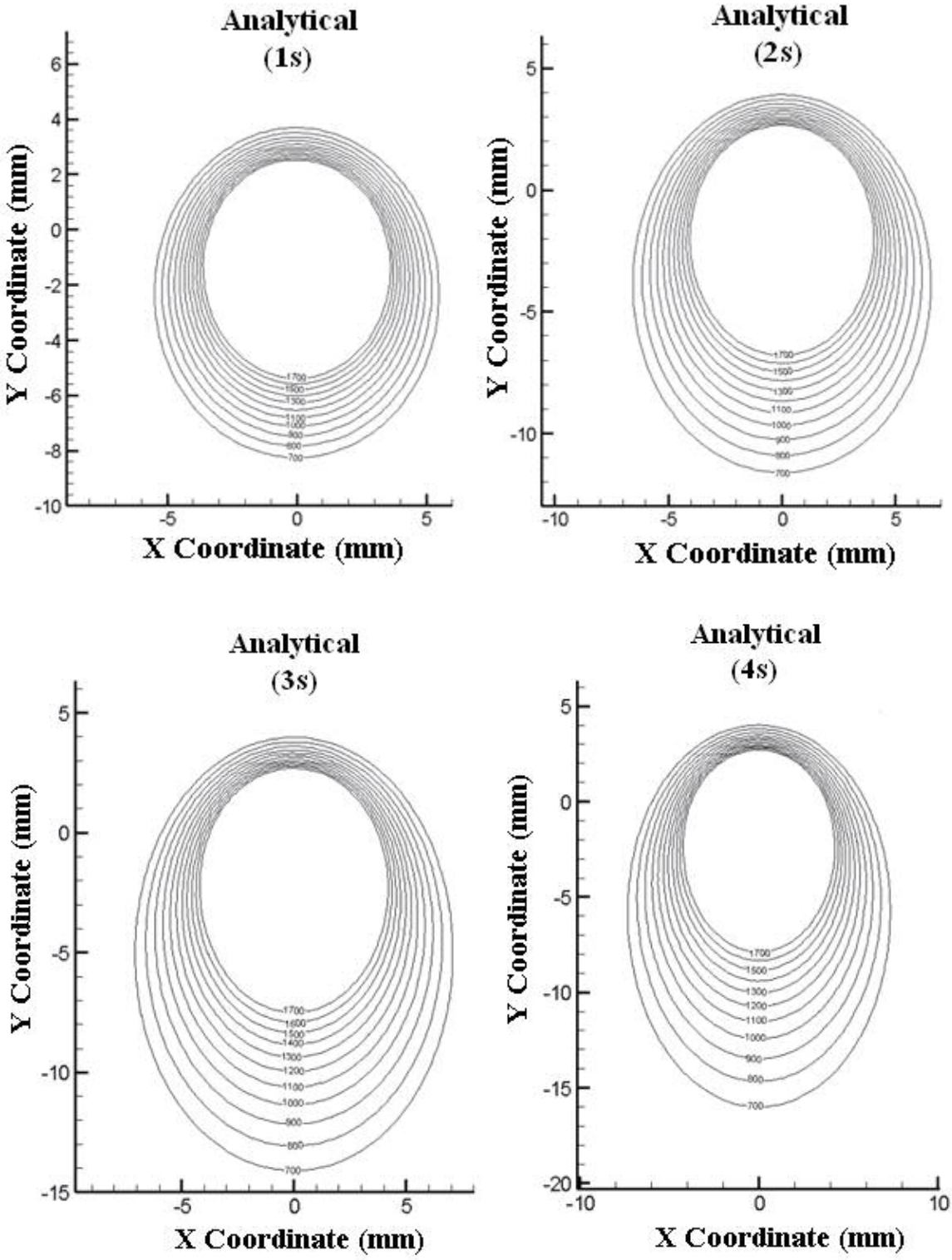

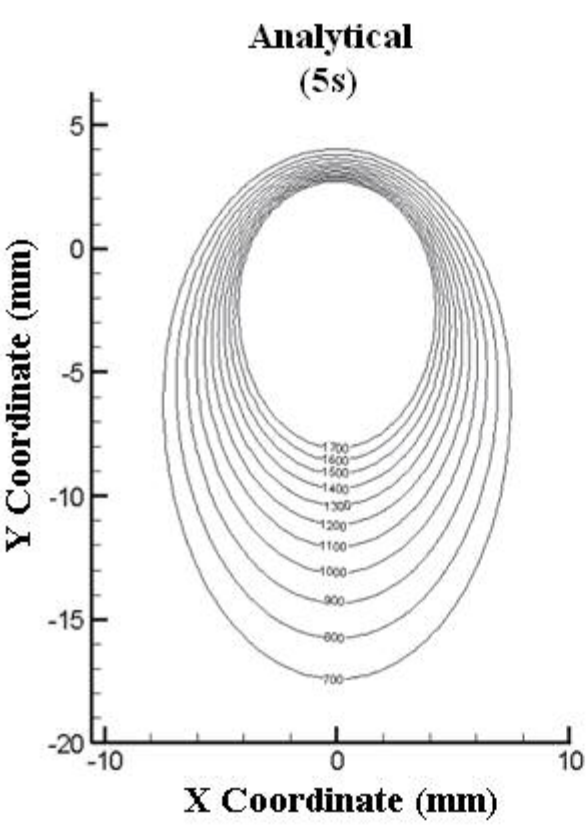
Analytical
(5s)
Y Coordinate (mm)
X Coordinate (mm)
5
0
-5
-10
-15
-20
-10
0
10
1700
1600
1500
1400
1300
1200
1100
1000
900
800
700

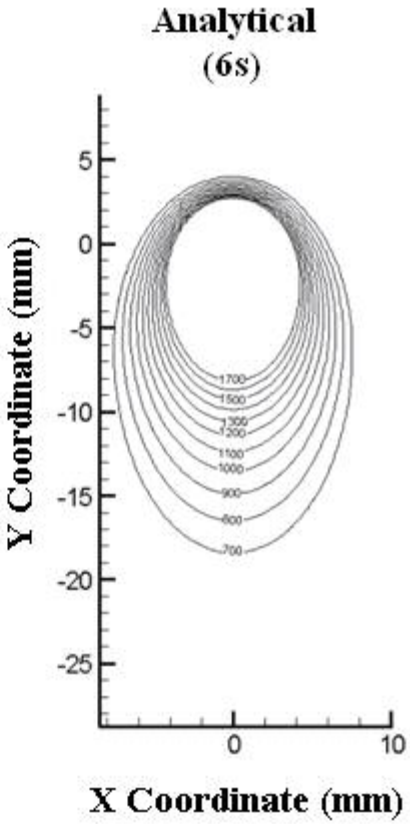
Analytical
(6s)
Y Coordinate (mm)
X Coordinate (mm)
5
0
-5
-10
-15
-20
-25
0
10
1700
1500
1300
1200
1100
1000
900
800
700

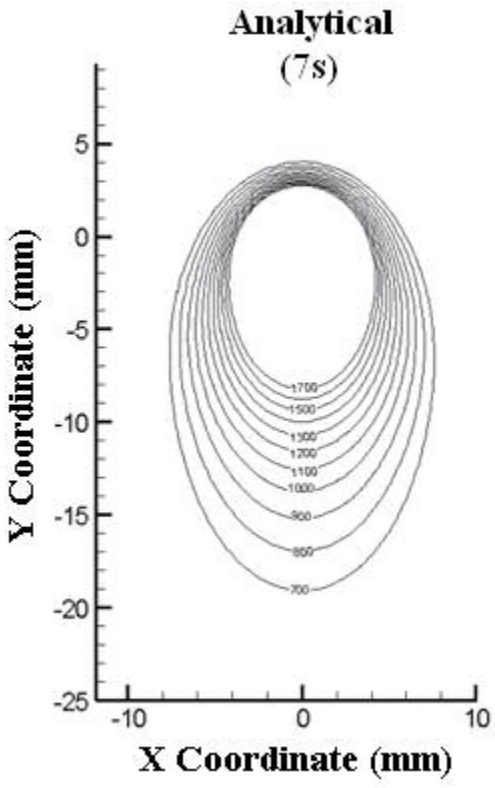
Analytical
(7s)
Y Coordinate (mm)
X Coordinate (mm)
5
0
-5
-10
-15
-20
-25
-10
0
10
1700
1500
1300
1200
1100
1000
900
800
700

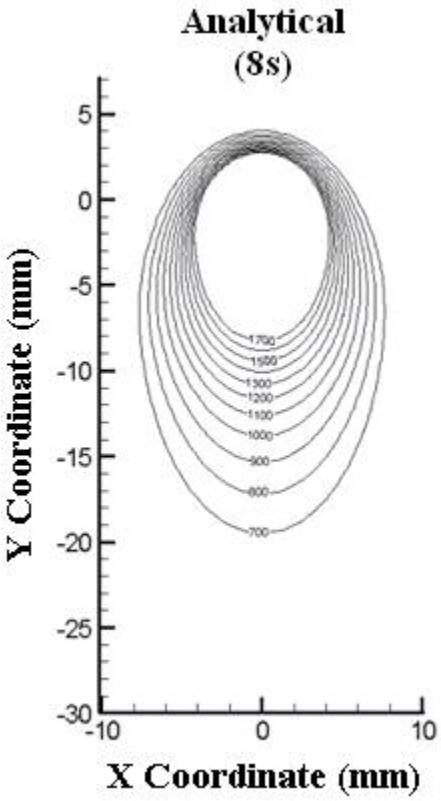
Analytical
(8s)
Y Coordinate (mm)
X Coordinate (mm)
5
0
-5
-10
-15
-20
-25
-30
-10
0
10
1700
1500
1300
1200
1100
1000
900
800
700

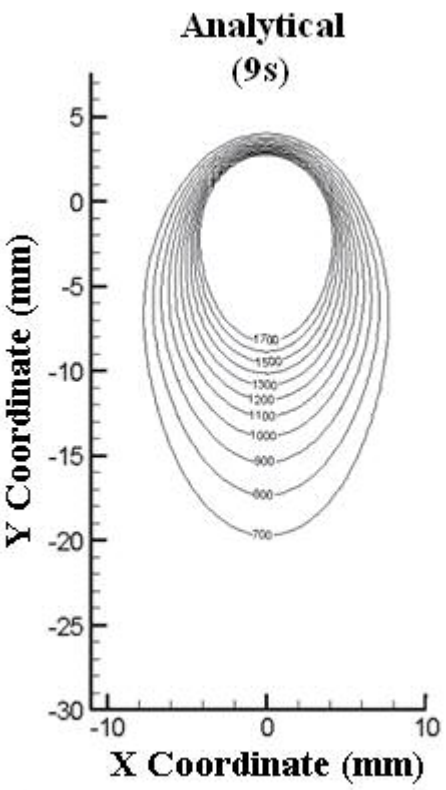
Analytical
(9s)
Y Coordinate (mm)
X Coordinate (mm)
5
0
-5
-10
-15
-20
-25
-30
-10
0
10
1700
1500
1300
1200
1100
1000
900
800
700

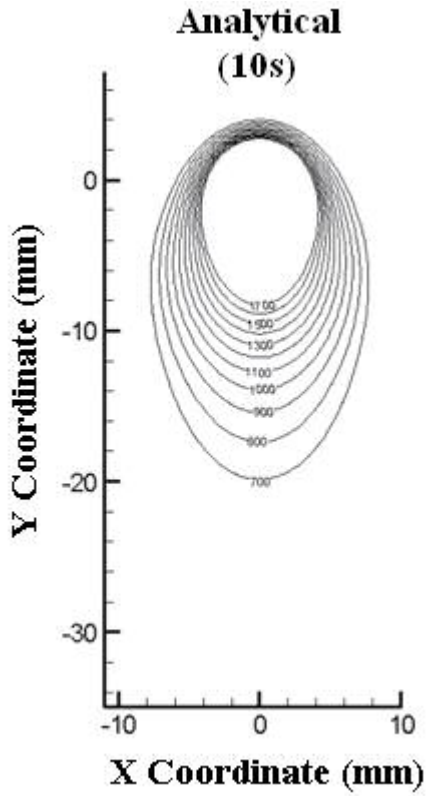
Analytical
(10s)
Y Coordinate (mm)
X Coordinate (mm)
0
-10
-20
-30
-10
0
10
1700
1500
1300
1100
1000
900
800
700

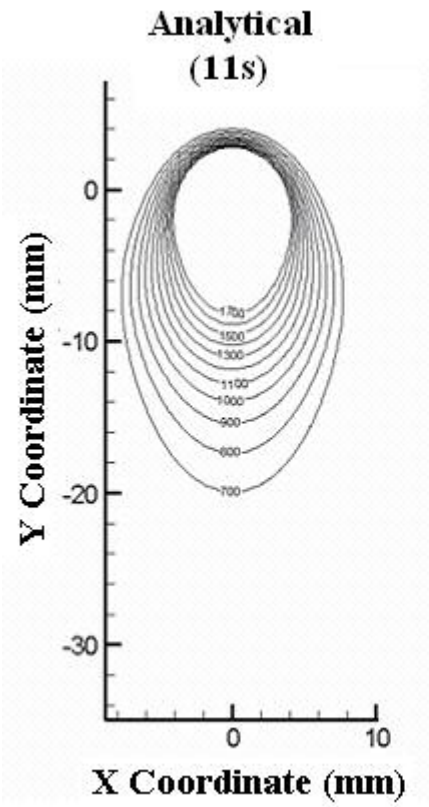
Analytical
(11s)
Y Coordinate (mm)
X Coordinate (mm)
0
-10
-20
-30
0
10
1700
1500
1300
1100
1000
900
800
700

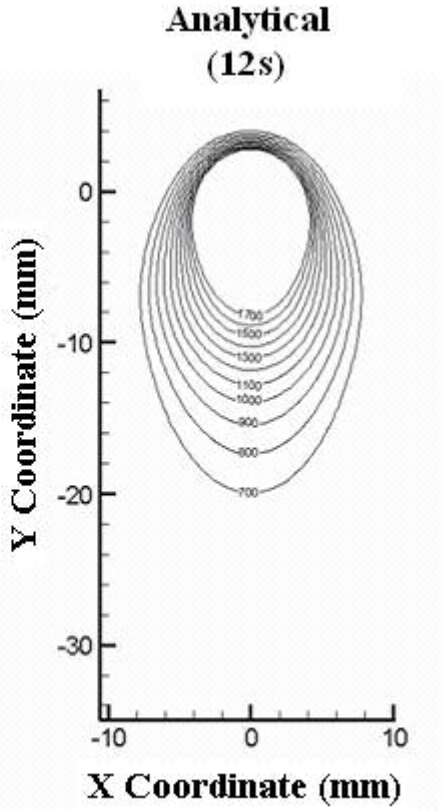
Analytical
(12s)
Y Coordinate (mm)
X Coordinate (mm)
0
-10
-20
-30
-10
0
10
1700
1500
1300
1100
1000
900
800
700

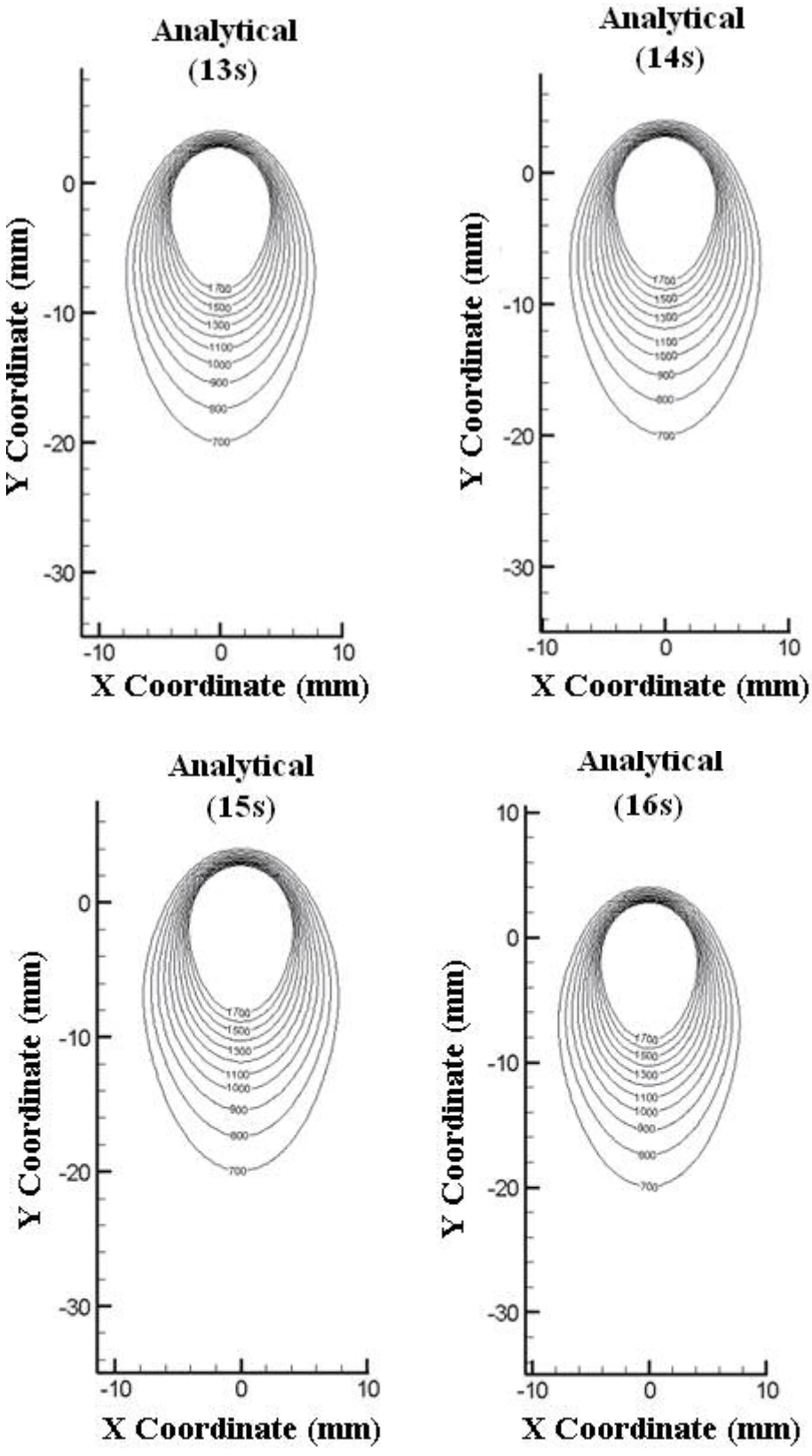
Analytical
(13s)
Analytical
(14s)
Analytical
(15s)
Analytical
(16s)
Y Coordinate (mm)
X Coordinate (mm)
0
-10
-20
-30
10
1700
1500
1300
1100
1000
900
800
700

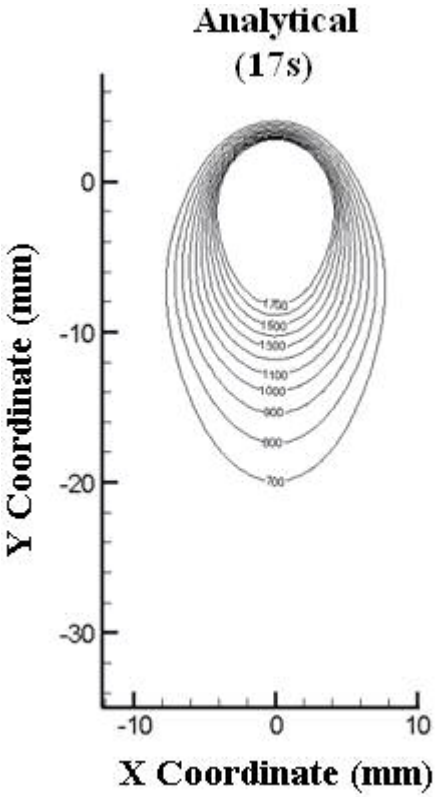
Analytical
(17s)
Y Coordinate (mm)
X Coordinate (mm)
0
-10
-20
-30
-10
0
10
1700
1500
1300
1100
1000
900
800
700

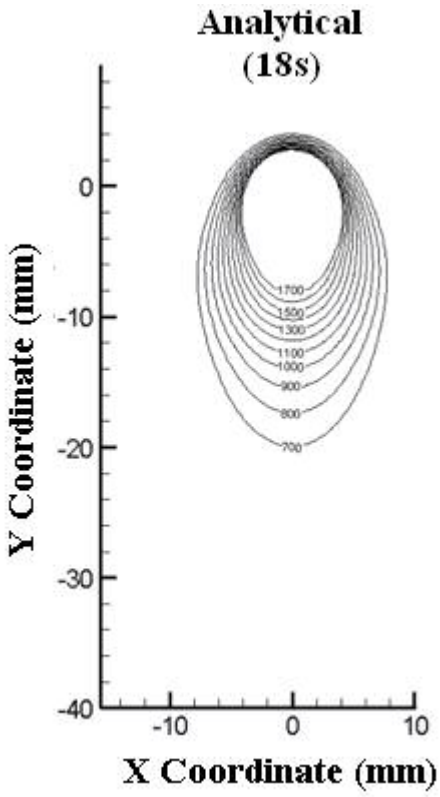
Analytical
(18s)
Y Coordinate (mm)
X Coordinate (mm)
0
-10
-20
-30
-40
-10
0
10
1700
1500
1300
1100
1000
900
800
700

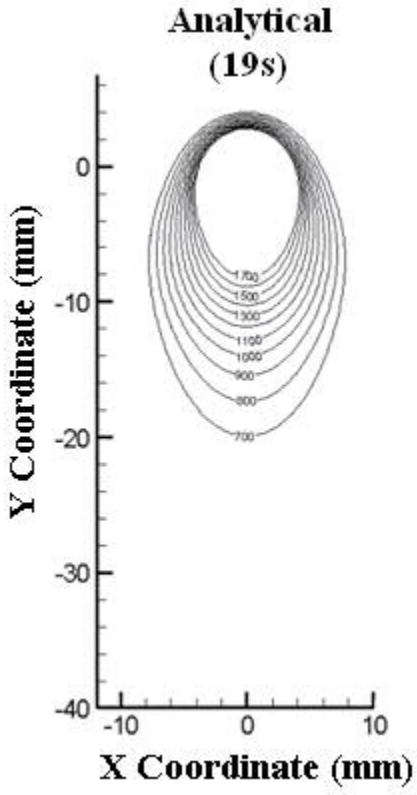
Analytical
(19s)
Y Coordinate (mm)
X Coordinate (mm)
0
-10
-20
-30
-40
-10
0
10
1700
1500
1300
1100
1000
900
800
700

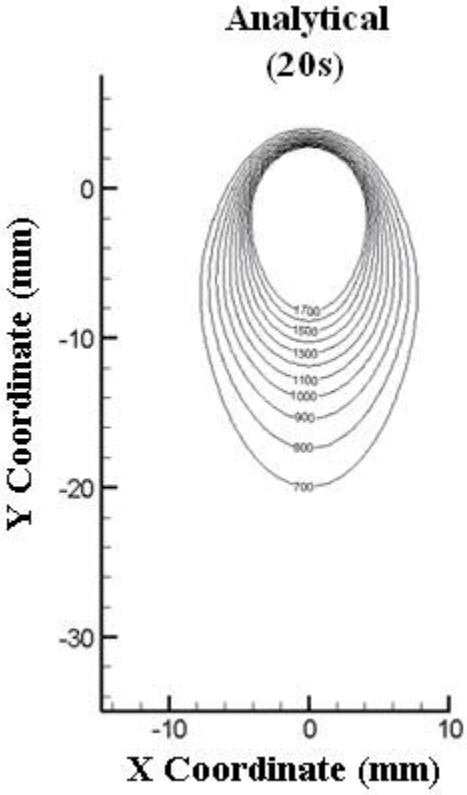
Analytical
(20s)
Y Coordinate (mm)
X Coordinate (mm)
0
-10
-20
-30
-10
0
10
1700
1500
1300
1100
1000
900
800
700

Quasi-steady state temperature distribution for analytical data at 21 s, 25 s, and 29 s for a weld velocity of 0.545 cm/s

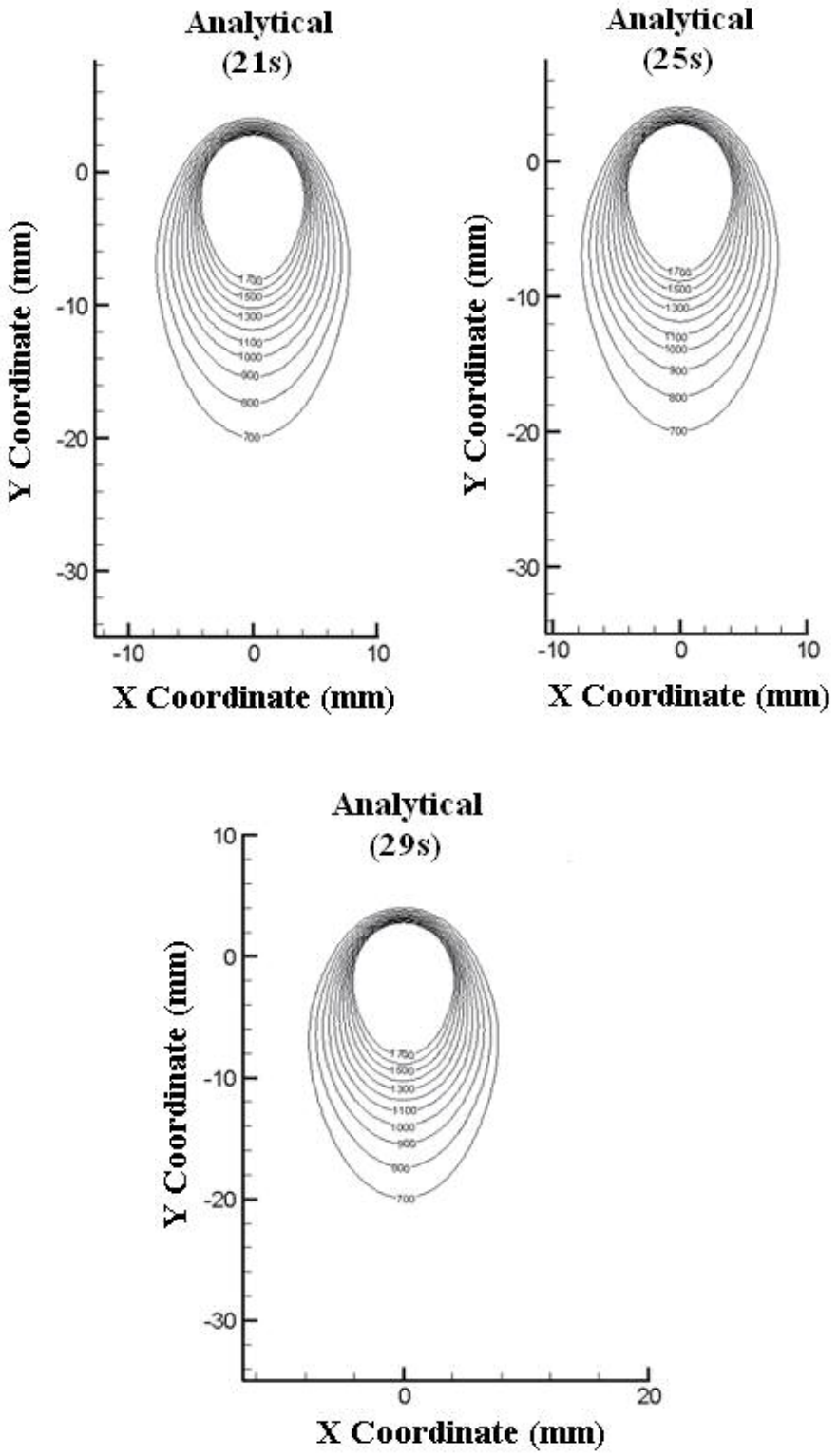

Transient to quasi-steady state temperature distributions for 1 s to 20 s in 1 s increments for comparison of experimental data and analytical data for a weld velocity of 0.545 cm/s

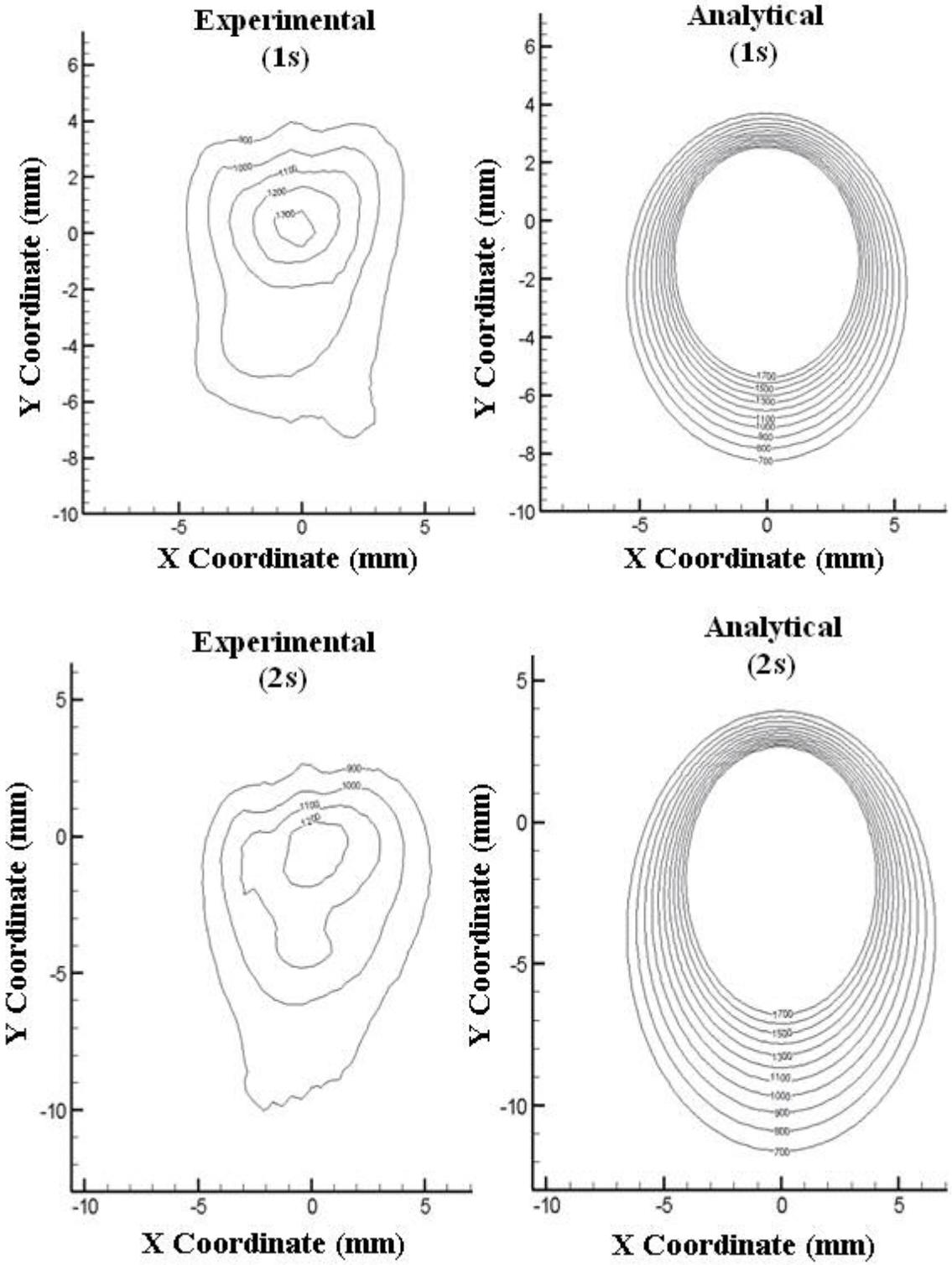

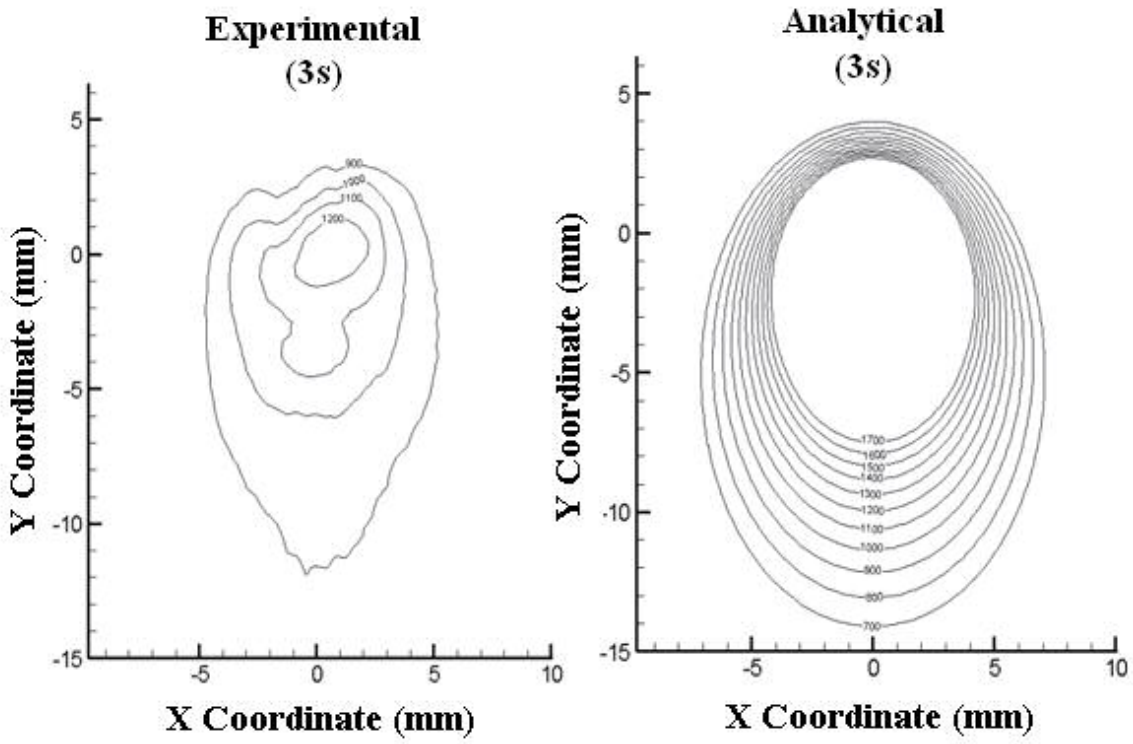
Experimental
(3s)
Analytical
(3s)
Y Coordinate (mm)
X Coordinate (mm)
5
0
-5
-10
-15
-5
0
5
10
900
1000
1100
1200
1700
1600
1500
1400
1300
1200
1100
1000
900
800
700

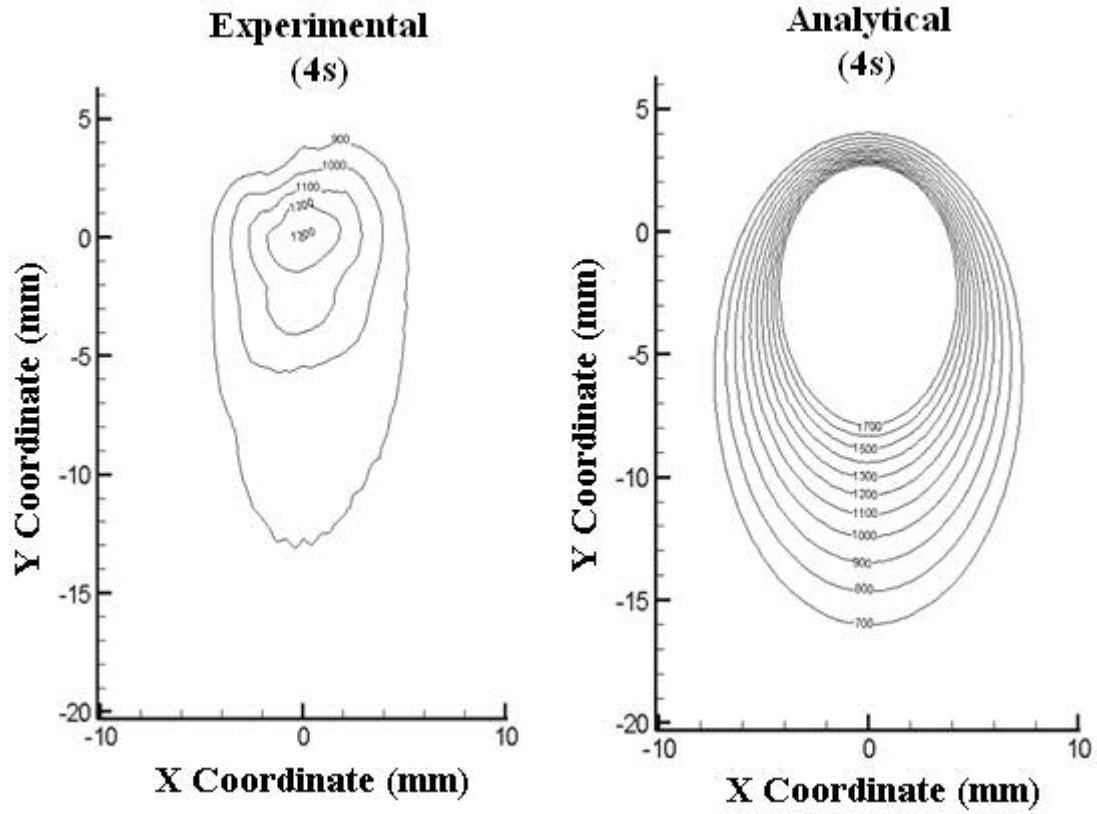
Experimental
(4s)
Analytical
(4s)
Y Coordinate (mm)
X Coordinate (mm)
5
0
-5
-10
-15
-20
-10
0
10
900
1000
1100
1700
1500
1300
1200
1100
1000
900
800
700

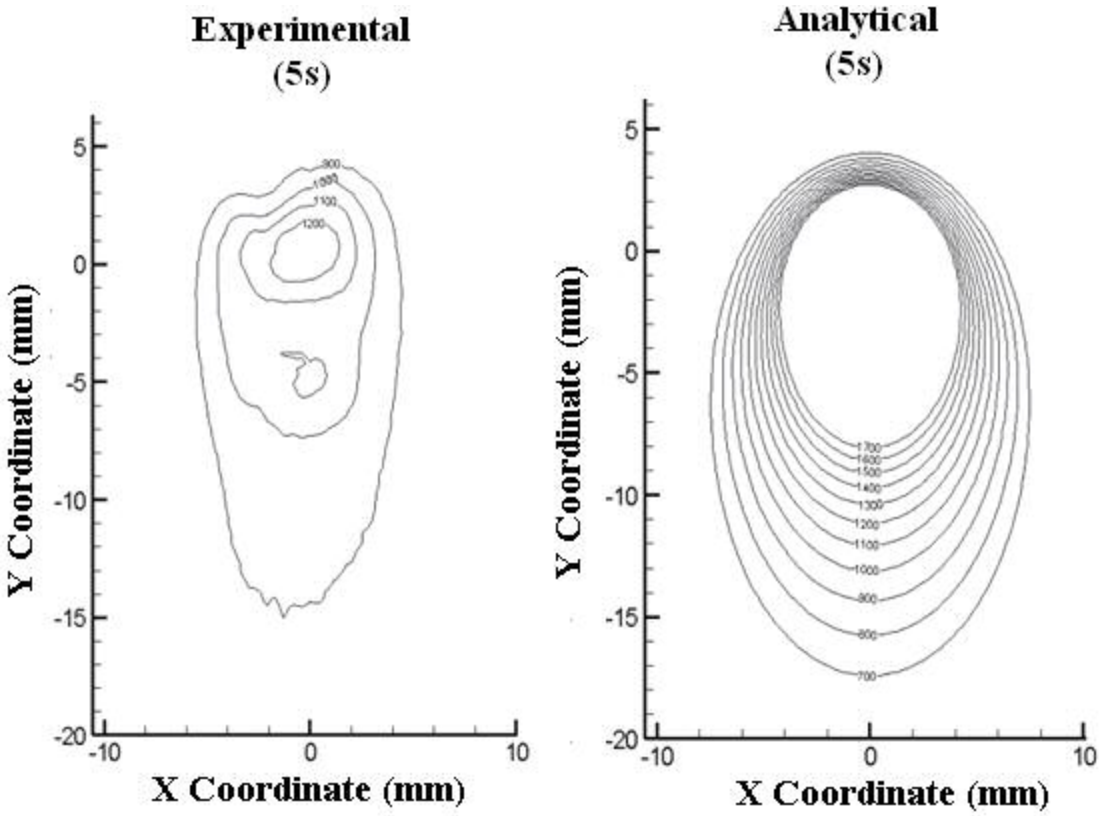
Experimental
(5s)
Analytical
(5s)
Y Coordinate (mm)
X Coordinate (mm)
5
0
-5
-10
-15
-20
-10
0
10
900
1000
1100
1200
1700
1600
1500
1400
1300
1200
1100
1000
900
800
700

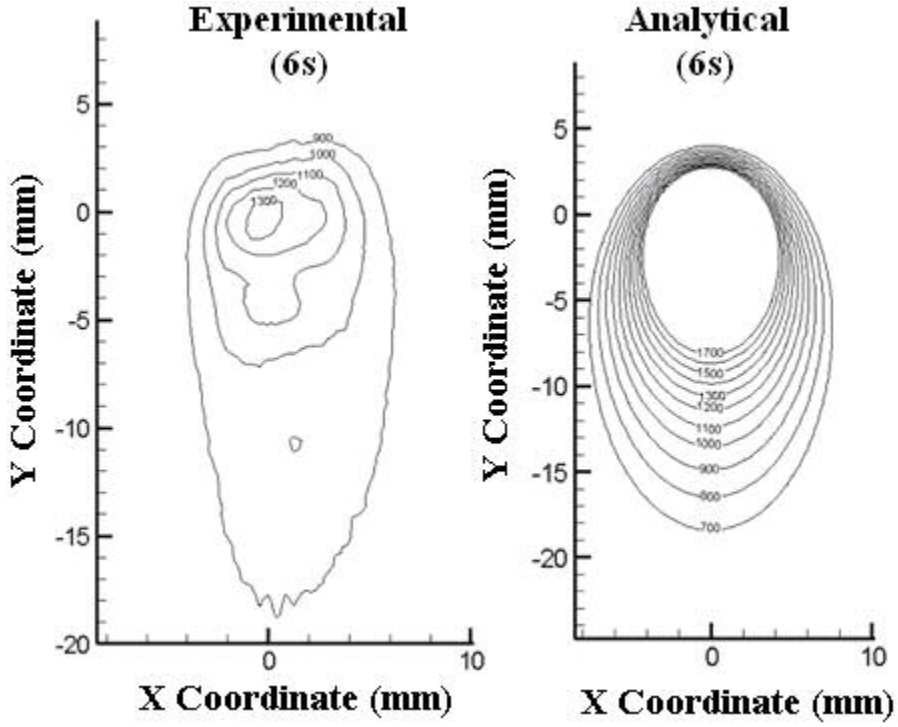
Experimental
(6s)
Analytical
(6s)
Y Coordinate (mm)
X Coordinate (mm)
5
0
-5
-10
-15
-20
-10
0
10
900
1000
1100
1200
1300
1700
1500
1300
1200
1100
1000
900
800
700

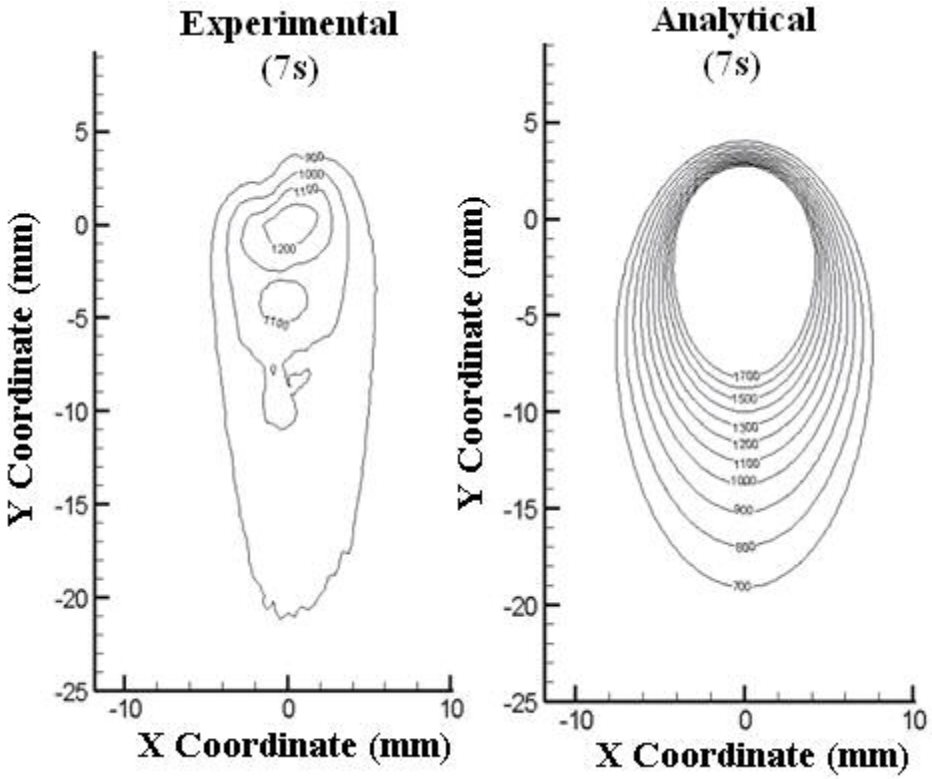
Experimental
(7s)
Analytical
(7s)
Y Coordinate (mm)
X Coordinate (mm)
5
0
-5
-10
-15
-20
-25
-10
0
10
900
1000
1100
1200
1700
1500
1300
1200
1100
1000
900
800
700

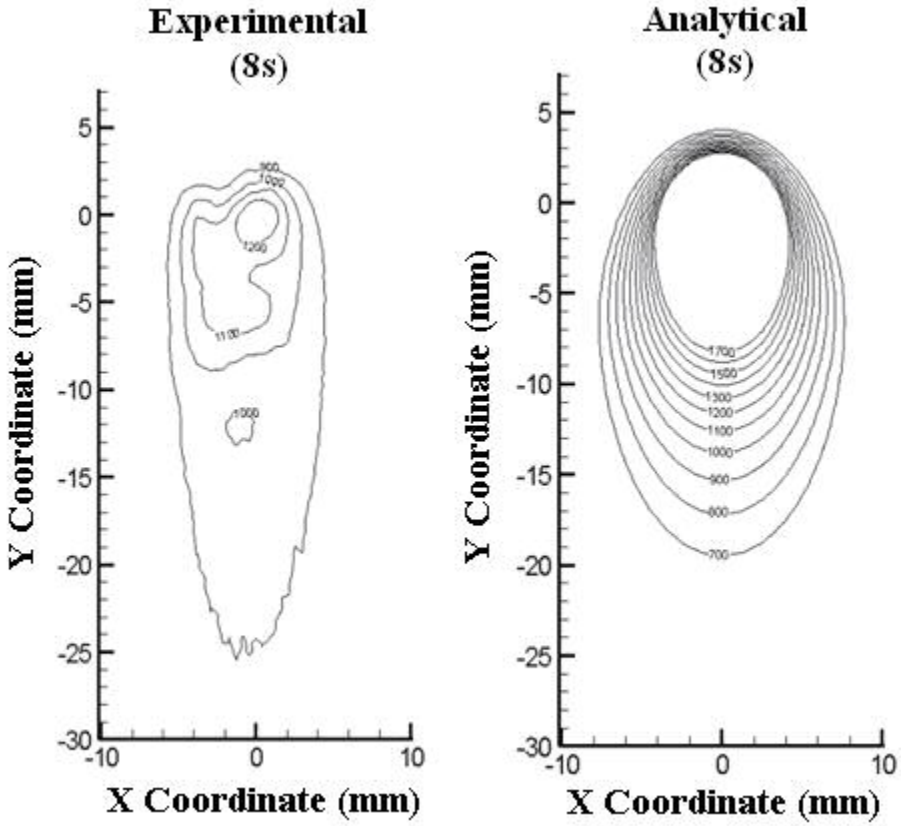
Experimental
(8s)
Analytical
(8s)
Y Coordinate (mm)
X Coordinate (mm)
5
0
-5
-10
-15
-20
-25
-30
-10
0
10
1200
1100
1000
1700
1500
1300
1200
1100
1000
900
800
700

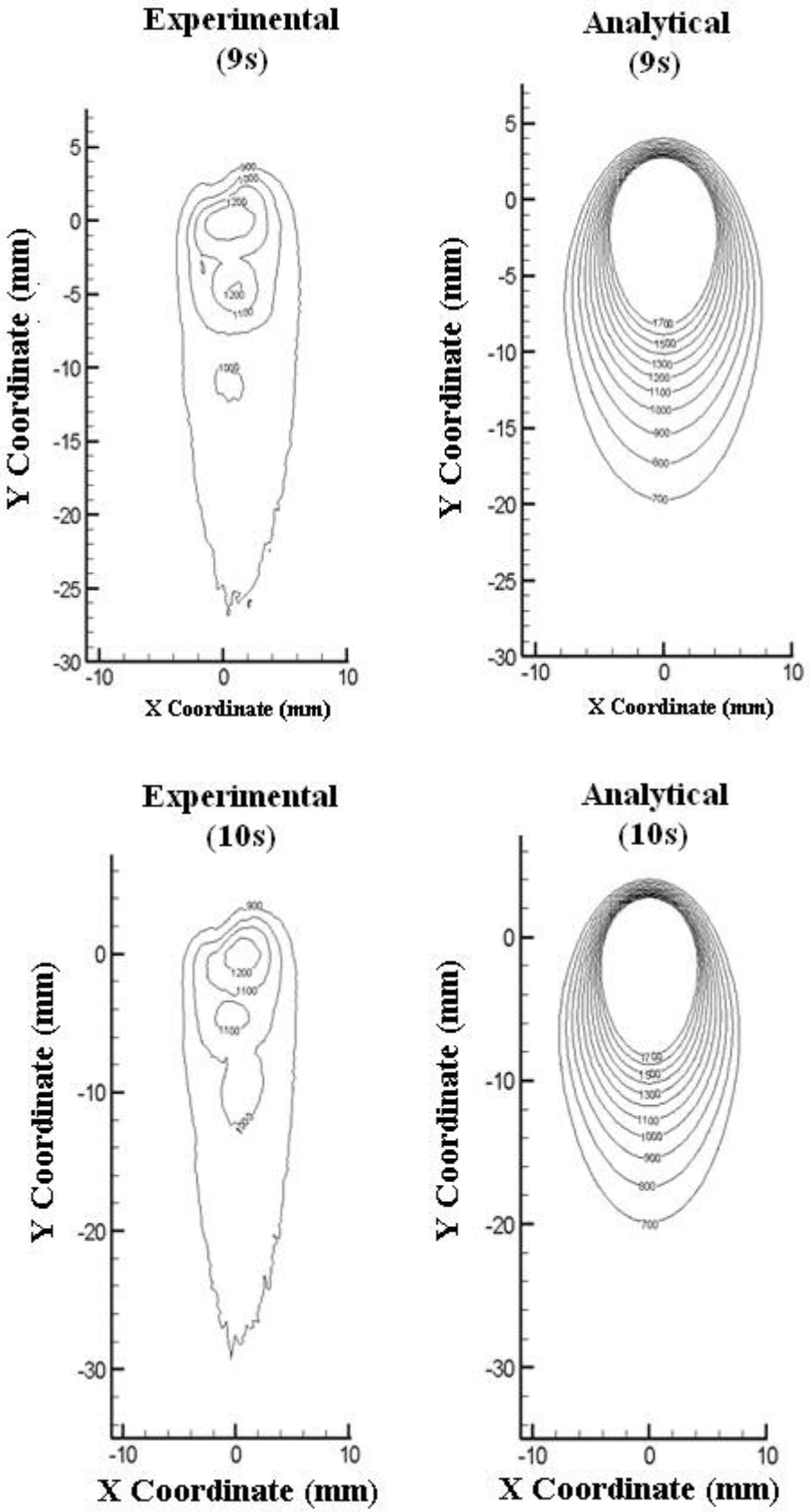
Experimental
(9s)
Analytical
(9s)
Experimental
(10s)
Analytical
(10s)
Y Coordinate (mm)
X Coordinate (mm)
5
0
-5
-10
-15
-20
-25
-30
-10
0
10

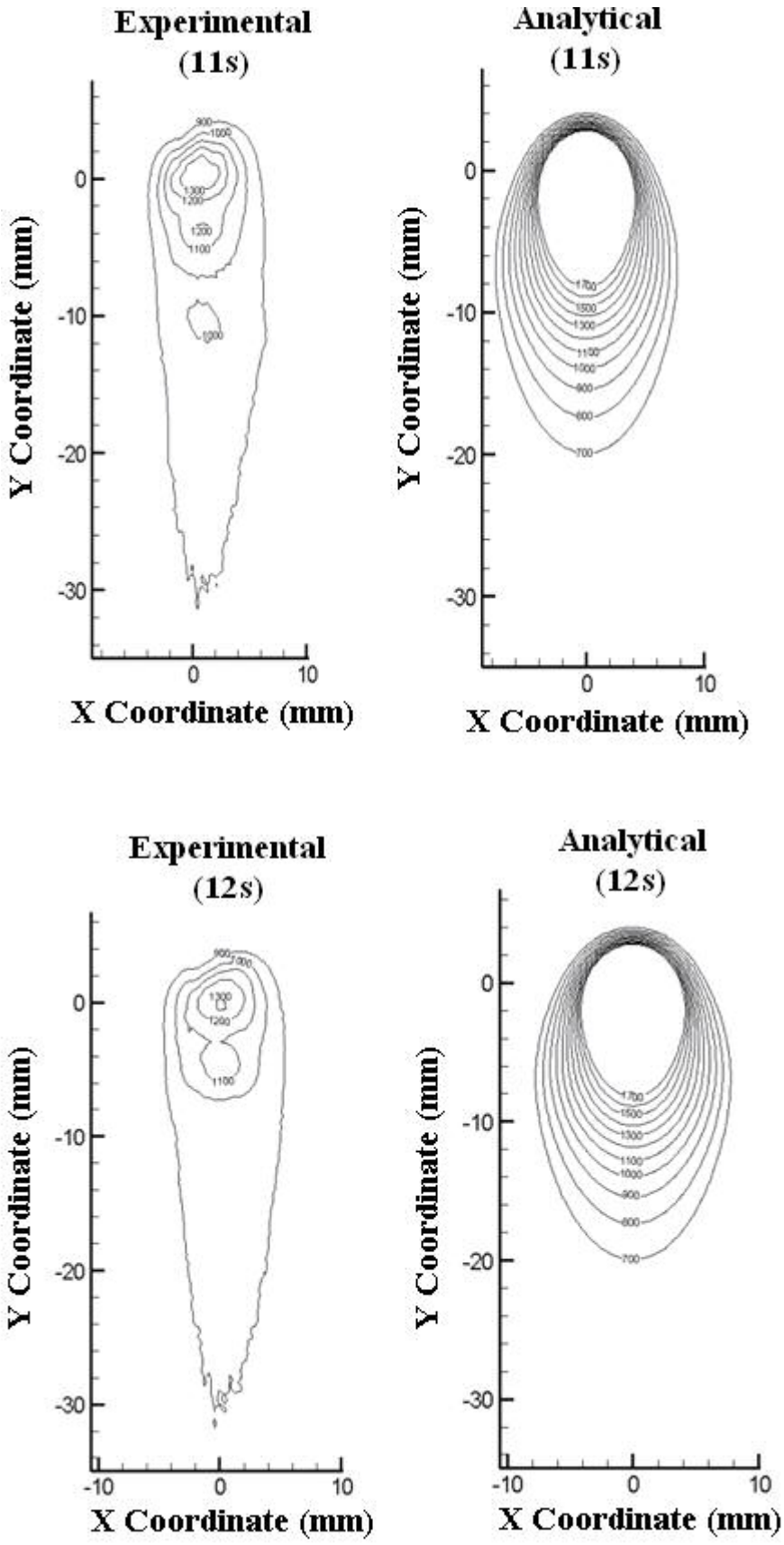
Experimental
(11s)
Analytical
(11s)
Experimental
(12s)
Analytical
(12s)
Y Coordinate (mm)
X Coordinate (mm)
0
-10
-20
-30
10

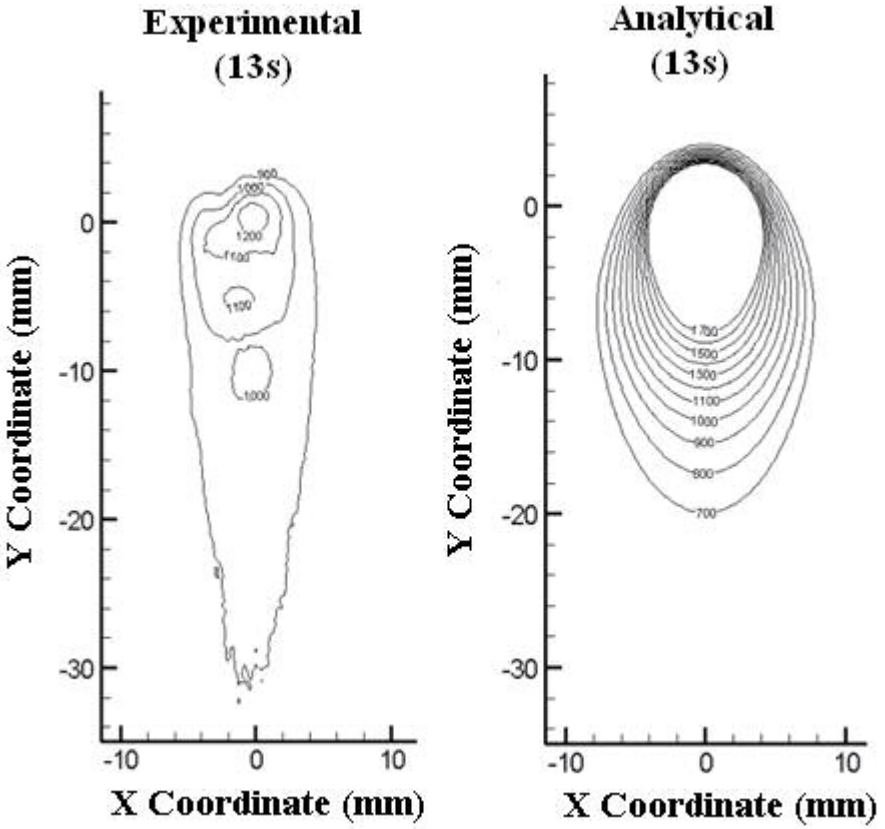
Experimental
(13s)
Analytical
(13s)
Y Coordinate (mm)
X Coordinate (mm)
0
-10
-20
-30
-10
0
10
1700
1500
1300
1100
1000
900
800
700

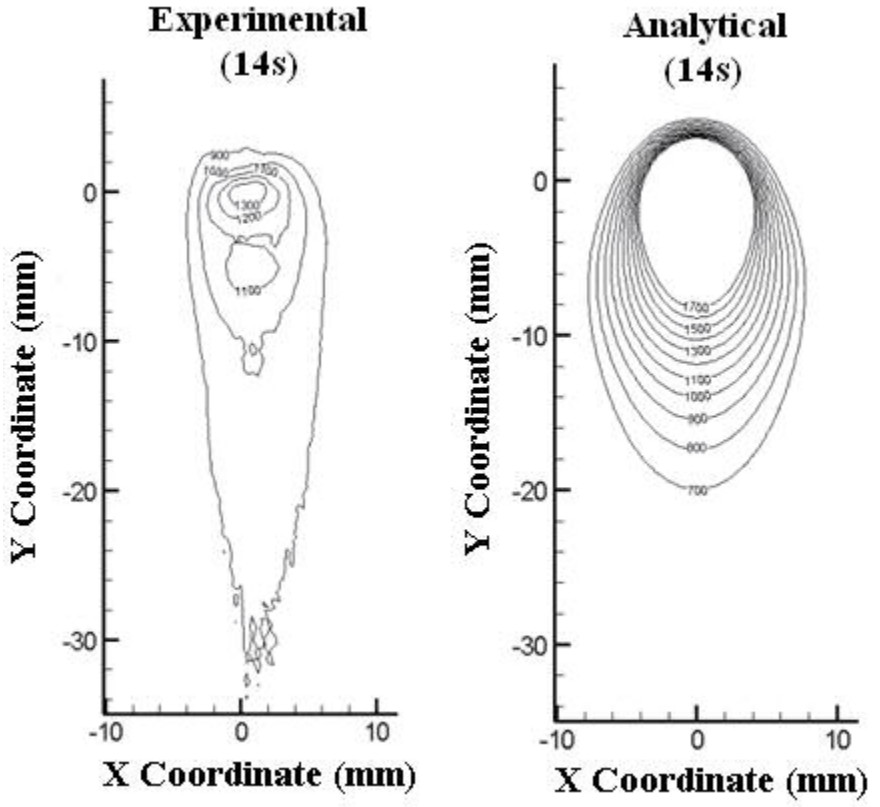
Experimental
(14s)
Analytical
(14s)
Y Coordinate (mm)
X Coordinate (mm)
0
-10
-20
-30
-10
0
10
1700
1500
1300
1100
1000
900
800
700

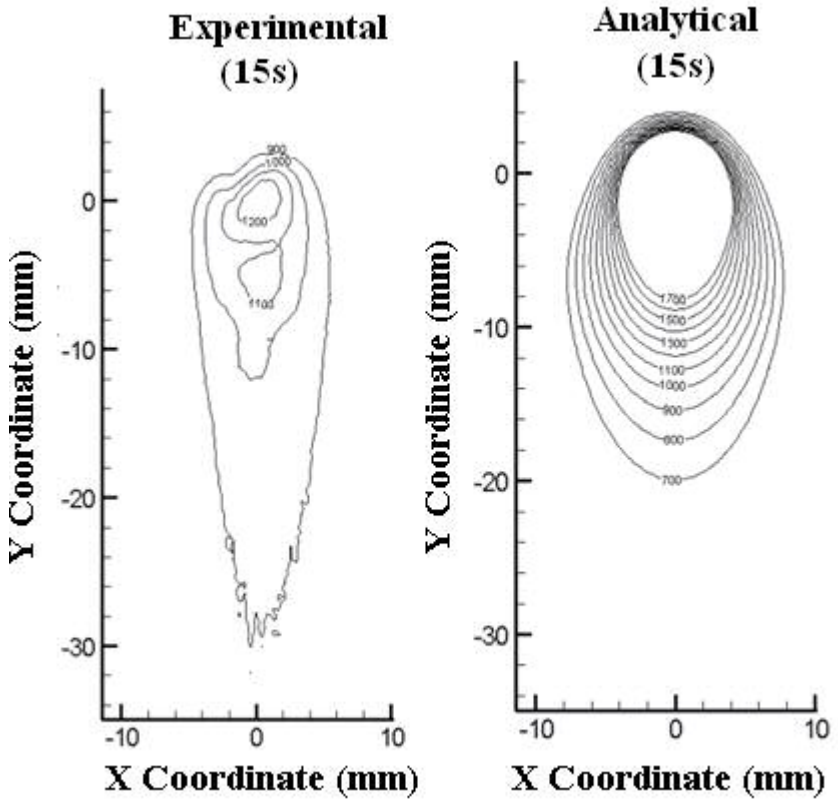
Experimental
(15s)
Analytical
(15s)
Y Coordinate (mm)
X Coordinate (mm)
0
-10
-20
-30
10
900
1000
1200
1100
1700
1500
1300
1100
1000
900
800
700

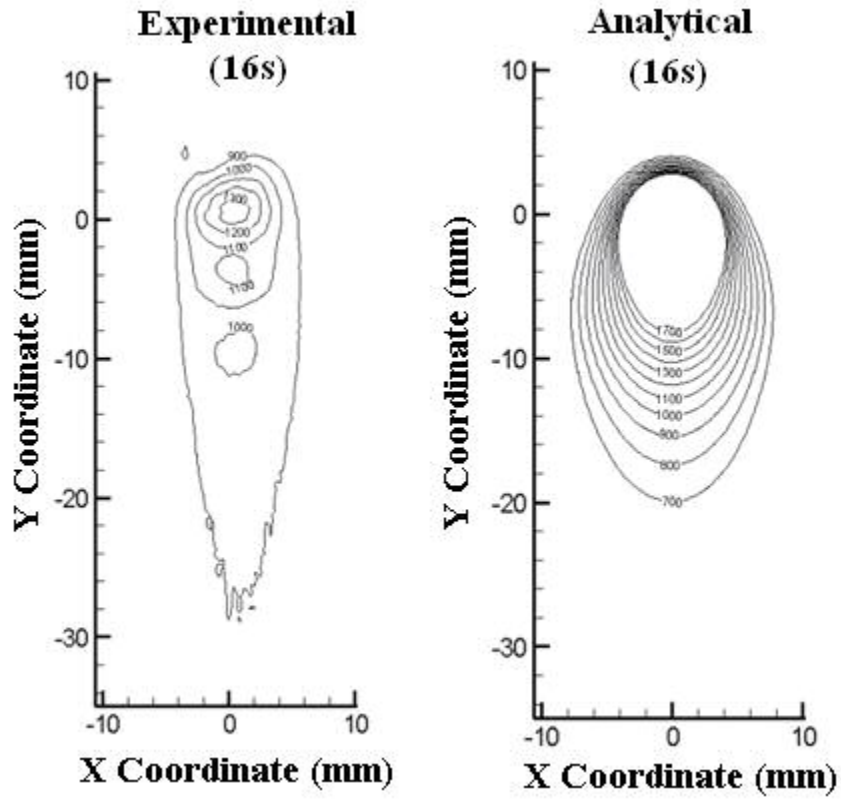
Experimental
(16s)
Analytical
(16s)
Y Coordinate (mm)
X Coordinate (mm)
10
0
-10
-20
-30
900
1000
1200
1100
1700
1500
1300
1100
1000
900
800
700

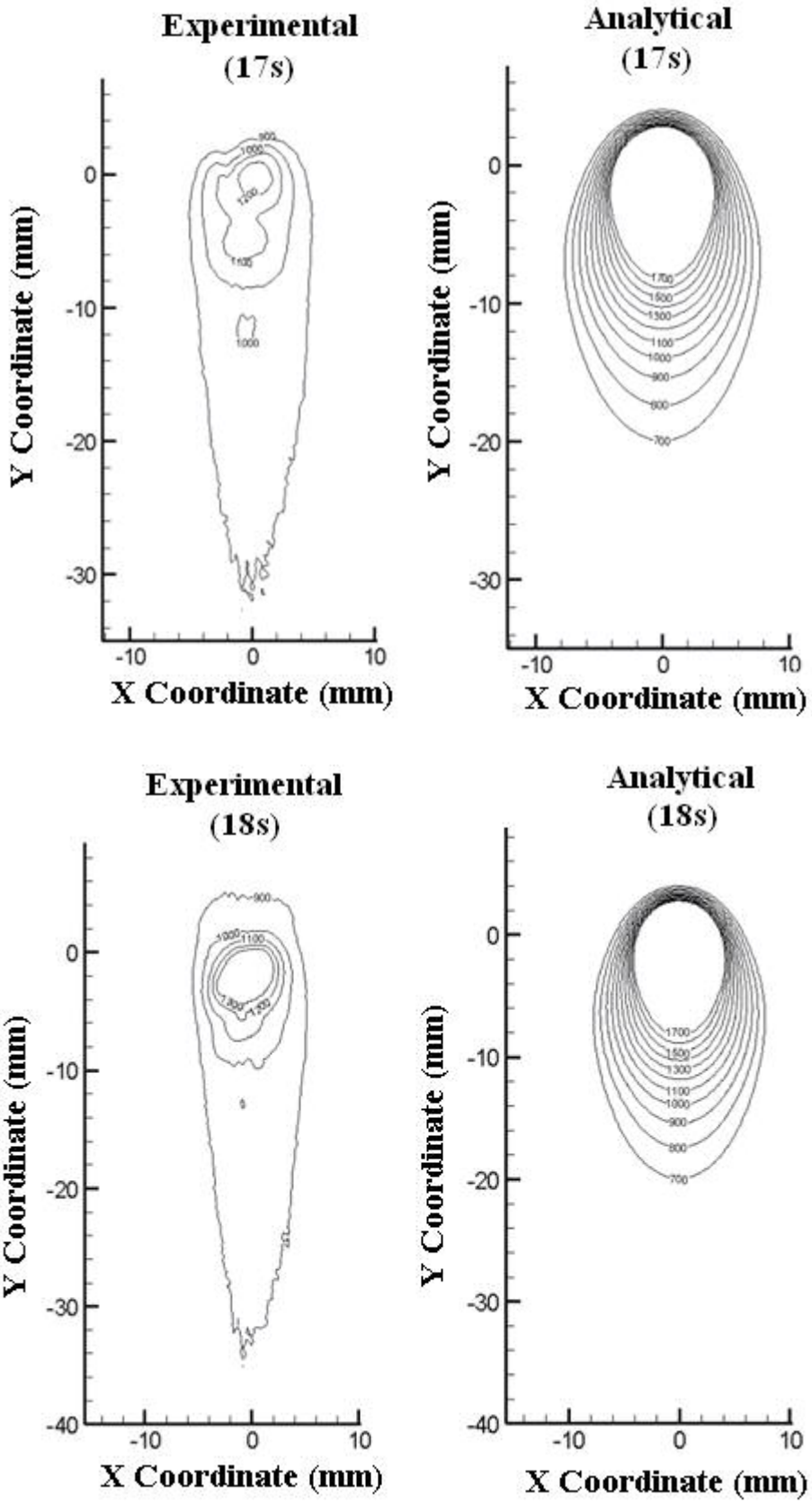
Experimental
(17s)
Analytical
(17s)
Experimental
(18s)
Analytical
(18s)
Y Coordinate (mm)
X Coordinate (mm)
0
-10
-20
-30
-40
10

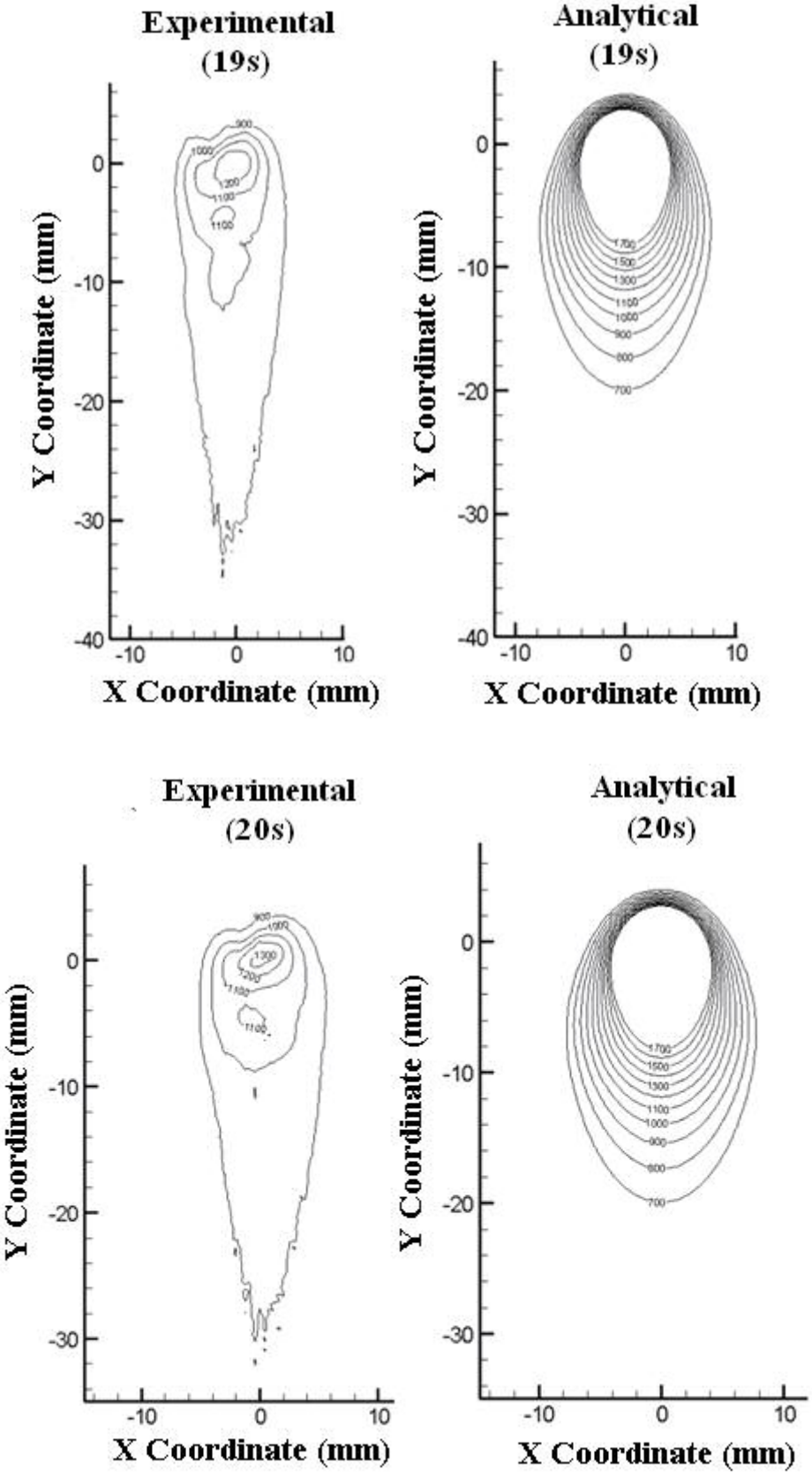
Experimental
(19s)
Analytical
(19s)
Experimental
(20s)
Analytical
(20s)
Y Coordinate (mm)
X Coordinate (mm)
0
-10
-20
-30
-40
10

Quasi-steady state temperature distribution for analytical data at 21 s, 25 s, and 29 s for a weld velocity of 0.545 cm/s

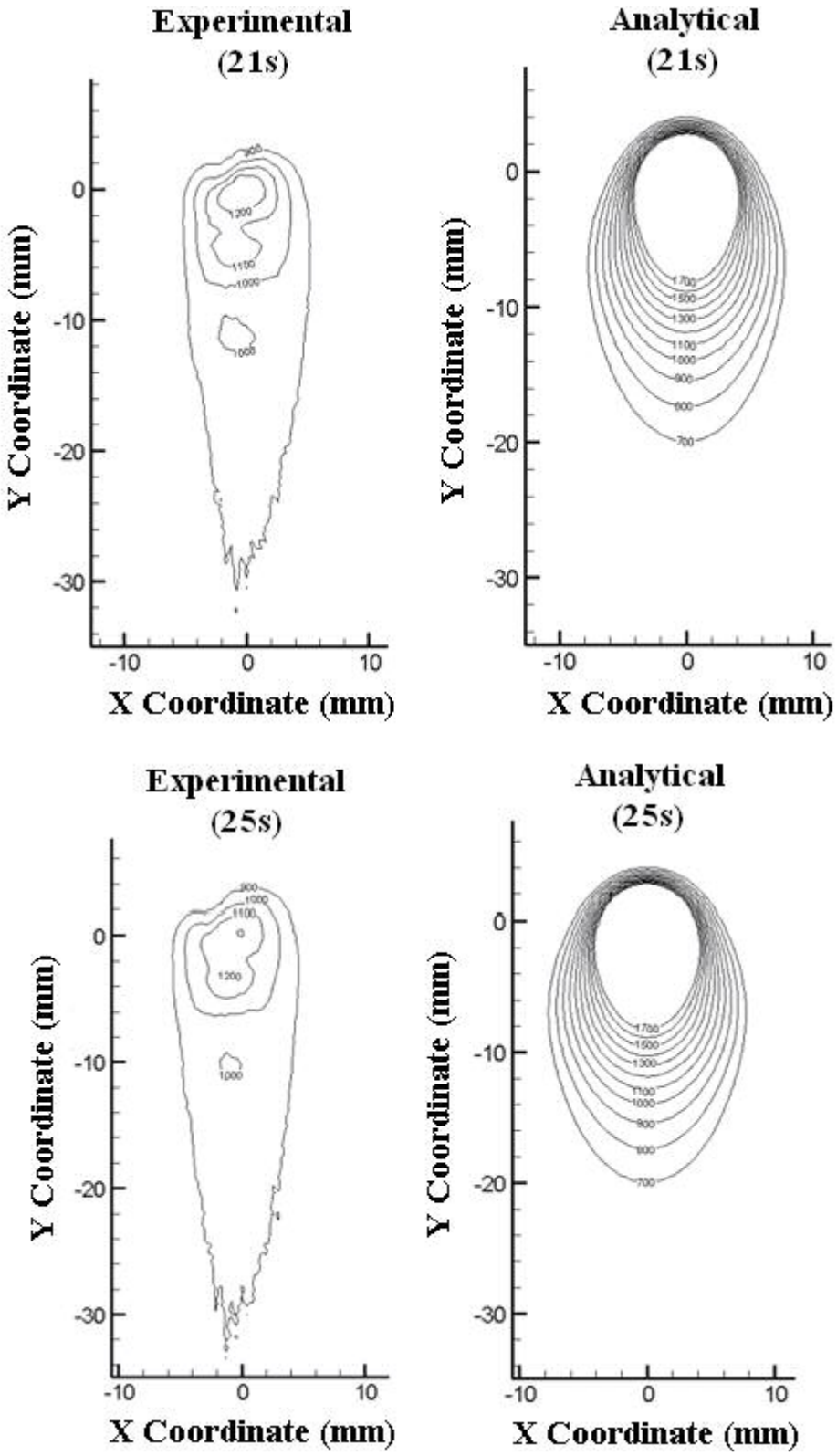

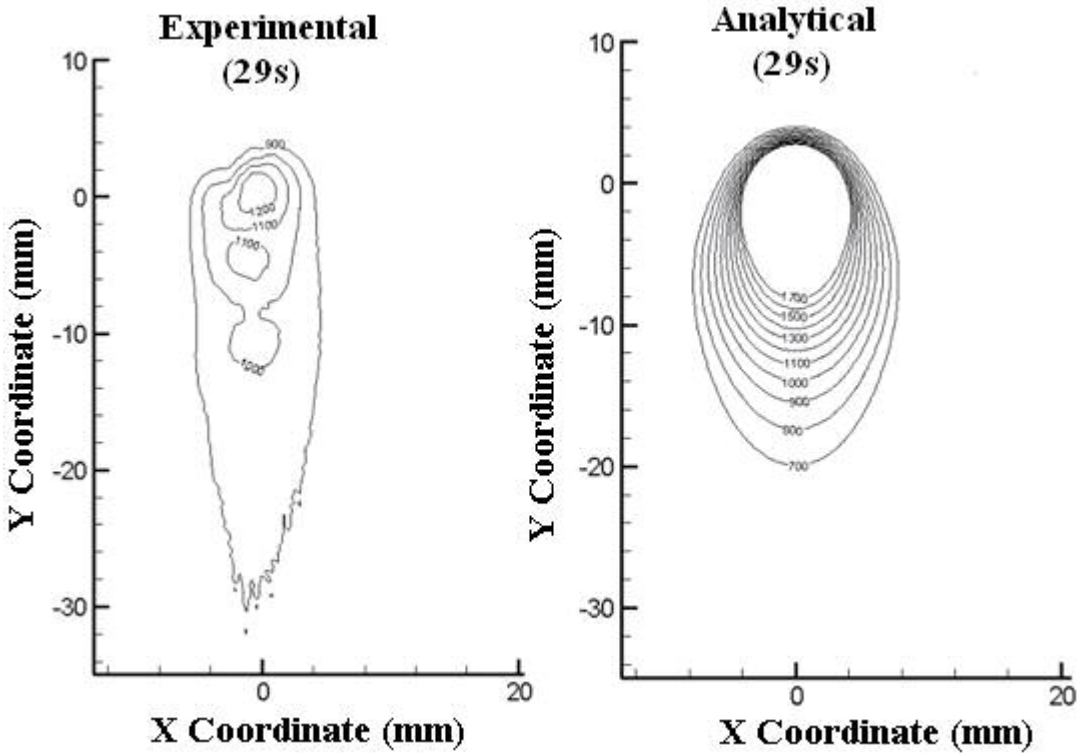
Experimental
(29s)
Analytical
(29s)
Y Coordinate (mm)
X Coordinate (mm)
10
0
-10
-20
-30
20
900
1200
1100
1000
1700
1500
1300
1100
1000
900
700

APPENDIX V

Experimental and analytical images and comparison for a weld velocity of 0.514 cm/s.

Data interface for the analytical solution for a weld velocity of 0.514 cm/s

Given Parameters	Value (Entered by User)	Units
Welding Speed (Arc Velocity)	5.142	mm/s
Arc Beam diameter	0.900	cm
Thickness of Steel Pipe	0.762	mm
Thermal Diffusivity	0.136	cm^2/s
Pipe (outer) diameter	165	mm
Time Elapsed		s
No of Experimental Data Points		
Heat Liberation Qpl	2444.46	W
Thermal Conductivity	0.52	J/(cm.s.K)
Z-Coordinate	0	cm

Transient to quasi-steady state temperature distributions at 1 s to 20 s in 1 s increments of experimental data for a weld velocity of 0.514 cm/s

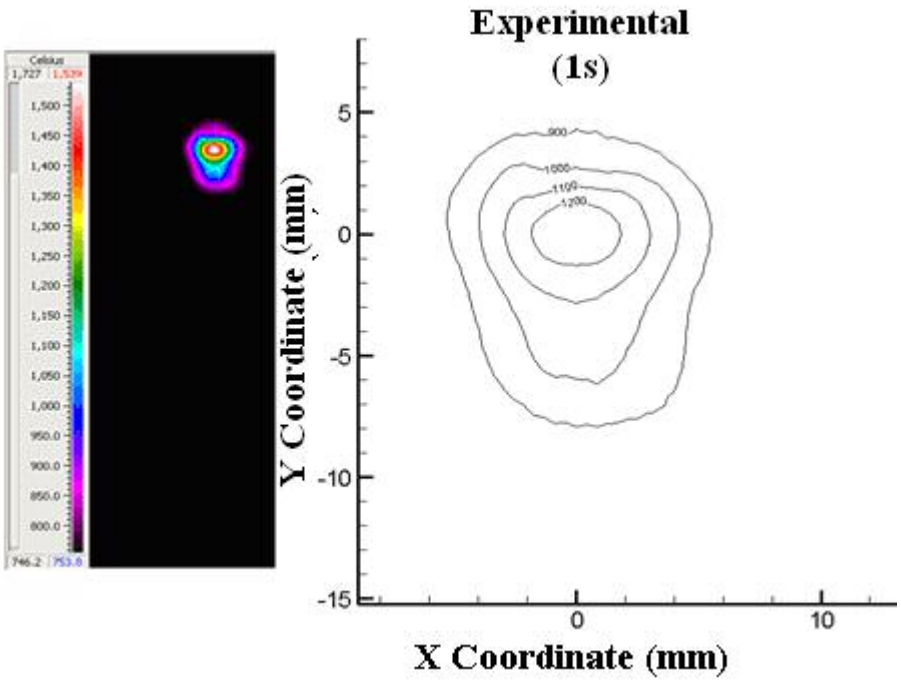

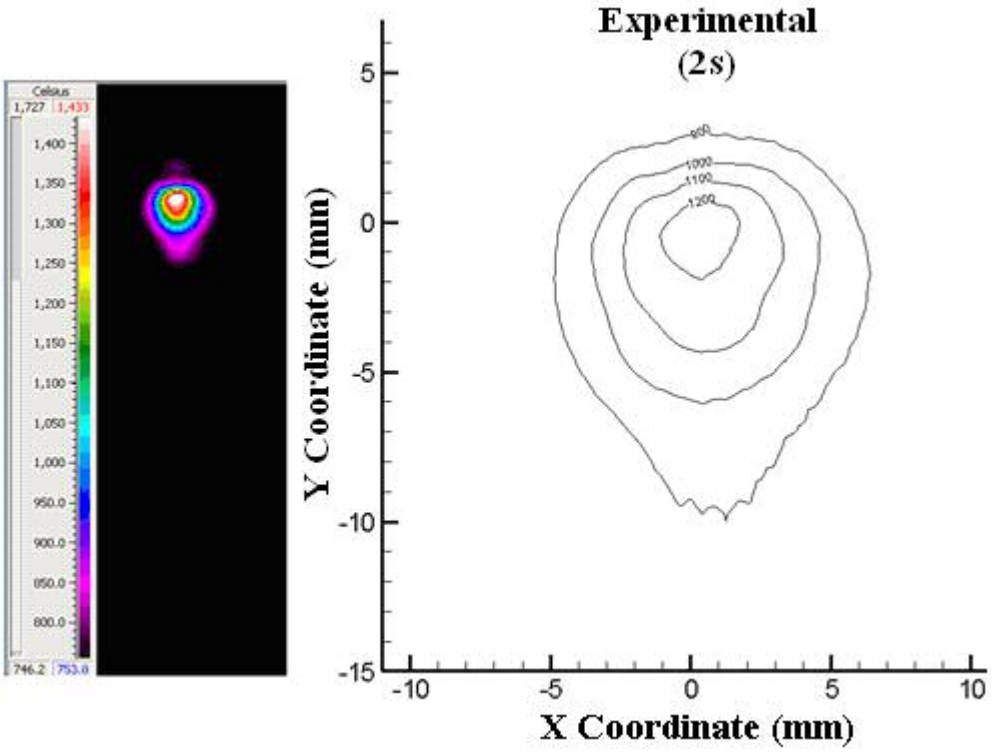
Celsius
1,727 1,433
1,400
1,350
1,300
1,250
1,200
1,150
1,100
1,050
1,000
950.0
900.0
850.0
800.0
746.2 753.0
Experimental
(2s)
900
1000
1100
1200
5
0
-5
-10
-15
Y Coordinate (mm)
-10
-5
0
5
10
X Coordinate (mm)

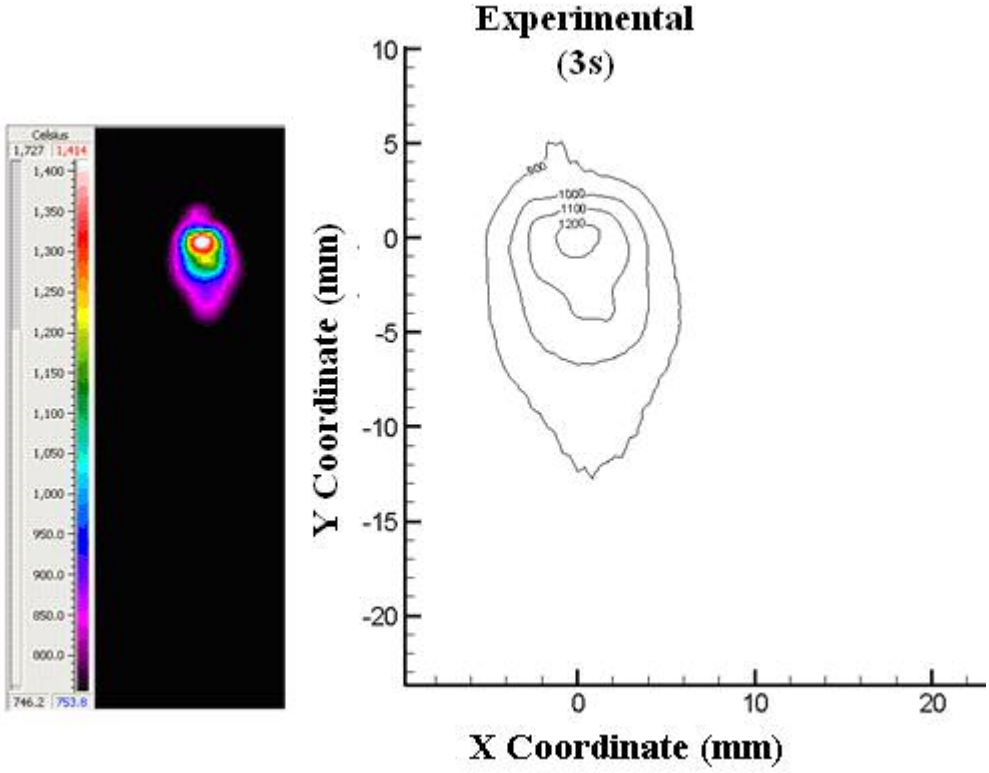
Celsius
1,727 1,414
1,400
1,350
1,300
1,250
1,200
1,150
1,100
1,050
1,000
950.0
900.0
850.0
800.0
746.2 753.8
Experimental
(3s)
900
1000
1100
1200
10
5
0
-5
-10
-15
-20
Y Coordinate (mm)
0
10
20
X Coordinate (mm)

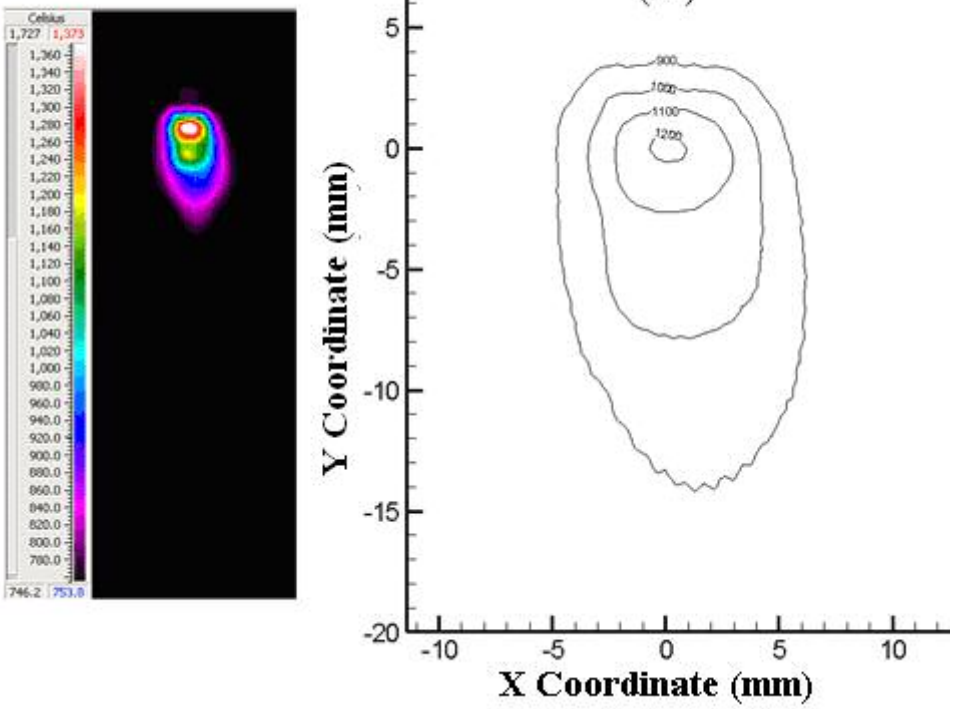
Experimental
(4s)
Celsius
1,727
1,373
1,360
1,340
1,320
1,300
1,280
1,260
1,240
1,220
1,200
1,180
1,160
1,140
1,120
1,100
1,080
1,060
1,040
1,020
1,000
980.0
960.0
940.0
920.0
900.0
880.0
860.0
840.0
820.0
800.0
780.0
746.2
753.8
900
1000
1100
1200
5
0
-5
-10
-15
-20
-10
-5
0
5
10
Y Coordinate (mm)
X Coordinate (mm)

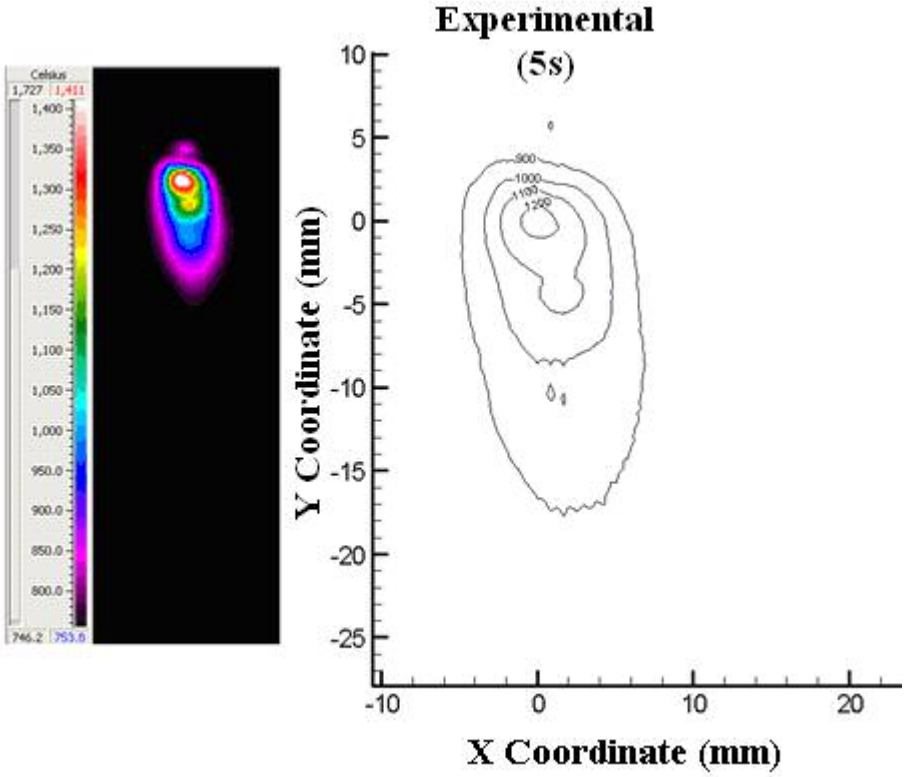
Experimental
(5s)
Celsius
1,727
1,411
1,400
1,350
1,300
1,250
1,200
1,150
1,100
1,050
1,000
950.0
900.0
850.0
800.0
746.2
753.8
900
1000
1100
1200
10
5
0
-5
-10
-15
-20
-25
-10
0
10
20
Y Coordinate (mm)
X Coordinate (mm)

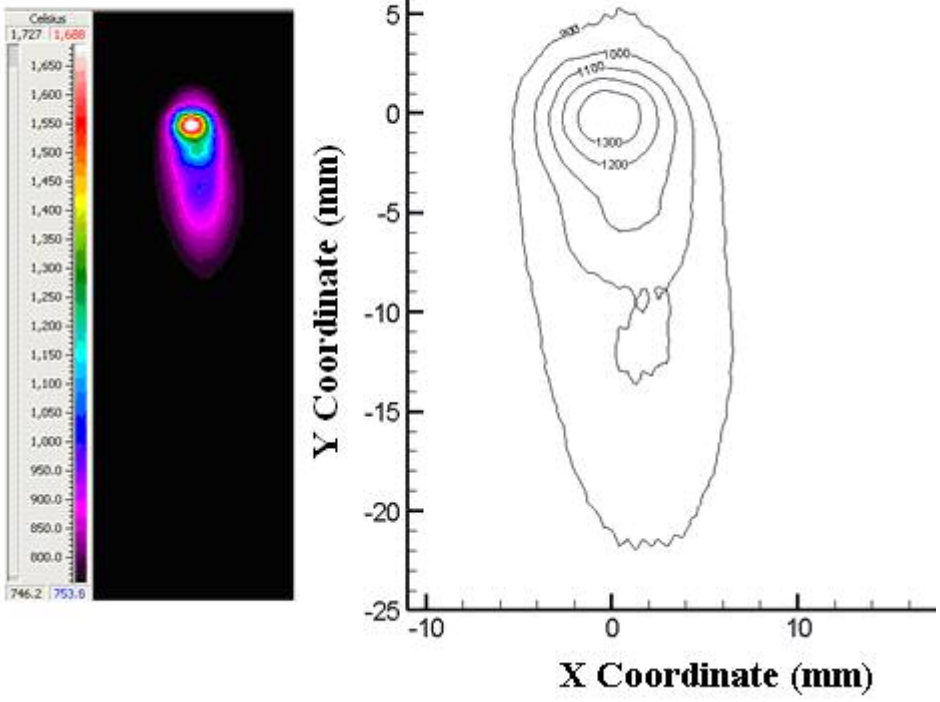
Experimental
(6s)
Celsius
1,727
1,688
1,650
1,600
1,550
1,500
1,450
1,400
1,350
1,300
1,250
1,200
1,150
1,100
1,050
1,000
950.0
900.0
850.0
800.0
746.2
753.6
900
1000
1100
1300
1200
5
0
-5
-10
-15
-20
-25
-10
0
10
Y Coordinate (mm)
X Coordinate (mm)

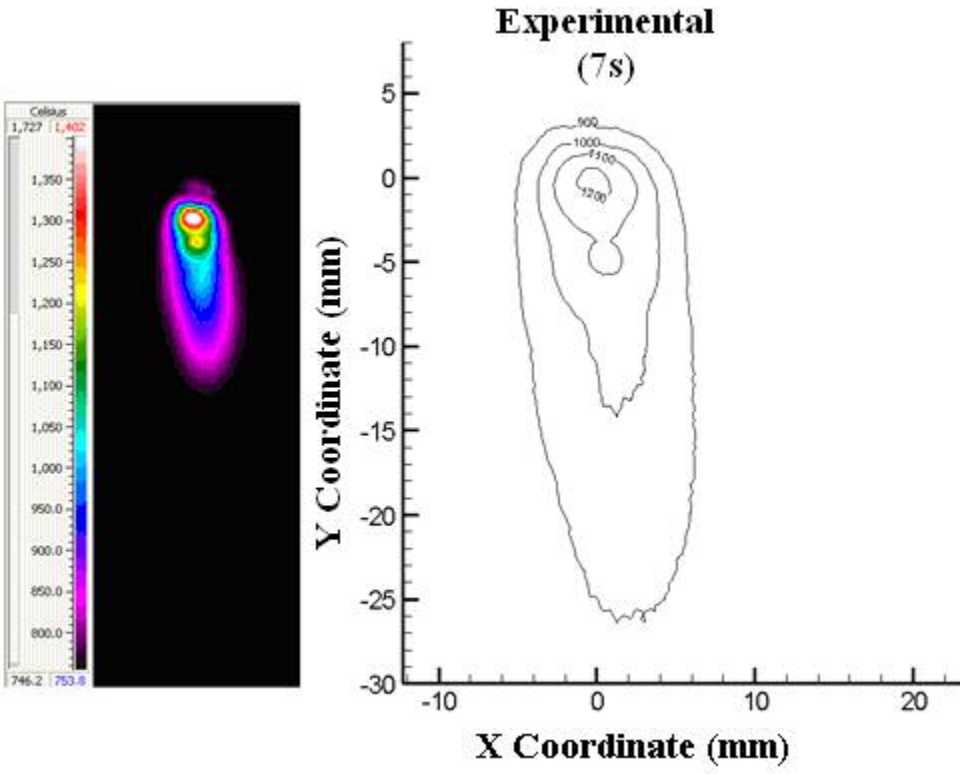
Experimental
(7s)
Celsius
1,727
1,402
1,350
1,300
1,250
1,200
1,150
1,100
1,050
1,000
950.0
900.0
850.0
800.0
746.2
753.6
900
1000
1100
1200
5
0
-5
-10
-15
-20
-25
-30
-10
0
10
20
Y Coordinate (mm)
X Coordinate (mm)

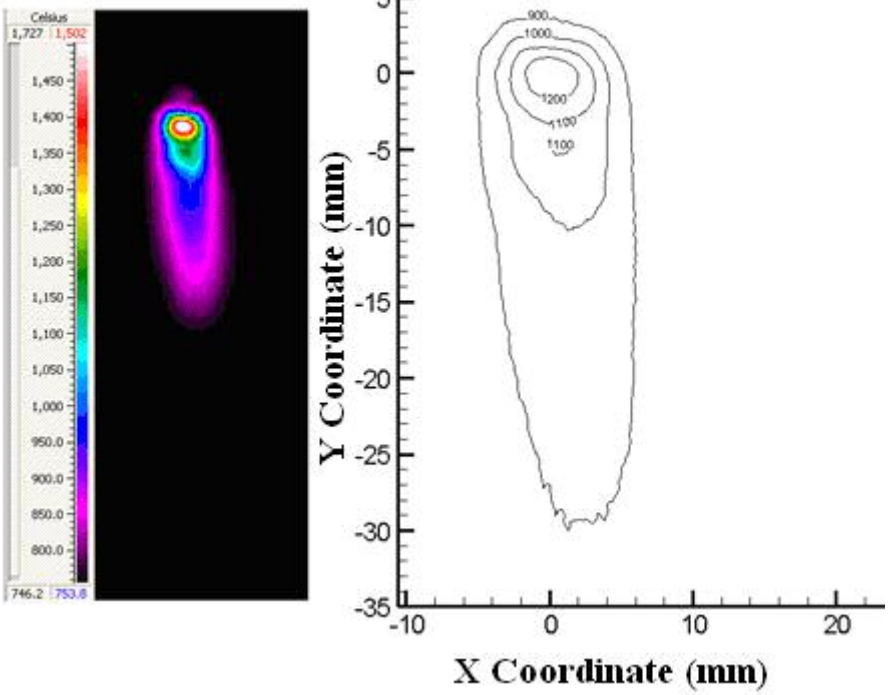
Experimental
(8s)
Celsius
1,727
1,502
1,450
1,400
1,350
1,300
1,250
1,200
1,150
1,100
1,050
1,000
950.0
900.0
850.0
800.0
746.2
753.8
900
1000
1200
1100
1100
5
0
-5
-10
-15
-20
-25
-30
-35
-10
0
10
20
Y Coordinate (mm)
X Coordinate (mm)

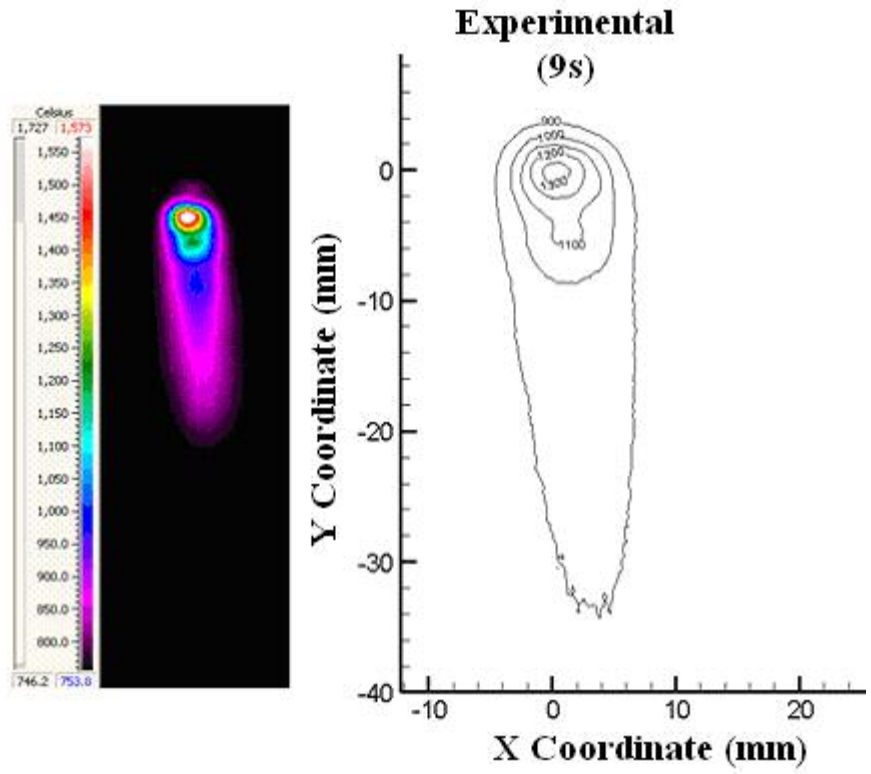
Experimental
(9s)
Celsius
1,727
1,573
1,550
1,500
1,450
1,400
1,350
1,300
1,250
1,200
1,150
1,100
1,050
1,000
950.0
900.0
850.0
800.0
746.2
753.8
900
1000
1200
1300
1100
0
-10
-20
-30
-40
-10
0
10
20
Y Coordinate (mm)
X Coordinate (mm)

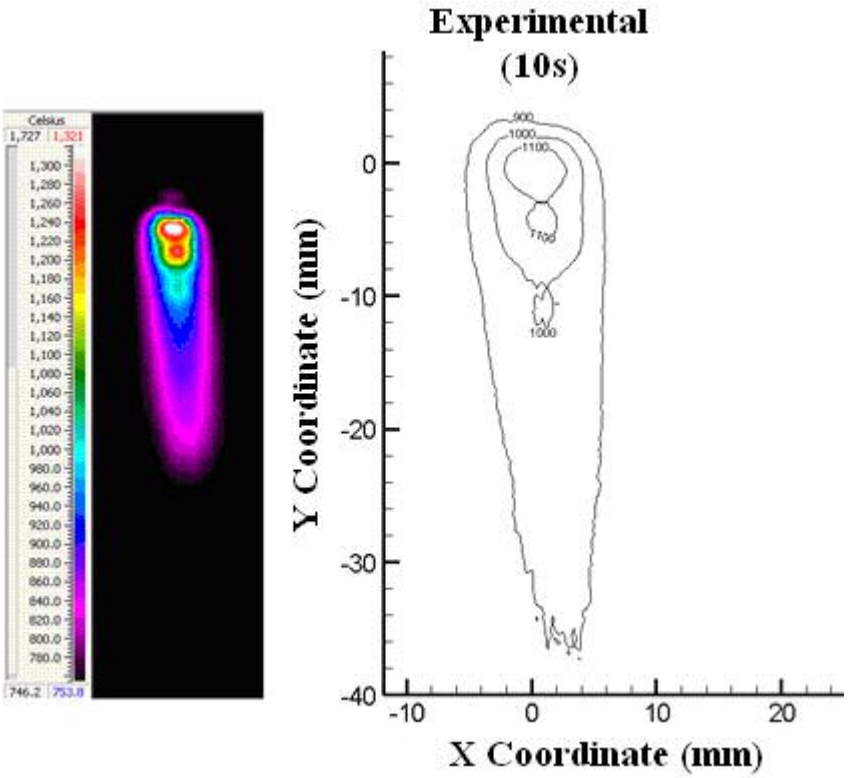
Experimental
(10s)
Celsius
1,727
1,321
Y Coordinate (mm)
X Coordinate (mm)
0
-10
-20
-30
-40
-10
0
10
20
900
1000
1100
1100
1000

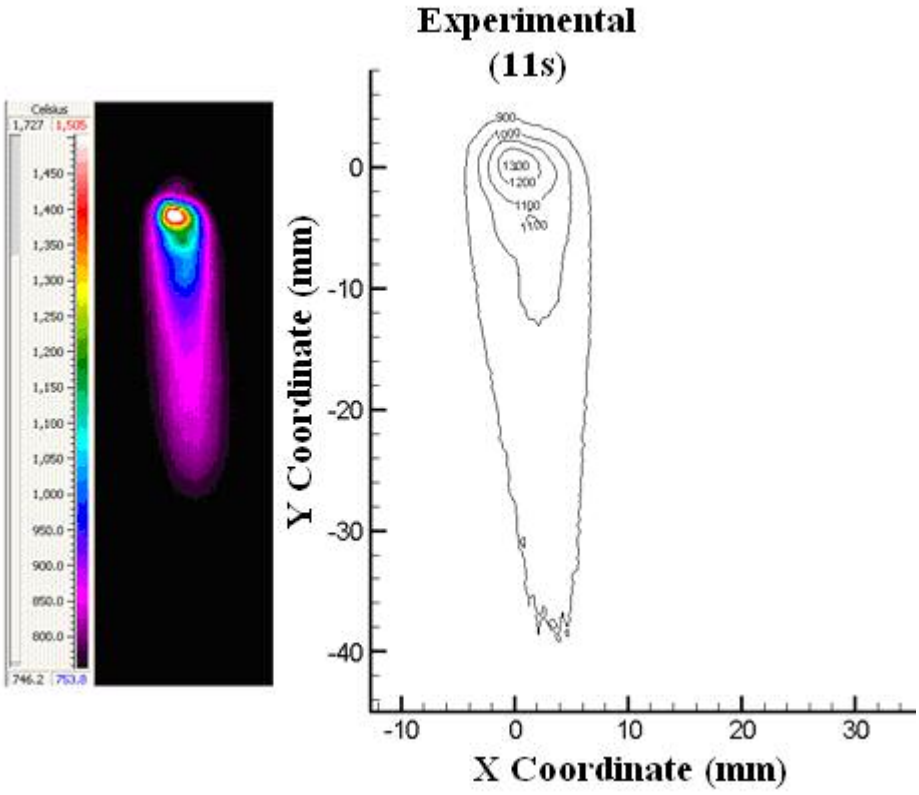
Experimental
(11s)
Celsius
1,727
1,505
Y Coordinate (mm)
X Coordinate (mm)
0
-10
-20
-30
-40
-10
0
10
20
30
900
1000
1300
1200
1100
1100

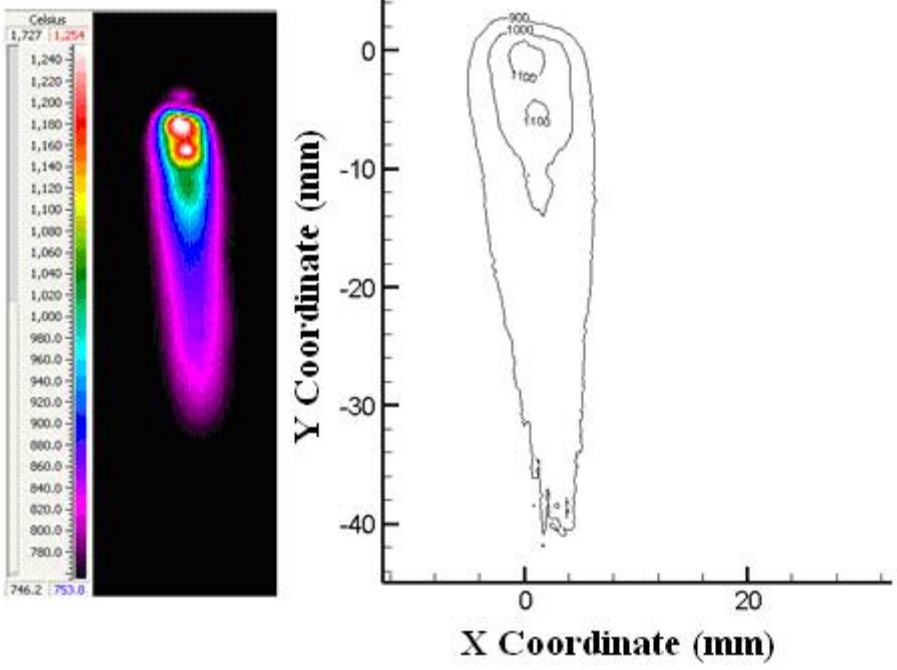
Experimental
(12s)
Celsius
1,727
1,254
746.2
753.0
900
1000
1100
1100
0
-10
-20
-30
-40
Y Coordinate (mm)
0
20
X Coordinate (mm)

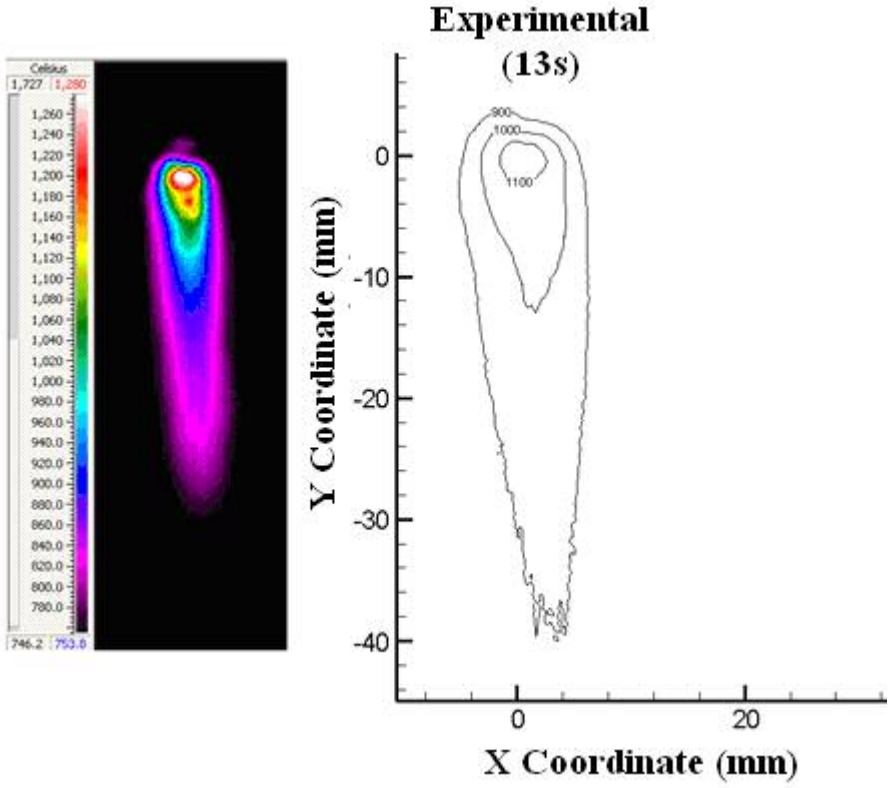
Experimental
(13s)
Celsius
1,727
1,280
746.2
753.0
900
1000
1100
0
-10
-20
-30
-40
Y Coordinate (mm)
0
20
X Coordinate (mm)

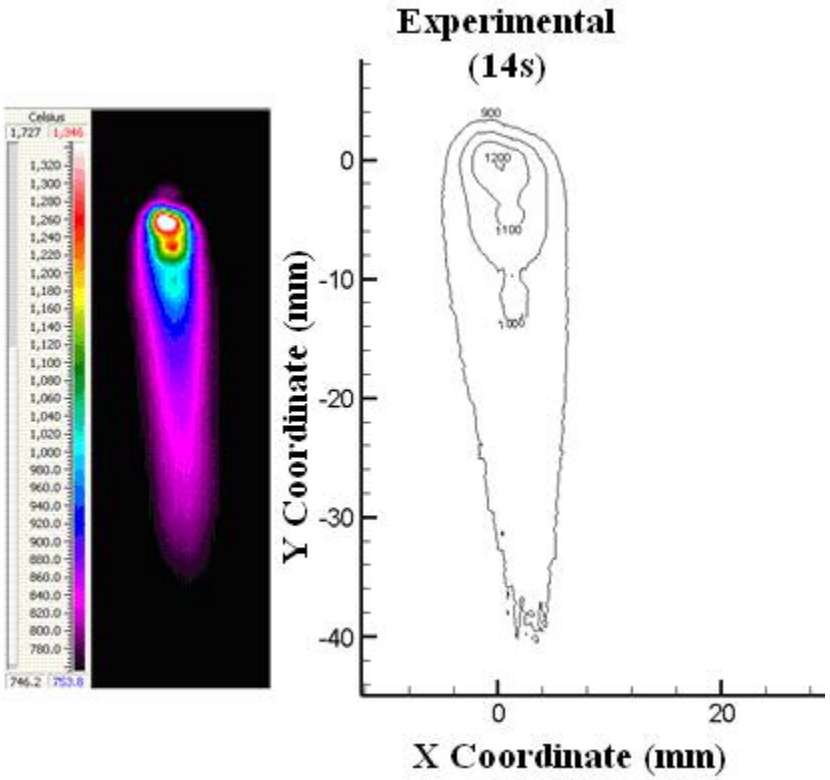
Experimental
(14s)
Celsius
1,727 1,946
1,320
1,300
1,280
1,260
1,240
1,220
1,200
1,180
1,160
1,140
1,120
1,100
1,080
1,060
1,040
1,020
1,000
980.0
960.0
940.0
920.0
900.0
880.0
860.0
840.0
820.0
800.0
780.0
746.2 753.8
900
1200
1100
1000
0
-10
-20
-30
-40
Y Coordinate (mm)
0
20
X Coordinate (mm)

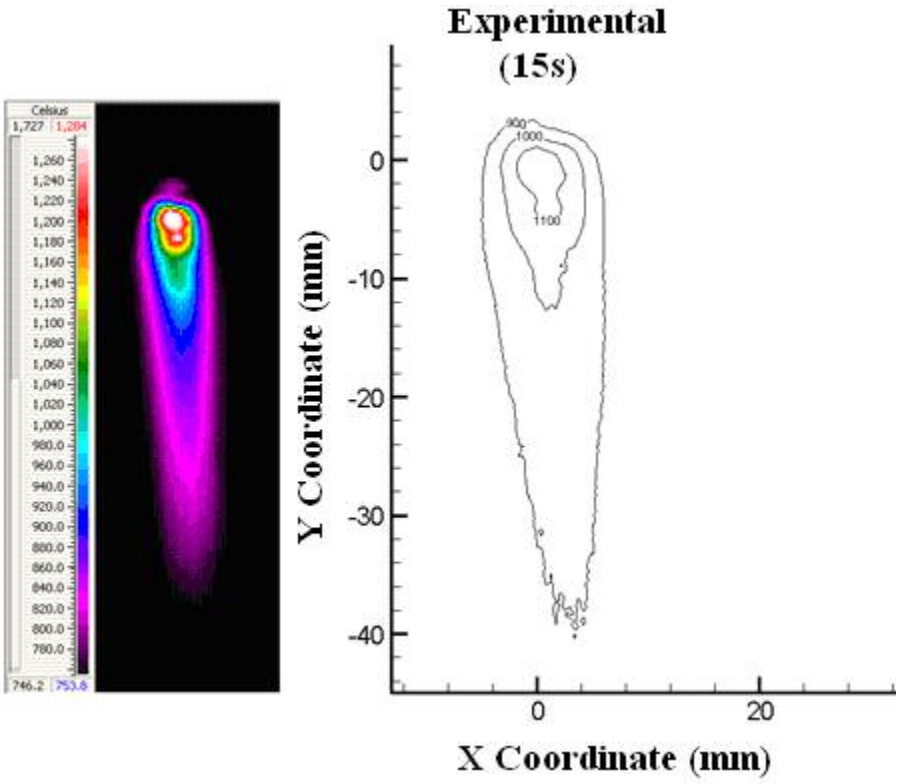
Experimental
(15s)
Celsius
1,727 1,284
1,260
1,240
1,220
1,200
1,180
1,160
1,140
1,120
1,100
1,080
1,060
1,040
1,020
1,000
980.0
960.0
940.0
920.0
900.0
880.0
860.0
840.0
820.0
800.0
780.0
746.2 753.8
900
1000
1100
0
-10
-20
-30
-40
Y Coordinate (mm)
0
20
X Coordinate (mm)

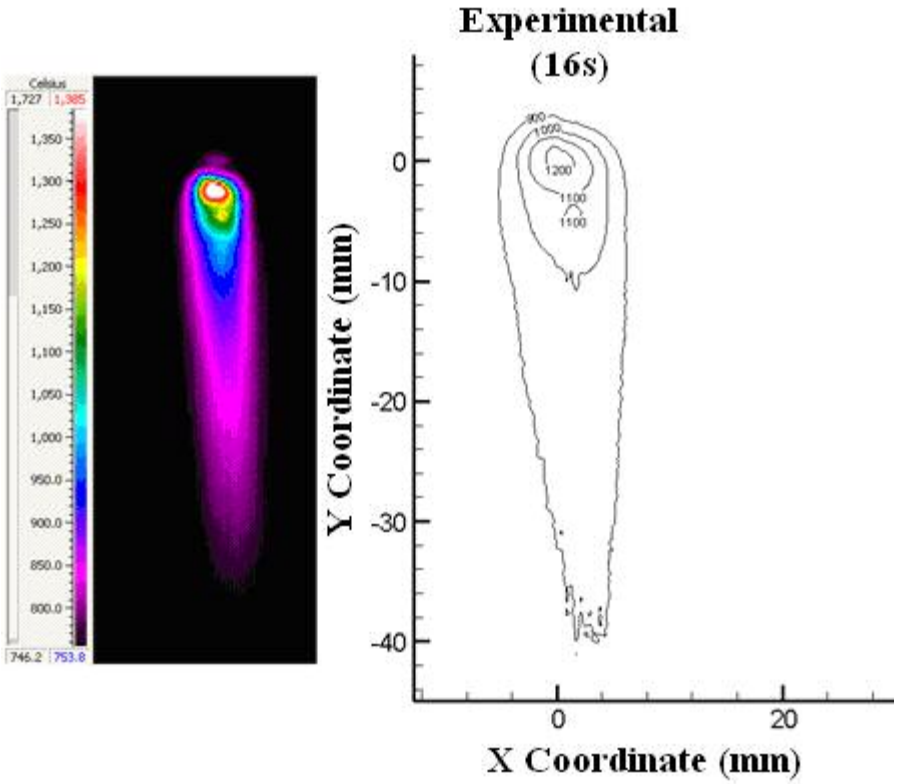
Experimental
(16s)
Celsius
1,727
1,385
1,350
1,300
1,250
1,200
1,150
1,100
1,050
1,000
950.0
900.0
850.0
800.0
746.2
753.8
800
1000
1200
1100
1100
0
-10
-20
-30
-40
0
20
Y Coordinate (mm)
X Coordinate (mm)

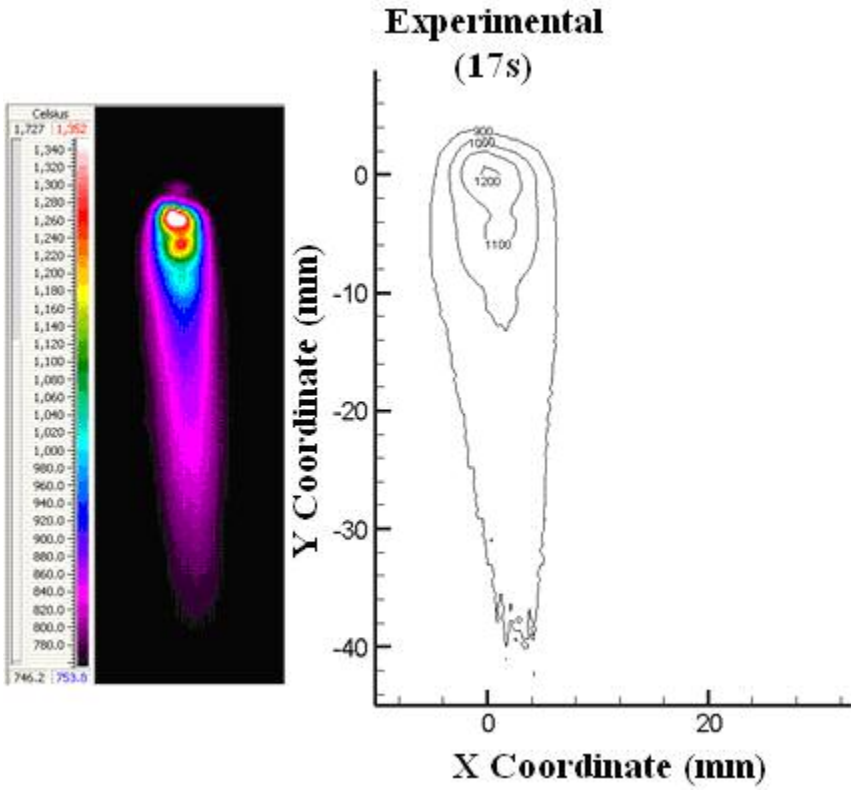
Experimental
(17s)
Celsius
1,727
1,362
1,340
1,320
1,300
1,280
1,260
1,240
1,220
1,200
1,180
1,160
1,140
1,120
1,100
1,080
1,060
1,040
1,020
1,000
980.0
960.0
940.0
920.0
900.0
880.0
860.0
840.0
820.0
800.0
780.0
746.2
753.0
800
1000
1200
1100
0
-10
-20
-30
-40
0
20
Y Coordinate (mm)
X Coordinate (mm)

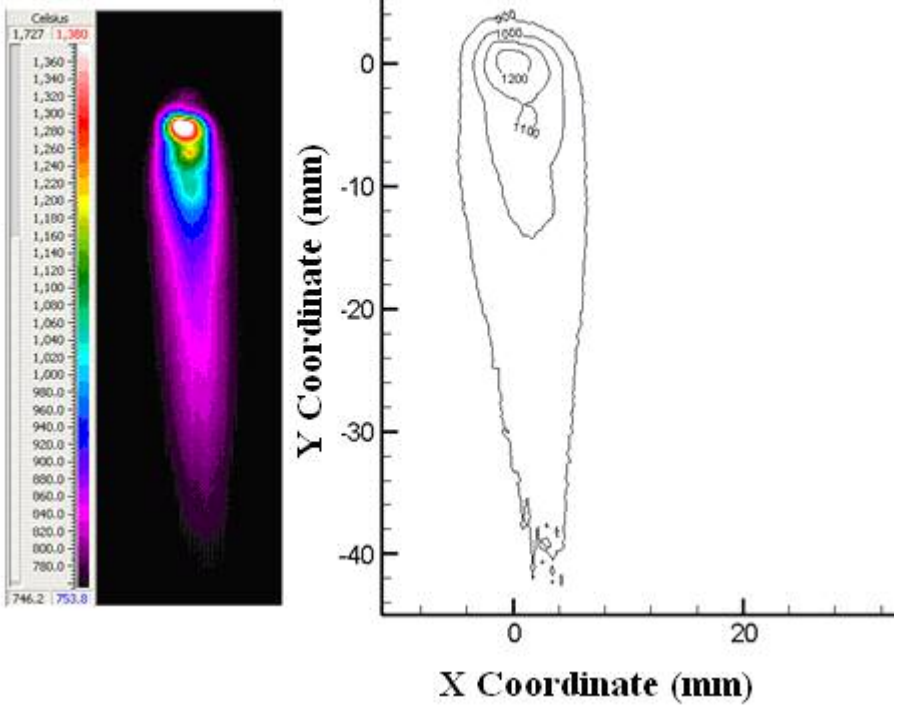
Experimental
(18s)
Celsius
1,727
1,360
746.2
753.8
900
1000
1200
1100
0
-10
-20
-30
-40
0
20
Y Coordinate (mm)
X Coordinate (mm)

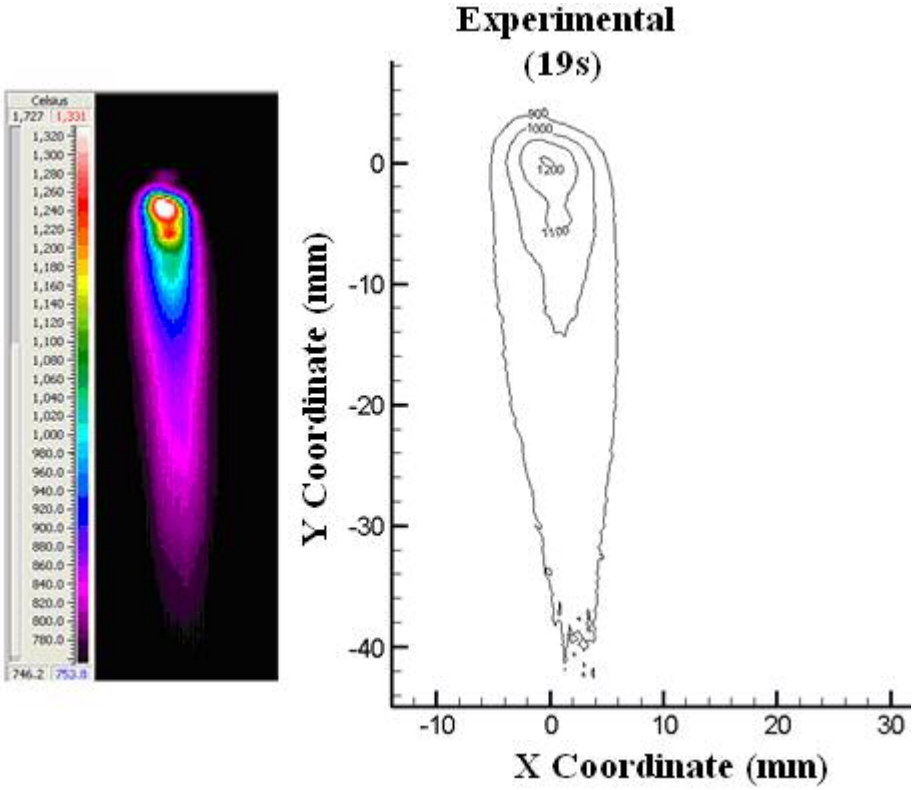
Experimental
(19s)
Celsius
1,727
1,331
746.2
753.8
900
1000
1200
1100
0
-10
-20
-30
-40
-10
0
10
20
30
Y Coordinate (mm)
X Coordinate (mm)

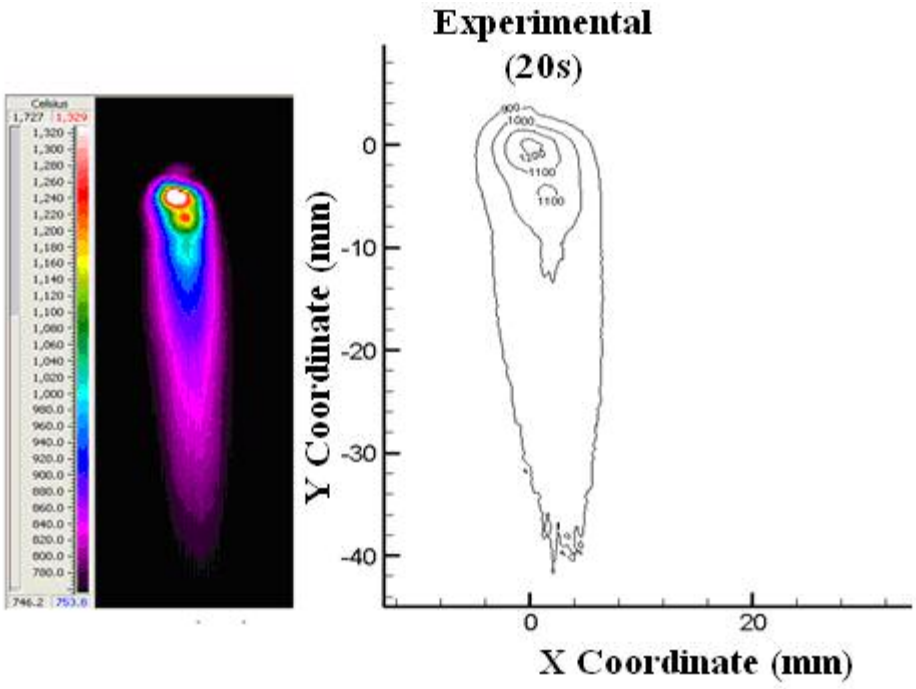

Quasi-steady state temperature distribution for experimental data at 21 s, 25 s, and 29 s for a weld velocity of 0.514 mm/s

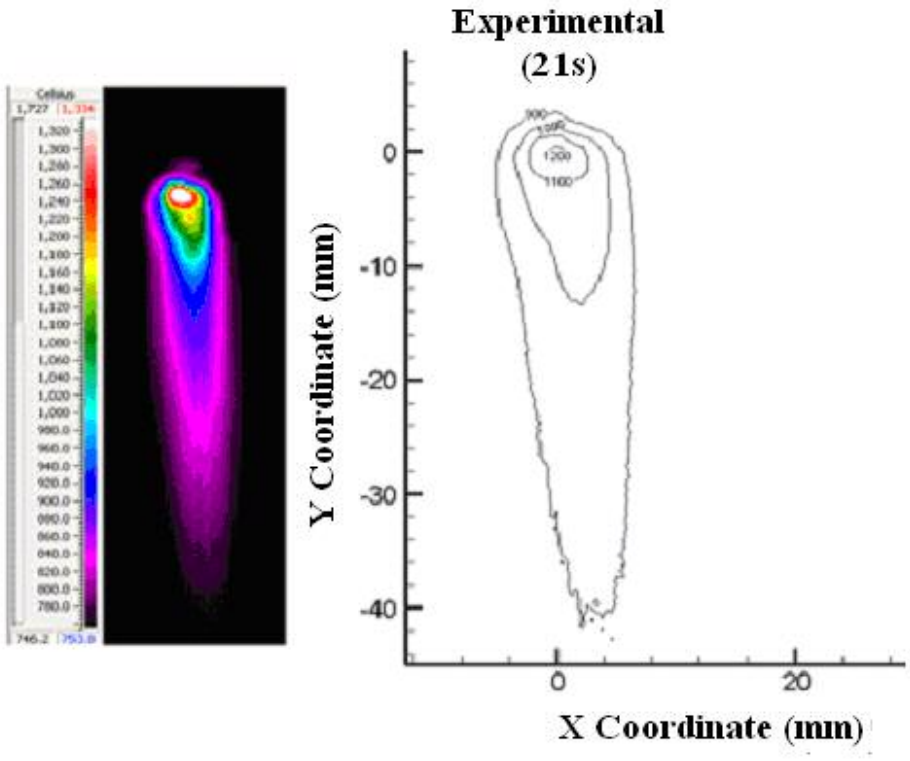

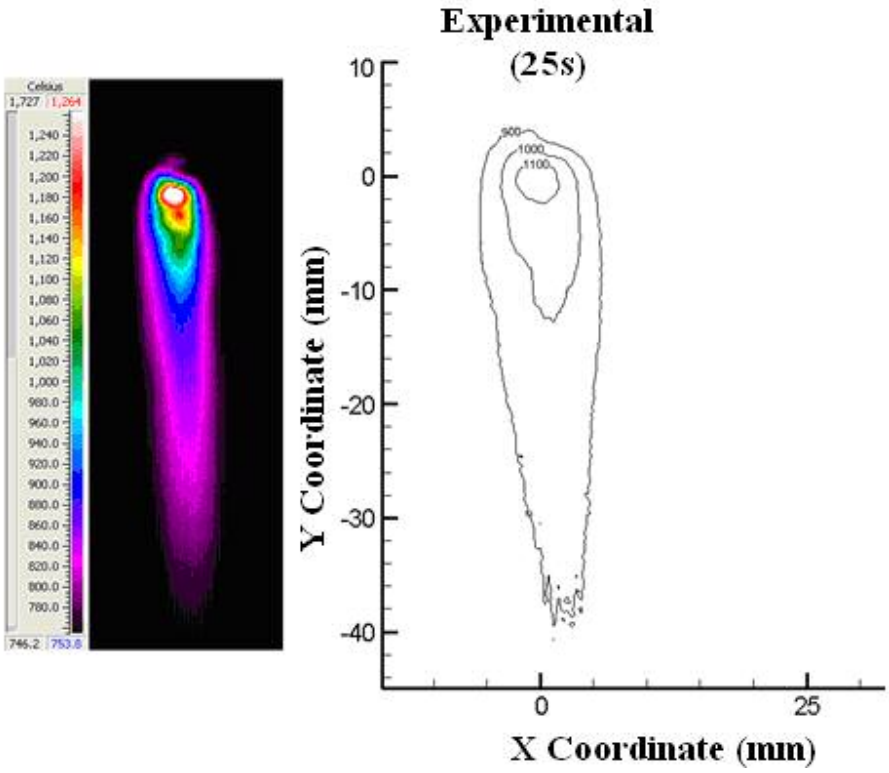
Experimental
(25s)
Celsius
1,727
1,264
746.2
753.8
900
1000
1100
10
0
-10
-20
-30
-40
0
25
Y Coordinate (mm)
X Coordinate (mm)

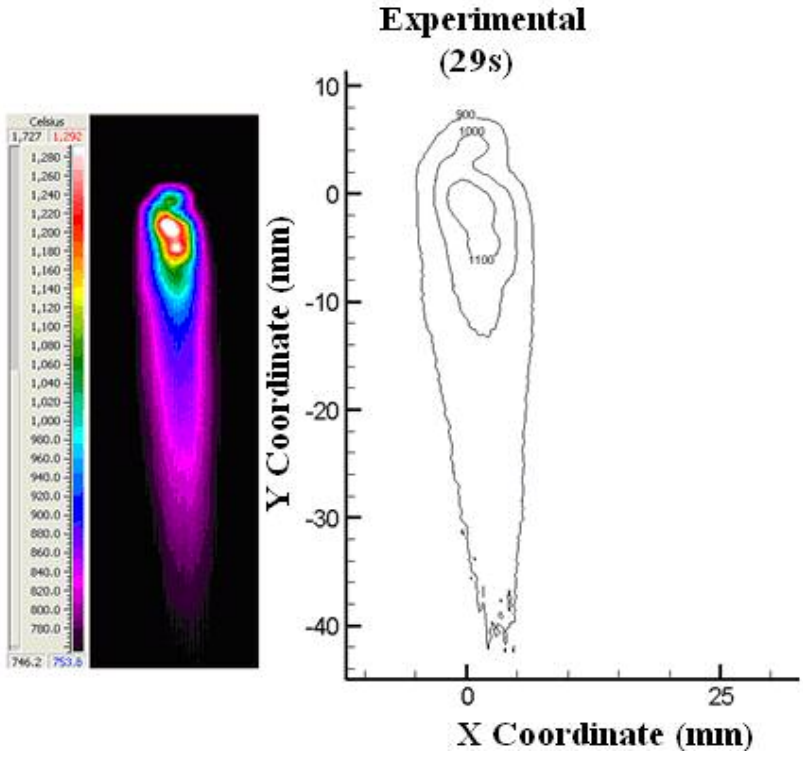
Experimental
(29s)
Celsius
1,727
1,292
746.2
753.8
900
1000
1100
10
0
-10
-20
-30
-40
0
25
Y Coordinate (mm)
X Coordinate (mm)

Transient to quasi-steady state temperature distributions for 1 s to 20 s in 1 s increments of analytical data for a weld velocity of 0.514 cm/s

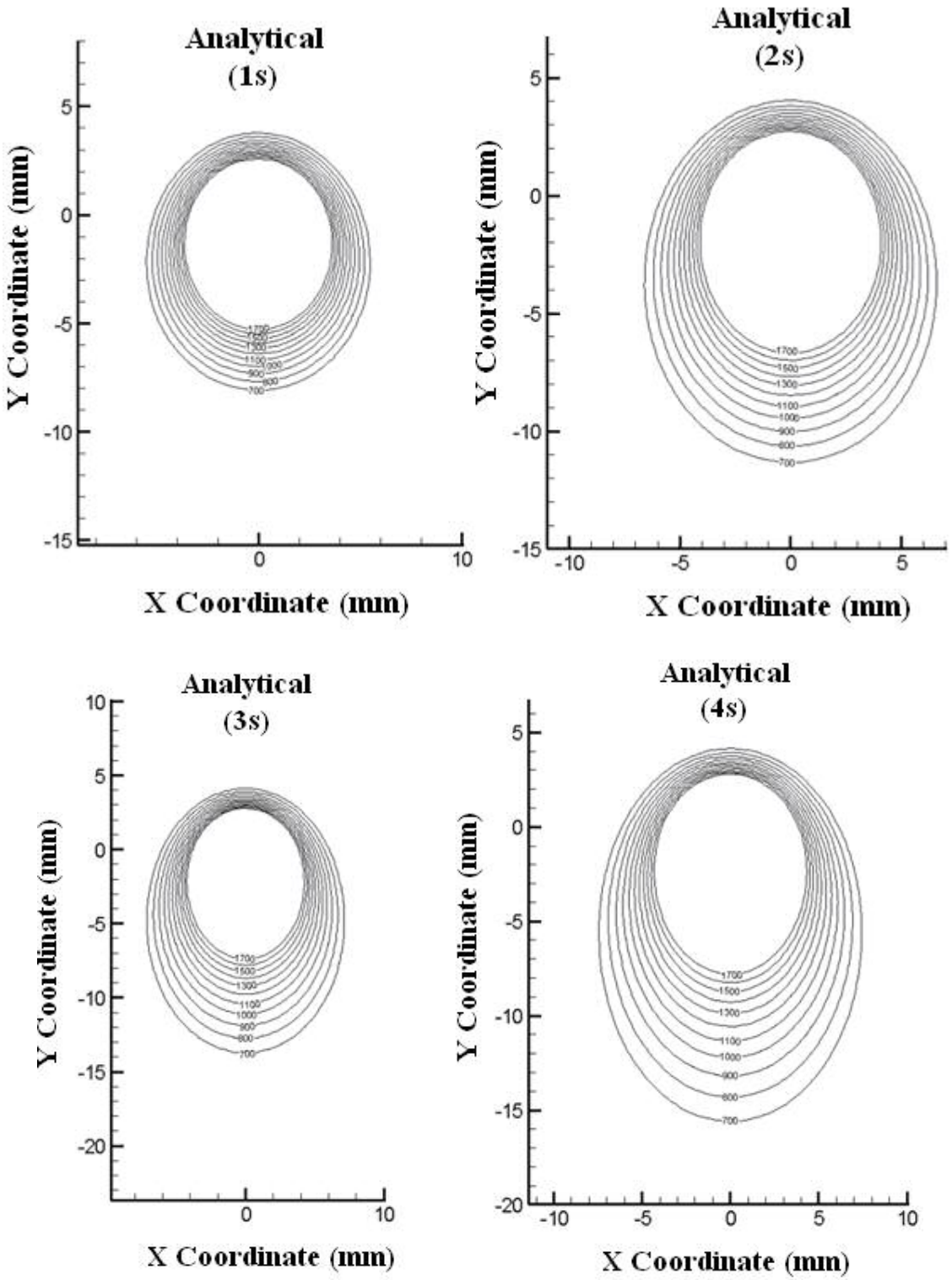

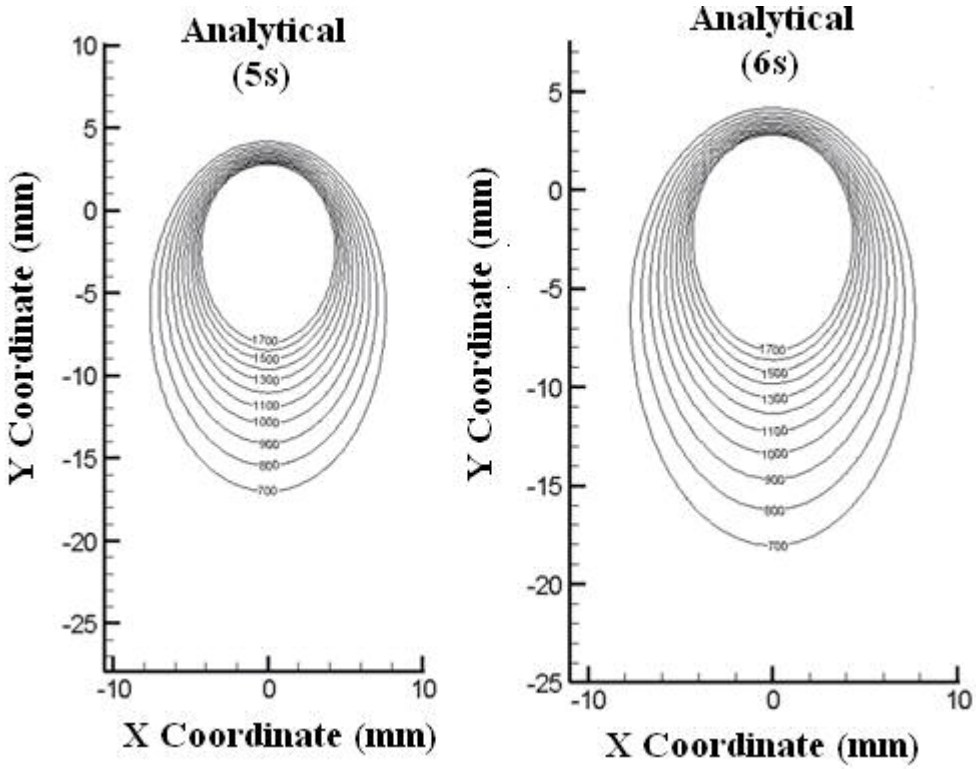
Analytical
(5s)
Analytical
(6s)
Y Coordinate (mm)
X Coordinate (mm)
1700
1500
1300
1100
1000
900
800
700

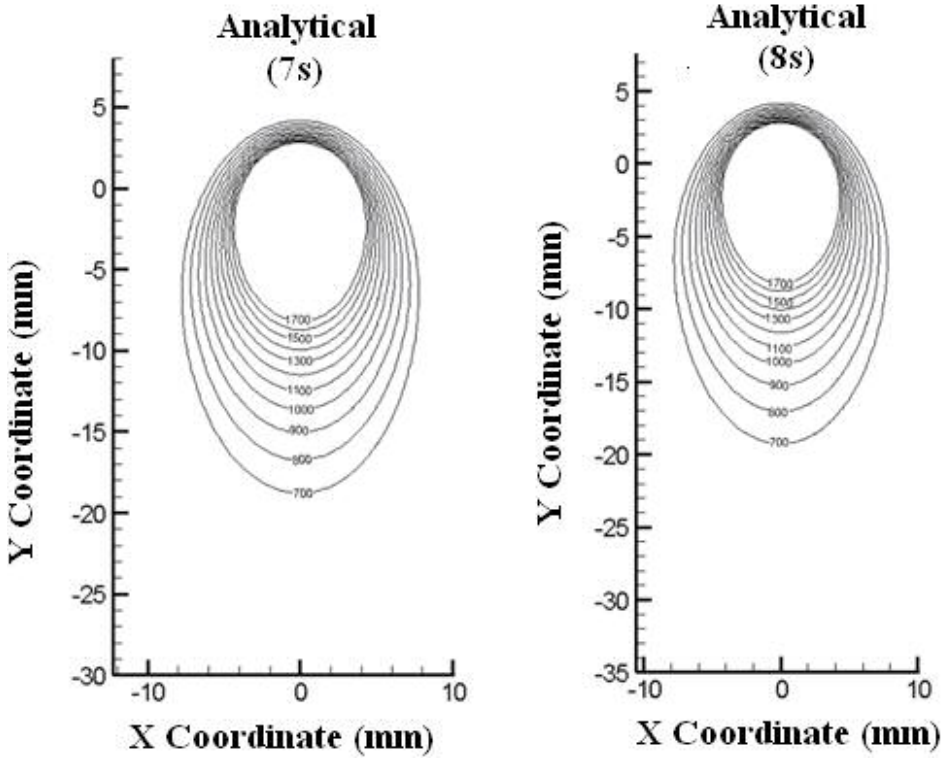
Analytical
(7s)
Analytical
(8s)
Y Coordinate (mm)
X Coordinate (mm)
1700
1500
1300
1100
1000
900
800
700

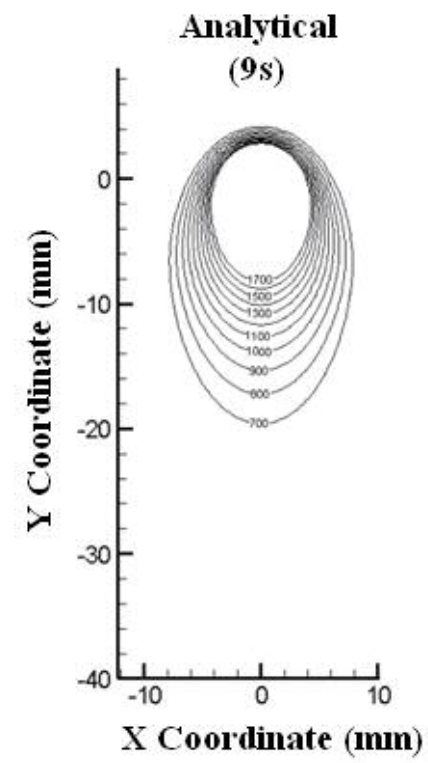
Analytical
(9s)
Y Coordinate (mm)
X Coordinate (mm)
0
-10
-20
-30
-40
-10
0
10
1700
1500
1300
1100
1000
900
800
700

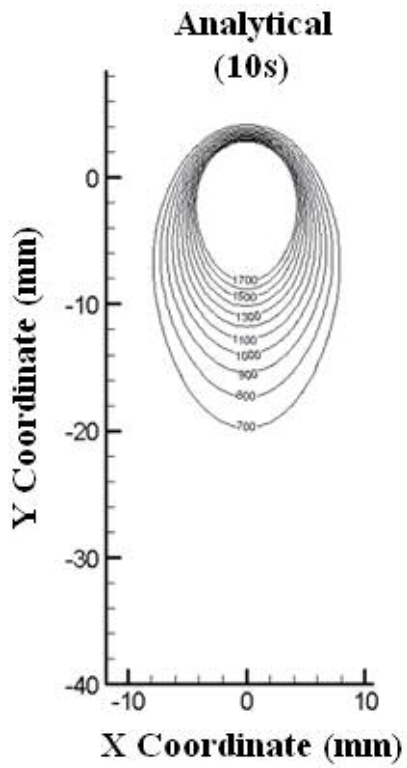
Analytical
(10s)
Y Coordinate (mm)
X Coordinate (mm)
0
-10
-20
-30
-40
-10
0
10
1700
1500
1300
1100
1000
900
800
700

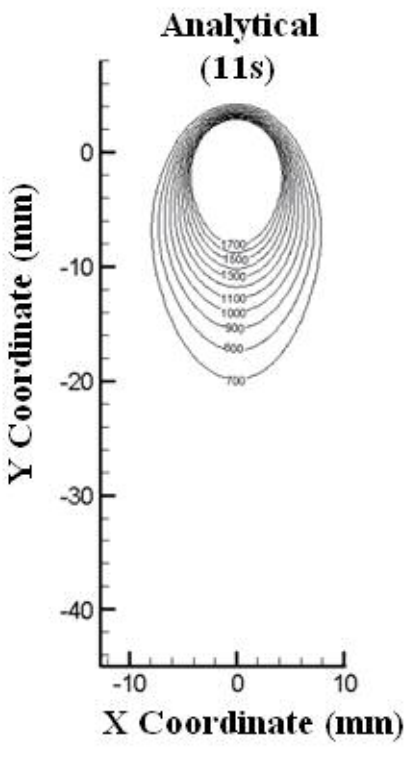
Analytical
(11s)
Y Coordinate (mm)
X Coordinate (mm)
0
-10
-20
-30
-40
-10
0
10
1700
1500
1300
1100
1000
900
800
700

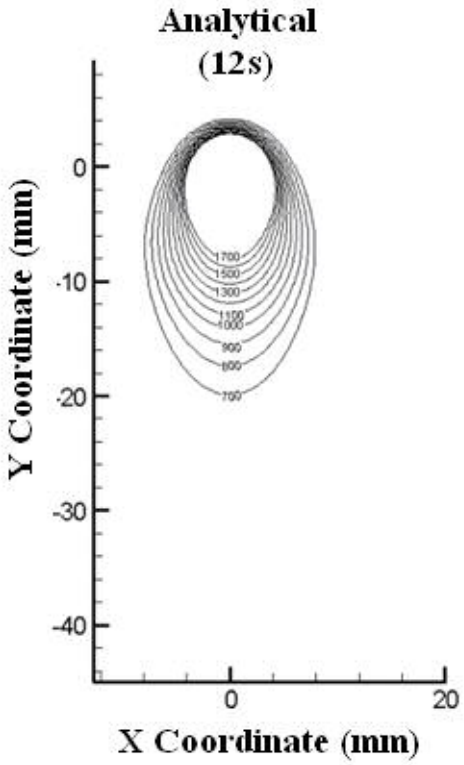
Analytical
(12s)
Y Coordinate (mm)
X Coordinate (mm)
0
-10
-20
-30
-40
0
20
1700
1500
1300
1100
1000
900
800
700

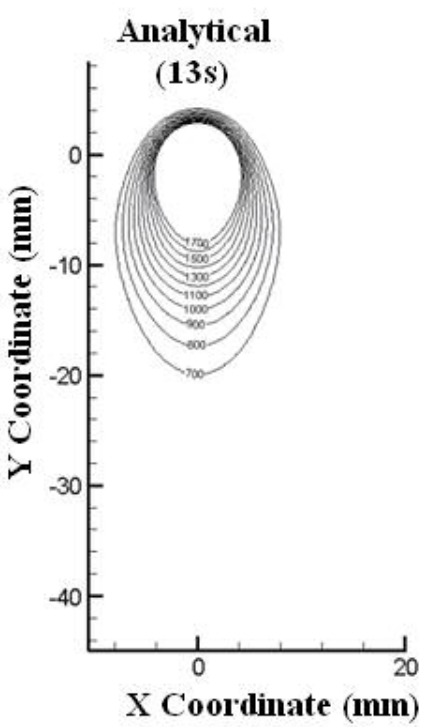
Analytical
(13s)
Y Coordinate (mm)
X Coordinate (mm)
0
-10
-20
-30
-40
0
20
1700
1500
1300
1100
1000
900
800
700

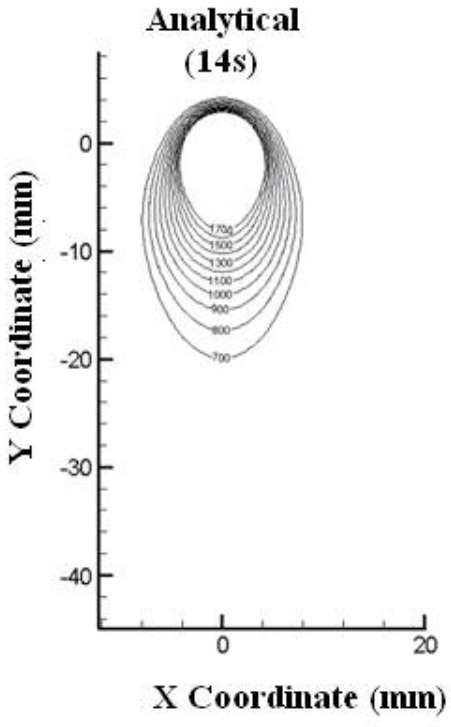
Analytical
(14s)
Y Coordinate (mm)
X Coordinate (mm)
0
-10
-20
-30
-40
0
20
1700
1500
1300
1100
1000
900
800
700

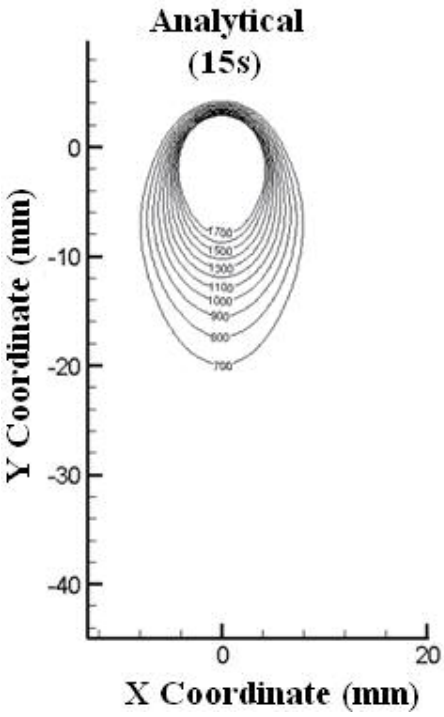
Analytical
(15s)
Y Coordinate (mm)
X Coordinate (mm)
0
-10
-20
-30
-40
0
20
1700
1500
1300
1100
1000
900
800
700

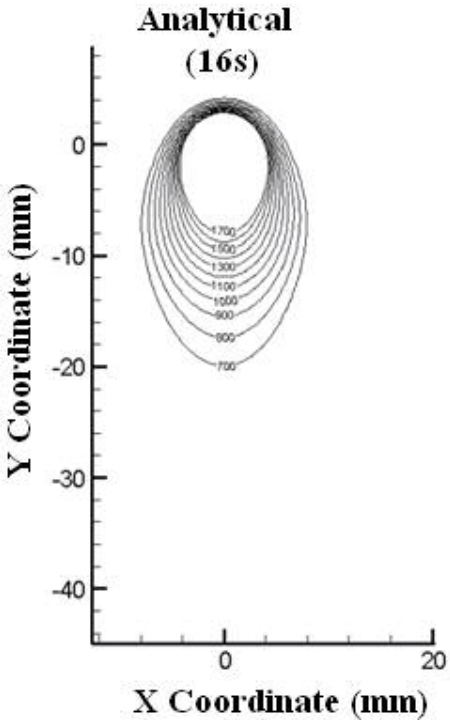
Analytical
(16s)
Y Coordinate (mm)
X Coordinate (mm)
0
-10
-20
-30
-40
0
20
1700
1500
1300
1100
1000
900
800
700

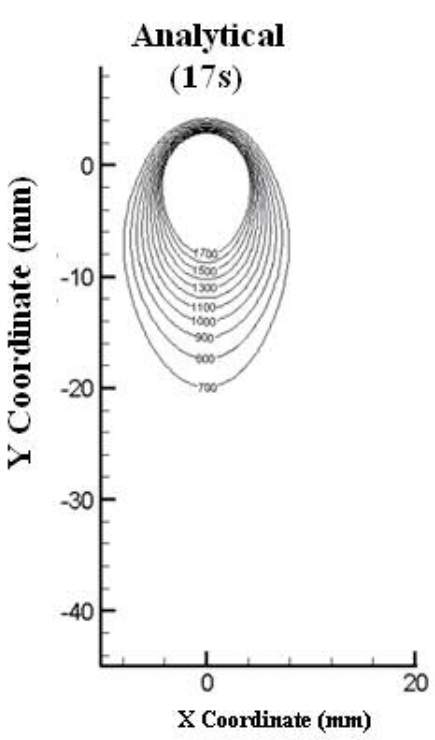
Analytical
(17s)
Y Coordinate (mm)
X Coordinate (mm)
0
-10
-20
-30
-40
0
20
1700
1500
1300
1100
1000
900
800
700

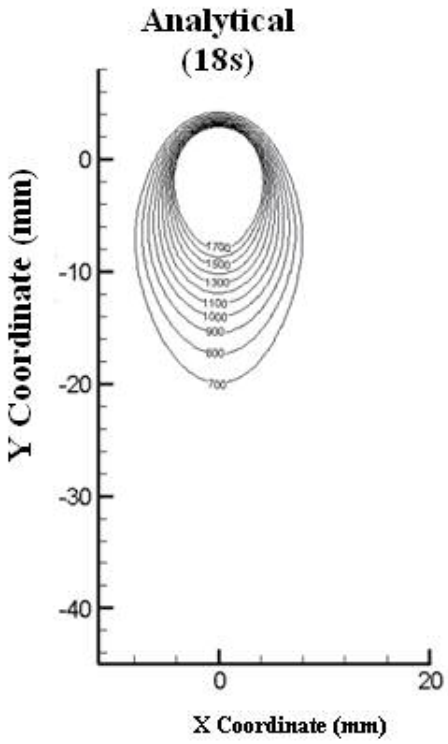
Analytical
(18s)
Y Coordinate (mm)
X Coordinate (mm)
0
-10
-20
-30
-40
0
20
1700
1500
1300
1100
1000
900
800
700

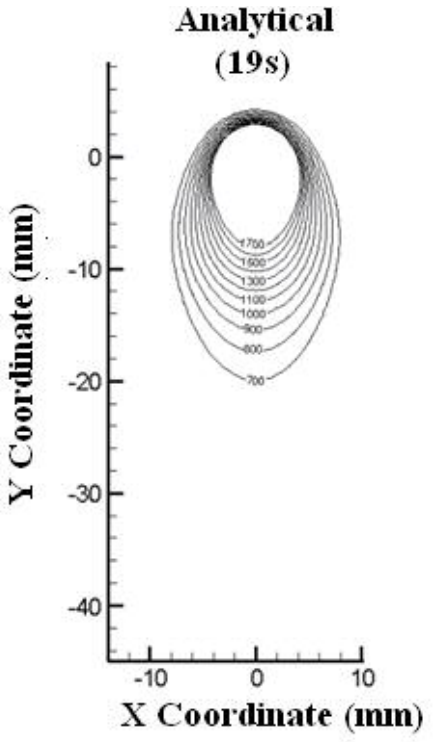
Analytical
(19s)
Y Coordinate (mm)
X Coordinate (mm)
0
-10
-20
-30
-40
-10
0
10
1700
1500
1300
1100
1000
900
800
700

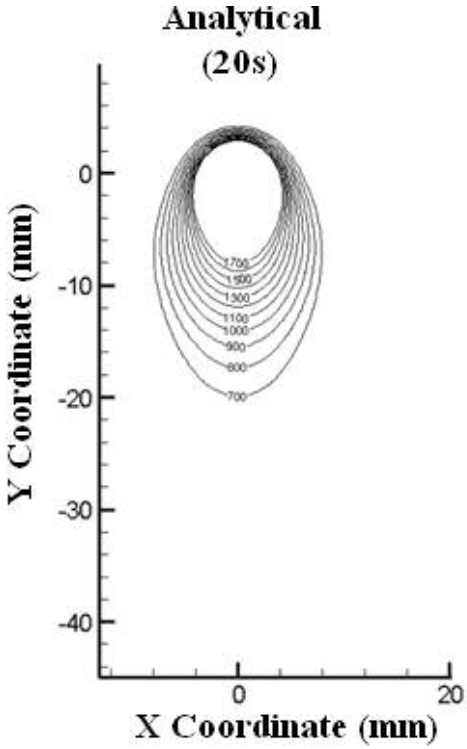
Analytical
(20s)
Y Coordinate (mm)
X Coordinate (mm)
0
-10
-20
-30
-40
0
20
1700
1500
1300
1100
1000
900
800
700

Quasi-steady state temperature distribution of analytical data for 19 s, 20 s, and 25 s for a weld velocity of 0.514 cm/s

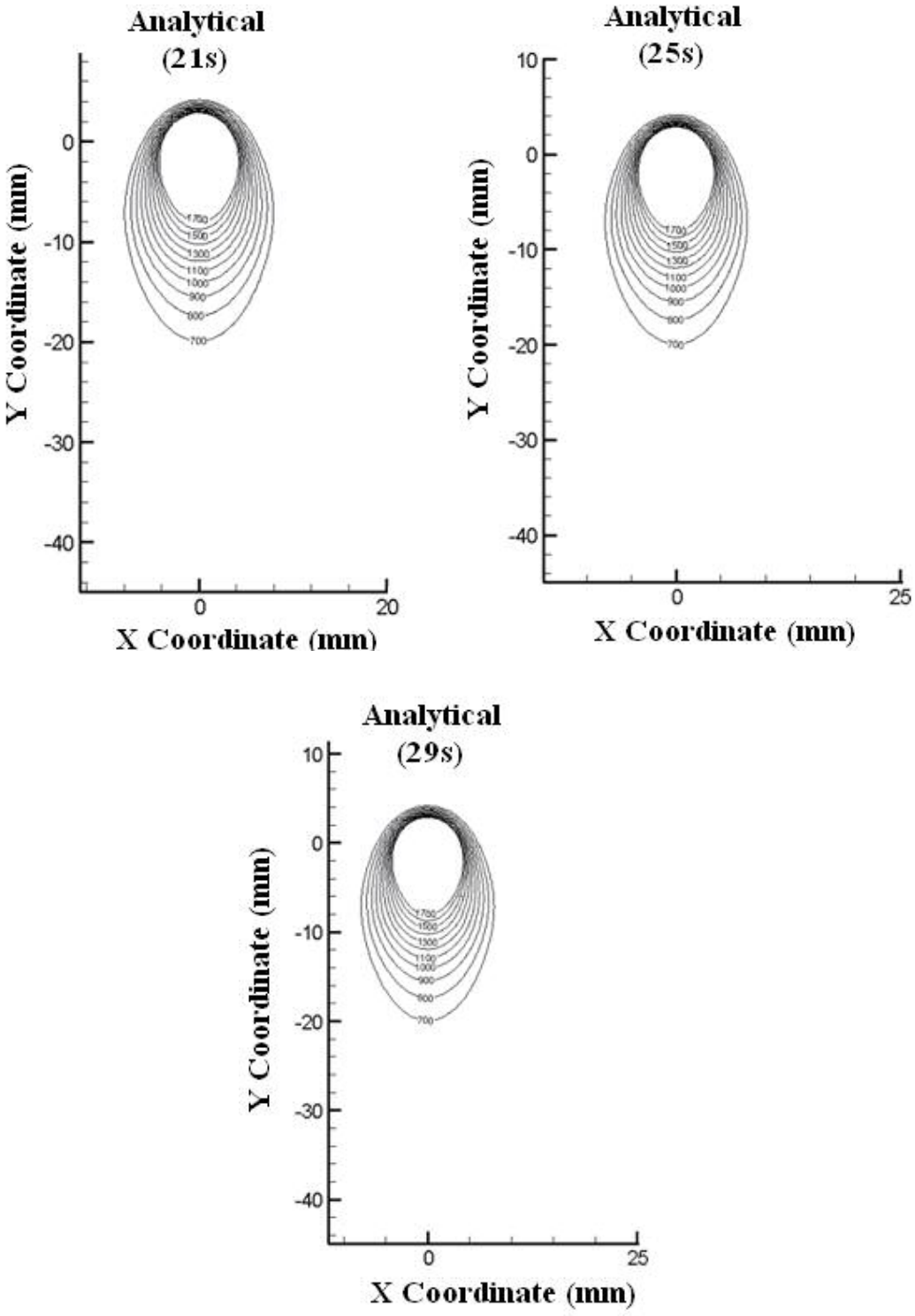

Transient to quasi-steady state temperature distributions for 1 s to 20 s in 1 s increments of experimental data and analytical data comparison for a weld velocity of 0.514 cm/s

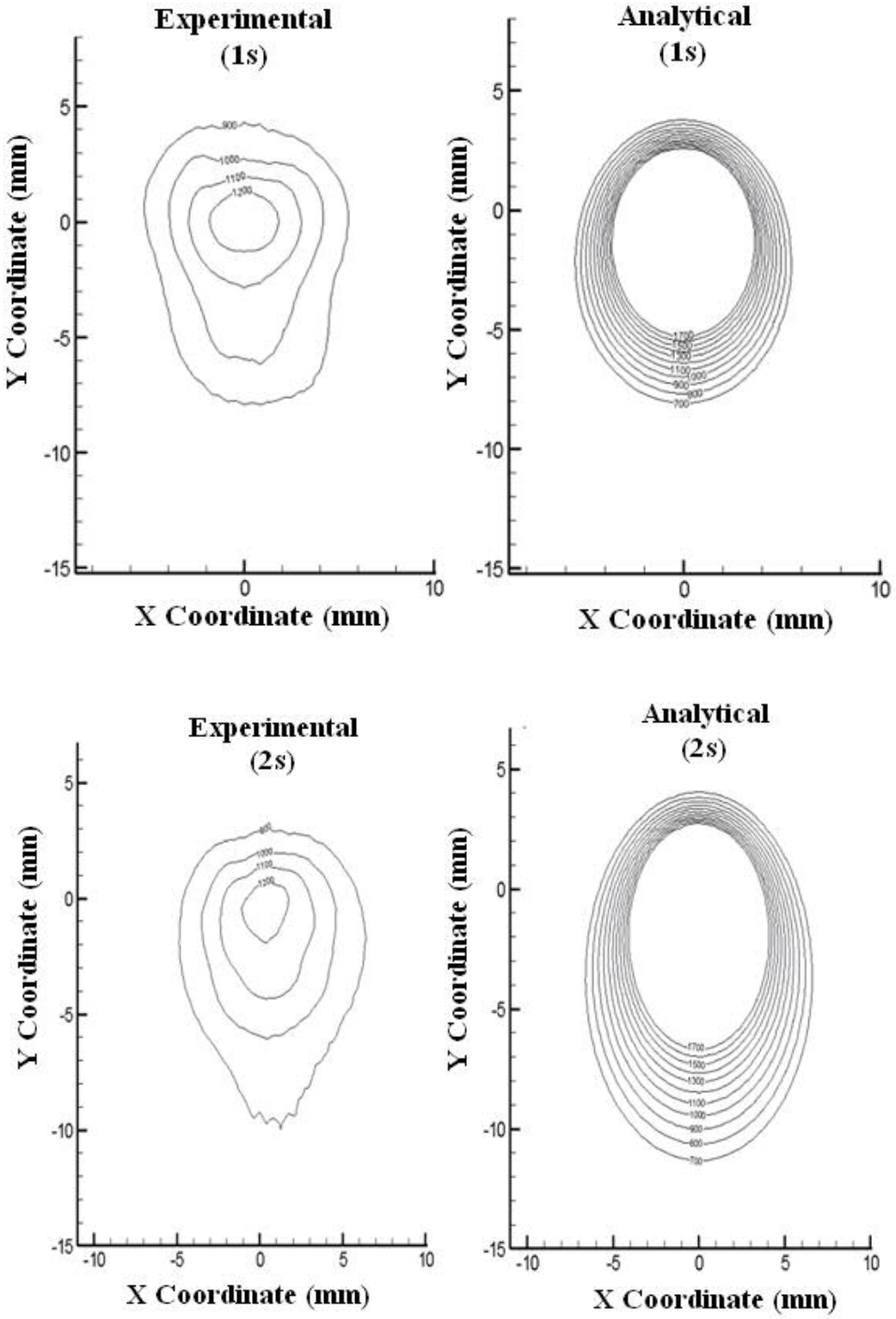

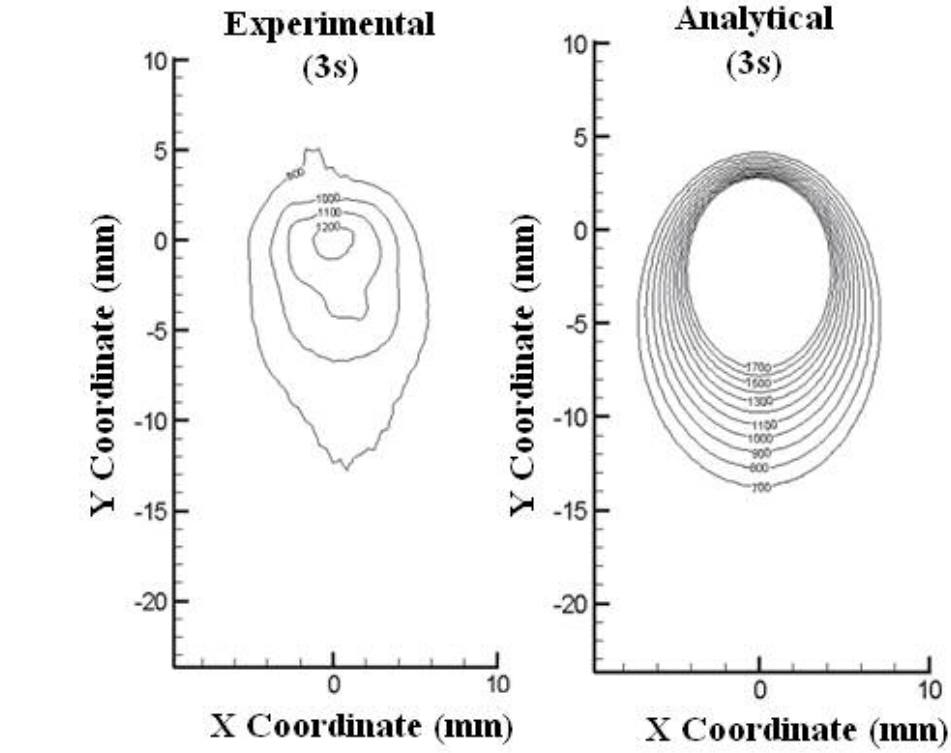
Experimental
(3s)
Analytical
(3s)
Y Coordinate (mm)
X Coordinate (mm)
10
5
0
-5
-10
-15
-20
1000
1100
1200
1700
1500
1300
1100
1000
900
800
700

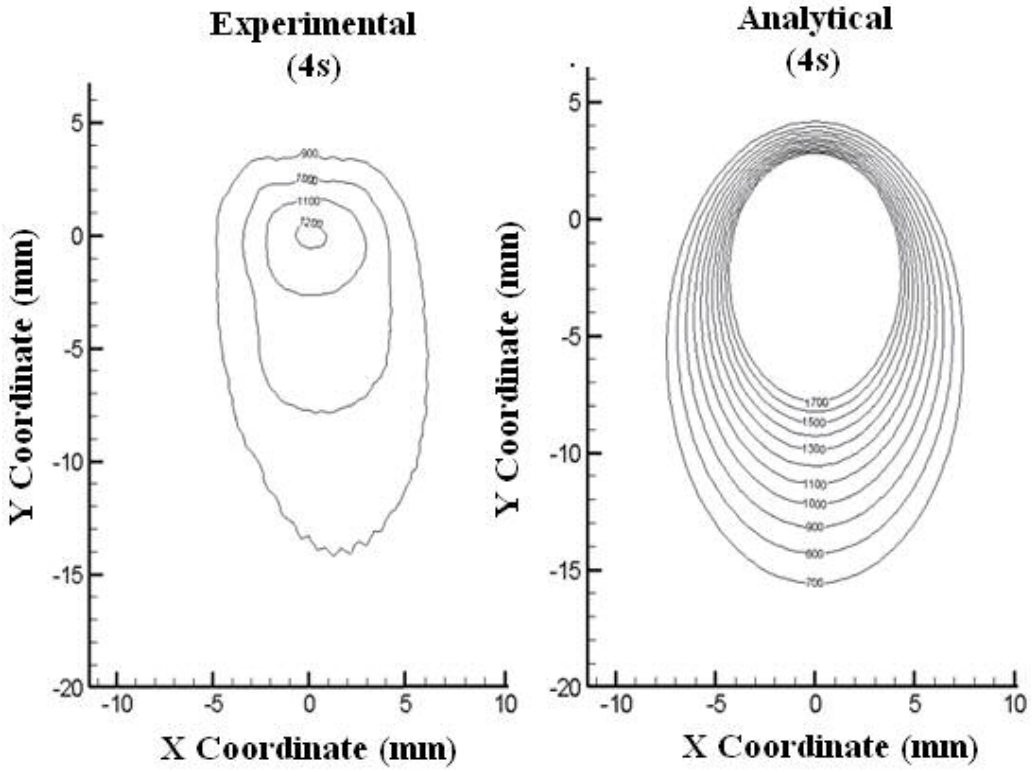
Experimental
(4s)
Analytical
(4s)
Y Coordinate (mm)
X Coordinate (mm)
5
0
-5
-10
-15
-20
-10
-5
0
5
10
900
1000
1100
1200
1700
1500
1300
1100
1000
900
800
700

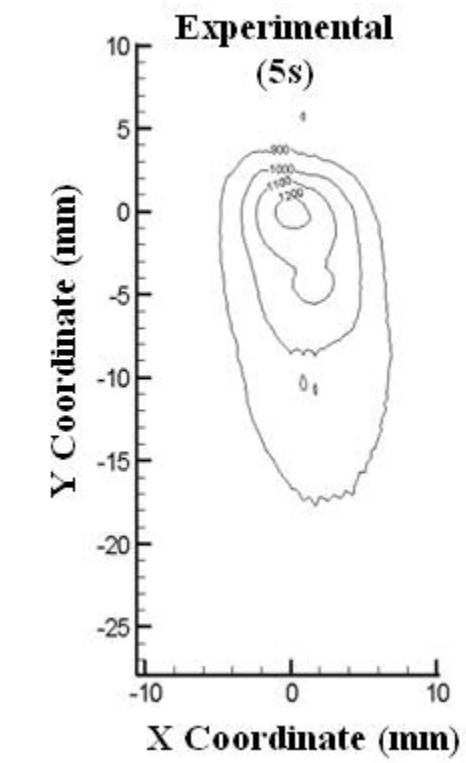
Experimental
(5s)
Y Coordinate (mm)
X Coordinate (mm)
10
5
0
-5
-10
-15
-20
-25
-10
0
10
900
1000
1100
1200

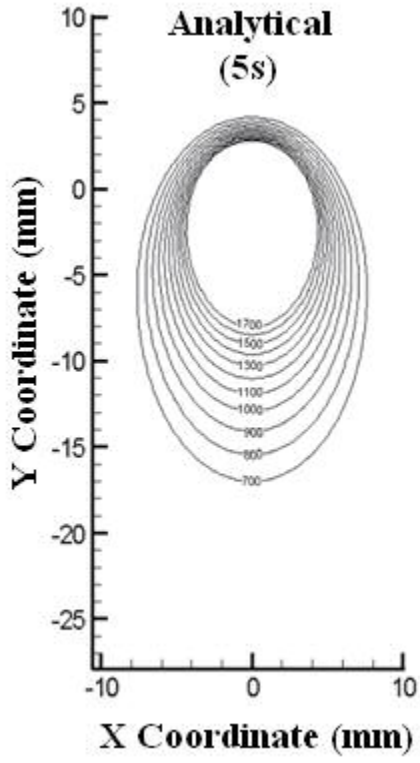
Analytical
(5s)
Y Coordinate (mm)
X Coordinate (mm)
10
5
0
-5
-10
-15
-20
-25
-10
0
10
1700
1500
1300
1100
1000
900
800
700

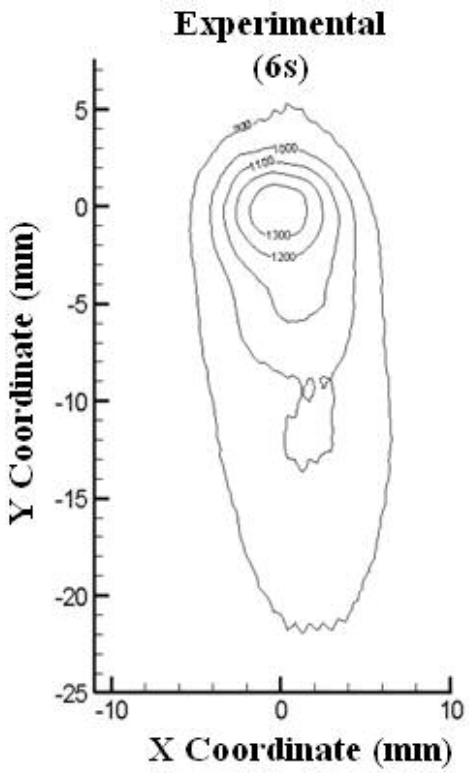
Experimental
(6s)
Y Coordinate (mm)
X Coordinate (mm)
5
0
-5
-10
-15
-20
-25
-10
0
10
900
1000
1100
1300
1200

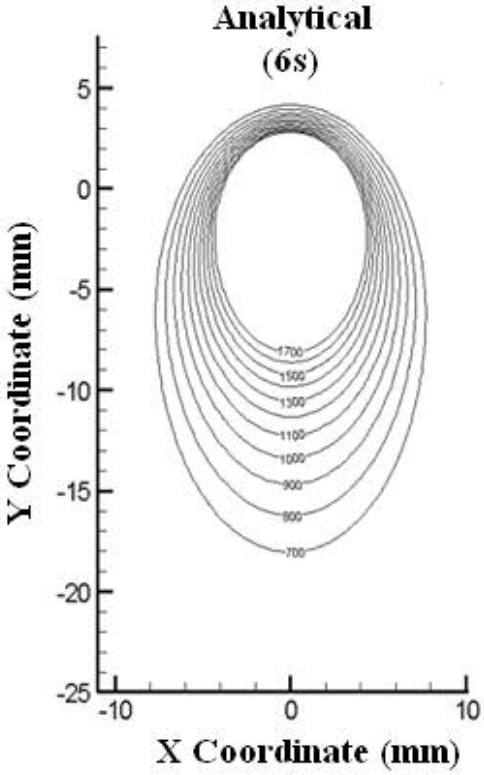
Analytical
(6s)
Y Coordinate (mm)
X Coordinate (mm)
5
0
-5
-10
-15
-20
-25
-10
0
10
1700
1500
1300
1100
1000
900
800
700

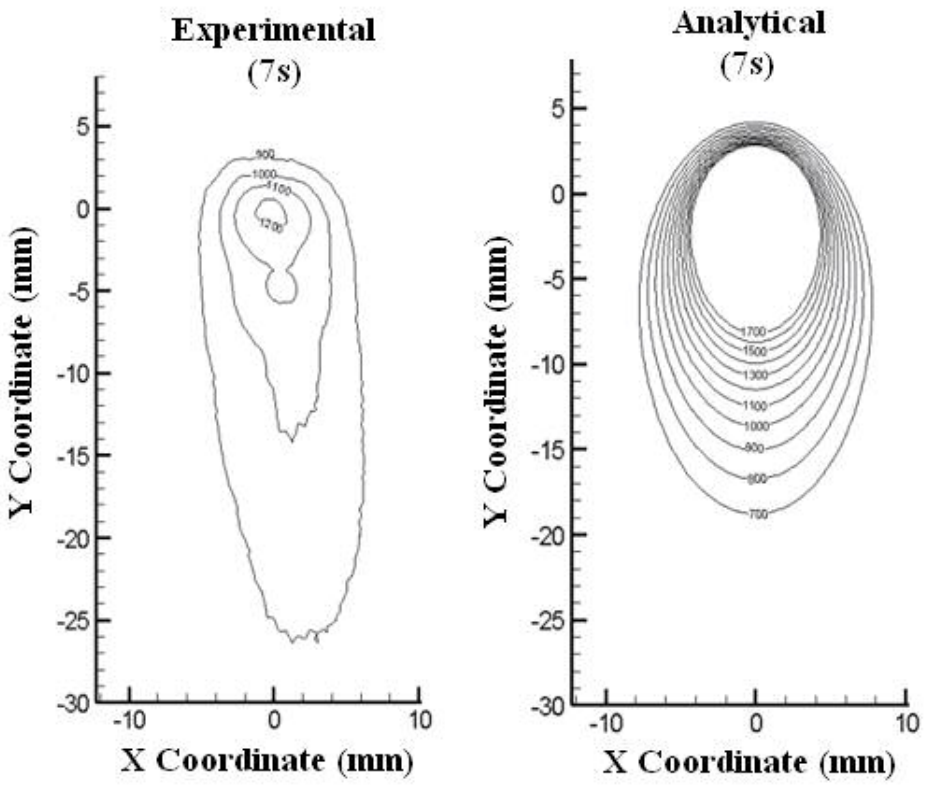
Experimental
(7s)
Analytical
(7s)
Y Coordinate (mm)
X Coordinate (mm)
5
0
-5
-10
-15
-20
-25
-30
-10
0
10
900
1000
1100
1200
1700
1500
1300
1100
1000
900
800
700

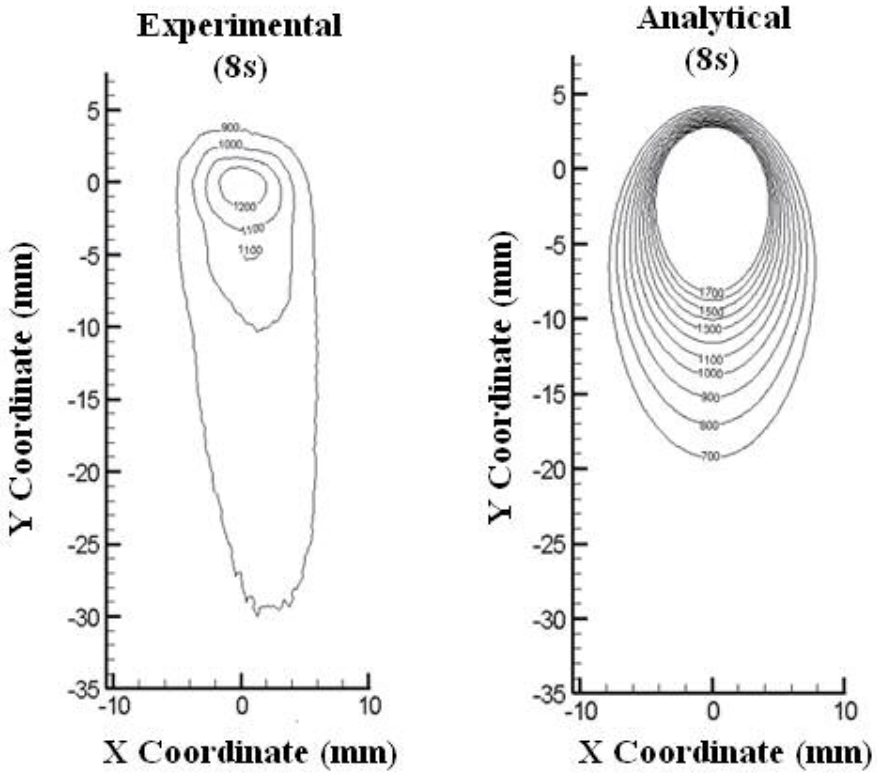
Experimental
(8s)
Analytical
(8s)
Y Coordinate (mm)
X Coordinate (mm)
5
0
-5
-10
-15
-20
-25
-30
-35
-10
0
10
900
1000
1200
1100
1700
1500
1300
1100
1000
900
800
700

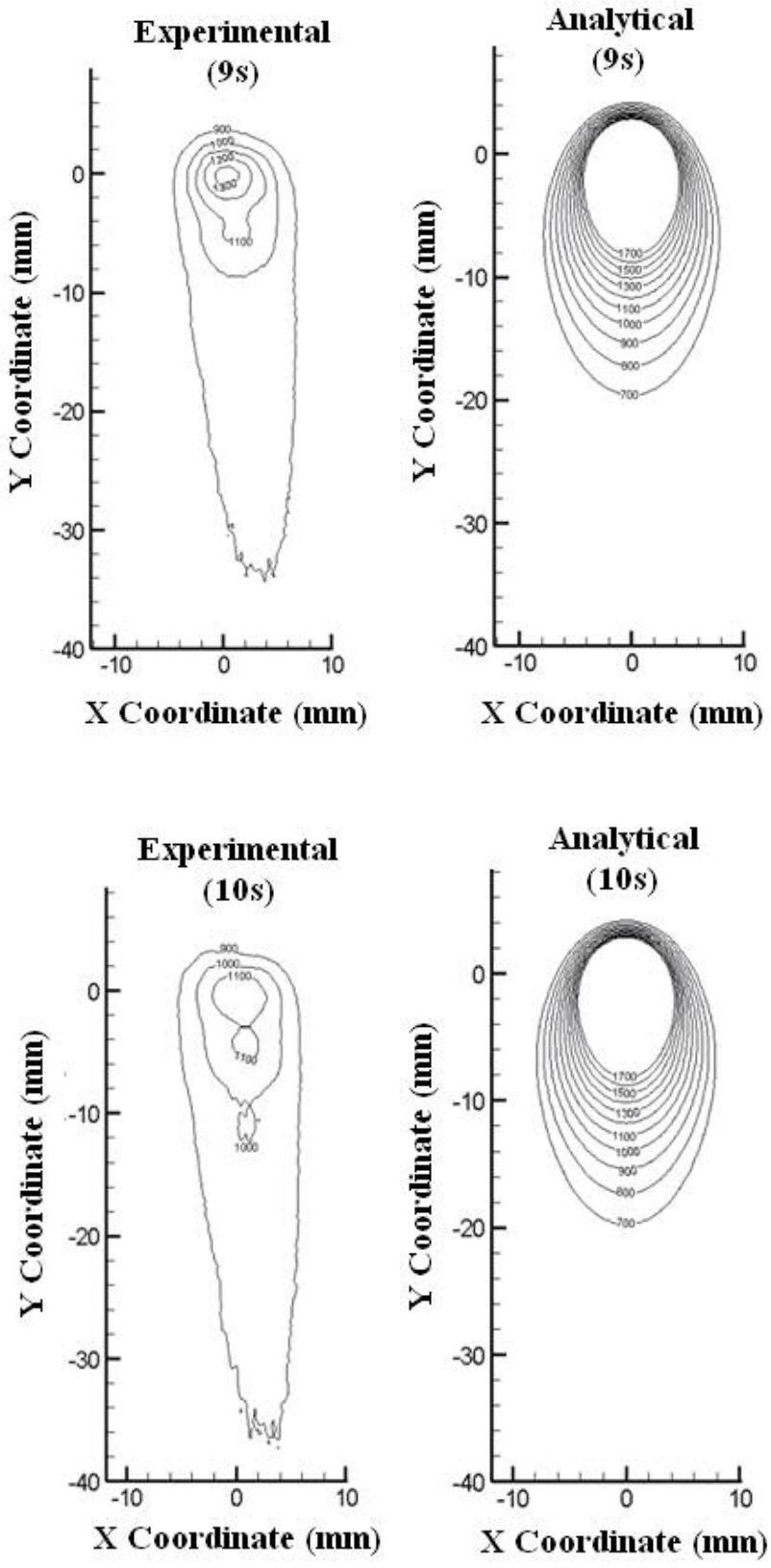
Experimental
(9s)
Analytical
(9s)
Experimental
(10s)
Analytical
(10s)
Y Coordinate (mm)
X Coordinate (mm)
0
-10
-20
-30
-40
10

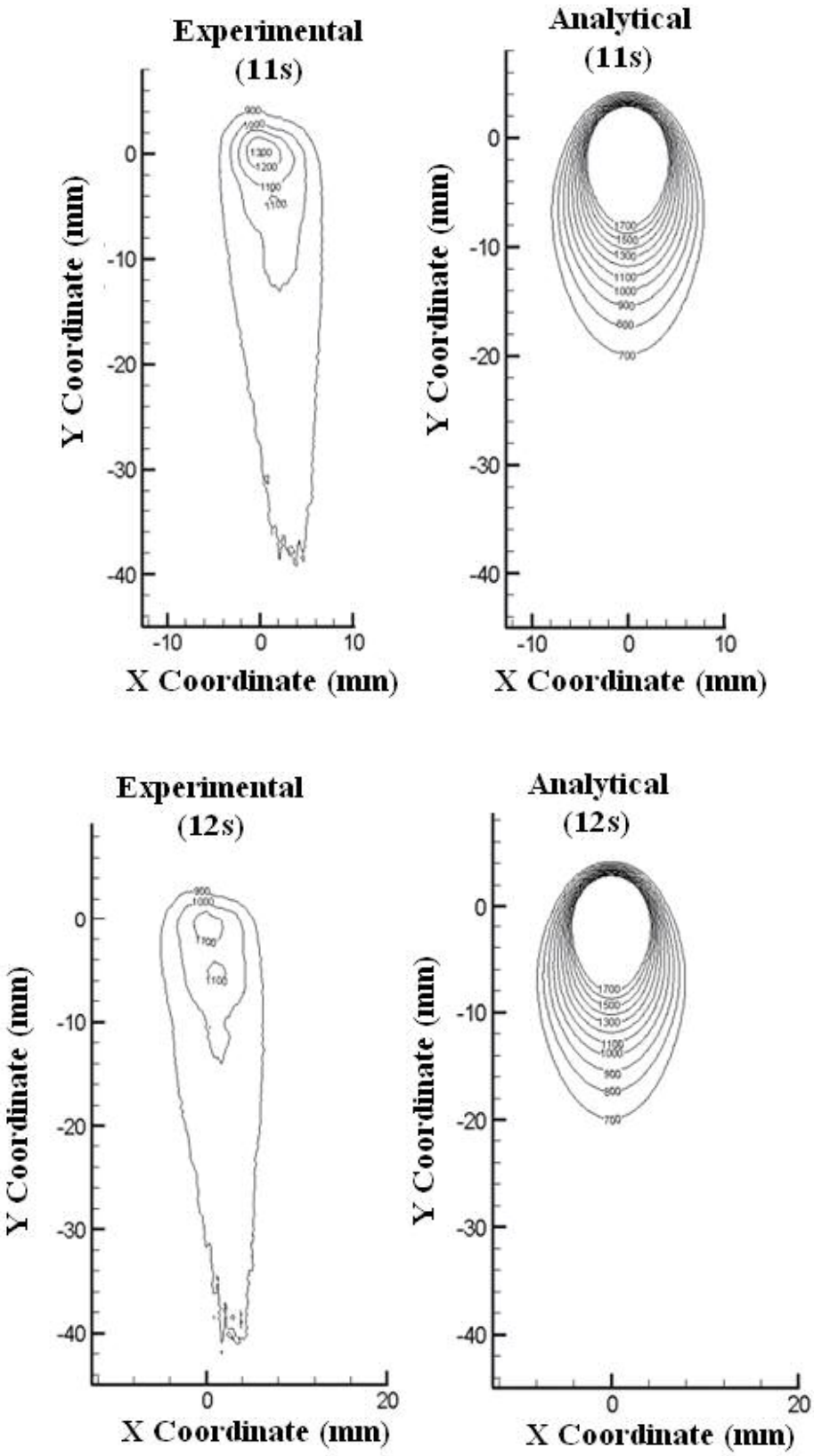
Experimental
(11s)
Analytical
(11s)
Y Coordinate (mm)
X Coordinate (mm)
Experimental
(12s)
Analytical
(12s)
Y Coordinate (mm)
X Coordinate (mm)

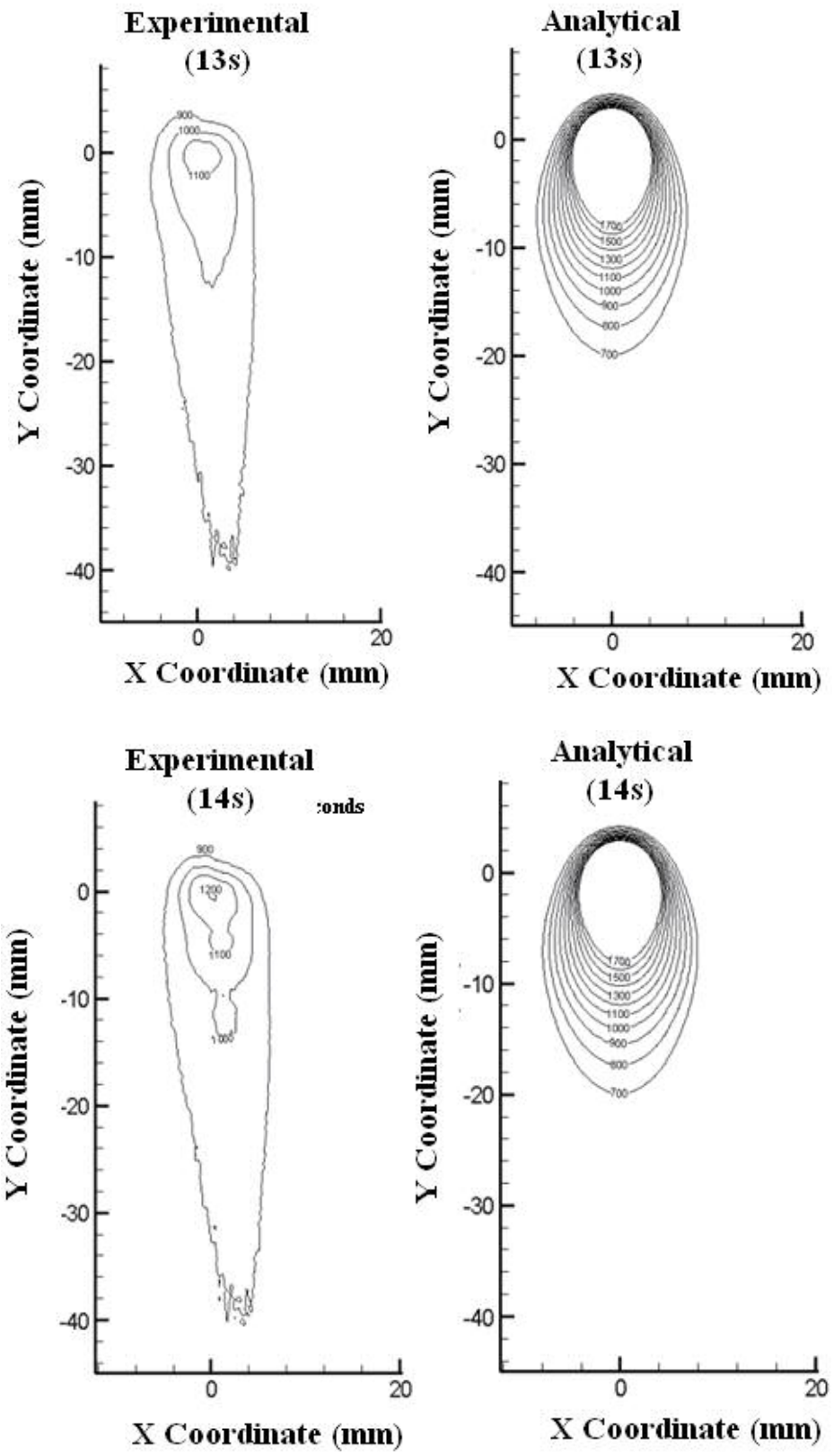
Experimental
(13s)
Analytical
(13s)
Experimental
(14s)
Analytical
(14s)
Y Coordinate (mm)
X Coordinate (mm)
0
-10
-20
-30
-40
20

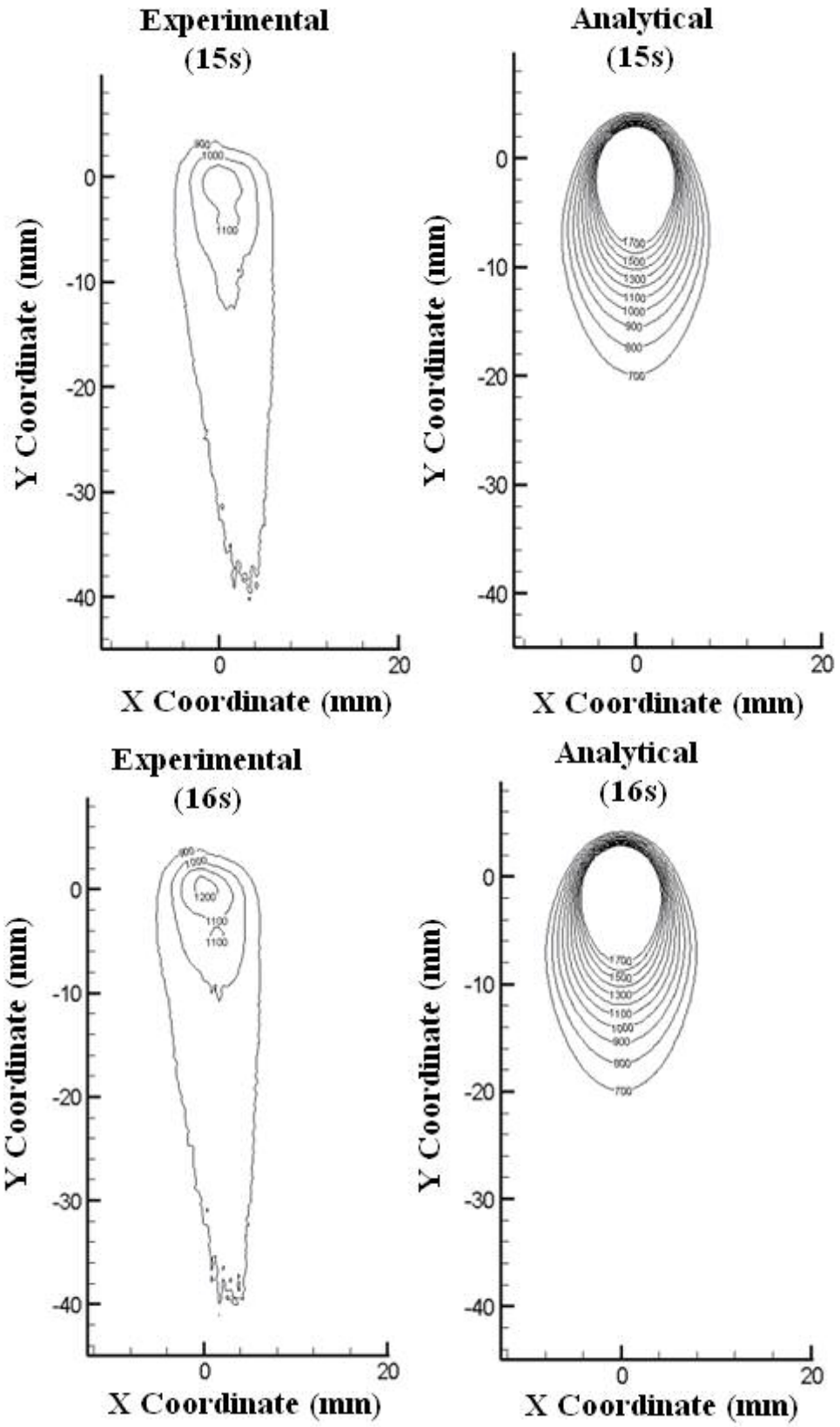
Experimental
(15s)
Analytical
(15s)
Experimental
(16s)
Analytical
(16s)
Y Coordinate (mm)
X Coordinate (mm)
0
-10
-20
-30
-40
20
900
1000
1100
1200
1300
1500
1700

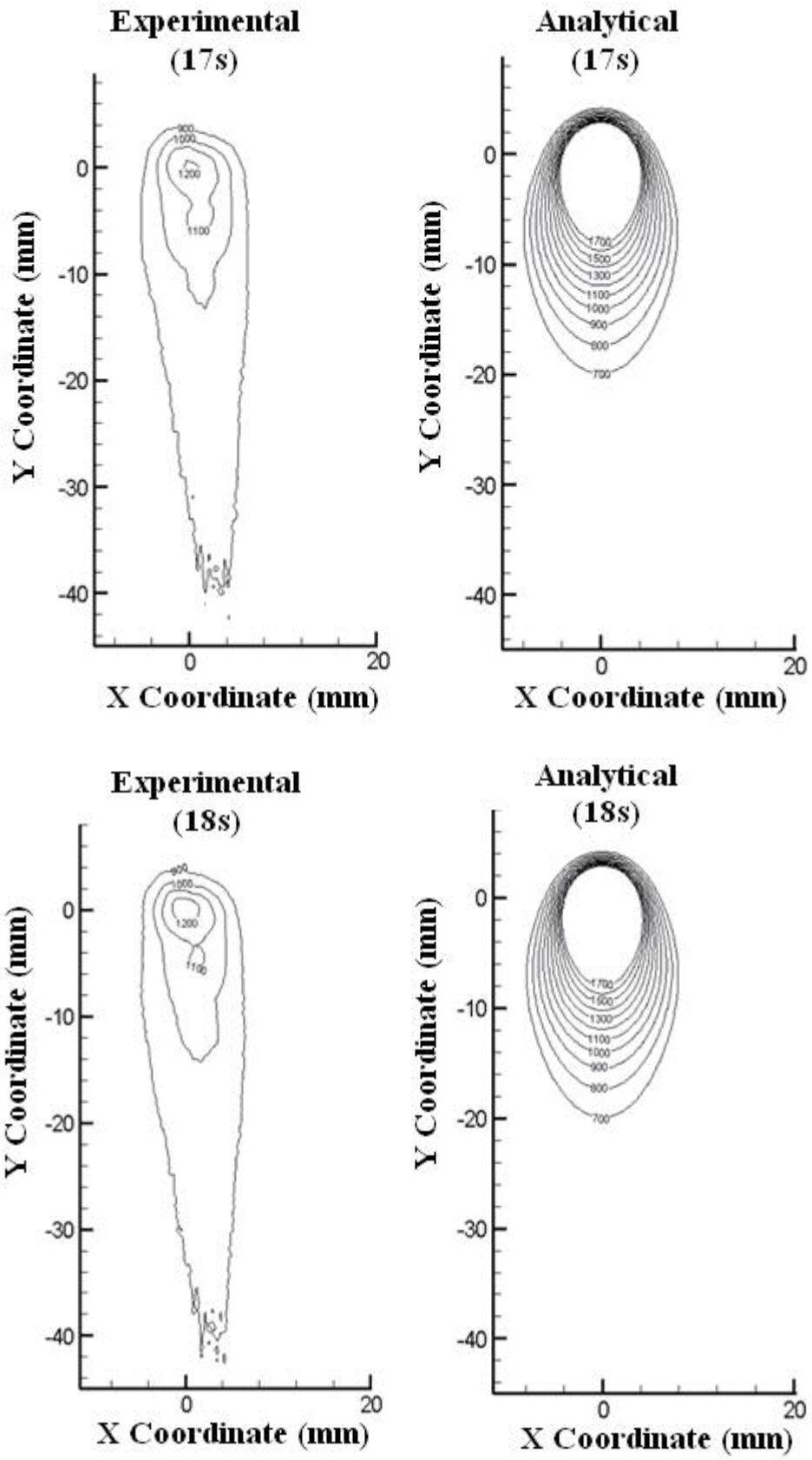
Experimental
(17s)
Analytical
(17s)
Experimental
(18s)
Analytical
(18s)
Y Coordinate (mm)
X Coordinate (mm)
0
-10
-20
-30
-40
20
1200
1100
1700
1500
1300
1100
1000
900
800
700

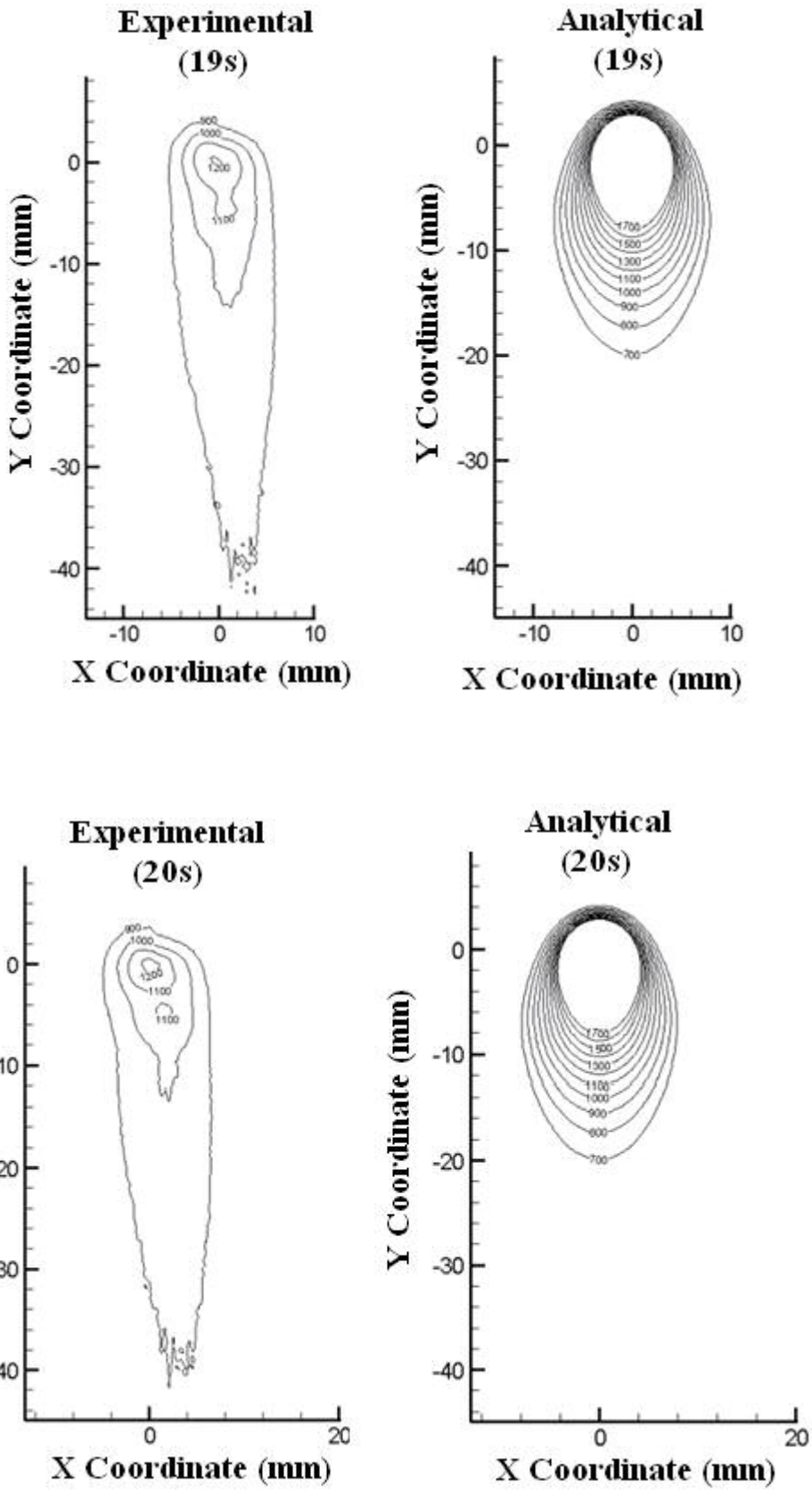
Experimental
(19s)
Analytical
(19s)
Experimental
(20s)
Analytical
(20s)
Y Coordinate (mm)
X Coordinate (mm)
0
-10
-20
-30
-40
10
20
900
1000
1200
1100
1700
1500
1300
800
700

Quasi-steady state temperature distribution comparison of experimental data and analytical data for 21 s, 25 s, and 29 s for a weld velocity of 0.514 cm/s

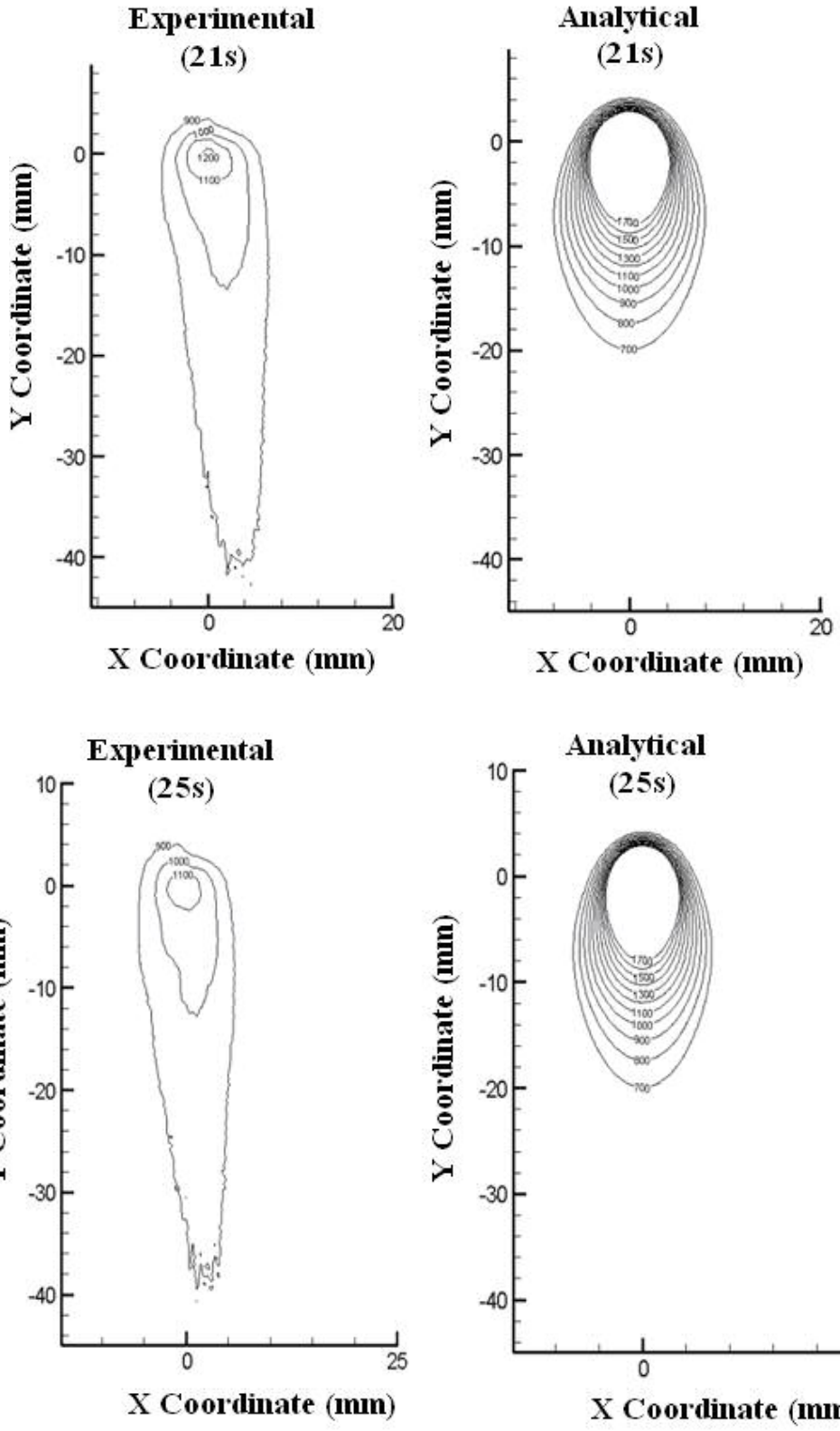

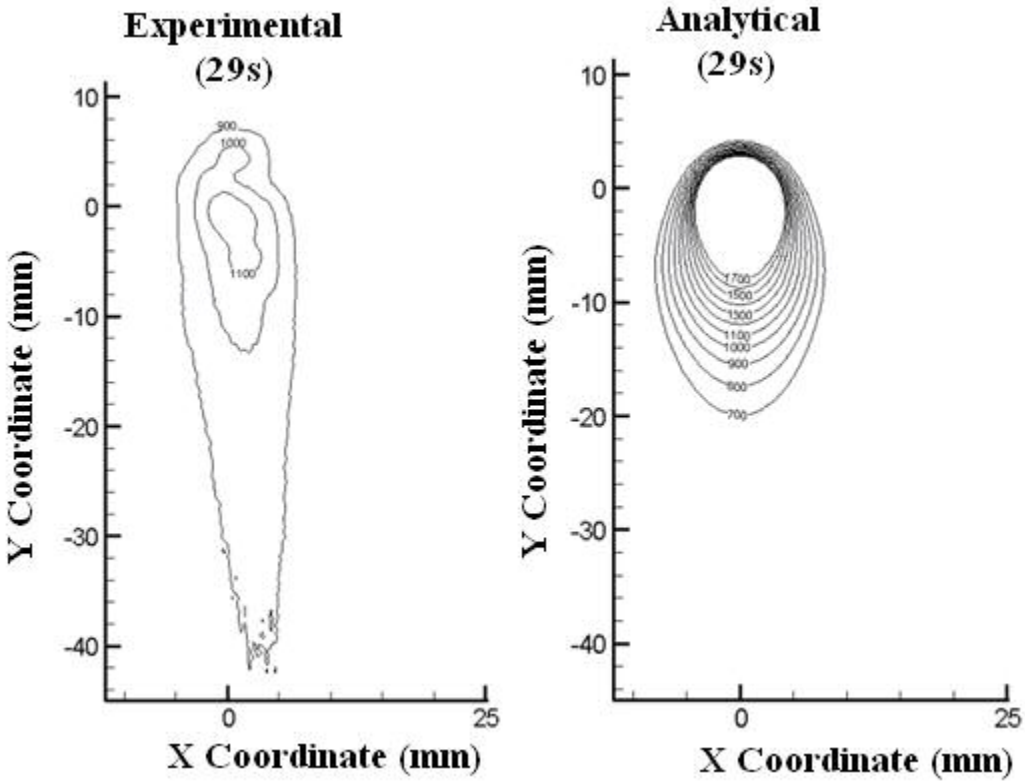
Experimental
(29s)
Analytical
(29s)
Y Coordinate (mm)
X Coordinate (mm)
10
0
-10
-20
-30
-40
25
900
1000
1100
1700
1500
1300
1100
1000
900
800
700

VITA

Catherine Antes Higgins

Candidate for the Degree of

Master of Science

Thesis: METAL INERT GAS (MIG) WELDING OF ASTM A500 GRADE B STEEL PIPES: INFRARED THERMAL IMAGING AND ANALYSIS

Major Field: Mechanical Engineering

Biographical:

Personal Data: Born in Coupeville, Washington, On May 22, 1980, the daughter of Dr. Joseph and Sunny Higgins, Sibling to Joseph, Brian, Daniel, and Jimmy Higgins.

Education: Attended Skagit Valley College for two years. Transferred and earned a bachelor's degree at Oklahoma State University in May 2003.
Completed the requirements for the Master of Science degree with a major in Mechanical Engineering at Oklahoma State University, Stillwater, Oklahoma in December, 2005.

Experience: Worked for the National Institute of Standards and Technology July to August 2004.
Research Assistant from June 2003 to December 2005.

Professional Memberships: American Society of Mechanical Engineers

Name: Catherine Higgins **Date of Degree:** December, 2005

Institution: Oklahoma State University **Location:** Stillwater, Oklahoma

Title of Study: METAL INERT GAS (MIG) WELDING OF ASTM A500 GRADE B STEEL PIPES: INFRARED THERMAL IMAGING AND ANALYSIS

Pages in Study: 209 Candidate for Degree of Master of Science

Major Field: Mechanical Engineering

Scope and Methodology of Study: Welding is a complex manufacturing process that generates extremely high temperatures and temperature gradients at and near the weld bead. In this investigation, welding of circular pipes is undertaken. An experimental setup was designed and built to observe the welding process and gather temperature isotherms under different welding conditions.

In the present experimental investigation, thermal images of welding of ASTM A500 Grade B steel pipes are collected using an infrared camera. A V-groove on a single pipe simulates welding of two pipes using a metal inert gas (MIG) welding process as the pipe rotates in a pipe-welding machine. An analytical solution is used to calculate the temperature isotherms for comparison with the experimental data.

The analytical approach, developed by Komanduri and Hou, uses Jaegers moving heat source method, is extended to calculate spot temperature data in pipe welding to determine the temperature profiles under various welding conditions. The analytical and experimental temperature isotherms were compared.

Findings and Conclusions: Some differences in the temperature distributions produced by the analytical and experimental results were observed. They include the geometry and magnitude of the temperature distributions. An attempt has been made to explain for these differences.

Advisor's Approval: Dr. Ranga Komanduri